DOCTOR OF PHILOSOPHY

The Development of a Low pH Mycobacterial Fuel Cell

Ahmed, Nawzad

Award date:
2013

Awarding institution:
Bangor University

The Development of a Low pH Mycobacterial Fuel Cell

A thesis submitted for the degree of

Doctor of Philosophy

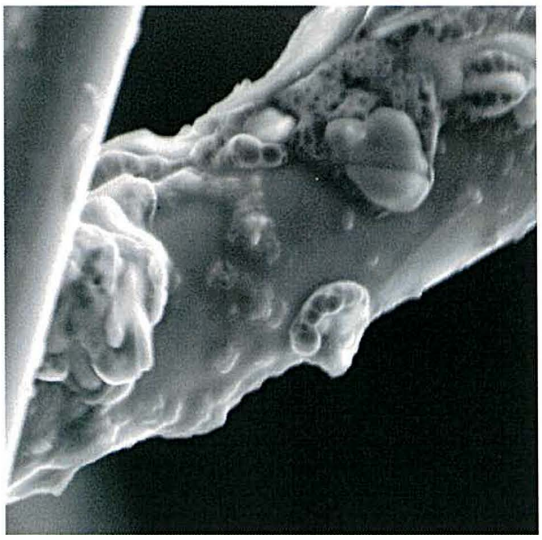

PRIFYSGOL BANGOR UNIVERSITY

1884

Prifysgol Bangor • Bangor University

by

Nawzad Noori Ahmed

Contents

Abstract

The development of a low pH mycobacterial fuel cell

by Nawzad Noori Ahmed

Microbial fuel cells offer an efficient and environmentally-friendly method of producing electricity and as such are an attractive green energy source especially as they can potentially produce power whilst recycling waste. The first objective of this study was to test the possibility of generating electricity with *Acidiphilium SJH* bacteria operating at a low pH as biocatalysts, with the ferric ion as the electron shuttle and glucose as the electron donor in a two-compartment microbial fuel cell.

This study is focused on a comparison between different microbial fuel cell designs that were constructed to test their energy performances. The resulting power densities ranged from 18.3 mW/m^2 to 25 mW/m^2 and the coulombic efficiency based on the contained substrates is in the range of 6 % to 7 %. Unfortunately the design of microbial fuel cells and scale-up is limited by the large cost of the platinum electrodes. Hence the electrode material used in the design is an important parameter when deciding the performance and cost effectiveness of microbial fuel cell.

This work demonstrates a potentially large reduction in cost by utilising the catalytic activity of platinum nano-sized particles on a Ketjen Black cathode that is able to diffuse oxygen from the air, eliminating the need for an external oxygen supply. The low pH redox behaviour of the ferric ion has been paired with an iron-reducing *Acidiphilium* sp. to form an effective fuel cell. At room temperature a power output of 20.7 m W/m^2 was achieved with nano particulate platinum loading of 150 $\mu g /cm^2$ within a Ketjen Black cathode. The modified cathode retained an equivalent of 80 % efficiency when compared to a solid platinum electrode; which is significant considering that the mass of platinum used in the modified electrode was only 0.1 % of that in a solid platinum electrode. Platinum nanoparticles were electrodeposited on carbon felt from an aqueous electrolyte containing hydrogen hexachloroplatinate by a potential cycling method. The modified Pt/KB cathode achieved higher power density when compared with the platinum electrodeposition on the carbon felt cathode electrode.

Acknowledgments

I would like to express my deepest gratitude and profound appreciation to my supervisor Dr C. D. Gwenin for his infinite support, inspiration and constant encouragement throughout my research work. I am indebted for his patience concerning the accomplishment of this thesis and passing on his knowledge of the microbial fuel cells and for all of his enthusiastic support. Throughout my research, he provided encouragement, sound advice, good teaching and a lot of ideas.

I am a grateful to Prof. Barry Johnson for his kind help and support to carry out my research work. I would also like to thank: John Charles and Alan Johns from the glass workshop for all of their hard work producing both cell designs. I would like to thank: electrochemical group.

Thanks also to the support staff Mr. Mike Lewis for their computational and electrical wisdom: Tracy, Caroline, Siobhan, and Bryony for their unconditional support.

I would like to thank the Government of Iraq for financial support of this project. My heartfelt thanks to my wife for her love, constant encouragement and support through my research period.

Chapter 1

INTRODUCTION

1.1 Energy sustainability

Energy sustainability is a serious challenge that faces our world today. Shortages in natural resources such as fossil fuels, natural gas[1] and fresh water are inevitable, and humanity cannot depend on available energy resources forever. The population growth in the world is also has a high demand on our limited available energy resources, contributing to a rise in energy prices.[2] In addition, climate change and global warming give rise to the environmental problems of the world.[3] However, treatment of wastewater has become one of the most crucial strategies, regardless of the intensive energy required which is almost 3 % of the total energy consumption in developed countries as a result less than 1 % of water is currently being treated.[4]

In a developed country, such as the USA, the wastewater treatment cost was $3.09 billion per year in 2010.[5] There is a significant amount of energy present in the wastewater in the form of organic matter; however, isolating the organic matter from wastewater is currently very costly.[6] Classical wastewater treatment technology is no longer considered as an economic option. Hence there is a clear need for the development of an environmentally clean alternative source of energy. Different biotechnologies have appeared recently that can not only treat wastewater but also utilise the wastewater as renewable energy source in the production of fuel simultaneously; using techniques such as fermentation,[7] production of biogas[8] and microbial fuel cells (MFCs).[9,10]

One of the technologies that are at the frontier of wastewater treatment is MFCs, a bio-processing strategy in producing sustainable energy and treating water. MFCs can produce electrical energy and biogas (*from biodegradable compounds*) which ultimately can minimise carbon compounds in domestic and industrial wastewater.[11] A typical MFC contains both an anaerobic anode and aerobic cathode chamber, separated by a proton exchange membrane. In the anode chamber, fuel (*substrate*) is oxidised by microorganisms, producing electrons and protons. Electrons are transferred to the cathode chamber through an external electric circuit, and protons are transferred through the membrane to the cathode. Here they react with oxygen and electrons to form water, with the production of electricity as a by-product. MFCs can minimise the amount of organic material in the wastewater which in turn cleans the water body. In order for the MFCs to be used in industry, they would need to be

scaled up. To achieve that goal, different geometries have been designed and optimised to be able to treat domestic and industrial wastewater effectively.[12, 13,14,15,16]One of the emphases is on the type of anode materials to optimise the electricity production and then in enhancing the interaction with anaerobic bacteria and replacing the chemical catalyst which is currently being used by cheaper material; this is an important factor which has a direct influence on the performance and cost effectiveness of an MFC.[17,18,19]

In summary, the optimised geometry of MFCs has great potential in improving the quality of water and minimising and converting organic matter in wastewater *via* bio-energy to sustainable fuel energy. A better understanding in MFCs geometry and mechanism are essential to gain a better future in sustainable fuel energy.

1.2 Background on fuel cells

A fuel cell system is usually classified by the type of electrolyte used. Different types of electrolytes identify the specific properties of a fuel cell, like fuel type, temperature or efficiency. There are several types of fuel cells currently under development, each with its own advantages, limitations and applications; these are explained in the following text.

Solid oxide fuel cells

These cells operate using solid oxide electrolyte (SOFC) in the form metal oxide (*calcium or zirconium oxide*). They generally operate at a high temperatures of around 500-1000 °C,[20] and they have reliability issues due to the low conductivity of their solid electrolyte. SOFCs have an efficiency of about 50-60 % in converting fuel to electricity. However, at a high operating temperature it produces a large amount of steam which is used in turbines to generate electricity; efficiencies are therefore over 70 %. SOFCs are best suited for large-scale stationary power generators that could provide electricity for factories or towns. In the mechanism of operation of the SOFC, electrons transfer from the anode to the cathode *via* an external circuit; however, the electrolyte negative ions (O^{2-}) are transferred from the cathode to the anode where electrons are generated by oxidation of hydrogen.[21]

Anode $H_2 + O^{2-} \rightarrow H_2O + 2e^-$ *Equation 1-1*
Cathode $O_2 + 4e^- \rightarrow 2O^{2-}$ *Equation 1-2*

Alkaline fuel cells

Alkaline fuel cells (AFC) produce heat and electricity using aqueous alkaline solution (*such as KOH*) as the electrolyte in the presence of oxygen and hydrogen. However, to avoid the possibility of CO_2 poisoning, pure oxygen, hydrogen and an operating temperature of 50-200 °C is required.[20] AFCs have an efficiency of about 70-80 %; during their operation electrons are transferred from the anode to the cathode *via* an external circuit and the electrolyte negative ions (OH^-) are transferred from the cathode to the anode.[22]

Anode $H_2 + 2OH^- \rightarrow 2H_2O + 2e^-$ *Equation 1-3*
Cathode $O_2 + 4e^- + 2H_2O \rightarrow 4OH^-$ *Equation 1-4*

Phosphoric acid fuel cells

Phosphoric acid fuel cells (PAFC) belong to the first generation of fuel cells and were the first to be made commercially.[23] They have good ionic conductivity by producing electricity using liquid phosphoric acid (H_3PO_4) as the electrolyte at an operating temperature of 150-200 °C. PAFCs have an efficiency of about 37-42 %; however, efficiencies could top 90 % when used as a heat and power system. The PAFC has the potential for use in small stationary power-generation systems. The most common electrolytes are permeable for protons and chemical reactions in phosphoric acid fuel cells:[20]

Anode $H_2 \rightarrow 2H^+ + 2e^-$ *Equation 1-5*
Cathode $O_2 + 4e^- + 4H^+ \rightarrow 2H_2O$ *Equation 1-6*

Molten carbonate fuel cells

Another type of high temperature fuel cell is molten carbonate fuel cells (MCFC) which operates at a temperature of about 650 °C.[20] MCFC use compounds of salts like lithium and sodium carbonates (CO_3^{2-}) or lithium and potassium carbonates as the electrolyte. Their efficiency is about 60-80 % and the high operating temperature helps to reduce the effect of possible carbon monoxide contamination, as well as increasing electricity generation by recycling waste heat.[24] MCFCs are best suited for large stationary power generators. The chemical reactions which occur are:[25]

Anode $H_2 + CO_3^{2-} \rightarrow H_2O + CO_2 + 2e^-$ *Equation 1-7*
Cathode $\frac{1}{2}O_2 + CO_2 + 2e^- \rightarrow CO_3^{2-}$ *Equation 1-8*

Polymer electrolyte membrane fuel cells

Polymer electrolyte membrane (PEM) fuel cells are also called proton exchange membrane fuel cells and operate at a temperature of about 30-100 °C.[20] PEM fuel cells use thin porous polymers as an electrolyte, with the porous membrane allowing proton transfer to the cathode chamber. PEM fuel cells have an efficiency of about 50-60 %; their possible fields of application are mobile systems, and transportation. The most common electrolytes are permeable for protons and the chemical reaction is in the PEM fuel cells are:[26]

Anode $H_2 \rightarrow 2H^+ + 2e^-$ *Equation 1-9*

Cathode $O_2 + 4e^- + 4H^+ \rightarrow 2H_2O$ *Equation 1-10*

1.3 Microbial fuel cell principles

History of microbial fuel cell development

The bioelectric phenomenon started from the first observation by Luigi Galvani (1791) of the twitching of an isolated frog's leg, when a small electrical discharge was passed through it.[27] Later, in 1839, William Grove made the first FC by reversing the process of electrolysis of water; hydrogen and oxygen were produced and combined back to water producing electricity.[28] Michael Potter (1911) observed that electrical energy was generated from living cultures of yeast and *Escherichia coli (E. coli)* using platinum electrodes.[29] Cohen (1931) developed the field later showing that a batch-biological FC generates more than 35 V.[30] Although these studies may be a starting point for MFC development, it was not until the 1960s that biofuel FCs became frontier science due to the need of this technology for spacecraft as the conversion of organic wastes to energy was of interest to NASA.[31] In 1969, a biofuel FC was made using a platinum black electrode as the working electrode where it was shown that glucose could be used for energy generation.[32] In 1976, Rao readdressed the principles of the biofuel FC.[33] It was believed that bacteria can transfer electrons onto the anode (*an electron acceptor*) with the current produced *via* an external circuit. For completion of the electrical circuit, protons migrate though the proton exchange membrane to the cathode where protons and electrons are recombined. However, the term and concept of the MFC was found by Roller *et al*, in the1980s.[34] The result was that in 1991, Habermann and Pommer combined the concepts of wastewater treatment and MFCs.[35]

1.4 Types of biological fuel cells

Two types of fuel cells are common; MFC and enzymatic fuel cells. It's very important to distinguish between these two types; MFCs utilise microorganisms as the biocatalyst to produce electrons and protons, while in enzymatic fuel cells, enzymes are isolated from the microorganisms and then used in the system for energy production in a similar operation as MFCs. Enzymatic fuel cells have higher efficiency due to the catalytic effectiveness of enzymes, but it's more convenient, practical and economic to apply bacteria in MFCs.[36,37,38,39] Based on the electron transfer mechanisms within the bacteria, MFCs could be classified into three types:

(1) Mediated electron transfer MFCs. This type depends on extracellular redox mediators, like neutral red,[40,41] or thionin.[42,43] Mediators are costly chemicals and in general cannot be recycled.

(2) Mediator-less MFCs. This type is a more environmentally friendly system, where there is no concern about the effects of mediators. The earliest concept of electron exchange by electrochemically active bacteria (EAB) to electrodes was recorded by dissimilatory metal reduction by neutrophilic bacteria of the family *Geobacter* , *Shewanella* and *Thermincola potens* strain JR species, which can generate electricity in MFCs.[44,45,46,47] This ability has also been identified in acidophilic bacterium *Acidiphilium 3.2 Sup 5,*[48] where the EAB transferred electrons to a solid anode electrode through an extracellular electron transfer (EET) mechanism. The mechanism of EET has been elucidated by three different routes:

(i) Outer membrane associated cytochromes.[45,49,50,51]
(ii) Redox mediators (i.e., phenazines or quinones) excreted from the microorganisms.[52,53,54]
(iii) Conducting molecular pili or elongated appendages (nanowires) that interconnect bacterial cells to the electrode surface.[55,56,57]

(3) Photo heterotrophic MFC: this type uses an extra source of light to input extra energy into the MFCs system.[58]

Figure 1.1 illustrates the chemical compounds suggested to be involved in the electron transfer chain from electron carriers (NADH) in the intracellular matrix to the solid- anode electrode of electrochemically active bacteria.[59,60]

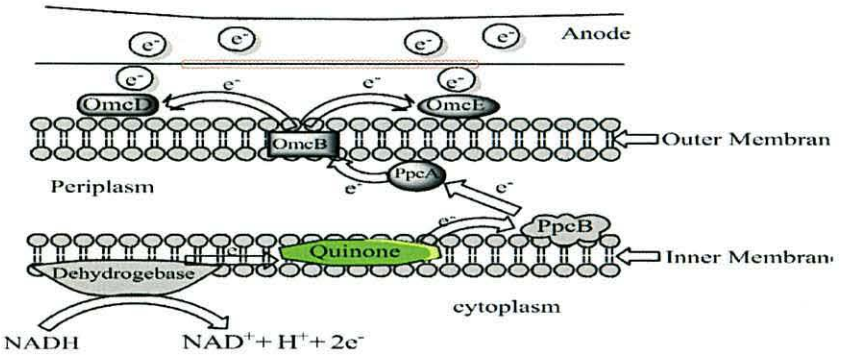

Figure1. 1- Electron transport from cells to the anode in MFCs.[60]

Microbial fuel cells for renewable electricity production

While MFCs convert the chemical energy into electricity directly similar to traditional FCs, the principle difference is their configuration, materials, fuels and products generated. MFCs are capable of using different kinds of fuel which include but are not limited to: environmental waste, reduced carbohydrates, glucose, sucrose, acetate, lactate, starches and municipal or industrial wastewaters in the form of liquid or sludge.[61,62,63]

Another factor which affects the MFCs electron transfer is the attachment and growth of bacteria to the anode surface; forming layers which are collectively known as biofilms Figure 1.2. Electrons are transferred to the cathode chamber through an external electric circuit, and protons are transferred through the membrane to the cathode. Here they react with oxygen and electrons to form water with the production of electricity as a by-product.

$$O_2 + 4e^- + 4H^+ \Longrightarrow 2H_2O \qquad \textit{Equation 1-11}$$

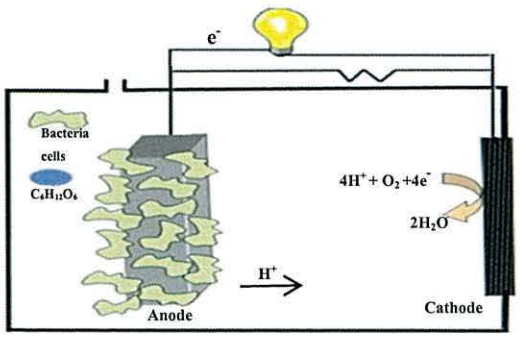

Figure1. 2- Homemade bacterial fuel cell (open air cathode) single chamber with carbon cloth (anode), Pt/KB (cathode).

1.5 Microbial fuel cell materials

Anode materials

An important factor which has a direct influence on the performance of a MFC and the subsequent production cost is the material used for the anode electrode.[64] This is related to the reaction between the microorganisms and the anode electrode. In addition, the anode must be able to transfer electrons, and then reduce the protons to react with the oxygen at the cathode.[44,65] An ideal anodic material is conductive, chemically stable in the MFC reactor solution, non-corrosive, with a high porosity and has a high surface area for bacteria to easily attach to and grow on the surface.[61] The most common materials used for anode electrode are carbon-based materials; they traditionally include carbon paper, carbon cloth, carbon felt, carbon mesh, graphite rod, granular graphite, and reticulated vitrified carbon (RVC).[66,67] Carbon cloth is a good material for anodic biofilms in MFCs, but it is expensive (*approximately $1,000/m^2*).[66] Carbon mesh is a much less expensive material (*approximately $10–50/m^2*) and can work as well or better than both carbon cloth and paper.[68] To improve surface modification of the anode electrode, treatment with ammonia gas at a high temperature is a good factor for increasing bacterial adhesion and power densities,[69] while carbon mesh is sufficient to produce good performance with a simple heat treatment.[68] Graphite fibre brush is one of the more promising materials and configurations for anode electrodes.[70,71,72]

The function of a bio-electrode is not just conducting; it also works as a carrier of microbes, and some special surface characteristics of electrode materials, such as high surface roughness, good biocompatibility, and the electron transfer efficiency between microbes and electrode surface, are essential for high bio-catalytic activity. In order to enhance bacterial adhesion and charge transfer, surface modification of the anode electrode has become a new topic of interest in the research field of MFCs.[73] Table 1.1 on the following page serves as a comparison of these studies.

Table 1. 1 - Anode materials, reactor configuration, and power generation performance in MFC.

Anodes	MFC configuration	Performance improvements	References
Carbon brush treated with ammonia	Single chamber	1280 mW/m^2	74
Antimony(V)-graphite	Sediment	108 mW/m^2	75
Fe_2O_3 coated Carbon paper	Two chamber	30 mW/m^2	76
Mn^{4+} - graphite	Two chamber	788 mW/m^2	77
Carbon nanotube -textile composite	Unreported	1098 mW/m^2	78
Polypyrole coated Plain C. Cloth	Single chamber	160 mW/m^2	79
Graphite-ceramic composite-Mn^{4+}, Ni^{2+}	Sediment	105 mW/m^2	80
Neutral red-Carbon paper	Two chamber	900 mW/m^2	81

Cathode materials

The cathode material and construction are the most challenging aspect of any MFC design.[73] There are many types of materials used for cathodic electrodes: carbon paper, carbon cloth, graphite foil, graphite granules, platinum (Pt), platinum black, activated carbon (AC), graphite based cathodes and biocathodes.[60,82] The most widely used cathode catalyst for a MFC is platinum and its alloys, due to its excellent catalytic efficiency.[83,84,85,86,87] However, Pt is expensive and hence prevents up scaling of the fuel cell for industrial applications. In aerobic cathodes, oxygen is the terminal electron acceptor. Oxygen reduction is the most common electrochemical reaction that takes place at the surface of cathodic electrodes, and is commonly used because of its low cost, sustainability, and its high standard redox potential.[61,88,65]

The cathode reaction, also called oxygen consumption is certainly one of the most serious factors which has a direct influence on the performance of MFC due to the low reaction kinetics of the oxygen reduction at the cathode unless the expensive Pt catalyst is used.[89,90,91] Consequently, current research has focused on the reduction of the amount of the used platinum for electrocatalyst purposes.[92,93,94,95] The use of cheaper metals to create new catalytic electrode materials for cost reduction, Fe(II) and cobalt-based cathodes, have also been investigated as a useful alternative to a platinum catalyst (*metal porphyrins and phthalocyanines*).[96,97,98]

Currently, biocathode catalysts are an attractive alternative to chemical catalysts to improve the oxygen reduction reaction, because of their low cost and sustainability.[99] Bacteria were used to catalyse the oxygen reduction reaction (ORR) *via* a mediating species like manganese, manganese-oxidising bacteria deposited on the surface of the cathodic electrode which increases current density.[100]

Bacteria have also been utilised *via* a (Fe^{2+}/Fe^{3+}) couple redox at low pH (2.5) for biological cathodes using *Acidithiobacillus ferrooxidans*,[101] the biocathode was biocatalyzed by Ferro/manganese-oxidising microorganisms[102] or directly in the case of *acidophilic Acidithiobacillus ferrooxidans*,[103] ɣ-, β-, and α -*Proteobacteria, Bacteroidetes* and *Actinobacteria*,[104] in both wastewater,[105] and freshwater.[106] The performance and cost effectiveness of an MFC using a bacteria biocathode with different cathode electrode materials have been show to provide a substantial cost saving.[107] However, the ORR can be improved by using more effective oxidants (*e.g. Ferricyanide* ($K_3Fe(CN)_6$),[108,109,110] *acidic permanganate* (MnO_4^-),[111] or acidic hexavalent chromium[Cr(VI)],[112] persulfate ferrous ion ($K_2S_2O_8$-Fe^{2+}) as the electron acceptors.[113]

Surface modification provide a new and interesting approach for oxygen reduction in MFC at cathodic activated carbon materials.[114,115,116] In essence ORR improvements have been studied and developed with cathode alternatives [*Lead dioxide* using a titanium base (*PbO_2/Ti*), *Iron phthalocyanine* supported on Ketjen black (*FePc-KJB*), Polypyrrole/carbon black (Ppy/C), manganese oxide on carbon cloth (*MnOx/C*) and *cobalt tetramethoxyphenylporphyrin* (*CoTMPP*)]and have shown to improve MFC performance similar to or better than that of platinum contained cathodes, as shown in Table 1.2.

Table 1. 2 - Non Pt cathode catalyst, configuration and performance in MFC.

Cathode composition	Configuration	Types of reactor	Max Power density mW/m^2	References
Graphite-CoTMPP	Plane	Single chamber	449	117
Activated carbon fibre felt	Plane	Two chamber	315	115
Fe^{3+} -graphite	Plane	Two chamber	788	77
Pb O_2/Ti	Plane	Two chamber	25	118
FePc-KJB	Plane	Single chamber	2011	98
Ppy/C	Plane	Single chamber	401.8	119
MnOx/C	Plane	Two chamber	193	120

Carbon supports for electrocatalysts

Another important component of the MFC is the catalytic support which has been shown to have a major role in catalyst performance.[121] Carbon black materials have been used as carbon support for MFCs electrocatalyst applications.[122] These carbon black materials differ in sulphur, ash, moisture content, porosity, surface area, and electroconductivity.[123,124]

Ketjen Black

Ketjen Black (KB), which was used for this study, is a commercially available carbon black from Akzo Nobel and is generally used as a carbon support for MFCs electrocatalysts.[98] The main property of KB is low ash content; large pore volume and a high surface area.[125] KB is treated through chemical oxidation of carbon supports in order to enhance the interaction between carbon support and catalytic particles. [126] Table 1.3 shows the properties of four types of carbon blacks generally used for electrocatalyst applications (*KB EC-600JD, KB EC-300J, Black Pearls and Vulcan XC-72*).

Table 1. 3 - Some properties of carbon black materials.[125,127]

Carbon support	Surface area m^2/g	Pore volume cm^3/g	Ash content Wt %
KB EC-600JD	1400	4.80-5.10	<0.10
KB EC-300J	886	3.10-3.45	<0.05
Vulcan XC-72	267	0.46	0.10
Black Pearls	1475	2.67	0.36

Previous work by Subramanian *et al* studied the effect of surface area and distribution of pore sizes on the activity of cobalt-ethylene diamine (Co-EDA) catalysts using three different carbon supports, Ketjen Black EC 300 J, Vulcan XC-72 and Black Pearl 2000. Their results revealed that with an increase in the amount of quinone groups on an oxidised carbon surface the activity of the heat treated Co-EDA/C catalyst decreased in the following sequence: KJ300 > Black Pearls 2000 > Vulcan XC-72.[128]

Because carbon black materials are cheap and environmentally-friendly many new carbon black materials have been discovered, these include: graphitised carbon,[129] carbon nanotubes,[130,131,132] highly mesoporous carbons,[133] carbon nanofibres,[134,135] and even carbon nano-onion like structures.[136] These new carbon structures generally have the following features: increased volume-to-mass aspect ratio, higher surface

areas, and greater electroconductivity. Furthermore, they can be prepared or post-treated to give diverse functions, for example, nitrogen doped carbon nanotubes.[137]

Membranes

Membrane plays an important role in MFCs. Several types of membranes have been documented in the literature for MFCs, including salt bridge, cation exchange membrane (CEM), anion exchange membrane (AEM), bipolar membrane (BPM), microfiltration membrane (MFM), ultrafiltration membrane (UFM), glass fibres, porous fabrics and other course pore filter materials to separate the liquid in the anode from that of the cathode chamber.[138] A Nafion ionomer membrane is the most widely used in proton exchange membrane fuel cell devices because of its high chemical stability, high ionic conductivity and good mechanical strength. Recently, a number of proton conducting membranes were developed for high temperature operation; these are classified into four groups:[139] Perfluorosulfonic Acid Polymer Membranes, alternative sulfonated polymers and their inorganic composite membranes, acid base complex membrane, and ionic liquid-based gel-type proton conducting membranes. The disadvantage of the membrane is the reduced performance of the MFC which results from an increased internal resistance.[140]

Microbial fuel cell design developments

There has been an unprecedented development in the design and the technology of MFCs; this has given rise to different configurations of MFCs with outstanding performance. The development of the air-cathode single chamber MFC is membraneless and increases power output and cost effectiveness.[141,142] The presence of membranes between the electrodes can lead to pH gradients.[143] An important factor, which has a direct influence on the performance of the air-cathode single chamber MFC, is membrane deformation when the membrane is placed next to the cathode electrode, and performance of the system is enhanced through control of the membrane deformation.[144] For the first time, cloth separators were used to replace membranes in air-cathode single chamber MFCs.[145] Wei, B *et al* demonstrated the importance of pressing separators against the cathode electrode in single-chamber air cathode MFC.[146] For instance, Liu, H *et al* designed an MFC cylindrical chamber used in wastewater treatment (Figure 1.3).[147] This design has been shown to be useful in both batch and continuous modes as opposed to other previously illustrated

two chamber cells in section. The larger surface area of the anode helps to facilitate more bacterial activity and passive air transfer to the cathode, thus producing more energy.

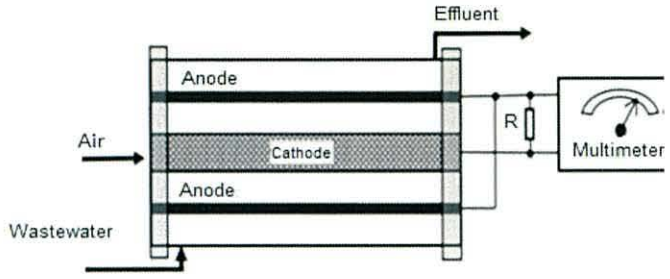

Figure 1. 3 - Schematic single chamber MFC cylindrical shape with inner cathode.[147]

An Upflow MFC design is where the anode and cathode were placed in one reactor chamber with the cathode electrode located at the top through which an air flow can be passed. The anode and the cathode chamber are separated by a PEM membrane. The long distance between the anode and cathode increases the internal resistance therefore; the performance of an upflow MFC design was lower than the cylindrical MFC design. Due to the cheap and large surface area of the anode, an air supply must be injected into the cathode, hence costing more energy.[65] K Rabaey, *et al.,* designed a tubular MFC reactor using an inner granular packed bed graphite anode and a woven graphite mat served as the outer cathode. In this system the cathode was wrapped around the anode and was separated by a cation exchange membrane. Although there is a need to replenish the used up $K_3Fe(CN)_6$, in the long run however this design was works with high performance due to low internal resistance.[148]

Bruce Logan's group[52,58,141,147] developed many different configurations (*batch and continuous*) of MFC reactors, as shown in (Figure 1.4 on the following page). One of the easy reactors to construct and assemble is an H-type design. Two chambers are separated with a PEM membrane. H-type systems present some difficulties in optimizing performance, due to large electrode separation, large dead volume in the head space, large reactor volume compared to the small dimension of the electrode and small membrane areas, and the large amount of trapped bacterium in the narrow membrane joints.[149]

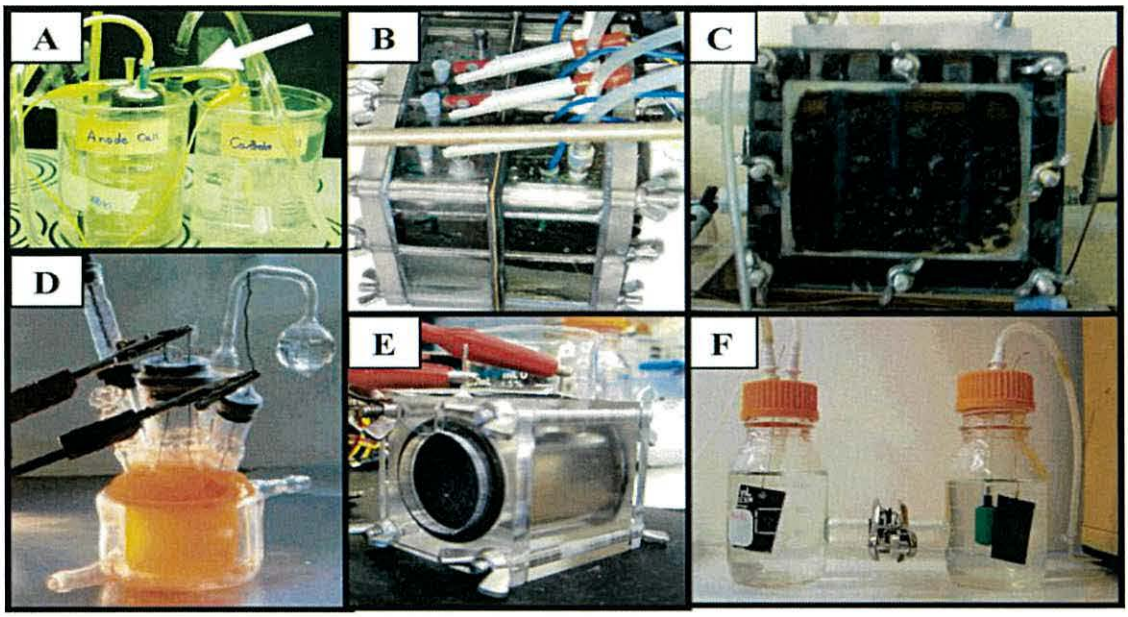

Figure 1. 4 - Types of MFC configurations for batch mode application,[140] (A) Salt bridge two chamber MFC;[150] (B) Four batch mode MFCs configuration where the compartments are separated by membrane; [52]C) same as B but with a continuous flow-through anode;[151] (D) photoheterotrophic type MFC;[58] (E) single-chamber air-cathode MFC;[141](F) Two-chamber MFC.[152]

In essence the MFC design has very significantly lowered the internal resistance, whilst increasing the power output, performance and coulombic efficiency; however, subsequent MFC design with high performance and low cost is still desired. Until now, due to heterogeneity in function and mode of operation, there is no consensus on the best MFC design. Whereas the power output performance is affected by the MFC design, other factors such as electrode materials, mediums, separation membrane and bacteria species, influence the MFC performance.

Microbial fuel cell configuration and designs

There are many types of MFC reactors but they all share the same working principles. Various configurations have been designed using different materials. They are worked under different conditions to improve the performance, power generation and reduce the overall cost.

1-Two chamber configurations: - This is the most generally used design consisting of two chambers with the anode and cathode compartments separated by a proton exchange membrane, ion exchange membrane and salt bridge. Two chamber MFCs are generally run in a fed-batch mode. This design is used in basic research and the literature suggests that the power output from these systems is low due to their complex design, high internal resistance and electrode based losses.[60,153]

2- Single chamber configurations: - This configuration contains only one chamber that has both the anode and the cathode electrode. One of the significant advantages of single chambered MFCs is improved power generation along with simple structures, cost savings and more practical than two chamber MFC.[77,141] However, in a system lacking a proton exchange membrane configuration, bacterial contamination and back diffusion of oxygen from cathode to anode without PEM are the major drawbacks.[154]

3- Up-flow configurations: - An up-flow construction generally consists of a cylindrical cathode sitting on the top and the anode on the bottom partitioned by glass wool and glass bead layers of an MFC operating in continuous flow mode.[155]

4-Stacked configurations: - A stacked MFC consists of several single cells of MFCs connected in series or in parallel. Stacked MFCs raise the voltage and currents produced in MFCs. The parallel connection can produce more power than a series connection when worked at the same volumetric flow rate. The parallel connection stack has a higher short circuit current compared to a series connection stack.[156]

1.6 Microbiological fundamentals of microbial fuel cells

Cell Wall

Almost all bacteria cell membranes can be classified as Gram-positive or Gram-negative cell walls. The arrangement of the surface layers of the bacterial cell are examined in the scanning electron microscopy of thin sections.

Gram-positive bacteria

The cell wall of gram-positive bacteria consists of a membrane and many layers of peptidoglycan. Also, in addition, gram-positive bacteria cell walls contain teichoic acids, which consists principally of an alcohol and phosphate. The cell wall of gram-positive bacteria is significantly thicker when compared to gram-negative cell walls.[157,158]

Gram-negative bacteria

Gram-negative bacteria have been identified to be made up of a three layer covering: (i) the cytoplasmic membrane (CM) or inner membrane, (ii) the peptidoglycan layer which is exterior to the CM, and (iii) the lipopolysaccharide-rich outer membrane (OM). Lipids and proteins are the major constituents of the double layer structure of

CM; with its properties comparable to that of other defined biological membranes. Some of the significant cellular roles carried out by CM are mechanical protection, passive and active transport, electron transport, oxidative phosphorylation, protein export, biosynthesis of phospholipids, peptidoglycan and proteins, and a number of other known enzymatic functions. The OM is a distinctive characteristic of gram-negative bacteria with a disproportionate double layer that consists of lipid, protein, and lipopolysaccharide; it provides a partial permeability barrier, contains receptors, serves as an attachment for outside structures, is partly involved in protein transfer and contains lesser enzymes and proteins as compared to CM.[159,160]

Electron transport out of the bacteria

A series of membrane-associated electron carriers compose an electron transport system within the bacteria, such as from NADH [the reduced form of nicotinamide adenine dinucleotide (NAD)] to flavoprotein and from quinine to cytochrome.[161] The electron carriers are bound to the proteins of membrane, and the order of electron transfer is based on the reduction potentials, from lower to higher, with higher reduction potential required to release the electrons to the outside environment.

Proton transport out of bacteria

In the internal transport process, protons are separated from electrons, like, removal of hydrogen from NADH (*oxidation*), and are separated into protons and electrons. Protons are moved across an internal membrane which creates a proton gradient and difference in potential across the cell membrane. The protons flow back into the cell to generate adenosine triphosphate (ATP) from ADP through ATPasc.[161]

Mediators

Routinely, electron shuttles or electrochemical mediators were added to MFCs resulting in electron transfer by microorganisms to the anode. The development of effective electrochemical mediators is clearly significant for improving the performance of MFC. To facilitate electron shuttling from the cell to the electrode a variety of chemicals have been used.[140]Mediators are typically redox molecules with a low molecular weight e.g. *neutral red*,[40] mixed mediator systems (*ferric chelate compounds and thionine*),[162] and others, and quinones that can form reversible redox couples that are stable in both oxidised and reduced forms, the rate of the electron

transfer is accelerated by this cyclic process, and this raises the power output.[163] There are two redox mechanisms have been :(a) electron shuttle from outer cell membrane cytochrome, (b) shuttling *via* cytoplasmatic redox couples (Figure 1.5).[164]

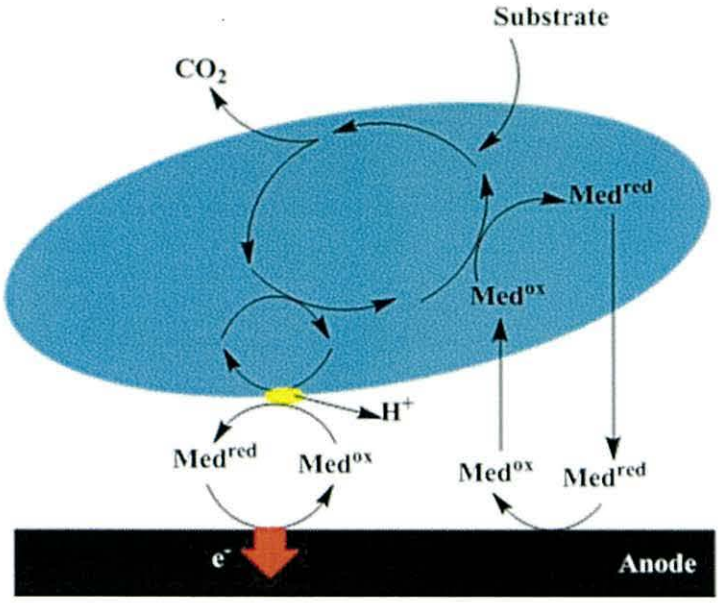

Figure 1. 5 - How redox mediators works.[164]

The disadvantage of reversible redox electron-mediator on performance of the MFC is usually a result in environmental contamination and low cost-effectiveness. These limitations may be overcome by fast and cost effective immobilizing electron-mediator molecules (e.g. conductive polymers, neutral red, and methylene blue) coated anode electrode surface.[165,166]

Bacterial anode biofilms

A century ago, production of electrical current from electrodes placed in microorganisms' cultures was noticed.[29] Microorganisms can attach and grow to solid surfaces, embed themselves in protective matrix [Extracellular Polymeric Substance (EPS)] and form layers which are called biofilms. Biofilms consist of active, inert biomass and EPS. Extracellular Polymeric Substance is mostly composed of polysaccharides, proteins, lipids and nucleic acids.[167,168,169,170,171,172] Attachment of microbials on a solid surface is crucial in the creation of biofilms, transporting of the microorganisms in porous media, and in situ bioremediation. Deposition of bacteria on surfaces is governed by a number of biophysical and biochemical factors, like type of the bacteria cell, motility, hydrophobic interactions, the outer membrane proteins, and lipopolysaccharides.[173,174,175]

One of the significant roles of biofilm is the electrochemically active process, and shows marked effect on bioelectricity production.[176,177] As the density of the cells is high in the matrix, cell to cell contact is increased in the biofilm which stimulates the electron transfer mechanism.[178] Anode associated biofilm of MFCs is pivotal for the efficient electron transfer in an MFC.[179,180] Also extracellular polymeric substances immobilise the bacterial cells play important roles in extracellular electron transfer reactions.[181] Micro-sized MFC design has very significantly improved biofilm formation and power generation.[182]

In summary, bacteria colonised anode biofilm of an MFC has three vital parameters: the electron donor (*carbon source*), microorganisms oxidising the electron donor, and electrons transferred to the anode surface. These parameters are commonly expressed as the electron donor concentration, colonisation of microorganisms on the anode, and production of electricity respectively.

The majority of the electrochemically active bacteria reported in the literature relate to systems operated at neutral pH, however, a new approach to the anode biofilm *Acidiphilium SJH* bacteria will be adopted for this work due to the *Acidiphilium* low pH requirements which are ideal for iron electron redox chemistry.[183]

Acidophilic heterotroph

An acidophilic heterotroph (SJH) bacterium is comprised of gram-negative, rod-shaped bacteria; they have also been reported to be obligate aerobes and useful model organism for the study of extremophilic bacteria in bioremediation applications. The environments in which they are characteristically found are invariably rich in ferrous and ferric iron. The *Acidiphilium sp* SJH bacteria used in this study was isolated from a subterranean, high acidic environment (pH 2.3), metal-rich stream located within a derelict pyrite mine (*Cae Coch*) in North Wales.[183]

A microbiological study on dissimilatory iron reduction in extremely acidic environments is one of the most abundant electron sinks for the oxidation of organic matter.[184] Recent studies have reported dissimilatory iron reduction by neutrophilic bacteria of the family *Geobacteraceae, Shewanella* spp., and hyperthermophilic microorganisms.[59] This ability has also been identified in a significant number of

Acidiphilium and *Acidiphilium*-related bacteria that carry out a dissimilatory reduction of ferric iron under anoxic as well as microaerophilic conditions.[48]

In acidic media, ferric ion tends to be more available due to its stability, which has relatively high redox potential Fe^{3+}/Fe^{2+} 770 mV, at nearly pH of 2, while the same couples have less potential at neutral pH at -88 to 430 mV. Based on the thermodynamic view, ferric ion is considered as an attractive electron acceptor to molecular oxygen in highly acidic media.[185]

1.7 Aim and objectives

Aim

The aim of this PhD thesis is to study the efficiency of a microbial fuel cell capable of utilising iron due to its ideal redox behaviours.

Objectives

The program of this research is divided into five main parts:

1. Using acidophilic microorganisms (*Acidiphilium sp* SJH) as iron reducing bacteria in the anodic chamber of the MFC in order to enhance the production of electricity.
2. Developing the scale up potential of MFC by studying various construction configurations of MFC.
3. Improve the cathode material and compartment in order to increase the catalytic activity of the cathode reaction and cost effectiveness.
4. To study the influence of anodic biofilm growth from *Acidiphilium sp* SJH bacteria at low pH.
5. Utilise an air-cathode single chamber MFC on bioelectricity production to remove the need to supply oxygen from outside the cell.

1.8 References

1. Klass, D. L. A critical assessment of renewable energy usage in the USA, *Energy Policy* **2003**, *31*, 353 - 367.
2. World population balance, population and energy consumption, USA, **2013**.
3. Lewis, J. I. Climate change and security: examining China's challenges in a warming world, *Int. Affairs, Int. Affairs* **2009**, *85*, 1195 - 1213.
4. McCarty, P. L.; Bae, J.; Kim, J. Domestic Wastewater Treatment as a Net Energy Producer-Can this be Achieved. *Environ. Sci. Technol.* **2011**, *45*, 7100 - 7106.
5. Lorenzo, M. D.; Scott, K.; Curtis, T. P.; Katuri, K. P.; and Head, I. M. Continuous Feed Microbial Fuel Cell Using An Air Cathode and A Disc Anode Stack for Wastewater Treatment, *Energy Fuels* **2009**, *23*, 5707 - 5716.
6. Sustainable Infrastructure for Water & Wastewater, U.S. Environmental Protection Agency (EPA), 2012.
7. Ziemiński, K.; and Frąc, M. Methane fermentation process as anaerobic digestion of biomass: Transformations, stages and microorganisms. *Afr. J. Biotechnol.* **2012**, *11*, 4127 - 4139.
8. Ueno, Y.; Fukui, H.; and Goto, M. Operation of a Two-Stage Fermentation Process Producing Hydrogen and Methane from Organic Waste. *Environ. Sci. Technol.* **2007**, *41*, 1413 - 1419.
9. Kim, I. S.; Chae, K. J.; Choi, M. J; and Verstraete, W. Microbial Fuel Cells: Recent Advances, Bacterial Communities and Application Beyond Electricity Generation. *Environ. Eng. Res.* **2008**, *13*, 51 - 65.
10. Oh, S. T.; Kim, J. R.; Premier, G. C.; Lee, T. H. Kim, C. Sloan, W. T. Sustainable wastewater treatment: How might microbial fuel cells contribute. *Biotechnol Adv.* **2010**, *28*, 871 - 881.
11. Barua, P. K.; Deka, D. Electricity Generation from Biowaste Based Microbial Fuel Cells. *Int. J. Energy Information. Commun.* **2010**, *1*, 77 - 92.
12. Li, Z.; Zhang, X. Zeng, Y.; and L. Lei, Electricity production by an overflow-type wetted-wall microbial fuel cell. *Bioresour. Technol.* **2009**, *100*, 2551 - 2555.
13. Cheng, K. Y.; Ho, G.; and Ruwisch, R. C. Energy-efficient treatment of organic wastewater streams using a rotatable bioelectrochemical contactor (RBEC). *Bioresour Technol.* **2012**, *126*, 431 - 436.
14. Zhang, Y.; and Angelidaki, I. Self-stacked submersible microbial fuel cell (SSMFC) for improved remote power generation from lake sediments. *Biosens. Bioelectron.* **2012**, *35*, 265 - 270.
15. Zhang, G.; Zhao, Q.; Jiao, Y. Wang, K.; Lee, D. J.; and Ren, N. Biocathode microbial fuel cell for efficient electricity recovery from dairy manure. *Biosens. Bioelectron.* **2012**, *31*, 537 - 543.
16. Cheng, S.; Logan, B. E. Increasing power generation for scaling up single-chamber air cathode microbial fuel cells. *Bioresour. Technol.* **2011**, *102*, 4468 - 4473.
17. Wang, Y.; Liu, L.; Zhang, D.; Xu, S.; Li, M. A New Strategy for Immobilization of Electroactive Species on the Surface of Solid Electrode, *Electrocatal.* **2010**, *1*, 230 - 234.

18. Li, X.; Hu, B. X.; Suib, S.; Lei, Y.; Li, B. K. Manganese dioxide as a new cathode catalyst in microbial fuel cells. *J. Power Sources* **2010**, *195*, 2586 - 2591.
19. Zhang, F.; Xia, X.; Luo, Y.; Sun, D.; Call, D. F; Logan, B. E. Improving startup performance with carbon mesh anodes in separator electrode assembly microbial fuel cells. *Bioresour. Technol.* **2013**, *133*, 74 - 81.
20. Larminie, J.; Dicks, A. *Fuel Cell Systems Explained*, Second Edition, John Wiley and Sons Ltd. England, 2003.
21. Singhal, S. C. Advances in solid oxide fuel cell technology. *Solid State Ionics* **2000**, *135*, 305 - 313.
22. Gulzow, E. Alkaline fuel cells: A critical view. *J. Power Sources* **1996**, *61*, 99 - 104.
23. Sammes, N.; Bove, R.; Stahl, K. Phosphoric acid fuel cells: Fundamentals and applications. *Curr. Opin. Solid State Mater. Sci.* **2004**, *8*, 372 - 378.
24. Silveira, J. L.; Leal, E. M.; Jr, L. F. R. Analysis of a molten carbonate fuel cell: cogeneration to produce electricity and cold water. *Energy*, **2001**, *26*, 891 - 904.
25. Dicks, A. L. Molten carbonate fuel cells. *Curr. Opin. Solid State Mater. Sci.* **2004**, *8*, 379 - 383.
26. Vishnyakov, V. M. Proton exchange membrane fuel cells. *Vacuum* **2006**, *80*, 1053 - 1065.
27. Galvani, L. Electricitatis in Motu Musculari Commentaries, *Bon. Sci. Art. Inst. Acad. Comm.*, **1791**, *7*, 363 - 418.
28. Grove, W. R. Series and the Combination of Gases by Platinum. *Philos. Mag. J. Sci.* **1839**, *14*, 127 - 130.
29. Potter, M. C. Electrical effects accompanying the decomposition of organic compounds. *Roy. Soc. Lond. Ser. B.* **1911**, *84*, 260 - 276.
30. Cohen, B. The bacterial culture as an electrical half-cell, *J. Bacteriol.* **1931**, *21*, 18 - 19.
31. Canfield, J. H.; Goldner, B. H; and Lutwack, R. *NASA Technical Report*, Magna Corporation, Anaheim, CA. **1963**, P: 63.
32. Yao, S. J.; Appleby, A. J.; Geise, A.; Cash, H. R.; and Wolfson, S. K. Anodic oxidation of carbohydrates and their derivatives in neutral saline solution. *Nat.* **1969**, *224*, 921 - 922.
33. Rao, J. R.; Richter, G. J.; Sturm, F. V.; and Weidlich, E. The Performance of Glucose Electrodes, and the Characteristics of Different .Biofuel Cell Constructions. *Bioelectrochem. Bioenerg.* **1976**, *3*, 139 - 150.
34. Roller, S. D.; Bennetto, H. P.; Delaney, G. M.; Mason, J. R.; Stirling, J. L.; and Thurston, C. F. Electron-transfer coupling in microbial fuel Cells: 1.Comparison of redox-mediator reduction rates and respiratory rates of bacteria. *J. Chem. Technol. Biotechnol.***1984**, *34*, 3 - 12.
35. Habermann, W.; and Pommer, E. Biological fuel cells with sulphide storage capacity. *Appl. Microbiol. Biotechnol.* **1991**, *35*, 128 - 133.
36. Kim, N.; Choi, Y.; Jung, S.; Kim, S. Effect of initial carbon sources on the performance of microbial fuel cells containing *Proteus vulgaris*. *Biotechnol. Bioeng.* **2000**, *70*, 109 - 114.
37. Nevin, K. P.; Richter, H.; Covalla, S. F.; Johnson, J. P.; Woodard, T. L.; Orloff, A. L.; Jia, H. ; Zhang, M.; Lovley, D. R. Power output and columbic efficiencies from biofilms of *Geobacter sulfurreducens* comparable to mixed community microbial fuel cells. *Environ. Microbiol.* **2008**, *10*, 2505 - 2514.

38. Luo, H.; Liu, G.; Zhang, R.; Jin, S. Phenol degradation in microbial fuel cells. *Chem. Eng. J.* **2009**, *147*, 259 - 264.
39. Luo, Y.; Liu, G.; Zhang, R. Zhang, C. Power generation from furfural using the microbial fuel cell. *J. Power Sources* **2010**, *195*, 190 - 194.
40. Park, D. H.; and, Zeikus, J. G. Utilization of Electrically Reduced Neutral Red by Actinobacillus succinogenes: Physiological Function of Neutral Red in Membrane-Driven Fumarate Reduction and Energy Conservation. *J. bacteriol.* **1999**, *181*, 2403 - 2410.
41. McKinlay, J. B.; and Zeikus, J. G. Extracellular Iron Reduction Is Mediated in Part by Neutral Red and Hydrogenase in Escherichia coli. *Appl. Environ. Microbiol.* **2004**, *70*, 3467 - 3474.
42. Choi, Y.; Kim, N.; Kim, S.; and Jung, S. Dynamic Behaviours of Redox Mediators within the Hydrophobic Layers as an Important Factor for Effective Microbial Fuel Cell Operation. *Bull. Korean chem. Soc.* **2003**, *24*, 437 - 440.
43. Rahimnejad, M.; Najafpour, G. D. Ghoreyshi, A. A.; Talebnia, F.; Premier, G. Bakeri, G, C.; Kim, J. R.; and Oh, S. E. Thionine Increases Electricity Generation from Microbial Fuel Cell Using *Saccharomyces cerevisiae* and Exoelectrogenic Mixed Culture. *J. Microbiol.* **2012**, *50*, 575 - 580.
44. Kim, H. J.; Park, H. S.; Hyun, M. S.; Chang, I. S.; Kim, M.; Kim, B. H. A mediator-less microbial fuel cell using a metal reducing bacterium, *Shewanella putrefaciens. Enzyme Microb. Technol.* **2002**, *30*, *145* - 152.
45. Bond, D. R.; Lovley, D. R. Electricity production by Geobacter sulfurreducens Attached to Electrodes, *Appl. Environ. Microbiol.* **2003**, *69*, 1548 - 1555.
46. Zuo, Y.; Xing, D.; Regan, J. M.; and B. E. Logan, Isolation of the exoelectrogenic bacterium *Ochrobactrum anthropi* YZ-1 by using a U-tube microbial fuel cell. *Appl. Environ. Microbiol.* **2008**, *74*, 3130 - 3137.
47. Wrighton, K. C.; Thrash, J. C.; Melnyk, R. A.; Bigi, J. P.; Byrne-Bailey, K. G.; Remis, J. P.; Schichnes, D.; Auer, M.; Chang, C. J.; and Coates, J. D. Evidence for Direct Electron Transfer by a Gram-Positive Bacterium Isolated from a Microbial Fuel Cell. *Appl. Environ. Microbiol.* **2011**, 77, 7633 - 7639.
48. Malki, M.; De Lacey, A. L.; Rodríguez, N.; Amils, R.; and Fernandez, V. M. Preferential use of an anode as an electron acceptor by an acidophilic bacterium in the presence of oxygen. *Appl. Environ. Microbiol.* **2008**, *74*, 4472 - 4476.
49. Summers, Z. M.; Fogarty, H. E.; Leang, C.; Franks, A. E.; Malvankar, N. S.; and Lovley, D. R. Direct exchange of electrons within aggregates of an evolved Syntrophic coculture of anaerobic bacteria, *Sci.* **2010**, *330*, 1413 - 1415.
50. Rollefson, J. B.; Stephen, C. S.; Tien, M.; and Bond, D. R. Identification of an Extracellular Polysaccharide Network Essential for Cytochrome Anchoring and Biofilm Formation in *Geobacter sulfurreducens. J. bacteriol.* **2011**, *193*, 1023 - 1033.
51. Okamoto, A.; Hashimoto, K.; Nakamura, R. Long-range electron conduction of Shewanella biofilms mediated by outer membrane C-type cytochromes. *Bioelectrochem.* **2012**, *85*, 61- 65.
52. Rabaey, K.; Boon, N.; Hofte, M.; Verstraet, W. Microbial Phenazine production enhances electron transfer in biofuel cells. *Environ. Sci. Technol.* **2005**, *39*, 3401 - 3408.
53. Rabaey, K.; Boon, N.; Siciliano, S. D.; Verhaege, M.; Verstraete, W. Biofuel Cells Select for Microbial Consortia That Self-Mediate Electron Transfer. *Appl. Environ. Microbiol.* **2004**, *70*, 5373 - 5382.

54. Coursolle, D.; Baron, D. B.; Bond, D. R.; Gralnick, J. A. The Mtr Respiratory Pathway Is Essential for Reducing Flavins and Electrodes in *Shewanella oneidensis*. *J Bacteriol.* **2010**, *192*, 467 - 474.
55. Reguera, G.; Nevin, K. P; Nicoll, J. S.; Covalla, S. F.; Woodard, T. L.; and Lovley, D. R. Biofilm and nanowire production leads to increased current in *Geobacter sulfurreducens* fuel cells. *Appl. Environ. Microbiol.* **2006**, *72*, 7345 - 7348.
56. Reguera, G.; Pollina, R. B.; Nicoll, J. S.; and Lovley, D. R. Possible Nonconductive Role of *Geobacter sulfurreducens* Pilus Nanowires in Biofilm Formation. *J. Bacterial.* **2007**, *189*, 2125 - 2127.
57. Malvankar, N. S.; and Lovley, D. R. Microbial nanowires: A new paradigm for biological electron transfer and bioelectronics. *Chem Sus Chem.* **2012**, *5*, 1039 - 1046.
58. Rosenbaum, M.; Schroder, U.; and Scholz, F. In Situ Electrooxidation of Photobiological Hydrogen in a Photobioelectrochemical Fuel Cell Based on Rhodobacter sphaeroides. *Environ. Sci. Technol.* **2005**, *39*, 6328 - 6333.
59. .Lovley, D. R; Holmes, D. E. Nevin, K. P. Dissimilatory Fe^{+3} and Mn^{+4} reduction. *Adv. Microb. Physiol.* **2004**, *49*, 219 - 286.
60. Du, Z.; Li, H.; Gu, T. A state of the art review on microbial fuel cells: A promising technology for wastewater treatment and bioenergy. *Biotechnol. Advan.* **2007**, *25*, 464 - 482.
61. Logan, B. E.; Hamelers, B.; Rozendal, R.; Schroder, U. Keller, J.; Freguia, S.; Aelterman, P. Verstraete, W.; and Rabaey, K. Microbial Fuel Cell: Methodology and Technology. *Environ. Sci. Technol.* **2006**, *40*, 5181 - 5192.
62. Lovley, D. R. Microbial fuel cells: novel microbial physiologies and engineering approaches. *Curr. Opin. Biotechnol.* **2006**, *17*, 327 - 332.
63. Rabaey, K.; and Verstraete, W. Microbial fuel cells: novel biotechnology for energy generation. *Trends Biotechnol.* **2005**, *23*, 291 - 298.
64. Ahn, Y.; and Logan, B. E. Altering Anode Thickness To Improve Power Production in Microbial Fuel Cells with Different Electrode Distances. *Energy Fuels* **2013**, *27*, 271 - 276.
65. He, Z.; Minteer, S. D.; and Angenent, L. Electricity Generation from Artificial Wastewater Using an Upflow Microbial Fuel Cell. *Environ. Sci. Technol.* **2005**, *39*, 5262 - 5267.
66. Logan, B. E. Scaling up microbial fuel cells and other bioelectrochemical systems. *Appl. Microbiol. Biotechnol.* **2010**, *85*, 1665 - 1671.
67. Zhou, M.; Chi, M.; Luo, J.; He, H.; Jin, T. An overview of electrode materials in microbial fuel cells. *J. Power Sources* **2011**, *196*, 4427 - 4435.
68. Wang, X.; Cheng, S.; Feng, Y.; Merrill, M. D.; Saito, T.; and Logan, B .E. Use of Carbon Mesh Anodes and the Effect of Different Pre-treatment Methods on Power Production in Microbial Fuel Cells. *Environ. Sci. Technol.* **2009**, *43*, 6870 - 6874.
69. Cheng, S.; Logan, B. E. Ammonia treatment of carbon cloth anodes to enhance power generation of microbial fuel cells. *Electrochem. Commun.* **2007**, *9*, 492 - 496.
70. Logan, B. E.; Cheng, S.; Watson, V.; Estadt, G. Graphite fiber brush anodes for increased power production in air-cathode microbial fuel cells. *Environ. Sci. Technol.* **2007**, *41*, 3341 - 3346.

71. Nielsen, M.; Reimers, C.; and Stecher, H. Enhanced Power from Chambered Benthic Microbial Fuel Cells. *Environ. Sci. Technol.* **2007**, *41*, 7895 - 7900.
72. Hays, S.; Zhang, F.; Logan, B. E. Performance of two different types of anodes in membrane electrode assembly microbial fuel cells for power generation from domestic wastewater. *J. Power Sources* **2011**, *196*, 8293 - 8300.
73. Wei, J.; Liang, P.; Huang, X. Recent progress in electrodes for microbial fuel cells. *Bioresour. Technol.* **2011**, *102*, 9335 - 9344.
74. Feng, Y.; Yang, Q.; Wang, X.; Logan, B. E. Treatment of carbon fiber brush anodes for improving power generation in air-cathode microbial fuel cells. *J. Power Sources* **2010**, *195*, 1841-1844.
75. Lowy, D. A.; Tender, L. M. Harvesting energy from the marine sediment-water interface III. Kinetic activity of quinone- and antimony-based anode materials. *J. Power Sources* **2008**, *185*, 70 - 75.
76. Kim, J. R.; Min, B.; and Logan, B. E. Evaluation of procedures to acclimate a microbial fuel cell for electricity production. *Appl. Microbiol. Biotechnol.* **2005**, *68*, 23 -30.
77. Park, D. H.; Zeikus, J. G. Improved fuel cell and electrode designs for producing electricity from microbial degradation. *Biotchnol. Bioeng.* **2003**, *81*, 348 - 355.
78. Xie, X.; Hu, L.; Pasta, M.; Wells, G. F.; Kong, D.; Criddle, C. S.; and Cui, Y. Three-Dimensional Carbon Nanotube-Textile Anode for High-Performance Microbial Fuel Cells. *Nano Lett.* **2011**, *11*, 291 - 296.
79. Jiang, D. Q.; Li, B. K. Novel electrode materials to enhance the bacterial adhesion and increase the power generation in microbial fuel cells (MFCs). *Water Sci. Technol.* **2009**, *59*, 557 - 563.
80. Lowy, D. A.; Tender, L. M.; Zeikus, J. G.; J. G., Park, D. H. and D. R. Lovley, Harvesting energy from the marine sediment-water interface II Kinetic activity of anode materials. *Biosen. Bioelectron.* **2006**, *21*, 2058 - 2063.
81. Wang, K.; Liu, Y.; Chen, S. Improved microbial electrocatalysis with neutral red immobilized electrode. *J. Power Sources* **2011**, *196*, 164 - 168.
82. Chen, G. W.; Choi, S. J.; Lee, T. H.; Lee, G. Y.; Cha, J. H.; and Kim, C. W. Application of biocathode in microbial fuel cells: cell performance and microbial community. *Appl. Microbiol. Biotechnol.* **2008**, *79*, 379 - 388.
83. Yano, H.; Kataoka, M.; Yamashita, H.; Uchida, H.; and Watanabe, M. Oxygen Reduction Activity of Carbon-Supported Pt-M (M) V, Ni, Cr, Co, and Fe) Alloys Prepared by Nanocapsule Method. *Langmuir* **2007**, *23*, 6438 - 6445.
84. Stamenkovic, V. R.; Fowler, B.; Mun, B. S.; Wang, G.; Ross, P. N.; Lucas, C. A.; Markovic, N.M. Improved Oxygen Reduction Activity on Pt3Ni(111) via Increased Surface Site Availability. Sci. **2007**, *315*, 493 - 497.
85. Yang, J. H.; Zhou, W. J.; Cheng, C. H.; Lee J. Y.; and Liu, Z. L. Pt- decorated PdFe nanoparticles as methanol-tolerant oxygen reduction electrocatalyst, *ACS. Appl. Mater. Interfaces* **2010**, *2*, 119 - 126.
86. Stephens, I. E. L.; Bondarenko, A. S.; Grønbjerg, U.; Rossmeisl, J.; and Chorkendorff, I. Understanding the electrocatalysis of oxygen reduction on platinum and its alloys. *Energy Environ. Sci.* **2012**, *5*, 6744 - 6762.
87 Jayasayee, K.; Veen, J. A. R. V.; Manivasagam, T. G.; Celebi, S.; Hensen, E. J. M.; de Bruijn, F. A. Oxygen reduction reaction (ORR) activity and durability of carbon supported PtM (Co, Ni, Cu) alloys: Influence of particle size and non-noble metals. *Appl. Catal. B*: *Environ.* **2012**, *111 - 112*, 515 - 526.

88. You, S.; Zhao, Q.; Zhang, J.; Jiang, J.; Wan, C.; Du, M.; and Zhao, S. A. graphite-granule membrane-less tubular air-cathode microbial fuel cell for power generation under continuously operational conditions. *J. Power Sources* **2007**, *173*, 172 - 177.
89. Gil, G. C.; Ghang, I. S.; Kim, B. H.; Kim, M.; Jang, J. K.; Park, H. S.; and Kim, H. J. Operational parameters affecting the performance of a mediator-less microbial fuel cell. *Biosen. Bioelectron.* **2003**, *18*, 327 - 334.
90. Renslow, R.; Donovan, C.; Shim, M.; Babauta, J.; Nannapaneni, S.; Schenk J.; and Beyenal, H. Oxygen reduction kinetics on graphite cathodes in sediment microbial fuel cellsw. *Phys. Chem. Chem. Phys.* **2011**, *13*, 21573 - 21584.
91. Zhao, F.; Harnisch, F.; Schröder, U.; Scholz, F.; Bogdanoff, P.; Herrmann, I. Challenges and Constraints of Using Oxygen Cathodes in Microbial Fuel Cells. *Environ. Sci. Technol.* **2006**, *40*, 5193 - 5199.
92. Qi, Z.; Kaufman, A. Low Pt loading high performance cathodes for PEM fuel cells. *J. Power Sources* **2003**, *113*, 37 - 43.
93. Ota, K.; Ishihara, A.; Mitsushima, S.; Lee, K.; Suzuki, Y.; Horibe, N.; Nakagawa, T.; and Kamiya, N. Improvement of Cathode Materials for Polymer Eletrolyte Fuel Cell. *J. New Mater. Electrochem. Syst.* **2005**, *8*, 25 - 35.
94. X. Yang, J. Lu, Y. Zhu, J. Shen, Z. Zhang, J. Zhang, C. Chen, C. Li, Microbial fuel cell cathode with dendrimer encapsulated Pt nanoparticles as Catalyst. *J. Power Sources* **2011**, *196*, 10611 - 10615.
95. Yan, Z.; Wang, M.; Huang, B.; Liu, R.; Zhao, J. Graphene Supported Pt-Co Alloy Nanoparticles as Cathode Catalyst for Microbial Fuel Cells. *Int. J. Electrochem. Sci.* **2013**, *8*, 149 - 158.
96. Cheng, S.; Liu, H.; and Logan, B. E. Power Densities Using Different Cathode Catalyst(Pt and CoTMPP) and Polymer Binders (Nafion and PTEF) in Single Chamber Microbial Fuel Cells. *Environ. Sci. Technol.*, **2006**, *40*, 364 - 369.
97. Hao, E.; Yu, S. Cheng, Logan, B. E.; Scott, K. Electrochemical reduction of oxygen with iron phthalocyanine in neutral media. *J. Appl. Electrochem.* **2009**, *39*, 705 - 711.
98. Yu, E.; Cheng, S.; Scott, K.; and Logan, B. E. Microbial fuel cell performance with non-Pt cathode catalysts, *J. Power Sources* **2007**, 171, 275 - 281.
99. Huang, L.; Regan, J. M.; Quan, X. Electron transfer mechanisms, new applications, and performance of biocathode microbial fuel cells. *Bioresour. Technol.* **2011**, *102*, 316 - 323.
100. Rhoads, A.; Beyenal, H.; Lewandowski, Z. Microbial fuel cell using anaerobic respiration as an anodic reaction and biomineralized manganese as a cathodic reactant. *Environ. Sci. Technol.* **2005**, *39*, 4666 - 4671.
101. Heijne, H. V.; Hamelers, M.; and Buismana, C. N. Microbial Fuel Cell Operation with Continuous Biological Ferrous Iron Oxidation of the Catholyte. *Environ. Sci. Technol.* **2007**, *41*, 4130 - 4134.
102. Mao, Y. P.; Zhang, L. H.; Li, D. M.; Shi, H. F.; Liu, Y. D.; Cai, L. K Power generation from a biocathode microbial fuel cell biocatalyzed by ferro/manganese-oxidizing bacteria. *Electrochim Acta* **2010**, *55*, 7804 - 7808.
103. Carbajosa, S.; Malki, M.; Caillard, R.; Lopez, M. F.; Palomares, F. J.; Gago, J. A M.; Rodríguez, N.; Amils, R.; Fernández, V. M.; Lacey, L. D. Electrochemical growth of Acidithiobacillus ferrooxidans on a graphite electrode. *Biosens. Bioelectron.* **2010**, *26*, 887 - 880.

104. G. Zhang, Zhao, Q.; Jiao, Y.; Wang, K.; Lee D. J.; and Ren, N. Biocathode microbial fuel cell for efficient electricity recovery from dairy manure. *Biosens. Bioelectron.* **2012**, *31*, 537 - 543.
105. Heijne, A. T.; Strik, D. P. B. T. B.; Hamelers, H. V. M.; Buisman, C. J. N. Cathode potential and mass transfer determine performance of oxygen reducing biocathodes in Microbial Fuel Cells. *Environ. Sci. Technol.* **2010**, *44*, 7151 - 7156.
106. Freguia, S.; Tsujimura, S.; Kano, K. Electron transfer pathways in microbial oxygen biocathodes. *Electrochimica Acta* **2010**, *55*, 813 - 818.
107. Sun, Y.; Wei, J.; Liang P.; and Huang, X. Microbial community analysis in biocathode microbial fuel cells packed with different materials. AMB. *Express* **2012**, *2*, 1 - 8.
108. OH, S.; Min, B.; and Logan, B. E. Cathode Performance as a Factor in Electricity Generation in Microbial Fuel Cells. Environ. *Sci. Technol.* **2004**, *38*, 4900 - 4904.
109. Logan, B. E.; Regan, J. M. Microbial fuel cells- challenges and application. *Environ. Sci. Technol.* **2006**, *40*, 5172 - 5180.
110. Wei, L.; Han, H.; Shen, J. Effects of cathodic electron acceptors and potassium ferricyanide concentrations on the performance of microbial fuel cell. *Int. j. hydrogen energy* **2012**, *37*, 12980 - 12986.
111. You, S. Zhao, Q.; Zhang, J. Jiang, J.; Zhao, S. A microbial fuel cell using permanganate as the cathodic electron acceptor. *J. Power Sources* **2006**, *162*, 1409 - 1415.
112. Wang, G.; Huang, L.; and Zhang, Y. Cathodic reduction of hexavalent chromium [Cr(VI)] coupled with electricity generation in microbial fuel cells. *Biotechnol Lett.* **2008**, *30*, 1959 - 1966.
113. Wang, Y.; Niu, C. G.; Zeng, G.M.; Hu, W. J; Huang, D.W.; Ruan, M. Microbial fuel cell using ferrous ion activated persulfate as a cathodic reactant. *Int. J. Hydrogen Energy* **2011**, *36*, 15344 - 15351.
114. Erable, B.; Duteanu, N.; Kumar, S. M. S.; Feng, Y. J.; Ghangrekar, M. M.; Scott, K. Nitric acid activation of graphite granules to increase the performance of the non-catalyzed oxygen reduction reaction (ORR) for MFC applications. *Electrochem. Commun.* **2009**, *11*, 1547 - 1549.
115. Q .Deng, Li. X, J. E. Zuo, B. E. Logan, A. Ling, Power generation using an activated carbon fiber felt (ACFF) cathode in an upflow microbial fuel cell. *J. Power Sources* **2010**, *195*, 1130 - 1135.
116. Duteanu, N.; Erable, B.; Kumar, S. M. S.; Ghangrekar, M. M.; Scott, K. Effect of chemically modified Vulcan XC-72R on the performance of air-breathing cathode in a single-chamber microbial fuel cell. *Bioresour. Technol.* **2010**, *101*, 5250 - 5255.
117. Zuo, Y.; Cheng, S. A.; Logan, B. E. Ion exchange membrane cathodes for scalable microbial fuel cells. *Environ. Sci. Technol.* **2008**, *42*, 6967 - 6972.
118. Morris, J. M.; Jin, S.; Wang, J.; Zhu, C.; and Urynowicz, M. A. Lead dioxide as an alternative catalyst to platinum in microbial fuel cells. *Electrochem. Commun.* **2007**, *9*, 1730 - 1734.
119. Yuan, Y.; Zhou, S.; and Zhuang, L. Polypyrrole/carbon black composite as a novel oxygen reduction catalyst for microbial fuel cells. J. *Power Sources* **2010**, *195*, 3490 - 3493.

120. Roche, I.; Katuri, K.; and Scott, K. A microbial fuel cell using manganese oxide oxygen reduction catalysts. *J. Appl. Electrochem.* **2010**, *40*, 13 - 21.
121. Ahmed, J.; Yuan, Y.; Zhou, L. Kim, S. Carbon supported cobalt oxide nanoparticles–iron phthalocyanine as alternative cathode catalyst for oxygen reduction in microbial fuel cells. *J. Power Sources* **2012**, *208*, 170 - 175.
122. Kim, M.; Park, J. N.; Kim, H.; Song, S.; Lee, W. H. The preparation of Pt/C catalysts using various carbon materials for the cathode of PEMFC. *J. Power Sources* **2006**, *163*, 93 - 97.
123. Charreteur, F.; Jaouen, F.; Ruggeri, S.; Dodelet, J. Fe/N/C non-precious catalysts for PEM fuel cells: Influence of the structural parameters of pristine commercial carbon blacks on their activity for oxygen reduction. *Electrochimica Acta* **2008**, *53*, 2925 - 2938.
124. Tashima, D.; Yoshitama, H.; Otsubo, M.; Maeno, S.; Nagasawa, Y. Evaluation of electric double layer capacitor using Ketjen black as conductive nanofiller. *Electrochimica Acta* **2011**, *56*, 8941 - 8946.
125. Product Data Sheet, Akzo Nobel Polymer Chemicals B.V, **2011**.
126. Choi, J. Hsu, R. S.; and Chen, Z. Evaluation of electric double layer capacitor using Ketjen black as conductive nanofiller. *J. Phys. Chem. C,* **2010**, *114,* 8048 - 8053.
127. Wang, X.; Zhang, H.; Zhang, J.; Xu, H.; Tian, Z.; Chen, J.; Zhong, H.; Liang, Y.; Yi, B. Micro-porous layer with composite carbon black for PEM fuel cells. *Electrochimica Acta* **2006**, *51*, 4909 - 4915.
128. Subramanian, N.; Kumaraguru, S.; Mercado, H. C.; Kim, H.; Popov, B.; Black, T.; Chen, D. Studies on Co-based catalysts supported on modified carbon substrates for PEMFC cathodes. *J. Power Sources* **2006**, *157*, 56 - 63.
129. freund, A.; Lang, J. Lehmann, T.; Starz, K. Improved Pt Alloy catalysts for fuel cells. *Catal. Today* **1996**, *27*, 279 - 283.
130. Wang, X.; Li, W.; Chen, Z.; Waje, M.; Yan, Y. Durability investigation of carbon nanotube as catalyst support for proton exchange membrane fuel cell. *J. Power Sources* **2006**, *158*, 154 - 159.
131. Guo, D.; Li, H. High dispersion and electrocatalytic properties of Pt nanoparticles on SWNT bundles, *J. Electroanal. Chem.*, 2004, **573**, 197 - 202.
132. Yan, Z.; Wang, M.; Huang, B.; Zhao, J.; Liu, R. Carboxyl Multi-Wall Carbon Nanotubes Supported Pt-Ni Alloy Nanoparticles as Cathode Catalyst for Microbial Fuel Cells. *Int. J. Electrochem. Sci.* **2012**, *7*, 10825 - 10834.
133. Wen, Z.; Liu, J.; Li, J. Core/Shell Pt/C Nanoparticles Embedded in Mesoporous Carbon as a Methanol-Tolerant Cathode Catalyst in Direct Methanol Fuel Cells. *Adv. Mater.* **2008**, *20*, 743 - 747.
134. Zheng, J.; Zhang, X.; Li, P.; Zhou, X. Yuan, W. Microstructure effect of carbon nanofiber on electrocatalytic oxygen reduction reaction. *Catal. Today* **2008**, *131*, 270 - 277.
135. Qiu, Y.; Yu, J.; Wu, W.; Yin, J.; Bai, X. Fe–N/C nanofiber electrocatalysts with improved activity and stability for oxygen reduction in alkaline and acid solutions. *J. Solid State Electrochem.* **2013**, *17*, 565 - 573.
136. Ganesh, P.; Kent, P. R. C. and Mochalin, V.; Formation, characterization, and dynamics of onion-like carbon structures for electrical energy storage from nanodiamonds using reactive force fields. *J. Appl .Phys.* **2011**, *110*, 1 - 8.

137. Zhou, Z.; Gao, X. Yan, J.; Song, D.; Morinaga, M. A first-principles study of lithium absorption in boronor nitrogen-doped single-walled carbon nanotubes. *Carbon* **2004**, *42*, 2677 - 2682.
138. Li, W.; Sheng, G.; Liu, X.; and Yu, H. Recent advances in the separators for microbial fuel cells. *Bioresource. Technol.* **2011**, *102*, 244 - 252.
139. Lee, J. S.; Quan, N. D.; Hwang, J. M.; Lee, S. D. Kim, H.; and Lee, H. Polymer Electrolyte Membranes for Fuel Cells. *J. Ind. Eng. Chem.* **2006**, *12*, 175 - 183.
140. Logan, B. E. *Microbial Fuel Cells*, John Wiley and Sons, Inc. Hoboken, New Jersey, 2008.
141. Liu, H.; Logan, B. E. Electricity generation using an air-cathode single chamber microbial fuel cell in the presence and absence of a proton exchange membrane. *Environ Sci Technol.* **2004**, *38*, 4040 - 4046
142. Call, D.; Logan, B. E. Hydrogen production in a single chamber microbial electrolysis cell (MEC) lacking a membrane. *Environ Sci Technol.* **2008**, *42*, 3401 - 3406.
143. Kim, J. R.; Cheng, S.; Oh, S. E.; Logan, B. E. Power generation using different cation, anion and ultrafiltration membranes in microbial fuel cells. *Environ Sci Technol.* **2007**, *41*, 1004 - 1009.
144. Zhang, X.; Cheng, S.; Huang, X.; Logan, B. E. Improved performance of single-chamber microbial fuel cells through control of membrane deformation. *Biosens. Bioelectron.* **2010**, *25*, 1825 - 1828.
145. Fan, Y.; Hu, H.; Liu, H. Enhanced coulombic efficiency and power density of air-cathode microbial fuel cells with an improved cell configuration. *J Power Sources* **2007**, *171*, 348 - 354.
146. Wei, B.; Tokash, J. C.; Zhang, F.; Kim, Y. Logan, B. E. Electrochemical analysis of separators used in single-chamber, air-cathode microbial fuel cells. *Electrochimica Acta* **2013**, *89*, 45 - 51.
147. Liu, H.; Ramnarayanan, R.; and Logan, B. E. Production of Electricity during Wastewater Treatment Using a Single Chamber Microbial Fuel Cell. *Environ. Sci. Technol.* **2004**, *38*, 2281 - 2285.
148. Rabaey, K.; Clauwaert, P.; Aelterman, P.; and Verstraete, W. Tubular Microbial Fuel Cells for Efficient Electricity Generation. *Environ. Sci. Technol.* **2005**, 39, 8077 - 8082.
149. Oh, S.; Logan, B. E. Proton exchange membrane and electrode surface areas as factors that affect power generation in microbial fuel cells. *Appl. Microbiol. Biotechnol.* **2006**, *70*, 162 - 169.
150. Min, B.; Cheng, S.; Logan, B. E. Electricity generation using membrane and salt bridge microbial fuel cells, *Water Res.* **2005**, *39*, 1675 - 1686.
151. Rabaey, K.; Ossieur, W.; Verhaege, M.; Verstraete, W. Continuous microbial fuel cells convert carbohydrates to electricity. *Water Sci. Technol.*, **2005**, *52*, 515 - 523.
152. Logan, B. E.; Murano, C.; Scott, K.; Gray, N. D.; Head, I. M. Electricity generation from cysteine in a microbial fuel cell. *Water Res.* **2005**, *39*, 942 - 952.
153. Nwogu, N. G. Microbial Fuel Cells and Parameters Affecting Performance When Generating Electricity. *Basic Biotech.* **2007**, *3*, 73 - 79.
154. Kim, I. S.; Chae, K. J.; Choi, M. J. Electricity generation from cysteine in a microbial fuel cell. *Environ. Eng. Res.*, **2008**, *13*, 51 - 65.

155. Jang, J. K.; Pham, T. H; Chang, I. S.; Kang, K. H.; Moon, H.; S. Cho, K.; and Kim, B. H. Construction and operation of a novel mediator-and membrane-less microbial fuel cell. *Process Biochem.* **2004**, *39*, 1007 - 1012.
156. Aelterman, P.; Rabaey, K.; Pham, H. T.; Boon, N.; Verstraete, W. Continuous electricity generation at high voltages and currents using stacked microbial fuel cells. *Environ Sci Technol.* **2006**, *40*, 3388 - 3394.
157. Tortera, G. J.; Funke, B. R.; Case, C. L. *Microbiology an introduction*, Eighth Edition, Daryl Fox, New York, 2004.
158. Pugsley, A. P. The Complete General Secretory Pathway in Gram-Negative Bacteria. *Microbiol. Rev.*, **1993**, *57*, 50 - 108.
159. Salton, M. R. J. Bacterial Membranes. *Crit. Rev. Microbiol.*, **1971**. *1*, 161 - 197.
160. Kostakioti, M.; Newman, C. L.; Thanassi, D. G.; and Stathopoulos, C. C. Mechanisms of Protein Export across the Bacterial Outer Membrane. *J. Bacteriol.* **2005**, *187*, 4306 - 4314.
161. Madigan, M. T.; and Martinko, J. *Brock Biology of Microorganisms,* Prentice Hall, Upper Saddle River, NJ. USA, 2006.
162. Tanaka, K.; Vega, C. A.; and Tamamushi, R. 612bis-Thionine and ferric chelate compounds as coupled mediators in MFCs. *Bioenerg.* **1983**, *11,* 289 - 297.
163. Lovlely, D. R. Bug juice: harvesting electricity with microorganisms. *Nat. Rev.*, **2006**, *4*, 497 - 508.
164. Schröder, U. Anodic electron transfer mechanisms in microbial fuel cells and their energy efficiency. *Phys. Chem. Chem. Phys.* **2007**, *9,* 2619 - 2629.
165. Li, C.; Zhang, L.; Ding, L.; Ren, H.; Cui, H. Effect of conductive polymers coated anode on the performance of microbial fuel cells (MFCs) and its biodiversity analysis. *Biosensor. Bioelectron.* **2011**, *26*, 4169 - 4176.
166. Popov, A. L.; Kim, J. R.; Dinsdale, R. M.; Esteves, S. R.; Guwy, A. J.; and Premier, G. C. The Effect of Physico-chemically Immobilized Methylene Blue and Neutral Red on the Anode of Microbial Fuel Cell. *Biotechnol. Bioprocess Eng.* **2012**, *17*, 361 - 370.
167. Galament, P. S.; and Saravia, S. G. Laboratory Studies of Biocorrosion Control Using Traditional and Environmentally Friendly Biocides: an Overview. *Latin Am. Appl. Res.* **2005**, *35*, 295 - 300.
168. Costerton, J. W.; Philip S. Stewart,1; Greenberg, E. P. Bacterial Biofilms: A Common Cause of Persistent Infections. *Sci.* **1999**, *284*, 1319 - 1322
169. Sutherland, L. W. Biofilm expopolysaccharides: a strong and sticky frame work. *Microbiol.* **2001**, *147*, 3 - 9.
170. Whitchurch, C. B.; Nielsen, T. T.; Ragas, P. C.; Mattick, J. S. Extracellular DNA required for bacterial biofilm formation. *Sci.* **2002**, *295*, 1487.
171. Liu, Y., Li, J. Role of *Pseudomonas aeruginosa* biofilm in the initial adhesion, growth and detachment of *Escherichia coli* in porous media. *Environ. Sci. Technol.* **2008**, *42*, 443 - 449.
172. Laspidou, C. S.; and Rittmann, B. E. Modeling biofilm complexity by including active and inert biomass and extracellular polymeric substances. *Biofilms* **2004**, *1*, 285 - 291.
173. Lahlou, M.; Harms, H.; Springael, D.; Calvo, J. O. Influence of soil components on the transport of polycyclic aromatic hydrocarbon-degrading bacteria through saturated porous media. *Environ. Sci. Technol.* **2000**, *34*, 3649 - 3656.

174. Wick, L. A.; P. Mattle, Wattiau, P.; Harms, H. Electrokinetic transport of PAH-degrading bacteria in model aquifers and soil. *Environ. Sci. Technol.* **2004**, *38*, 4596 - 4602.
175. Casal, P. V.; Wick, L. Y.; Calvo, J. O. Chemoeffectors decrease the deposition of chemotactic bacteria during transport in porous media. *Environ. Sci. Technol.* **2008**, *42*, 1131 - 1137.
176. Biffinger, J. C.; Pietron, J.; Ray, R.; Little, B.; Ringeisen, B. R. A biofilm enhanced miniature microbial fuel cell using Shewanella oneidensis DSP10 and oxygen reduction cathodes. *Biosens. Bioelectron.* **2007**, *22*, 1672 - 1679.
177. Chen, K. Y.; Ho, G.; and Ruwisch, R. C. Affinity of microbial fuel cell biofilm for the anodic potential. *Environ. Sci. Technol.* **2008**, *42*, 3828 - 3834.
178. Mohan, S. V.; Raghavulu, S. V.; and Sarma, P. N. Influence of anodic biofilm growth on bioelectricity production in single chambered mediator-less microbial fue cell using mixed anaerobic consortia. *Biosensor. Bioelectron.* **2008**, *24*, 41 - 47.
179. Franks, A. E.; and Nevin, K. P. Microbial Fuel Cell, A Current Review. *Energies* **2010**, *3*, 899 - 919.
180. Borole, A. P.; Reguera, G.; Ringeisen, B.; Wang, Z.; Feng, Y.; and Kim, B. H. Electroactive biofilms: Current status and future research needs. *Energy Environ. Sci.* **2011**, *4*, 4813 - 4834.
181. Cao, B. B.; Shi, L.; Brown, R. N.; Xiong, Y.; Fredrickson, J. K.; Romine, M. F.; Marshall, M. J.; Lipton, M. S.; Beyenal, H. Extracellular polymeric substances from Shewanella sp. HRCR-1 biofilms: characterization by infrared spectroscopy and proteomics. *Environ. Microbiol.* **2011**, *13*, 1018 - 1031.
182. Choi, S.; Chae, J. Optimal biofilm formation and power generation in a micro-sized microbial fuel cell (MFC). *Sen. Actuators A: Phys.* **2012**, 177, 10 - 15.
183. Johnson, D. B.; Bridge, T. A. M. Reductive dissolution of ferric iron minerals by *Acidiphilium* SJH, *Geomicrobiol. J.* **2000**, 17, 193 - 206.
184. Pronk, J. T.; and Johnson, D. B. Oxidation and reduction of iron by acidophilic bacteria. *Geomicrobiol. J.* **1992**, *10*, 153 - 171.
185. Straub, K. L.; Benz, M.; and Schink, B. Iron metabolism in anoxic environments at near neutral pH. *FEMS. Microbiol. Ecol.* **2001**, *34*,181 - 186.

Chapter 2

THEORY

2.1 Introduction

The first part of this chapter describes the experimental theory associated with the design of a microbial fuel cell and the second section discusses their performance outputs. The third and final section provides an overview of the limitations of the power output related to the materials used for construction of the MFC.

2.2 Microbial fuel cell theory

Oxygen reduction reaction mechanism

The understanding of the oxygen reduction reaction (ORR) is of paramount importance to the successful operation of a MFC. The triplet state of oxygen in its ground state, has two unpaired electrons occupying a doubly degenerate π^* antibonding orbital, according to Hund's rule. The bonding order of oxygen is two, which is attributed to the $3\sigma_g$ orbital with two electrons, the doubly degenerate $1\pi_u$ and $1\pi_g^*$orbitals, where the $1\pi_u$ orbitals have double occupancy while the $1\pi_g^*$orbital has single occupancy. In the reduction of O_2, the added electrons will occupy anti-bonding orbitals, decreasing the bond order of O-O. This increases the O-O bond distance and the vibrational frequency decreases. This explains the high stability of the O_2 molecule and its relatively low reactivity, in spite of its high oxidising power.[1]

Generally two reaction paths are accepted for the ORR that takes place at the cathode.[2] Equations 2.1 to 2.4 express the reaction pathways in an acidic medium.

Direct reduction

$$O_2 + 4H^+ + 4e^- \rightarrow 2H_2O \qquad E^\circ = 1.23V$$ *Equation 2-1*

Indirect reduction

$$O_2 + 2H^+ + 2e^- \rightarrow H_2O_2 \qquad E^\circ = 0.682V$$ *Equation 2-2*

followed by a further reduction

$$H_2O_2 + 2H^+ + 2e^- \rightarrow 2H_2O \qquad E^\circ = 1.77V$$ *Equation 2-3*

or a chemical decomposition.

$$2H_2O_2 \rightarrow 2H_2O + O_2$$ *Equation 2-4*

Figure 2.1 shows a postulated scheme of the main steps of an oxygen reduction reaction. It shows the reduction process is a multielectron reaction which includes a number of elementary steps of different reaction intermediates. This scheme is considered as one of the most effective in describing the reduction of O_2 on metal surfaces.

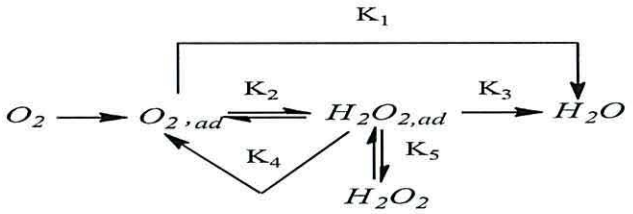

Figure 2.1 - Schematic presentation of ORR pathway.[1]

According to the proposed scheme an oxygen molecule can be reduced to a water molecule on the metallic surface either directly from adsorbed $O_{2(ads)}$ to water with a heterogonous rate constant K_1, or *via* another route by formation of adsorbed peroxide $H_2O_{2(ads)}$ with a heterogeneous rate constant K_2, then the adsorbed peroxide is further reduced chemically to water, with a heterogeneous rate constant K_3, then taking different routes to either decomposition on the electrode surface (K_4) or desorption into the solution (K_5).[3] The high stability of the O-O bond which has a dissociation energy of 118 Kcal.mol^{-1}, is probably the main reason for the tendency of the oxygen molecule to be reduced to H_2O_2 on the surface of most electrode materials. However, the O-O bond in H_2O_2 is only 35 Kcal.mol^{-1}.[4]

The various reaction pathways are interpreted as the consequence of different metal-dioxygen complex structures. Figure 2.2 shows the plausible mechanism 1:1 and 1:2 metal-dioxygen complex structures. Model (1) which is called the Griffiths model contains a side-on interaction of metal-oxygen.[5] Model (2), the Pauling model, is an end-on interaction of oxygen molecules with the surface of the metal to make an open angle ~ 120 degree.[6]

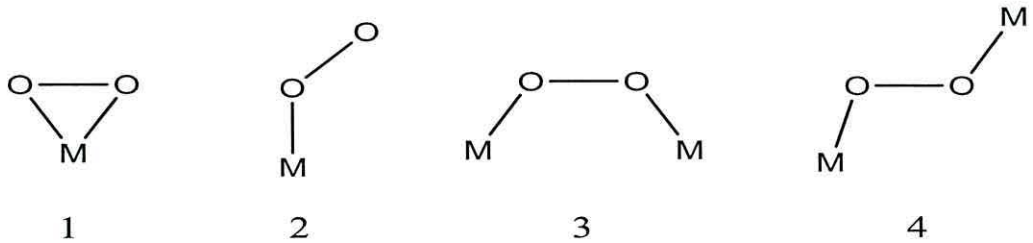

Figure 2. 2 - Possible configuration of oxygen molecule interaction with a metal in a complex.[4]

Thermodynamics of bioelectrochemical conversion in microbial fuel cell

Electricity from a MFC is spontaneously produced only when the overall reaction is thermodynamically favourable (change in Gibbs free energy < 0) To calculate the voltage generation in MFCs, it may be more convenient to calculate the reaction in terms of the overall cell electromotive force (E_{emf}), which is defined as the potential difference between the cathode and anode in an MFC that can be obtained relative to the theoretical amount of work (W). Both values are equal to the net release of Gibbs free energy (ΔG), as the reaction goes from reactant to product. This can be expressed according to the following equation:[7]

$$E_{emf}\, nF = W = -\Delta G \qquad \textit{Equation 2-5}$$

Where n the number of electrons transferred, F is Faraday's constant (96,485 C/mol)

$$E_{emf} = \frac{-\Delta G}{nf} \qquad \textit{Equation 2-6}$$

If all reactions are determined at standard conditions, then

$$E^{\Theta}{}_{emf} = \frac{-\Delta G^{\circ}}{nf} \qquad \textit{Equation 2-7}$$

The overall reaction in terms of the potential is given by

$$E_{emf} = E^{\Theta}{}_{emf} - \frac{RT}{nF} In(\Pi) \qquad \textit{Equation 2-8}$$

Where Π represents concentration the product/ reactant.

2.3 Microbial fuel cell performance

Power measurements

To study the MFC reactor performance and its effectiveness to generate power, it is essential to optimise the system for power production. The power obtained by an MFC is related to the measured cell voltage, E_{MFC}, across a fixed external load (R_{ext}) and the current by $P = IE_{MFC}$ where the current was determined using Ohms law based on the MFC voltage, $I = E_{MFC}/R_{ext}$. Hence the power can also be expressed as:

$$P = \frac{E_{MFC}^2}{R_{ext}} \qquad \textit{Equation 2-9}$$

Power output normalised by electrode surface area

Many studies use the surface area of the anode for determining power density; because the amount of power generated in an MFC is affected by the amount of anode surface area (A_{an}) available for bacteria to grow on. However, power

generation is not always affected by the surface of the anode. In some systems with very high anode surface area, alternates are used to obtain power density by the cathode surface area(A_{cat}). Thus, it is essential to normalise the power generation on the basis of surface area of the cathode.[8]

$$P_{an} = \frac{E_{MFC}^2}{A_{an}R_{ext}} \qquad \textit{Equation 2-10}$$

$$P_{cat} = \frac{E_{MFC}^2}{A_{cat}R_{ext}} \qquad \textit{Equation 2-11}$$

Power output normalised by membrane surface area

In reactor systems where the anode and cathode chamber are separated by a membrane, the membrane projected surface area may also be used to normalise the power. According to Oh and Logan,[9] the power production varied depending on the relative sizes of the anode, cathode and proton exchange membrane (PEM). A power density based on the membrane surface area is calculated as

$$P_A = \frac{E_{MFC}^2}{R_{ext}A_{PEM}} \qquad \textit{Equation 2-12}$$

Power output normalised by volume

The reactor liquid volume can also be used as a normalising factor. In the literature researchers sometimes normalise the power production on the basis of the total reactor volume (*including both the cathode and anode chambers*) or the anode liquid volume (*excluding membrane area and gas head space*). A volumetric power density based on the total reactor volume is calculated as:

$$P_V = \frac{E_{MFC}^2}{VR_{ext}} \qquad \textit{Equation 2-13}$$

Where P_V, is the volumetric power (W/m^3) and V the total reactor volume *(ie. the empty bed volume*). The literature reports power densities of several different types of reactor configuration (MFCs). Table 2.1 on the following page shows maximum power densities of these reference papers.

Table 2.1 - Substrate, configuration, and power generation performance in MFC.

Substrate	Max power density	Reactor configuration	References
Glucose	12.7 mW/m^2	Two-chamber	10
Glucose	2 mW/m^2	Two-chamber salt bridge	11
Wastewater	28 mW/m^2	Single	12
Glucose	4310 mW/m^2	Stacked	13
Acetate	90 W/m^3	Tubular	14
Wastewater	170 mW/m^2	Tubular upflow	15
Acetate	784 mW/m^2	Tubular upflow	16
Acetate	83 W/m^3	Cylindrical two chamber MFC	17

Polarisation curves

Polarisation curves provide a powerful tool for the characterisation of microbial fuel cells. Polarisation curve illustrates the amount of the produced current density as a function of the applied potential. Two ways are used for obtaining these polarisation curves; using a potentiostat, which can apply a fixed potential and measure the current, or using an external resistance circuit, of which the value is changed in several steps, measuring the potential. Figure 2.3 demonstrates a typical polarisation curve.

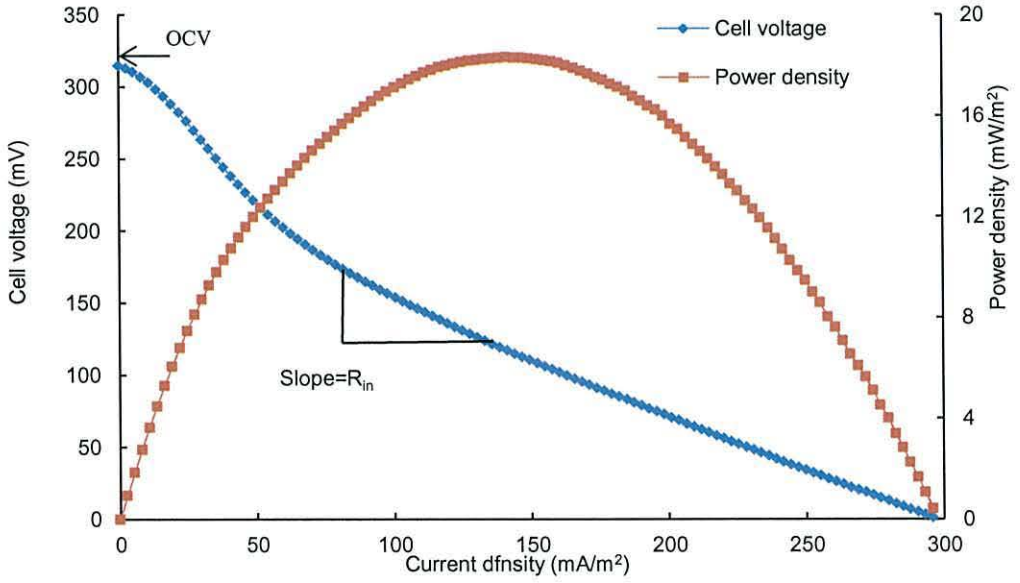

Figure 2.3 - Polarisation (blue line) and power density (red line) curve for a Microbial Fuel Cell. The OCV is the maximum cell voltage, found when no current flows. Cell voltage decreases with increasing current density as a result of increasing losses. Power density shows a maximum at a certain current density. The internal resistance can be determined from the slope of the cell voltage curve.

At the beginning (*intersect with x-axis*) there is no flowing of the current, no losses occur, and the maximum cell voltages could be found, which is called open circuit voltage (OCV). In the closed circuit, the current increases, and then the cell voltage will decrease. This decrease in cell potential is a result of increasing losses with

increasing current. The common losses are ohmic loss, activation loss and concentration losses. The Ohmic loss (*or resistance loss*) is due to low conductivity of the solution. This resistance leads to a voltage drop according to Ohm's law. Ohmic losses represent the energy loss as a result of the voltage drop in all conductive parts of the cell (*solution, electrical connections and electrodes*). The activation energy required to start the reaction leads to the loss of activation. The final loss is concentration losses, which are caused by the concentration gradients from the vicinity of the electrode. From the current density, decrease in cell voltage can be found, in which the higher the current density the higher the voltage loss in the system.

Coulombic efficiency

Coulombic efficiency (CE) is defined as the ratio of the number of coulombs recovered as electrical current versus the theoretical maximum number of coulombs recoverable from the initial organic matter added to the system.

$$C_E = \frac{Coulombs\ recovered}{Total\ coulombs\ in\ substrate} \qquad \textit{Equation 2-14}$$

Low level of CE of the MFC is dependent, partially, on the bacteria that are carrying out the oxidation of the organic carbon, and most of it is used for bacteria metabolism. Improvement of CE and highest theoretical amount of energy depend on complete oxidation of organic matter to carbon dioxide, with efficient electron transfer to the anode electrode.[18,19] An ampere is defined as the transfer of 1 Coulomb of charge per second, or 1 **A** = 1 C/S. Thus, if the current is integrated over time the total number of coulombs transferred in the system is obtained.

2.4 Limitations in microbial fuel cell processes related to materials

Anode

An important factor which has a direct influence on the potential losses of an MFC is the material used for the anodic electrode. This is related to the reaction between microorganisms and the anode electrode (*attachment and growth to the surface of the anode*). The common material and surface modification are mentioned in chapter 1, section (1.5).

Cathode

In practice, the actual voltage output OCV of an MFC is less than the cell electromotive force (EMF) due to irreversible losses (*i.e., overvoltage*). Commonly three types of potential losses can be identified that affect an MFC performance: activation losses, ohmic losses, and mass transport losses. These potential losses are known as the potential required to compensate for the current lost due to electrochemical reactions, charge transport, and mass transfer processes that take place in both the anode and cathode chambers.

Activation losses

The reduction reaction activity that takes place at the cathode electrode depends on the amount of current production in the MFCs. The reduction reaction kinetics are limited by an activation energy barrier which depends on the conversion of the oxidant into a reduced form (*Equation 2.15*).

Anode: $C_6H_{12}O_6 + 6H_2O \rightarrow 6CO_2 + 24H^+ + 24e^-$ *Equation 2-15*

The cathode potential produced at any specific current is considered to be the result of potential losses due to an activation barrier and is called cathodic activation loss (η_{act}).

Ohmic losses

The performance of a MFC is also limited by ohmic overpotentials of the cathode electrode, which can be identified as internal resistances. This loss arises from both the resistance of proton migration within the ion conducting electrolyte and the resistance due to the electron flow through the connection wire.

The ohmic overpotential (η *ohmic*) hence represents the potential which is lost in order to complete the charge transport (*electrons and protons*). Ohmic loss commonly follows Ohm's law on the following page.

$$\eta_{ohmic} = iR_{ohmic}$$ *Equation 2-16*

Where i is the current (A) and R_{ohmic} is the ohmic resistance (Ω) of the MFC. The ohmic resistance of the cathode electrode indicates the sum of ionic, R_{ion}, and electronic, R_{elec}, resistances, and includes the resistance from the electrode, electrolyte solution and contact resistances;

$$R_{ohmic} = R_{ion} + R_{elec}$$ *Equation 2-17*

Internal resistance is usually dominated by the electrolyte resistance since the ionic conductivity is an order of magnitude lower than the electrical conductivity of the electrode materials.[20] The ohmic resistance of the electrolyte R_{ion}, can be expressed by;

$$R_{ion} = \frac{l}{AK}$$ *Equation 2-18*

Where l is the distance (cm) and A is the cross-sectional area (cm^2) over which the ionic conduction occurs, and K is the specific conductivity $(\Omega\ cm)^{-1}$ of the electrolyte.[20] The cathodic ohmic loss is more pronounced at medium current densities and, following the Ohm's law, the operating voltage decreases linearly as current increases.

Mass transport losses

The process of supplying reactants (*oxidants, i.e., O_2*) and removing products (*i.e., H_2O*) at the cathode electrode of an MFC is termed mass transport. Insufficient mass transport can lead to low performance of the MFC, due to reactant depletion or product accumulation within the catalyst layer. Reactant depletion limits both the cell voltage and the reaction kinetics, leading to a performance loss. This loss is the voltage required to drive mass transport processes at the cathode and is referred to as cathodic concentration loss or mass transport loss, (η_{conc}) cathode. Cathodic concentration losses increase with increasing current density.

Minimising cathodic activation losses

Reduction of oxygen is the most common reaction that takes place at the cathode electrode. An important factor which has a direct influence on the performance of an MFC is the low reaction kinetics of the oxygen reduction on the surface of the cathode electrodes which leads to higher overvoltage.[21] Consequently, various methods are currently used to enhance the performance of the cathode in MFC with many requiring a high oxygen supply into the cathode chamber.[22] These methods include the use of more effective oxidants as the electron acceptors,[23 ,24 ,25] modification of the cathode electrode with catalyst,[26 ,27,28] Biocathode electrodes, and improving working conditions within the cathode chamber.[29,30 ,31]

Minimising cathodic ohmic losses

Currently, various methods are used to minimise cathodic ohmic losses, which include higher conductivity of the electrolyte solution, large size proton exchange membrane, and reducing the spacing between electrodes.[32,12,33,34]

Minimising cathodic mass transport losses

The mechanism of mass transport to the cathode electrode depends on both convection and diffusion. Convection plays an important role to transfer mass in a bulk solution. Conversely, diffusion controls the mass transport through the concentration gradient to the cathode surface. Mass transport losses can be reduced by keeping high concentrations of oxidant,[21,35] electrode material,[36,37] improving MFC working conditions, and optimised geometry of the cathode chamber.[38,39]

The material used for the cathode electrode needs to have high electrocatalytic activity to improve the slow rate of ORR which has a direct effect on the overpotential of a MFC. However, chemical catalyst materials (*i.e., Platinum*) are high cost and rare materials. Consequently current research has focused on alternative catalysts [27,40,41]

Membrane

MFCs can function with or without a membrane. When the anode and cathode chamber are separated by a proton exchange membrane, the CE is high due to low oxygen back diffusion to the anode.[12] The disadvantage of the membrane on MFC performance is usually a result of increased internal resistance and again high cost. However, the size of the membrane is also a significant factor because it controls the internal resistance of an MFC which facilitates fast diffusion of the proton through the membrane.[9]

Medium

While buffer solution can help stabilise pH and increase the conductivity of the solution, pH of buffer solution facilitating proton availability to the cathode, proton transfer efficiency depends on type and concentration of buffer solution.[42,43]

2.5 References

1. Valentine, J. S. The Dioxygen ligand in molecular group VIII transition metal complexes. Chem. Rev. **1973**, *73*, 235 - 245.
2. Li, L.; ZiDong, W.; Yi, Z.; XueQiang, Q.; MeiRong, X.; Jie, Z.; ZhiGang, S.; and CaiXin, S. DFT study of difference caused by catalyst supports in Pt and Pd catalysis of oxygen reduction reaction. *Sci. China Ser. B-Chem.* **2009**, *52*, 571 - 578.
3. Markovic, N. M.; Schmidt, T. J.; Stamenkovic, V.; and Ross. P. N. Oxygen Reduction, Reaction on Pt and Pt Bimetallic Surfaces. *Fuel Cells* **2001**, *1*, 105 - 116.
4. Zagal, Metallophthalocyanines as catalysts in electrochemical reactions. J. *Coord. Chem, Rev*, **1992**, *119*, 89 - 136.
5. Griffith, J. S. On the Magnetic Properties of Some Haemoglobin Complexes. *Proc. R. Soc. Lond.* **1956**, *235,* 23 - 36.
6. Pauling, L. Nature of iron-oxygen bond in oxyhaemoglobin. *Nat.* **1964**, *203,* 182 - 183.
7. Logan, B. E.; Hamelers, B.; Rozendal, R.; Schroder, U.; Keller, J.; Freguia, S.; Aelterman, P.; Verstraete, W.; and Rabaey, K. Microbial Fuel Cell: Methodology and Technology. *Environ. Sci. Technol.* **2006**, *40*, 5181 - 5192.
8. Cheng, S.; Liu, H.; and Logan, B. E. Increased performance of single-chamber MFCs using an improved cathode structure. *Electrochem. Commun.* **2006**, *8*, 489 - 494.
9. Oh, S.; Logan, B. E. Proton exchange membrane and electrode surface areas as factors that affect power generation in microbial fuel cells. *Appl. Microbiol. Biotechnol.* **2006**, *70*, 162 - 169.
10. Borole, A. P.; O'Neill, H.; Tsouris, C.; and Cesar, S. A microbial fuel cell operating at low pH using the acidophile *Acidiphilium cryptum*. *Biotechnol. Lett.* **2008**, *30*, 1367 - 1372.
11. Min, B.; Cheng, S.; Logan, B. E. Electricity generation using membrane and salt bridge microbial fuel cells. *Water Res.* **2005**, *39*, 1675 - 1686.
12. Liu, H.; Logan, B. E. Electricity generation using an air-cathode single chamber microbial fuel cell in the presence and absence of a proton exchange membrane. *Environ. Sci. Technol.* **2004**, *38*, 4040 - 4046.
13. Aelterman, P.; Rabaey, K.; Pham, H. T; Boon, N.; Verstraete, W. Continuous electricity generation at high voltages and currents using stacked microbial fuel cells. *Environ. Sci. Technol.* **2006**, *40*, 3388 - 3394.
14. Rabaey, K.; Clauwaert, P.; Aelterman, P.; and Verstraete, W. Tubular Microbial Fuel Cells for Efficient Electricity Generation. *Environ. Sci. Technol.* **2005**, *39*, 8077 - 8082.
15. He, Z.; Minteer, S. D.; and Angenent, L. Electricity Generation from Artificial Wastewater Using an Upflow Microbial Fuel Cell. *Environ. Sci. Technol.* **2005**, *39*, 5262 - 5267.
16. Deng, Q.; Li. X, J. E.; Zuo, B. E. Logan, Ling, A. Power generation using an activated carbon fiber felt (ACFF) cathode in an upflow microbial fuel cell. *J Power Sources* **2010**, *195*, 1130 - 1135.

17. Clauwaert, P.; Ha D.; Boon, N.; K. Verbeken, Verhaege, M.; Rabaey, K.; Verstraete, W. Open air biocathode enables effective electricity generation with microbial fuel cells. *Environ. Sci. Technol.* **2007**, *41*, 7564 - 7569.
18. Freguia, S.; Rabaey, K.; Yuan, Z.; Keller, J. Syntrophic processes drive the conversion of glucose in microbial fuel cell anodes. *Environ. Sci. Technol.* **2008**, 42, 7937 - 7943.
19. Franks, A. E.; and Nevin, K. P. Microbial Fuel Cells, *A* Current Review. *Energies* **2010**, *3*, 899 - 919.
20. O'Hayre, R.; Cha, S. W.; Colella, W.; Prinz, F. B. *Fuel cell fundamentals*, John Wiley and Sons, New York, 2006.
21. Gil, G. C.; Ghang, I. S.; Kim, B. H.; Kim, M.; Jang, J. K.; Park, H. S.; and Kim, H. J. Operational parameters affecting the performance of a mediator-less microbial fuel cell. *Biosen. Bioelectron.* **2003**, *18*, 327 - 334.
22. Zhao, F.; Harnisch, F.; Schröder, U.; Scholz, F.; Bogdanoff, P.; Herrmann, I. Challenges and Constraints of Using Oxygen Cathodes in Microbial Fuel Cells. *Environ. Sci. Technol.* **2006**, *40*, 5193 - 5199.
23. Wei, L.; Han, H.; Shen, J. Effects of cathodic electron acceptors and potassium ferricyanide concentrations on the performance of microbial fuel cell. *Int. J. Hydrogen Energy* **2012**, *37*, 12980 - 12986.
24. Wang, G.; Huang, L.; and Zhang, Y. Cathodic reduction of hexavalent chromium [Cr(VI)] coupled with electricity generation in microbial fuel cells. *Biotechnol. Lett.* **2008**, *30*, 1959 - 1966.
25. Wang, Y.; Niu, C. G.; Zeng, G. M.; Hu, W. J.; Huang, D. W.; Ruan, M. Microbial fuel cell using ferrous ion activated persulfate as a cathodic reactant. *Int. J. Hydrogen Energy* **2011**, *36*, 15344 - 15351.
26. Qi, Z.; Kaufman, A. Low Pt loading high performance cathodes for PEM fuel cells. *J. Power Sources* **2003**, *113*, 37 - 43.
27. Cheng, S.; Liu H.; and Logan, B. E. Power Densities Using Different Cathode Catalyst(Pt and CoTMPP) and Polymer Binders (Nafion and PTEF) in Single Chamber Microbial Fuel Cells. *Environ. Sci. Technol.* **2006**, *40*,364 - 369.
28. Yu, E.; Cheng, S.; Scott, K.; and Logan, B. E. Microbial fuel cell performance with non-Pt cathode catalysts. *J. Power Sources,* **2007**, *171*, 275 - 281.
29. Rhoads, A.; Beyenal, H.; Lewandowski, Z. Microbial fuel cell using anaerobic respiration as an anodic reaction and biomineralized manganese as a cathodic reactant. *Environ. Sci. Technol.* **2005**, *39*, 4666 - 4671.
30. Heijne, H. V.; Hamelers, M.; and Buismana, C. N. Microbial Fuel Cell Operation with Continuous Biological Ferrous Iron Oxidation of the Catholyte. *Environ. Sci. Technol.* **2007**, *41*, 4130 - 4134.
31. Sun, Y.; Wei, J.; Liang, P.; and Huang, X. Microbial community analysis in biocathode microbial fuel cells packed with different materials. *AMB. Express* **2012**, *2*, 1 - 8.
32. Jang, J. K.; Pham, T. H.; Chang, I. S.; Kang, K. H.; Moon, H.; Cho, K. S.; Kim, B. H. Construction and operation of a novel mediator-and membrane-less microbial fuel cell. *Process Biochem.* **2004**, *39*, 1007 - 1012.
33. Oh, S.; Logan, B. E. Proton exchange membrane and electrode surface areas as factors that affect power generation in microbial fuel cells. *Appl. Microbiol. Biotechnol.* **2006**, *70*, 162 - 169.

34. Cheng, S.; Liu, H.; Logan, B. E. Increased power generation in a continuous flow MFC with advective flow through the porous anode and reduced electrode spacing. *Environ. Sci. Technol.* **2006**, *40*, 2426 - 2432.
35. He, Z.; Shao, H. B.; Angenent, L. T. Increased power production from a sediment microbial fuel cell with a rotating cathode. *Biosensor. Bioelectron.* **2007**, *22*, 252 - 3255.
36. Park, D. H.; Zeikus, J. G. Improved fuel cell and electrode designs for producing electricity from microbial degradation. *Biotchnol. Bioeng.* **2003**, *81*, 348 - 355.
37. Cheng, S.; Liu, H.; and Logan, B. E. Increased performance of single-chamber MFCs using an improved cathode structure. *Electrochem. Commun.* **2006**, *8*, 489 - 494.
38. Pham, T. H.; Jang, J. K.; Moon, H. S.; Chang, I. S.; Kim, B. H. Improved performance of microbial fuel cell using membrane-electrode assembly. *J. Microbiol. Biotechnol.* **2005**, *15*, 438 - 441.
39. Liu, H.; Ramnarayanan, R.; and Logan, B. E. Production of Electricity during Wastewater Treatment Using a Single Chamber Microbial Fuel Cell, *Environ. Sci. Technol.* **2004**, *38*, 2281 - 2285.
40. Yu, E. H.; Cheng, S.; Logan, B. E.; Scott, K. Electrochemical reduction of oxygen with iron phthalocyanine in neutral media. *J. Appl. Electrochem.* **2009**, *39,* 705 - 711.
41. Yuan, Y.; Zhou, S.; and Zhuang, L. Polypyrrole/carbon black composite as a novel oxygen reduction catalyst for microbial fuel cells *J Power Sources* **2010**, *195*, 3490 - 3493.
42. Watanable, K. Recent developments in microbial fuel cell technologies for sustainable bioenergy. *J. Biosci. Bioeng.* **2008**, *106*, 528 - 536.
43. Fan, Y.; Hu, H.; and Liu, H. Sustainable power generation in microbial fuel cells using bicarbonate buffer and proton transfer mechanisms. *Environ. Sci. Technol.* **2007**, *41*, 8154 - 8158.

Chapter 3

EXPERIMENTAL METHODOLOGY

3.1 Introduction

3.2 Electrochemical methods

All measurements were performed using a computer-controlled Auto lab PGSTAT 30 electrochemical measurement system (*Eco Chemie, Holland*). The analysis was carried out with a three-electrode cell, using a saturated calomel reference electrode (SCE) and a platinum counter electrode unless stated otherwise. The platinum electrode was cleaned by means of a red-hot heating flame prior to use. Also prior to use, the cells were cleaned using a 50:50 mixture of concentrated H_2SO_4:HNO_3 followed by rinsing in deionised water (*nominal resistivity >18M_cm at 25 ˚C*), cleaning in a steam bath and drying in an oven. All tests were carried out at room temperature.

The effect of dissolved oxygen

The effect and/or interference of dissolved oxygen in the supporting electrolyte are determined using a glassy carbon (GC) working electrode; the GC electrodes were polished with alumina suspension (1 μm), and (300 nm) on Buehler felt pads and then ultrasonically cleaned for 15 minutes in doubly deionised water to remove any alumina residues. The working electrode was a 10 mm diameter GC electrode. A cyclic voltammogram of 500 mM H_2SO_4 with potential range was swept between 1500 mV and -500 mV was run. This was started at 0 V in the negative direction with a scan rate of 50 mV/s. The solution was then deoxygenated by purging with nitrogen for 15 min, and a cyclic voltammogram of the oxygen free-solution was recorded.

Study of ferricyanide by cyclic voltammetry

A 100 ml stock solution of 10 mM $K_3Fe(CN)_6$ was prepared in 1 M KNO_3. From this, 25 ml of 4 mM solution in 1 M KNO_3 was made. The working electrode was a 10 mm diameter GC electrode. A cyclic voltammogram of 4 mM $K_3Fe(CN)_6$ was 1 M KNO_3 with limits of -200 mV and 600 mV was run. This started at 0 V in the negative direction with a scan rate of 25, 50, 75, 100, 150, and 200 mV/s. The solution was then deoxygenated by purging with nitrogen for 15 min.

Anode treatment procedures

The physical treatment of the anode materials, carbon felt and carbon cloth was carried out using CO_2 gas at a flow rate of 100 mL/min in a tube furnace at three different temperatures of 400 °C, 500 °C, and 600 °C for two hours. The chemical treatment procedure of the anode materials carbon felt and carbon cloth involved one day of treatment in 3 M of, H_2SO_4, and KOH, respectively. The materials were then washed with distilled water at least three times.

Platinum particle deposition

Particles of platinum were electrodeposited on carbon felt from 1 mM aqueous solution of chloroplatinic acid hexahydrate and 1 mM of tri-sodium citrate (*Fisher Bio Reagents*). Tri-sodium citrate was used as a complexing agent. The solution was prepared by dissolving Chloroplatinic acid hexahydrate (518 mg) and Tri-sodium citrate (294 mg) in 50 ml de-ionised water. The approximate volume of the solution (10 ml) was taken in a cell for the electrodeposition of platinum particles. The carbon felt was cut into lengths of approximately 4.0 cm and a width of 0.7 cm to make rectangular electrodes. The electrical contact was made with a crocodile clip. For the deposition of particles, and for subsequent electrochemical experiments, approximately 1 cm of the carbon felt was immersed in the electrolyte.

For the deposition of the particles and their electrochemical characterisation a potentiostat was used. Platinum nanoparticles were deposited with limits of 100 and -500 mV *versus* a SCE. This was started at 0 V in the negative direction. The scan rates were varied between 50 and 1500 mV/s and the number of cycles was between 30 and 900. After the completion of the deposition of the nanoparticles the carbon felt electrode was washed with de-ionised water, then with ethanol, and was dried in an oven at 100 °C. Cyclic voltammetry was used for the electrochemical characterisation of the deposited platinum nanoparticles, in 1 M H_2SO_4. The potential range was swept between -200 and 1500 mV at a scan rate of 50 mV/s,[1] the resulting film was imaged under SEM.

3.3 Surface modification by polyaniline electrodeposition

According to standard literature procedure for polymerization of aniline,[2] i.e. 200 mM of aniline sulphate (*purum, 8.52 g*) was dissolved in 500 mM sulphuric acid in a volumetric flask to 150 mL of solution. The polyaniline were electrodeposited on a carbon felt (*Fisher Scientific UK*), with a surface area of 5 cm^2. For the deposition of the polyaniline films and their electrochemical characterisation a potentiostat was used. The polyaniline film was formed on the working electrode, platinum wire as the counter electrode, and SCE as reference electrode by cyclic voltammetry with the scan rate at 50 m V/s, and the potential range was swept between -200 to 1500 mV. The quantities of polyaniline deposited on the surface of the carbon felt were varied by changing the number of potential cycles; this was examined by weighing the carbon felt electrodes before and after electrodeposition. Previous reports used graphite paper or a platinum sheet electrode.[3] The modified carbon felt by polyaniline electrodeposition was sectioned and imaged using SEM.

3.4 Microbial experimental

Buffer solutions

One litre of a 100 mM stock solution of potassium hydrogen phthalate was made up of (20.422 g) in deionised water. The solution was then vacuum filtered through a 0.45 micron Millipore filter. To make pH (2.5, 3, 3.5, and 4) of 100 mL potassium hydrogen phthalate solution, the pH was adjusted by adding 100 mM Hydrochloric acid drop wise until the required pH was reached.

Media and growth conditions

Acidiphilium sp. SJH was isolated from a highly acidic (pH 2.3) metal-rich stream located within a derelict pyrite mine (*Cae Coch*) in North Wales.[4]The growth medium contained: glucose (1.8 g/L), tryptone soya broth (TSB, 250 mg/L), yeast extract (10 mg/L), ammonium sulphate (1.25 g/L) and magnesium sulphate (500 mg/L). The pH was adjusted to 2.5 with sulphuric acid (H_2SO_4, 1 M) and the liquid medium sterilised (120°C, 20 min). Next, 2.5 ml of filter-sterilised ferrous sulphate ($FeSO_4$, 1 M, pH 2.5) was added to 100 ml of the growth media which was then inoculated with 500 µl of stationary phase *Acidiphilium* sp. SJH. The culture was

incubated for 48 hours, unshaken, at 30 ±1 °C until an optical density (OD) of 1.0 (*at 600 nm*) was obtained.[4]

Preparation of *Acidiphilium* sp. SJH cells

Cells of *Acidiphilium* sp. SJH were prepared from cultures of *Acidiphilium* sp. SJH bacteria prepared as outlined in (Media and growth condition). The cells were harvested by centrifugation (13600 g, 5min). The supernatant was removed; the cells were washed three times in an iron-free liquid medium and re-centrifuged. *Acidiphilium* sp. SJH cells were redispersed in a small volume of the liquid medium. The number of *Acidiphilium* sp. SJH cells was assessed by measurement of the optical density at 600 nm, and by direct cell counts (*Thoma chamber*) using a Leitz Wetzlar microscopic.

Ferric ion reduction by *Acidiphilium* SJH bacteria

Ferrous ion concentration were analysed by UV-Visible spectrophotometry calibrated with a standard solution containing known ferrous ion content.[5] A double beam system with a single monochromator; wavelength range 190 – 900 nm; light source: Deuterium lamp (190 nm – 350 nm), and hydrogen lamp (330 nm – 900 nm), Jasco V- 550, with the Spectra Manger Software was used.

For (50 ml) cells of *Acidiphilium* sp. SJH bacteria was prepared as outlined in (Media and growth condition) 1 ml (20 mM) of filter-sterilised Ferric sulphate was added from (1 M stock solution pH 2.5), using 10 mM glucose as an energy source. The culture/Ferric iron suspensions were incubated at 30 ± 1 °C and ferrous iron concentration was estimated at regular intervals spectrophotometrically with the *ferrozine reagent*. The absorption spectra for ferrous ferrozine complexes were determined in a quartz cell at room temperature.[6] A series of standard ferrous solutions were prepared containing 0.1 to 2 mM dilution of the stock ferrous solution (10 mM was prepared by dissolving (278 mg) of ferrous sulphate in enough deionised water to make 100 ml of solution acidified to pH 1.8 with H_2SO_4).

A 50 µl sample of the culture supernatant (*after centrifuging*) was taken. If needed, the sample was diluted in deionised water acidified to pH 2.0 with H_2SO_4. 950 µl of the *ferrozine reagent* was added and mixed roughly. Absorbance of standards and samples were read at 562 nm against a blank without ferrous ions.

Effect of soluble ferric ion as electron shuttle on voltage generation

A series of tests were conducted to study the effect of different concentration soluble ferric ion on OCV in an H-type two chamber MFC. The anolyte consisted of pure cells of *Acidiphilium* sp. SJH (5.1 x 10^7 cells/ml), and glucose (10 mM) in (*potassium hydrogen phthalate, 100 mM*) buffer solution pH 2.5. The MFC was examined with different concentration soluble ferric ion (1mM, 5mM, and 10mM) on OCV as electron shuttle. Stock solution 1M ferric sulphate (*B.D.H Laboratory Reagent*) solution was prepared by dissolving (mg) in 100 ml deionised water. All experiments run in triplicate (*Error bars SD*).

Effect of Fe (III)-EDTA as an electron shuttle on voltage generation

The use of Fe (III)-EDTA as electron shuttle was studied to improve the efficiency of voltage output in MFC operating at low pH (2.5). The anolyte consisted of pure cells of *Acidiphilium* sp. SJH (5.1 x 10^7 cells/ml), and glucose (10 mM) in (*potassium hydrogen phthalate, 100 mM*) buffer solution pH 2.5. The MFC was tested with different concentration of soluble Fe (III)-EDTA (1m M, 5 mM, and 10 mM) as electron shuttle.

Electrochemical analysis ferric reduction by *Acidiphilium* SJH bacteria

Cyclic Voltammetry (CV) is used to understand the electrocatalysis mechanism of the microbial biofilms with an anode. However, most CV studies have focused on the suspensions of the microbial cells, and freshly immobilised microbials. CV on mature biofilms has rarely been reported.[7,8,9]

A reduction of ferric ions with or a without a washed cell suspensions of *Acidiphilium SJH* bacteria was incubated under anaerobic condition at pH 2.5 as a function of time (0, 6, 10, and 15 hours), followed by cyclic voltammograms. The working electrode was a 10 mm diameter GC electrode and measurements were performed with a scanning rate of 5 m V/s over the potential range 0 V and 900 mV. The electrochemical cell was purged with nitrogen for 20 min.

Open circuit voltage

Open circuit voltage is the maximum cell voltage observed when no current is running through the MFC electrical circuit. Hence the potential differences between

the anode and the cathode electrodes can be indicated by the OCV. The potential of the anode electrode is associated with coulombic efficiencies and the properties of the anode surface. The potential of the cathode depends on the electron accepters which are coated on the cathode, beside the rate of the reaction in the cell. The power density increases with low surface area and resistance, while it will increase with high OCV, according to equation 3.1.[10]

$$P = \frac{OCV^2}{AR_{total}} \qquad \textit{Equation 3-1}$$

Where: P is the power density of the system in mW/m^2, A is the anode surface area in cm^2 or m^2, the OCV of the cell in mV, and R_{total} is the total resistance (*internal and external resistance*).

An H-type two-chambered MFC was made using two glasses that had a volume of approximately 40 ml each. The membrane was held (*proton exchange membrane*) between two chambers. The anode electrode was made of carbon cloth with projected surface area (5 cm^2), the cathode electrode was made of platinum sheet. The cathode chamber was filled with (*potassium hydrogen phthalate, 100 mM*) buffer solution pH 2.5. Voltage generation from *Acidiphilium* sp. SJH bacteria (5.1 x 10^7 cells/ml) in an H-type MFC was studied when there was no external load, in presence glucose (1800 mg/L) as electron donor and soluble ferric ion (10 mM) as electron shuttle called open circuit voltage.

Electrochemical activity of *Acidiphilium* sp. SJH cells

The electrochemical activity of *Acidiphilium* sp. SJH bacteria was assayed by cyclic voltammetry of anaerobic SJH cells and tested using a potentiostat with a scanning rate of 5 mV/s over the potential range -800 and 800 mV. Cells of *Acidiphilium* sp. SJH were prepared from cultures of *Acidiphilium* sp. SJH bacteria were prepared as outlined in (Media and growth condition). The working electrode was a 10 mm diameter GC electrode. The electrochemical cell had a working volume of 5 mL,[11] and was purged with nitrogen for 20 min.

3.5 Construction of the microbial fuel cell

Two MFC designs were fabricated in the laboratory using polyacrylic plastic; the cells were identical apart from the air cathode (figure 3.1).

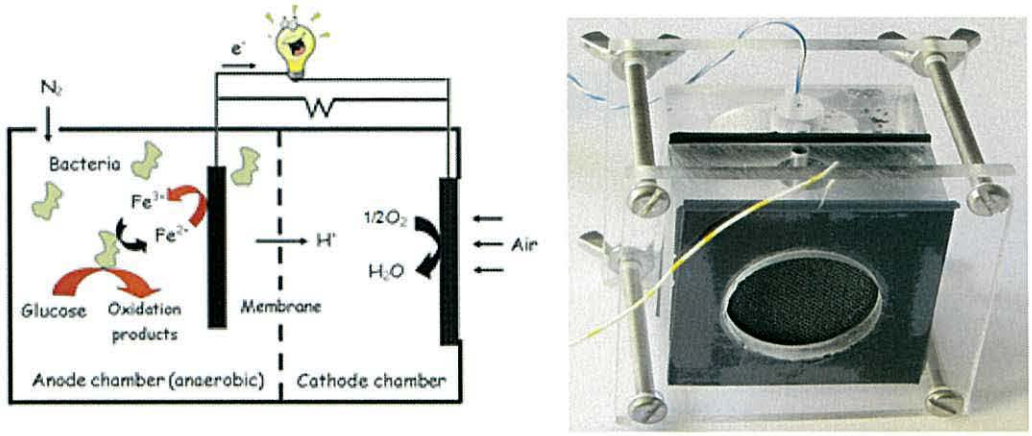

Figure 3.1 - (left) Schematic configuration and (right) cell of a two-chamber MFC with a carbon cloth (anode) and a carbon cloth modified with Pt/KB (air cathode).

The anode consisted of a non-wet-proofed carbon cloth (*Fuel Cell Store USA*), and carbon felt (*Fisher Scientific UK*) with a surface area of 5 cm^2. Figure 3.2 shows the material structure differences. The overall thickness of the carbon cloth was 1 mm and the carbon felt was 8 mm.

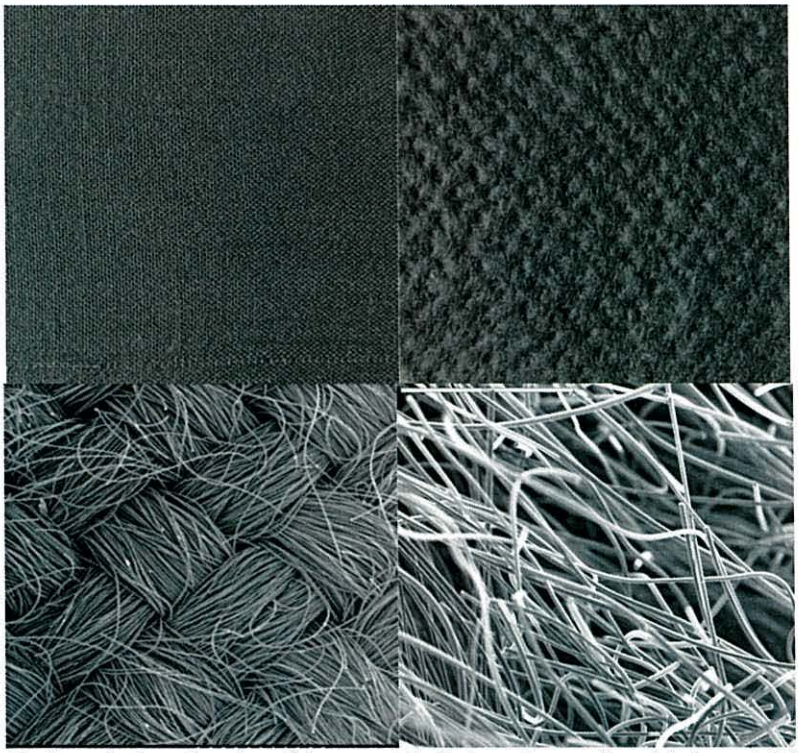

Figure 3.2 - Carbon cloth and carbon felt materials designation carbon felt (top right) and Carbon cloth (top left). An SEM image Carbon cloth and carbon felt at 50X magnification carbon felt (bottom left) and Carbon cloth (bottom right).

The cathode electrode consisted of a Platinum sheet (1 cm^2) or Pt/KB (*AkzoNobel*) (22 wt. % Pt/KB) coated on one side of the wet-proofed carbon cloth, also with a surface area of 5 cm^2. The two cylindrical chambers (*4 cm long with 3 cm in diameter*) were separated by a proton exchange membrane (PEM) with a rubber O-ring to prevent leakage. The distance between the two electrodes was 4 cm. the electrodes were soaked in distilled water for one day before measurements were taken. Copper wire (800 nm) was inserted inside the fluorinated ethylene propylene tubing and was used to connect the circuit; all exposed metal surfaces were sealed with a nonconductive epoxy. The proton exchange membrane (PEM) was pre-treated by boiling in H_2O_2 (30 %, Fluka) and deionised water, followed by 500 mM H_2SO_4 and deionised water before using them as a membrane.

3.6 Characterisation of the catalysts

X-ray powder diffraction

X-ray powder diffraction (XRD) data was measured between 5 and 75 degrees two theta using Ni-filtered Cu Kα1 radiation (λ = 1.54051 A°) on an X' Pert PRO theta-theta diffractometer (PAN Analytical Ltd) at 45 kV and 35 mA.

Transmission Electron Microscopy

In this study samples (Pt/KB and Ketjenblack particles) were suspended in H_2O by ultra-sonication, and then 10 ml drops were dried down onto a 200 mesh form var/carbon-coated gold grid and examined in a Philips CM12 transmission electron microscope at 80 kV. Images were captured with Megaview III digital camera and TEM software (*Soft Imaging System GmbH, Münster, Germany*).

Scanning electron microscopy

Scanning Electron Microscope (SEM) images were obtained using (S-520 Hitachi, Japan), Magnification 1000X, Beam current 150 μA max, Voltage 20KV).

Atomic Absorption Spectroscopy

Atomic Absorption Spectroscopy (AAS) was used to determine the Pt metal loading after the preparation of Pt/KB. For the AAS analysis, the Pt/KB catalysts were dissolved in *aqua regia* and examined in AAS, Apectr AA 220 FS, lamp current 10 mA, wavelength 226 nm, fuel: acetylene, support: nitrous oxide (*Australia*).

3.7 Preparation of the modified cathode

Oxidation of Ketjen Black

KB EC 600J (1 g KB EC 600J/ 10 ml of solution) was oxidised with a saturated solution of ammonium peroxydisulphate $(NH_4)_2S_2O_8$ in sulphuric acid (H_2SO_4, 1 M) at room temperature for 48 hours in a flask placed in a shaking bath. After oxidation, the samples were washed with distilled water to remove the sulphates (*determined with barium chloride*).[12]

Point of zero charge

The point of zero charge (PZC) experiment was carried out by contacting Ketjen Black EC 600J carbon with pH adjusted deionised water. The pH was adjusted using different molarities of HCl and NaOH. An eleven point PZC measurement was the most common experiment used to obtain PZC. Eleven different pH solutions were prepared. The Ketjen Black EC 600J was weighed out for each pH sample. The weight of the Ketjen Black EC 600J depends on the surface area, surface loading and volume of the bottle of sample. The weight of the Black EC 600J was calculated using equation 3.2: In the case of Ketjen Black EC 600J, having a surface area of 1415 m^2 g^{-1}, volume of the bottle of sample 0.050 m^3, surface loading 1000 m^2/L, and the weight of Ketjen Black EC 600J 353 mg was taken.[13]

M_{carbon}= *surface loading x volume / surface area.* *Equation 3-2*

Platinum catalyst preparation

In order to incorporate the platinum into the electrode oxidised Ketjen Black EC 600J (*AkzoNobel*) (350 mg) was dispersed by sonication for 15 min in 20 ml of distilled water, producing a homogeneous slurry; sodium carbonate (Na_2CO_3, 350 mg) was added to the slurry and sonicated for a further 15 min to make the solution more alkaline. The resulting slurry was boiled for 30 min at 80 C°, under continuous stirring. A solution of chloroplatinic acid hexahydrate ($H_2PtCl_6.6H_2O$, 500 mg) in 20 ml distilled water was then added to the slurry, and this was sonicated for a further 15 min. The slurry was then boiled for 30 min at 80 °C, again under continuous stirring. Next formic acid [HCO_2H, (98%) 1 ml] in 8 ml distilled water was added to the slurry and it was sonicated for 10 min to reduce the Pt^{4+}. The slurry was boiled for a further 60 min at 80 °C, under continuous stirring and it was then filtered and

washed with distilled water to pH 7. The precipitate was dried in a vacuum at 100 °C for 60 min and then supplementary dried for a further 12 hours at 100 °C.[14] The resulting Ketjen Black EC 600 JD supported (Pt/KB) was mixed with 5 % Nafion solution (*7 μL Nafion per mg platinum catalyst*).[15] The paste was applied to one side of the wet proofed carbon cloth, and dried at room temperature for 24 hours.

Determination of the amount of platinum metal in Pt/KB catalyst

The quantity of platinum metal after the preparation of the Pt/ KB catalyst was measured *via* AAS. A series of standard platinum solution was prepared containing 40 to 200 mg/L of the stock platinum solutions; 250 mg/L was prepared by dissolving 66.4 mg of Chloroplatinic acid hexahydrate, and then made up to 100 mL by deionised water. The Pt/KB catalysts were dissolved in *aqua regia* (3HCl:1 HNO_3, *by volume*), by filtration the supernatant was used, and then examined in AAS.

Electrochemical reduction of oxygen

Electrochemical activity of the ORR was assayed by cyclic voltammetry. The working electrode was a 10 mm diameter GC, which was polished with an alumina suspension (1 μm), and (300 nm) on Buehler felt pads and then ultrasonically cleaned for 15 minutes in doubly deionised water to remove any alumina residues. A thin-film electrode was prepared by mixing homemade KB carbon supported platinum powder 10 mg with 100 μL Nafion (5 %) and ethanol (900 μL). The platinum loading on the GC electrode was varied in the range [50 - 220 $\mu g/cm^2$ (22 wt % Pt/KB)]. The solution in the electrochemical cell was a buffer solution (*pH 2.5, Potassium hydrogen phthalate, and 100 mM*). ORR voltammograms were recorded in the potential range of 0 – 900 mV *vs.* at a scan rate of 5 mV/s for different Pt loading. All electrochemical tests were carried out at room temperature.

Polarisation curve

When the OCV was stable, polarisation curves were obtained by connecting the anode and cathode with external resistances (100 Ω to 100 KΩ), the potential was recorded at each resistance every 5 min or using a potentiostat, which can control the cell voltage or potentials at the desired level and measures the current. The power obtained was converted to power density, P (mW/m^2), according to $P = IV/A$, where

I (mA) is current, V (mV) is the voltage and A (m^2) the projected surface area of anode electrode (5 cm^2), the resulting current I (mA) was converted to current density, I (mA/m^2).

3.8 Power and coulombic efficiency as a function of glucose concentration

Glucose concentration

The concentration of glucose before and after each batch cycle (*duplicate samples*) was measured using the phenol-sulphuric method with glucose as standard. A series of standard glucose solutions were prepared containing 5 µL to 50 µL from the stock glucose solutions (*1000 mg/L by dissolving (1 g) of glucose filled up to 1000 mL with deionised water*).[16]

Power generation

Power production from a variety of concentrations of glucose was tested in the two-chamber MFC. For the tests with glucose at various concentrations, the anode chamber consisted of pure cells of *Acidiphilium* sp. SJH (5.1 x 10^7 cells/ml) and ferric ion (20 mM) in (*potassium hydrogen phthalate, 100 mM*) buffer solution pH 2.5 containing (360 – 1800 mg/L) of glucose. The cathode was made of 150 µg/cm^2 (22 wt % Pt/KB) coated on one side of the wet-proofed carbon cloth 5 cm^2 in buffer solution pH 2.5 (potassium hydrogen phthalate, 100 mM). The OCV was used to record the current based on the relationship between voltage and current at a given resistance ($I = V/RA$). Power density was obtained according to $P = IV/A$, and its polarisation curve. The optimal external resistance was found which showed the maximum power density.

Coulombic efficiency

The CE is correlated to the amount at which substrate is consumed by microorganisms and the transfer of electrons and protons in the MFC can be used for electricity production. CE is defined as the ratio of the number of coulombs recovered as electrical current versus the theoretical maximum number of coulombs recoverable from the initial organic matter added to the system.

$$C_E = \frac{Coulombs\ recovered}{Total\ coulombs\ in\ substrate}$$ *Equation 3-3*

pH of the anode chamber

A series of tests were conducted to study the effect of a variation of the pH (2.5, 3.5 and 4.5) on voltage, current density and power density. Using the two-chamber MFC system with cells of *Acidiphilium* sp. SJH (5.1 x 10^7 cells/ml), ferric ion, and buffer solution (*pH 2.5 ,potassium hydrogen phthalate, 100 mM*) referenced to the anode (*carbon cloth non wet proofing, or carbon felt 5 cm*^{2}) that oxidises glucose (10 mM). The cathode chamber was filled with buffer solution pH 2.5 (potassium hydrogen phthalate, 100 mM) with a platinum sheet (1 cm^2) as a cathode electrode. The OCV was used to record the current based on the relationship between voltage and current at a given resistance ($I = V/RA$). Power density was obtained according to $P = IV/A$, and its polarisation curve. The optimal external resistance was found which showed the maximum power density. During this operation, the anode chamber was purged with nitrogen while the cathode chamber was purged with air.

Effect pH changes in a microbial fuel cell using non-buffered solution

A set of experiments were performed using cells of *Acidiphilium* sp. SJH bacteria (5.1 x 10^7 cells/ml), glucose 1800 mg/L, and 10 mM ferric ion to measure pH changes, which was compared to that of the buffer solutions pH 2.5 experiment using Potassium hydrogen phthalate 100 mM.

Electrode potential

Open circuit potential (OCP) were measured of the electrodes (*anode and cathode*) of the MFC against a saturated calomel electrode, as a function of current with different resistor circuit (100 Ω to 100 KΩ).

The Pt loading on microbial fuel cell performance

Power production from a variety of platinum content was tested in the two-chamber MFC. Cells of *Acidiphilium sp. SJH* (5.1 x 10^7 cells/ml), ferric ion (20 mM), and buffer solution pH 2.5 (*potassium hydrogen phthalate, 100 mM*) were referenced to the anode (*carbon cloth non wet proofing 5 cm*^{2}) that oxidises glucose (10 mM). The platinum cathode consisted of various ranges [50 – 220 μg/cm^2 (22 wt % Pt/KB)],

coated on one side of the wet-proofed carbon cloth 5 cm^2 in buffer pH 2.5 (*potassium hydrogen phthalate, 100 mM*). A series of experiments examined the effect of different platinum contents recorded at power density. During this operation, the anode chamber was purged with nitrogen while the cathode chamber was purged with air.

Effect of cathode surface area on voltage generation

Different platinum cathode surface areas (1 cm^2, and 2 cm^2) were used for comparing voltage generation. Using the two-chamber MFC H-type design; the anolyte consisted of pure cells of *Acidiphilium* sp. SJH (5.1 x 10^7 cells/ml) ferric ion (20 mM), and glucose (10 mM). The catholyte was filled with buffer solution pH 2.5 (*potassium hydrogen phthalate, 100 mM*) with the Pt cathode at various surface areas (1 cm^2, and 2 cm^2). A series of experiments were conducted to study the effect of surface areas recorded in an OCV. During this operation, the anode chamber was purged with nitrogen while the cathode chamber was purged with air.

3.9 Aqueous cathodes using different electron acceptor

Effect of Potassium permanganate as the cathodic electron accepter

An aqueous catholyte of Potassium permanganate was used in the acidic medium of the two-chamber MFCs H-type design (Figure 3.3).

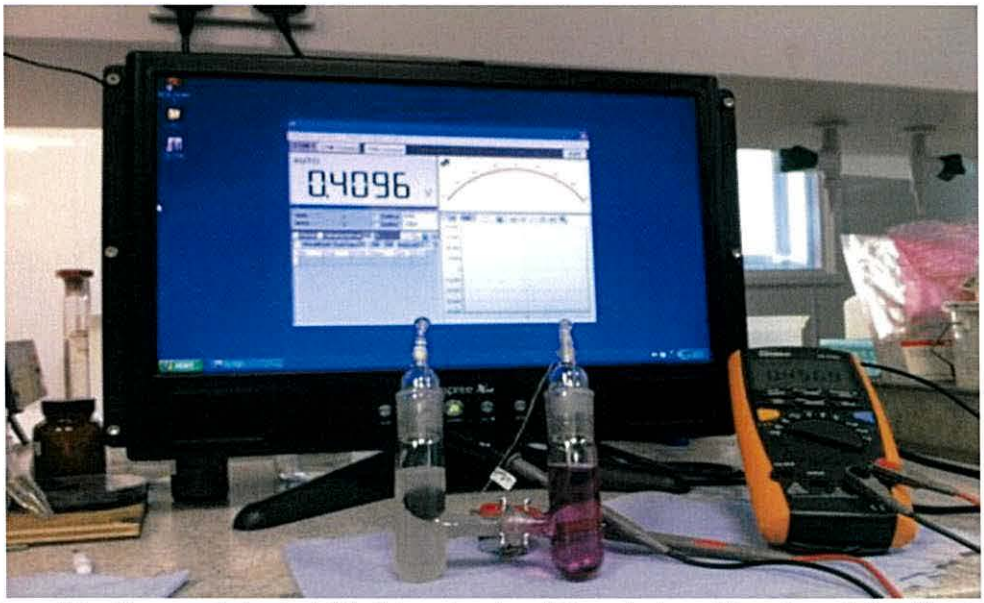

Figure 3.3 - Homemade bacterial fuel two-chamber H-type design with carbon cloth without wet proofing 5 cm^2 (anode) and carbon cloth wet-proofed carbon cloth 5 cm^2 (cathode) electrodes.

The anolyte consisted of pure cells of *Acidiphilium* sp. SJH (5.1 x 10^7 cells/ml) ferric ion (10 mM), and glucose (10 mM). The MFC was examined for OCV and cathode potential. A series of experiments were conducted to study the effect of different pH catholyte (2, 3.5, and 9) and various initial concentration of permanganate (20, 100, and 200 mg/L) respectively. They were recorded on OCV with cathode potential. A 10 mM Potassium permanganate (*B.D.H Laboratory Reagent*) solution was prepared by dissolving (150 mg) in 100 ml deionised water. Cathodic samples were fixed and dried overnight (25 °C) in a vacuum oven, followed by a direct examination. All experiments run in triplicate. The cathode surfaces were studied using SEM.[17]

Effect of Chromium [Cr (VI)] as the cathodic electron accepter

The two-chamber MFC system H-type design consisted of two glass tubes. The anode chamber (*carbon cloth non wet-proofed*) consisted of pure cells of *Acidiphilium* sp. SJH (5.1 x 10^7 cells/ml), ferric ion (10 mM), and glucose; 10 mM in (*potassium hydrogen phthalate, 100 mM*) with a buffer solution of pH 2.5. An aqueous catholyte of hexavalent chromium was used in the acidic medium with carbon cloth - wet-proofed. A 1000 mg/L hexavalent chromium (*B.D.H Laboratory Reagent*) solution was prepared by dissolving (2.83 g $K_2Cr_2O_7$) in 1 L deionised water. During the operation, the anode chamber and cathode chamber were purged with nitrogen for 30 min to remove oxygen. The MFC was examined for OCV and cathode potential under different pH catholyte (2, 3, 4, and 5) and various initial concentration of hexavalent chromium (20, 100, and 200 mg/L) respectively. All experiments run in triplicate).

Comparison Study

Using permanganate, hexavalent chromium, and oxygen as different electron acceptor and two electrodes carbon cloth, and [0.15 mg/cm^2 (22 wt % Pt/KB)], coated on one side of the wet-proofed carbon cloth 5 cm^2 in cathode chamber were tested.

3.10 Effect of different cathode materials on open circuit potentials

The OCPs produced using different cathode material (*carbon cloth, carbon felt, and carbon Ketjen Black EC 600J*) with same total cathode surface areas, (5 cm^2) were compared and examined in electrochemical tests.

Air cathode

A comparison of the MFCs performance was tested for power generation. Hence, two MFCs were obtained; the first cell was supplied with oxygen; the second cell was supplied with air (*as an external source of electron acceptors*). The anode chamber (*carbon cloth non wet-proofed)* consisted of pure cells of *Acidiphilium* sp. SJH (5.1 x 10^7 cells/ml), ferric ion (10 mM), and glucose (10 mM) in a buffer solution of pH 2.5 (*potassium hydrogen phthalate, 100 mM*). The cathode was made up of 0.15 mg/cm^2 (22 wt % Pt/KB) coated on one side of the wet-proofed carbon cloth in a buffer solution of pH 2.5 (*potassium hydrogen phthalate, 100 mM*). The cell design was two-chamber MFCs (*Sandwich design*).

3.11 Electrode Spacing

The two-chamber air cathode MFC was fabricated from polyacrylic plastic cylindrical (*3 cm in diameter*); (figure 3.4) spacing between the anode and cathode was varied (4 to 2 cm) in order to investigate the effect of decreasing the distance between the electrodes on power output. For the tests, the anode was made of carbon cloth (5 cm^2), and the cathode was made of 150 µg/cm^2 (22 wt % Pt/KB) coated on wet-proofed carbon cloth, (*coated side*) placed facing the solution, with the uncoated side exposed to the air. The anode was moved to a distance of 3 cm from the cathode, with either the anode exposed to both sides of the fluid with the total chamber distance of 4 cm (figure 3.4), or set at 2 cm fixed against a wall in a chamber 2 cm long (figure 2.5). The electrode spacing between the anode and the cathode was set at 4, 3 or 2 cm, resulting in a reactor empty bed volume of 28 ml, 28 ml and 14 ml respectively.

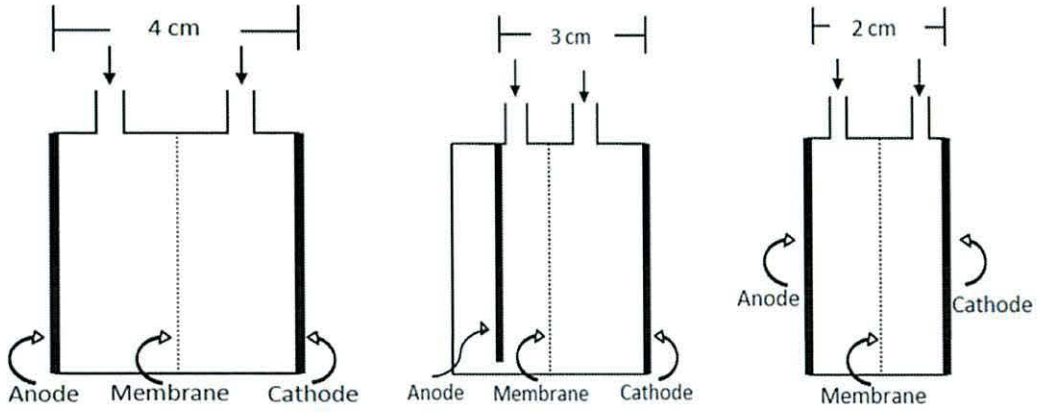

Figure 3.4 - MFC configurations showing different electrode spacing.

3.12 Preparation of the modified anode

A series of tests were conducted to study the effect of electrode spacing (4, 3 and 2 cm). All MFCs were tested for power generation using Cells of *Acidiphilium* sp. SJH (5.1 x 10^7 cells /ml) and ferric (10 mM) ion referenced to the anode. The cathode chamber was filled with a buffer solution of pH 2.5 (*potassium hydrogen phthalate, 100 mM*). During the operation, the anode chamber was purged with nitrogen while the cathode chamber obtained the oxygen from the atmosphere. Each test was repeated three times. The system was run until stable OCV was obtained. Polarisation curve power density curves were obtained by connecting the anode and cathode with external resistances (100 Ω to 100 KΩ), the potential was recorded for each resistance every 5 min or by using a potentiostat, recording maximum power over the complete cycle of the operation.

Construction of the microbial fuel cell for the anodic biofilm

Three single-chamber MFCs were fabricated in the laboratory using a polyacrylic plastic cylindrical chamber 4 cm long by 3 cm in diameter. The anode consisted of a non-wet-proofed carbon cloth (*Fuel Cell Store USA*), and carbon felt (*Fisher Scientific UK*) with a surface area of 5 cm^2. The cathode consisted of Pt/KB (150μg/cm^2) (*Akzo Nobel*) coated on one side of the wet-proofed carbon cloth, also with a surface area of 5 cm^2.

The biofilm on the surface of the anode was originated from laboratory substrate (glucose). The growth medium was made up as stated in media and growth conditions.

For the bacterial studies, carbon cloth (5 cm^2); carbon felt (5 cm^2) soaked in 200 mM H_2SO_4 for 24 h, pH 2.5, was used as the anode for the development of biofilm. The carbon cloth and carbon felt were inoculated with the cell suspension of SJH bacteria for a period of 7, 21 and 30 days. Anode associated biofilm growth experiments were carried in acidic medium (pH 2.5). Cell suspension of SJH bacteria was replaced once in 10 days. The sample was dried in a desiccator overnight before the imaged with SEM. *Acidiphilium* SJH bacterial (*stationary phase*) growth on the surface of the anode (*carbon cloth, carbon felt)* were evaluated using a SEM.

To examine the effect of the attached *Acidiphilium* sp. SJH bacteria, after 2 weeks of operation the anode was inoculated with the cell suspension of SJH bacteria, separated and inserted into the MFC with no attached *Acidiphilium* sp. SJH bacteria. Hence, two MFCs were obtained, the first cell contained a carbon cloth electrode and suspended bacteria in the anode solution, and the second cell contained the carbon cloth electrode with attached *Acidiphilium* sp. SJH bacteria from the preceding period and a new clear medium, as performed previously. The voltage and current density were measured simultaneously in order to calculate power density.

Using CV for the analysis of the anode-associated biofilm

Cyclic voltammetry was used to characterise the oxidation reduction reactions on the anode electrode surface by measuring the current response at an electrode surface to a specific range of potentials in an unstirred solution. The working electrode was 5 cm^2 carbon cloth or carbon felt electrodes colonised with *Acidiphilium* sp. SJH bacterial cells. Cyclic voltammetry was examined by applying a potential ramp at a scan rate of 5 mV/s over the potential range -800 and 800 mV to the working electrode (*anode*). The electrochemical cell was purged with nitrogen for 30 min.

Poised potential electrode

This study was used specifically to test the influence of a poised potential on the response of the anode-associated biofilm. The operated the MEC; the working electrode was 5 cm^2 carbon cloth or carbon felt electrodes were colonised with SJH bacterial cells with the anode potential poised at -200,-400,-600 mV. The production current was examined over time.

Anode materials

In the two-chamber MFC and single-chamber MFCs, non-wet proofed carbon cloth (*Fuel Cell Store USA*) and carbon felt (*Fisher Scientific UK*) were used as anode materials.

Cathode material

Cathode electrodes were prepared in the laboratory. Wet-proofed carbon cloth (*Fuel Cell Store USA, thickness 1 mm, and the area 5 cm^2*) was used as substrate, and a Pt

catalyst (22 wt % Pt/KB) was mixed with 5 % Nafion solution (*7 μL Nafion per mg platinum catalyst*) coated on one side of the carbon cloth (*a wet-proofed carbon cloth and a solid platinum electrode, thickness 1 mm and the area 1 cm^2*).

3.13 References

1. Dulal, S. M. S. I.; Won, M. S.; and Shim, Y. B. Characterization of Platinum Nanoparticles Electrodeposited on Carbon Felt. *J. Sci. Res.* **2010**, *2*, 303 - 312.
2. Niu, L.; Li, Q.; Wei, F.; Chen, X.; Wang, H. Formation optimization of platinum-modified polyaniline films for the electrocatalytic oxidation of methanol. *Synth. Met.* **2003**, *139*, 271 - 276.
3. Rimbu, G. A.; Stamatin, I.; Jackson, C. L.; Scott, K. The morphology control of polyaniline as conducting polymer in fuel cell technology. *J. Optoelectron Adv. Mater.* **2006**, *8*, 670 - 674.
4. Johnson, D. B.; Bridge, T. A. M., Reductive dissolution of ferric iron minerals by *Acidiphilium* SJH. *Geomicrobiol. J.* **2000**, *17*, 193 - 206.
5. Skoog, D. A.; West, D. M.; Holler: F. J. *Fundamentals of Analytical Chemistry*, Saunders College Publishing, Fort Worth, US. 1992.
6. Lovely, D. R. and Phillips, E. J. P. Rapid assay for microbially reduced ferric iron in aquatic sediments. *Appl. Environ.Microbiol.* **1987**, *53*, 1536 - 1540.
7. Lee, S. A.; Choi, Y.; Jung, S.; Kim, S. Effect of initial carbon sources on the electrochemical detection of glucose by Gluconobacter oxydans *Bioelectrochem.* **2002**, *57*, 173 - 178.
8. Choi, Y.; Jung, E.; Kim, S.; Jung, S. Membrane fluidity sensoring microbial fuel cell. *Bioelectrochem.* **2003**, *59*, 121-127.
9. Liu, H.; Cheng, S.; Logan, B. E. Production of Electricity from Acetate or Butyrate Using a Single-Chamber Microbial Fuel Cell. *Environ. Sci. Technol.* **2005**, *39*, 658 - 662.
10. Logan, B. E.; Hamelers, B.; Rozendal, R.; Schroder, U.; Keller, J.; Freguia, S.; Aelterman, P.; Verstraete, W.; and Rabaey, K. , Microbial Fuel Cell: Methodology and Technology. *Environ. Sci. Technol.*, **2006**, *40*, 5181 - 5192.
11. Cho, E. J. Ellington, A. D. Optimization of the biological component of a bioelectrochemical cell. *Bioelectrochem.* **2007**, *70*, 165 - 172.
12. Castilla, C. M.; Garcia, M. A. F.; Joly, J. P.; Toledo, I. B.; Marin, F. C.; Utrilla, J. R. Activated carbon surface modifications by nitric acid, hydrogen peroxide, and ammonium peroxydisulphate treatments, *Langmuir* **1995**, *11*, 4386 - 4392.
13. Lakshmi, N.; Rajalakshmi, N.; and Dhathathreyan, K. S. Functionalization of various carbons for proton exchange membrane fuel cell electrodes: analysis and characterisation. *J. Phys. D: Appl. Phys* **2006**, *39*, 2785 - 2790.
14. Rimbu, G. A.; Jackson, C. L.; Scoti, K. Platinum/ carbon/ polyaniline based nano composites as catalysts for fuel cell technology. *J. Optoelectron Adv. Mater.* **2006**, *8*, 611 - 616.
15. Cheng, S.; Liu, H.; and Logan, B. E. Power Densities Using Different Cathode Catalyst(Pt and CoTMPP) and Polymer Binders (Nafion and PTEF) in Single Chamber Microbial Fuel Cells *Environ. Sci. Technol.* **2006**, *40*, 364 - 369.
16 Dubois, M. M.; Gilles, K. A.; Hamilton, J. K.; Rebers, P. A.; and Smith, F. Colorimetric Method for Determination of Sugars and Related Substances. *Anal. Chem.* **1956**, *28*, 350 - 356.
17. You, S.; Zhao, Q.; Zhang, J.; Jiang, J.; Zhao, S. A microbial fuel cell using permanganate as the cathodic electron acceptor. *J. Power Sources,* **2006**, *162*, 1409 - 1415.

Chapter 4

EVALUATION OF THE MICROBIAL FUEL CELL

4.1 Introduction

Within this chapter the performance of the MFC was tested for power output, current density and rate of substrate combustion. The most important factors are the material and design of the reactor. Two different designs of MFCs are presented in this chapter the H-type and sandwich type.

4.2 Development of a batch mode microbial fuel cell

Electrochemistry study of carbon felt by cyclic voltammetry

Cyclic voltammograms of an oxygenated solution of 1.0 M H_2SO_4 have been shown to illustrate the effectiveness of purging the electrochemical cell with nitrogen to remove any oxygen from the cell as the presence of oxygen will mask the detection of the ion peak. Figure 4.1 shows cyclic voltammograms of 1.0 M H_2SO_4 on a carbon felt electrode with and without the presence of oxygen. Figure 4.1 also illustrates the removal of oxygen by deoxygenating with N_2 for 20 minutes. If the potential range is sufficiently limited, a very clean voltammogram can be obtained.[1]

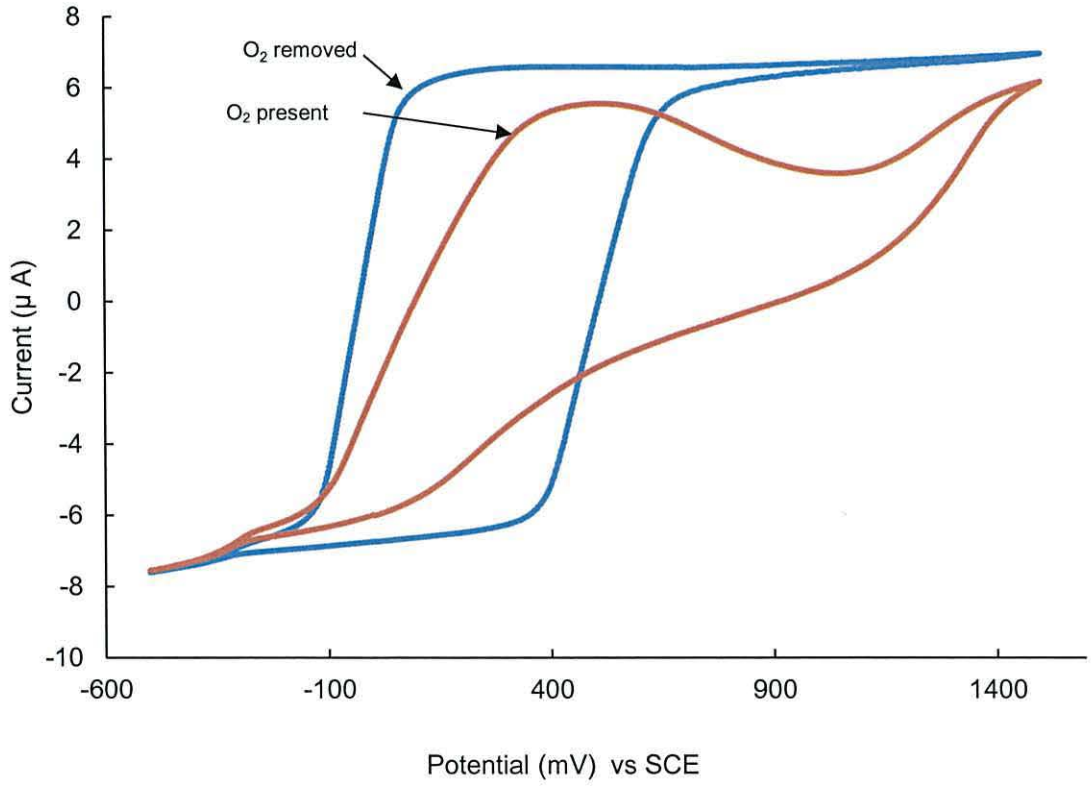

Figure 4. 1 - Cyclic Voltammogram of 1.0 M H_2SO_4 showing effect of O_2. Oxygen removed by sparging with nitrogen gas for (20 min). Carbon felt electrode, 50 mV scan rate.

Study of ferricyanide on cyclic voltammetry

To investigate the kinetics of the $K_3Fe(CN)_6/K_4Fe(CN)_6$ redox reaction qualitatively, the cyclic voltammograms at the following rates 25, 50, 75, 100, 150,and 200 mV/s are shown in (Figure 4.2); for a GC working electrode in a solution containing 4 mM $K_3Fe(CN)_6$ as the electro active species in 1 M KNO_3 as a supporting electrolyte. The shape of the cyclic voltammogram is dependent on the electron transfer kinetics and diffusional mass transport. The effect of scan rate on the shape voltammograms can be clearly seen. The voltammograms have a quasi-reversible shape with one electron transfer reaction with peak separations, more than 60 mV, which increases with potential scan rates.[2] However, the $K_3Fe(CN)_6$ species shows the lowest value of peak separations 70 mV close to a reversible system, which becomes slightly broader with potential scan rates, showing that the $K_3Fe(CN)_6$ species redox reaction would be fast.

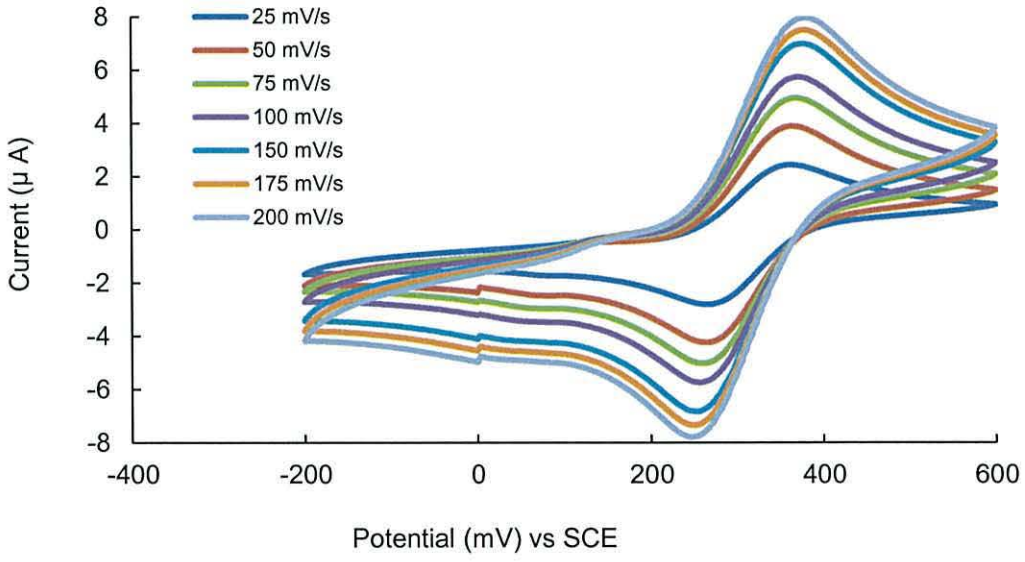

Figure 4. 2 - Cyclic Voltammograms recorded at different potential scan rates at a GC *electrode for 4 mM $K_3Fe(CN)_6$ in 1 M KNO3. Scan rate = 25, 50, 75, 100, 150, and 200 mV/s.*

From a cyclic voltammogram the cathodic and anodic peak current (i_{pc} *and* i_{pa}) can be measured. The ratio of the peak current (i_{pc} *and* i_{pa}) is equal to one, this is indicative of a reversible system. From the Randles- Sevcik[3]equation 4.1, cathodic and anodic peak current (i_{pc} *and* i_{pa}) increases as a function of square root of scan rate($v^{\frac{1}{2}}$). The same redox reaction of the $K_3Fe(CN)_6$/ $K_4Fe(CN)_6$ as deduced by the proportionality between the anodic peak current i_{pa} and cathodic peak current

(i_{pc}) vs square root($v^{\frac{1}{2}}$) of the scan rate can be seen in (Figure 4.3). A linear response is suggestive of relatively fast electrode kinetics and a diffusion controlled reaction.

$$i_p = (2.69 * 10^5) n^{\frac{3}{2}} A D^{\frac{1}{2}} C v^{\frac{1}{2}} \qquad \textit{Equation 4-1}$$

Where i_p is peak current (A), n is electron stoichiometry, A is electrode area (cm^2), D is diffusion coefficient (cm^2/s), C is concentration (mol/ cm^3), and υ is scan rate (V/s).

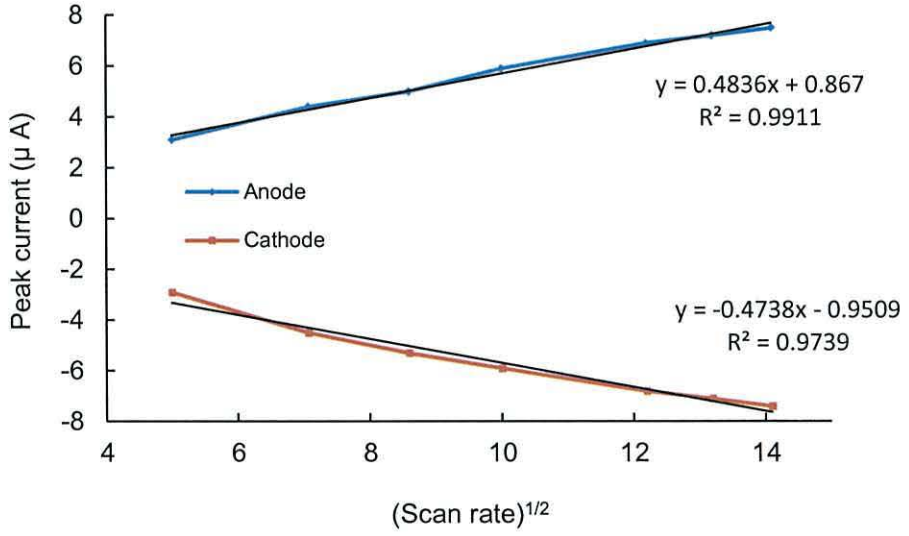

Figure 4. 3 - Plots of the anodic(■) and cathodic(♦) peak current vs. the square root of scan rate ($v^{\frac{1}{2}}$) *for the oxidation and reduction processes of the* $K_3Fe(CN)_6$.

Ferric ion reductions by *Acidiphilium* SJH bacteria

The ability of *Acidiphilium* SJH bacteria to reduce ferric ion using glucose as the energy source was estimated utilising a ferrozine reagent.[4] The ferrous iron concentration was estimated at regular intervals spectrophotometrically with the ferrozine reagent. Figure 4.4 shows that the SJH bacteria over a period of 15 hours incubation completely reduced the available ferric ion; confirming that an *Acidiphilium* SJH bacterium was enzymatically mediated and ferric ion could act as an electron shuttle.[5] Previous work reported was similar to that shown in figure 4.4.[6] This suggests a probability that ferric ion is more effective when competing for the electron at the space of periplasmic (*gram-negative bacteria is the space in between the cytoplasmic and outer membranes*). (Table 4.1) The proportionality between the ferric ion reduction and time was observed during which there was no visible change

in cell optical density. The anaerobic condition for the *Acidiphilium* SJH bacteria is more efficient when reducing the ferric ion but is not efficient in growing bacteria cells.[7,8]

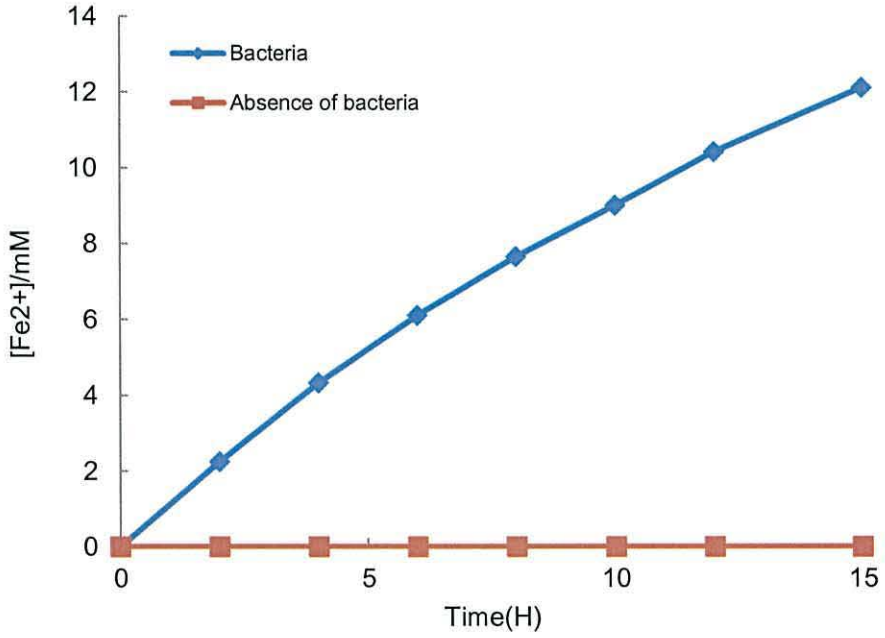

Figure 4. 4 - Ferric ion reduction by washed cell suspensions of Acidiphilium SJH incubated under anaerobic condition as a function of time, (■) with or (♦) in absence of bacteria.

Table 4. 1 - The effect of anaerobic condition on growth and ferric ion reduction by washed cell suspensions of Acidiphilium SJH, 540mg/L glucose.

Time (H)	*Concentration Ferrous iron*	*Optical density*
0	0	0.48
2	2.24 mM	0.51
6	6.13 mM	0.55
15	12.16 mM	0.56

A series experiments were carried out to examine the role of electron donor on the rate of reduction iron by *Acidiphilium* SJH bacteria. Ferrous iron concentration was estimated at regular intervals spectrophotometrically with the ferrozine reagent.[4] Figure 4.5 on the following page, shows differences in the rate of ferric iron reduction and that the amount ferrous ion which was obtained by *Acidiphilium* SJH had little effect on the specific rate of ferric iron reduction; with the amount being similar when either glucose or glycerol was supplied.

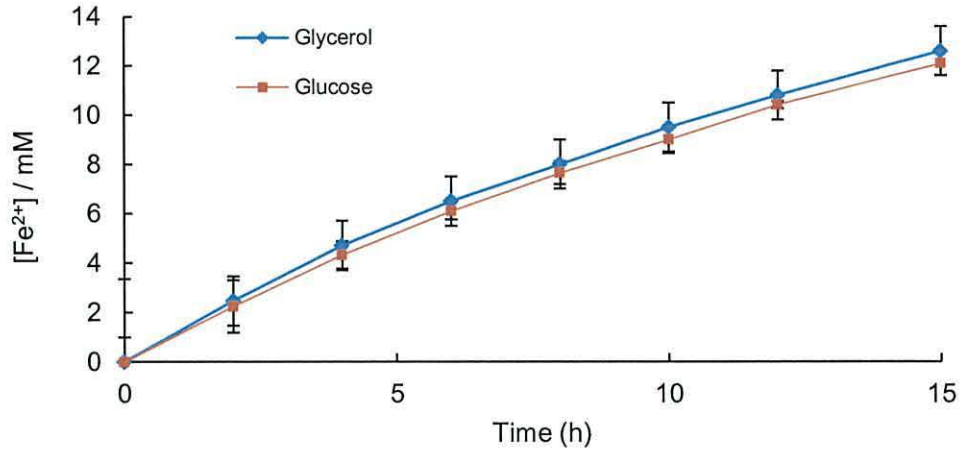

Figure 4. 5 - Ferric ion reduction by washed cell suspensions of Acidiphilium SJH incubated under anaerobic condition as a function of time, using glucose and glycerol as electron donor.

Using CV for the analysis of ferric reduction by *Acidiphilium*

After illustrating that *Acidiphilium* SJH bacteria was capable of reducing the ferric ion, cyclic voltammetry was used for the electrochemical characterisation of the reduced iron. Voltammograms for *Acidiphilium* SJH bacteria where recorded to illustrate the reduction of the soluble ferric ion (*ferric ion and their reduced forms ferrous ion*), the important variations in oxidation-reduction peaks and positions over a period of time under anaerobic conditions illustrated in (Figure 4.6).

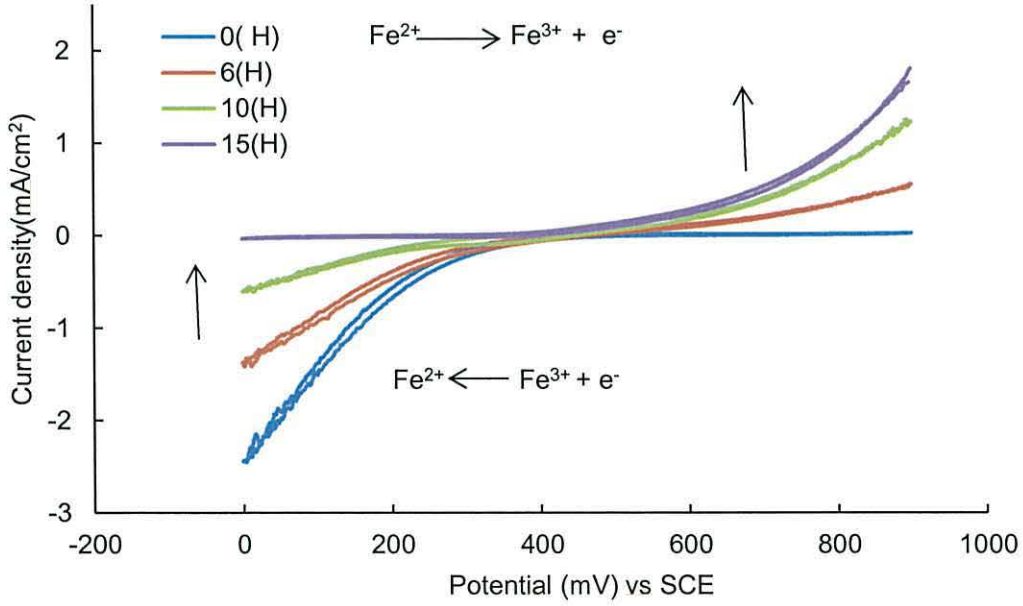

Figure 4. 6 - Cyclic voltammograms are shown rate of reduction Ferric ion in Acidiphilium SJH cells as a function of time, in 500 mM H_2SO_4 at scan rate 5mV/s.

The voltammogram for the Ferric/Ferrous couple (0 h) had no observable oxidation peak, and the reduction peak was at 0 mV (*vs.* SCE; -2.4 mA/cm^2) in the reverse scan, while the voltammogram for the Ferric/Ferrous couple (6, and 10 h) recorded an oxidation peaks at 900 mV (*vs.* SCE; 0.55 mA/cm^2, 1.3 mA/cm^2) in the forward scan and reduction peaks at 0 mV(*vs.* SCE; -1.3 mA/cm^2, -0.57 mA/cm^2) in the reverse scan. The voltammogram for the Ferric/Ferrous couple (15 h) recorded an oxidation peak at 900 mV (*vs.* SCE; 1.74 mA/cm^2) in the forward scan and had no observable reduction peak in the reverse scan, clearly illustrating the reduction of the soluble ferric ion.

4.3 Analysis of two-chamber H-type system

Operating mechanism of microbial fuel cell

A series of experiments were carried out to examine the role of soluble ferric ion as an electron shuttle in the MFC operating at pH 2.5. Electrons obtained from the oxidation of glucose in the presence of *Acidiphilium* sp. SJH bacteria are transferred to the anode with the aid of a soluble ferric ion. Glucose oxidation by *Acidiphilium* sp. SJH bacteria coupled with ferric reduction can be explained by the following reaction.[9]

$$24Fe^{3+} + C_6H_{12}O_6 + 6H_2O \Rightarrow 6CO_2 + 24Fe^{2+} + 24H^+ \qquad \textit{Equation 4-2}$$

The reduced iron is oxidised at the anode, giving a ferric ion as follows:

$$Fe^{2+} \Rightarrow Fe^{3+} + e^- \qquad \textit{Equation 4-3}$$

Electrons are transferred to the cathode chamber through an external electric circuit, and protons are transferred through the membrane to the cathode. Here they react with oxygen and electrons to form water with the production of electricity as a by-product.

$$O_2 + 4e^- + 4H^+ \Rightarrow 2H_2O \qquad \textit{Equation 4-4}$$

Effect of growing condition of Acidiphilium

The growth of *Acidiphilium* sp. SJH cells and their reduction capacity of ferric ion were compared between the growth of *Acidiphilium* sp. SJH bacteria in normal growth conditions and in generating an electricity system using MFC. Figure 4.7 shows that in the metabolism of *Acidiphilium* sp. SJH cells, cell optical density was

much higher, but the rate of reduction of the ferric ion was lower in the normal growing cells that were not coupled to the electrical generation system than in the presence of the generation of electricity system.

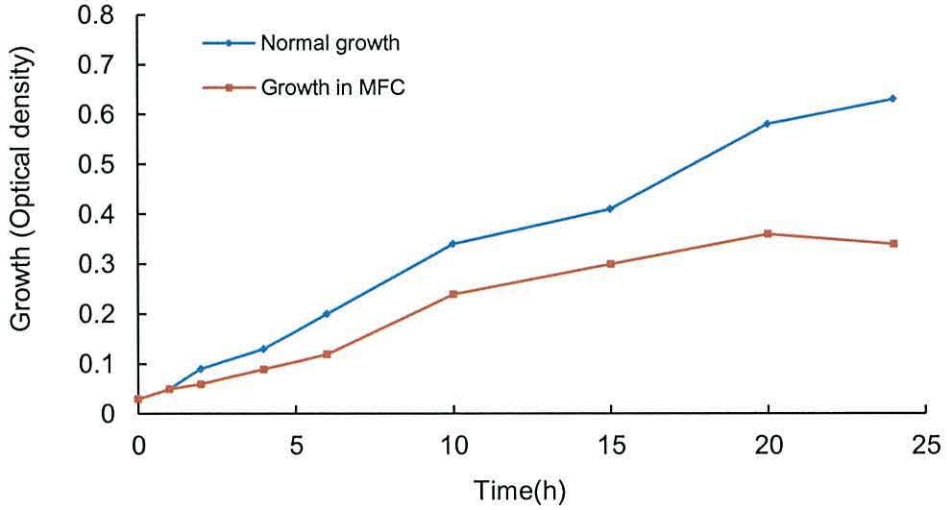

Figure 4. 7 - Growth Acidiphilium sp. SJH growing cells with glucose as electron donor and ferric iron as electron shuttle under anaerobic condition.

When growing *Acidiphilium* sp. SJH cells containing ferric ion in normal growth conditions a significant amount of ferrous ion was not detected because of the presence of oxygen which was a much better electron acceptor than the ferric ion. However, sparging anode chamber containing growing cells of *Acidiphilium* sp. SJH with nitrogen gases, the amount of cell density was reduced but the amount of ferrous ion was increased (figure 4.8).

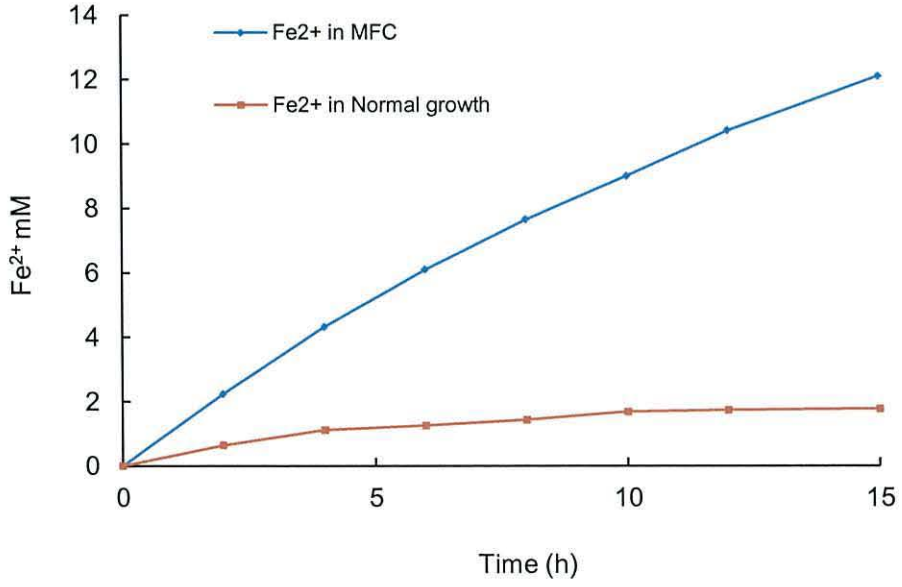

Figure 4. 8 - Ferric ion reduction by Acidiphilium SJH in normal growth conditions and in MFC with generation electricity.

These results suggest that the experiments under aerobic conditions, a significant amount of ferrous ion was not detected because ferric ion is not effective when competing for the electron at the space of periplasmic since presence oxygen, it had more redox potential than the ferric ion. However, the experiments under anaerobic conditions that ferric ion is more efficient when competing for the electron at the cell interaction.

Study of the effect of different concentration of ferric ion

MFCs were tested with different concentrations of ferric ion (1 mM, 5 mM, and 10 mM) to establish the voltage generation. Figure 4.9 shows voltage generation versus time curve for MFCs containing *Acidiphilium* sp. SJH cells (5.1 x 10^7 cells/ml) in the presence of different concentration of ferric ion (1 mM, 5 mM, and 10mM) as the electron shuttle and glucose (1800 mg/L) as the electron donor referenced to the anode. The cathode was made of a solid platinum electrode supplied with oxygen in buffer solution pH 2.5.

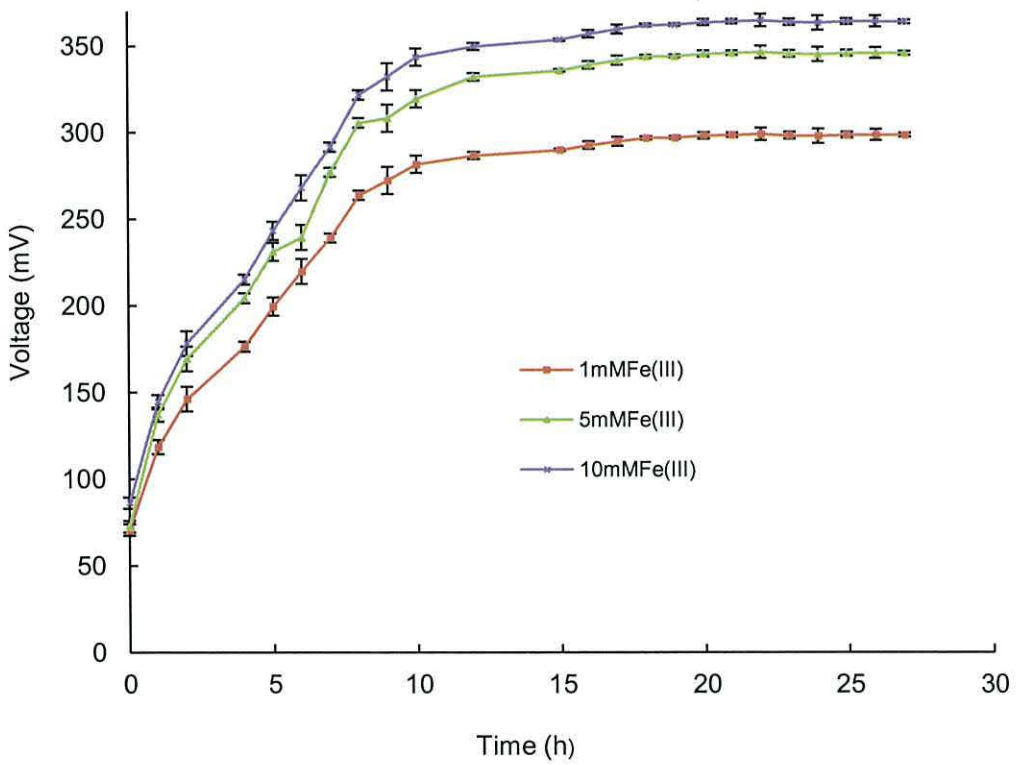

Figure 4. 9 - Voltage as a function of time of Acidiphilium sp. SJH cells in MFCs with different concentrations of Fe (III), experiments run in triplicate (Error bars equal ±1 SD).

As figure 4.9 shows, low ferric ion concentration (1 mM) has a limited electron shuttle effect, but a more concentrated solution of ferric ion gives maximum OCV (364 mV) and a good mediating effect (10 mM). No further improvement is detected

for the higher concentration of ferric ion. Previous work reported the use of ferric ion as electron shuttle with *Acidiphilium cryptum* as a biocatalyst operating at pH ≤ 4.[10] The results demonstrated that *Acidiphilium cryptum* was generating electricity using the ferric ion as the electron shuttle was similar to that shown here. Tests were run in triplicate and results averaged.

Open circuit voltage

Voltage generation was recorded from *Acidiphilium* sp. SJH bacteria (5.1 x 10^7 cells/ml) in an H-type MFC when there is no external load, in the presence of glucose (900 mg/L) as the electron donor and soluble ferric ion (10 mM) as the electron shuttle called OCV. The magnitude of the OCV over time for the MFC is illustrated in (Figure 4.10).

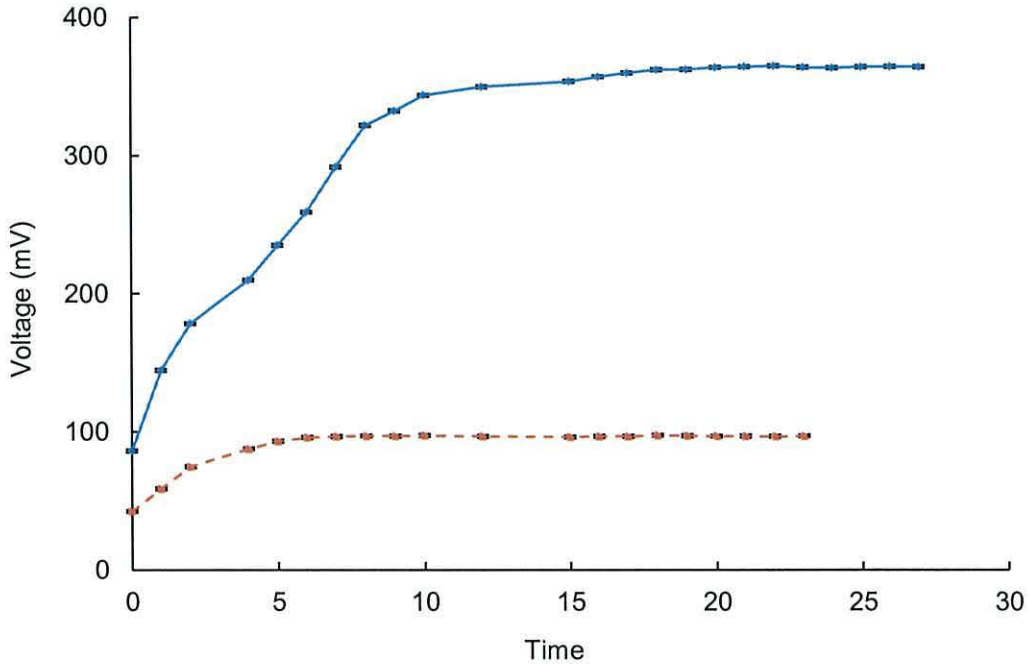

Figure 4. 10 - The resulting MFC voltage generation over time with (solid line) and without (dashed line) using Acidiphilium sp. SJH bacteria, experiments run in triplicate (Error bars equals ±1 SD).

The initial voltage in both cases was less than 100 mV, which was due to a capacitive charge at the electrodes which can be seen when abiotic control (*no bacteria*) are present, increasing with time and reaching a steady state after approximately 20 hours. Figure 4.10 also shows that a maximum OCV of 364 mV was reached over 18 hours, while that of the abiotic control was only 96 mV, at which point the voltage remained constant. These tests explained that *Acidiphilium* sp. SJH bacteria are

characterised by their use of a soluble ferric ion to couple cytoplasmic membrane electron exchange to electron transfer at the anode. This confirms that an *Acidiphilium* sp. SJH bacteria reduced ferric ion looks to be mediated by an enzyme system coupled to the bacterial cells. The position of this "iron reductase" is not currently known, it would be outside of the cell membrane, for example, in the periplasmic space.[5]

Polarisation curve

Polarisation and power density curves were obtained to calculate the maximum power densities and current densities for the MFC utilising *Acidiphilium* sp. SJH bacteria (5.1 x 10^7 cells/ml), in the presence of glucose (1800 mg/L) as the electron donor and soluble ferric ion (10 mM) as electron shuttle (Figure 4.11).

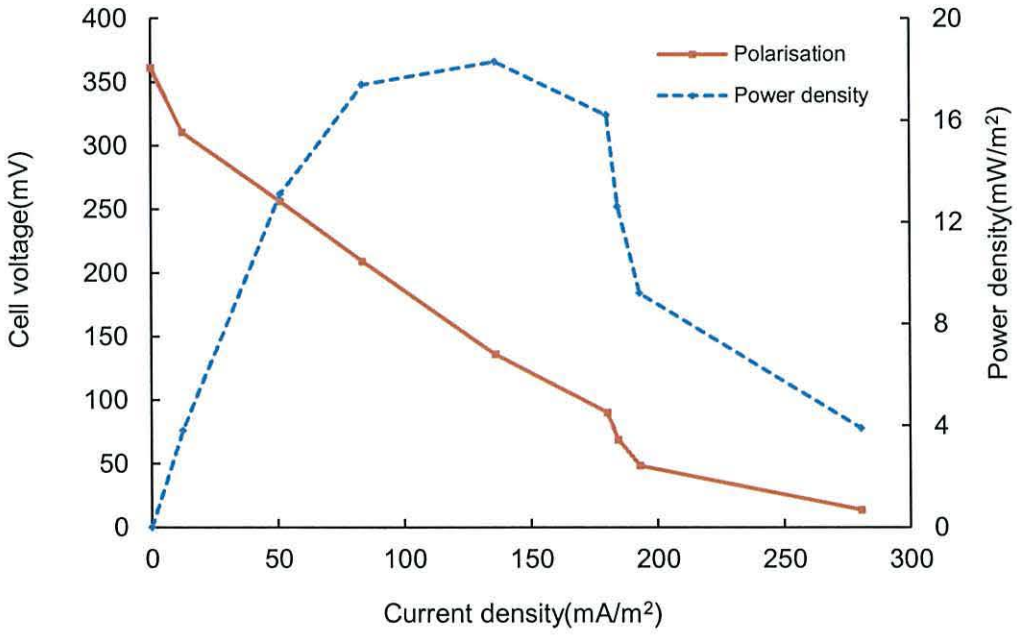

Figure 4. 11 - Power density (dashed line) and voltage (solid line) generated by the MFC as a function of current density, utilising an anodic carbon cloth and a cathodic Pt sheet.

When the OCV of MFC was reached the maximum voltage and stabilized. MFC polarisations were operated with different resistance across the anode and cathode, under optimal conditions (*pH 2.5, room temperature*). The potential was tested at each resistance and converted to power densities. The current density was determined using Ohms law based on the MFC voltage. From these measurements, the optimal external resistance was found (2000 Ω) which showed the maximum power density. The cell current and voltage data can be examined and recorded at the

maximum power density. As expected, during the operation period of the *Acidiphilium* sp. SJH bacteria, cell voltages, power densities as well as current densities are relatively low. The maximum value of power density is 18.3 mW/m^2, which was occurred when the current density (I_{mp}) was 136.8 m A/ m^2, with a corresponding cell voltage (V_{mp}) of 136 mV. This might be because of energy losses which occur due to low activity oxygen reduction reaction, and little consumed fuel (*glucose*) is used for electricity generation and most of it is consumed for bacteria metabolism, leading to extreme biomass yield but reduced electron recovery and higher energy gained by the bacterium.[11]

The total CE found here was 6 ± 1.1 % using (1800 mg/L glucose) (n = 3, using average) can be measured according to Equation 4.5

$$Coulombic\ efficency = \frac{M_s I t_b}{F b_{es} v_{An\Delta c}} x100 \qquad \textit{Equation 4-5}$$

Where M_s molecule weight of glucose($\frac{180g}{mol}$), I current, t_b time, F Faraday's constant which is 96485 *C/mol*, b_{es} the number of electrons exchanged per mol of glucose, which is 24 mol e^- per mol, v_{An} is the volume of liquid in the anode chamber, Δc is the glucose concentration difference between the starting of the experiment and the completion of the experiment. The internal resistance and the various voltage drops all contribute to the low coulombic efficiency.[12]

Study of pH on OCV, and power density

A two-chamber H-type system was used to study the effect of different pH on OCV. OCV of MFCs was evaluated at pH 2.0, 2.5, 3.0, 3.5, and 4.0. A PEM membrane was placed into the middle of the reactor, building two equally sized chambers (*10 cm long, with 3 cm in diameter*): connected by a narrow tunnel, the anode where the *Acidiphilium* sp. SJH bacteria, ferric ion, and glucose were placed, and the cathode containing just buffered solution that is sparged with air. As shown in (Figure 4.12 on the following page), the highest OCV was observed at pH 2.5 and the values were lower at pH 4.5.and below 2.0.

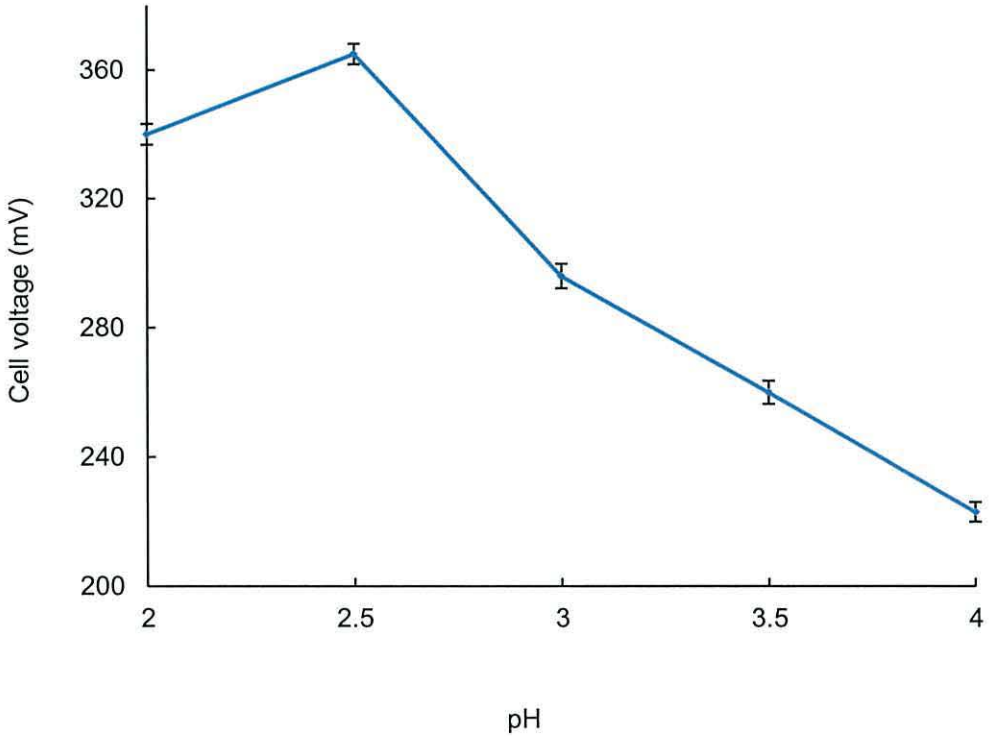

Figure 4. 12 - OCV variation with the function of pH during MFCs operation, experiments run in triplicate (Error bars equals ±1 SD).

These results show that the microbial activity is slower at sub-optimal pH than at optimal pH. The low value at pH 4.0 might be due to poor proton transfer at the reduced proton concentration gradient across the membrane and is suggested to be caused by the precipitation of Fe^{3+} forming Fe $(OH)_3$ which settles down from the solution.[13] However, below pH 2.0, the microbial will lose their biological activity (*bacterial community and metabolism*); as consistent with a previous report.[14] When MFC operated at pH 2.5 it showed visible influences on the performance of MFC. Figure 4.13 illustrates that a maximum current density and power density were observed 136 m A/m^2, and18.3 mW/m^2 at pH 2.5. This high performance at pH 2.5 was due to firstly, increasing the number of protons, which results in increasing transport of protons across the membrane. Secondly, solubility of ferrous ions is increased, which results in increasing the potential of improving the electron mediation to the electrode. The pH development in the anode and cathode chamber was due to H^+ diffusion through the membrane because of the pH gradient, coupled with the electrochemical production/consumption of protons on the anode and cathode.

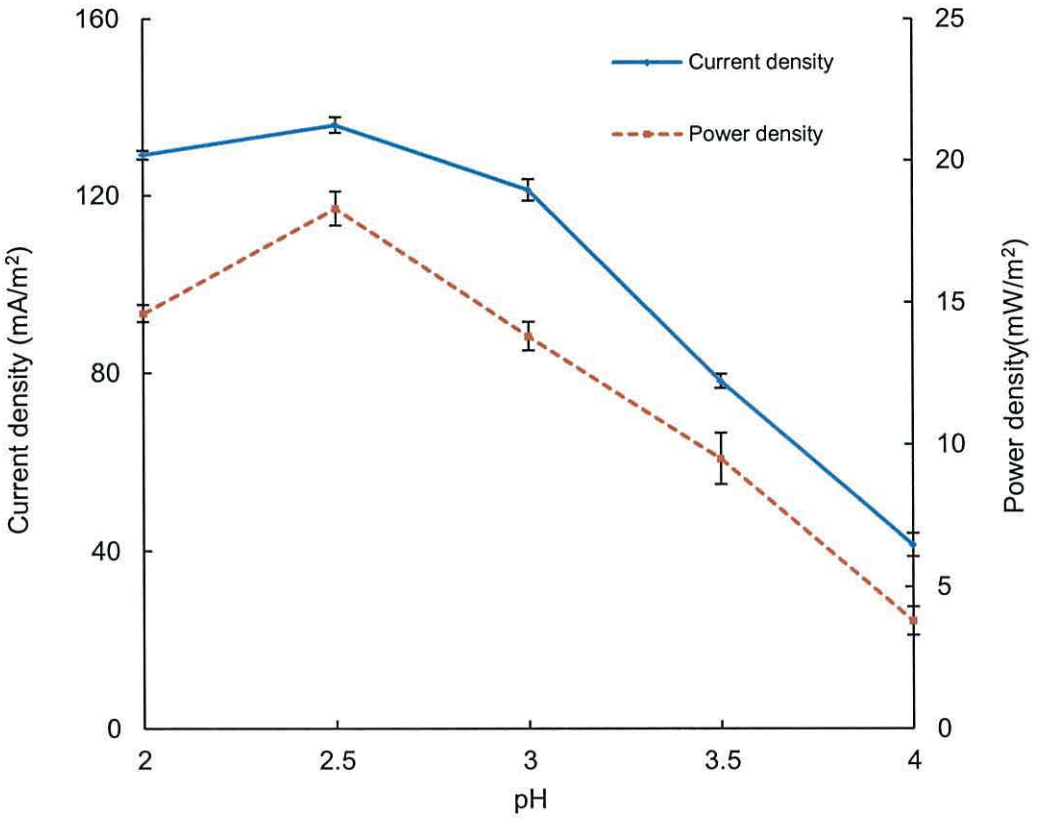

Figure 4. 13 - Power density (dashed line) and current density (solid line) with the function of pH during MFCs operation (2000 Ω resistor) experiments run in triplicate (Error bars equals ±1 SD).

Effect of cathode and anode surface area on power generation

The powers produced using the same cathode system with different total cathode surface areas; rectangular shaped (1 cm^2 to 2 cm^2), were compared and examined in the MFC tests (Table 4.2, Table 4.3 and Figure 4.14). The platinum catalyst was used as the cathode material. Nafion was used as a PEM (1 cm^2) material due to its high proton conductivity to allow the transfer of protons and electrons to the cathode electrode in the H-type system MFCs.

Table 4. 2 - Effect of cathode surface area on voltage production with 900 mg/L glucose concentration (2000Ω resistor).

Cathode surface area	Test 1 mV	Test 2 mV	Test 3 mV	Average mV
1 cm^2	133.1	132.9	135.4	133.8
2 cm^2	154.8	153.5	151.9	153.4

Table 4. 3 - Effect of cathode surface area on maximum power generation with 900 mg/L glucose concentration.

Cathode surface area	Test 1 mW/m^2	Test 2 mW/m^2	Test 3 mW/m^2	Average mW/m^2
1 cm^2	19.1	17.2	18.6	18.3
2 cm^2	20.6	21.7	21.4	20.9

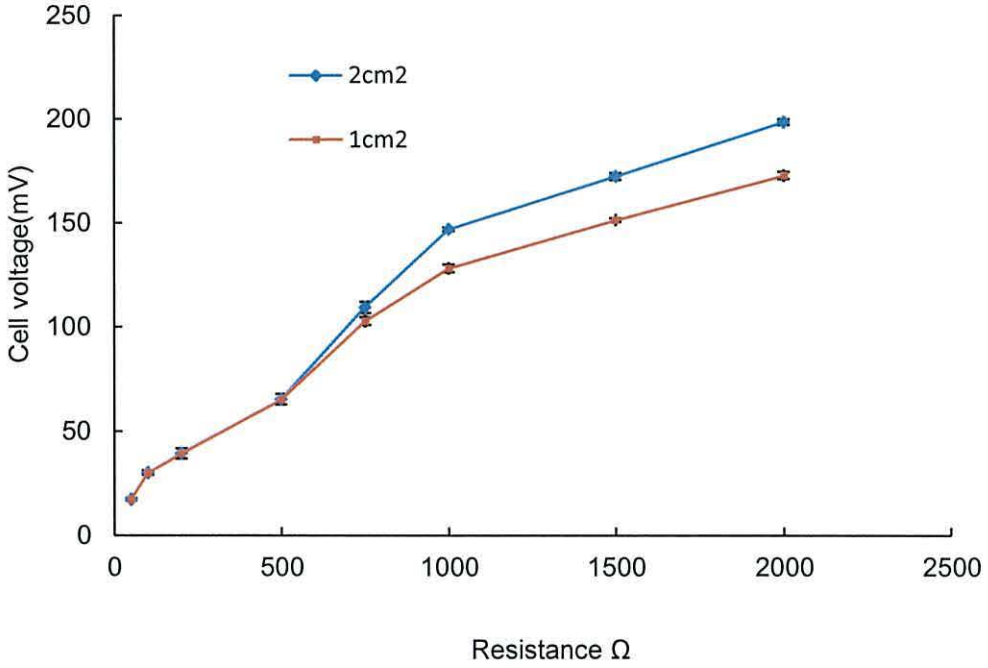

Figure 4. 14 - Voltage production as a function of external resistance at different cathode surface areas 1 cm^2, and 2 cm^2, experiments run in triplicate (Error bars equal ±1 SD).

As Figure 4.14 shows, increasing the cathode surface area of Pt sheet electrode by 100 % to 2 cm^2 increased the voltage by only 13 % compared to the case when the cathode surface area was 1 cm^2 at optimal external resistance (2000 Ω resistor). These results demonstrated that the surface area of the cathode in the certain experimental range of 1 – 2 cm^2 it seems from the H-type system MFC that a high cathode surface area may not necessary. Using a smaller surface area for the cathode can reduce the costs of the MFC construction and prevents up scaling of the fuel cell for industrial applications.

The OCV and power density generated by this MFC did not increase with increasing the anode surface area (3 – 6 cm^2) when the cathode and PEM sizes were kept constant. These results demonstrated that the surface area of the anode in the certain experimental range of 3 – 6 cm^2 does not limit OCV and power density generation in the H-type system (Table 4.4). In some reactor designs with high anode surface areas relative to the cathode areas, there was a limited power generation.[15]

Table 4. 4 - Effect of anode surface area on maximum power generation with 900mg/L glucose concentration.

Anode surface area	Test 1 mW/m^2	Test 2 mW/m^2	Test 3 mW/m^2	Average mW/m^2
3 cm^2	17.7	18.8	17.4	18.3
6 cm^2	18.1	16.8	19.6	18.5

Effect of O_2 as an electron acceptor

The most suitable electron acceptor for an MFC is oxygen, which is commonly used because of its low cost, sustainability (*unlimited availability from atmosphere*), and its high reduction potential.[16]When pure oxygen was used as an electron acceptor in the cathode chamber, the OCV, higher power density and current density were obtained than with the non-electron acceptor (*closed cell*) case (Figure 4.15), and (Table 4.5). The performance of MFC in accepting electrons will decrease if the concentration of oxygen is low. Then the produced electricity of the MFC will decrease with time as the amount of oxygen is consumed, as shown in equation 4.4. This study demonstrates that oxygen (*electron acceptor*) plays an important role in electricity generation of the MFC. In addition, the redox potential of the oxygen/water couple at pH 2 is 1.1V, means 0.3V more positive than at pH 7 (0.8V), making oxygen a more energetically favourable electron acceptor for acidophilic microorganisms.[17]

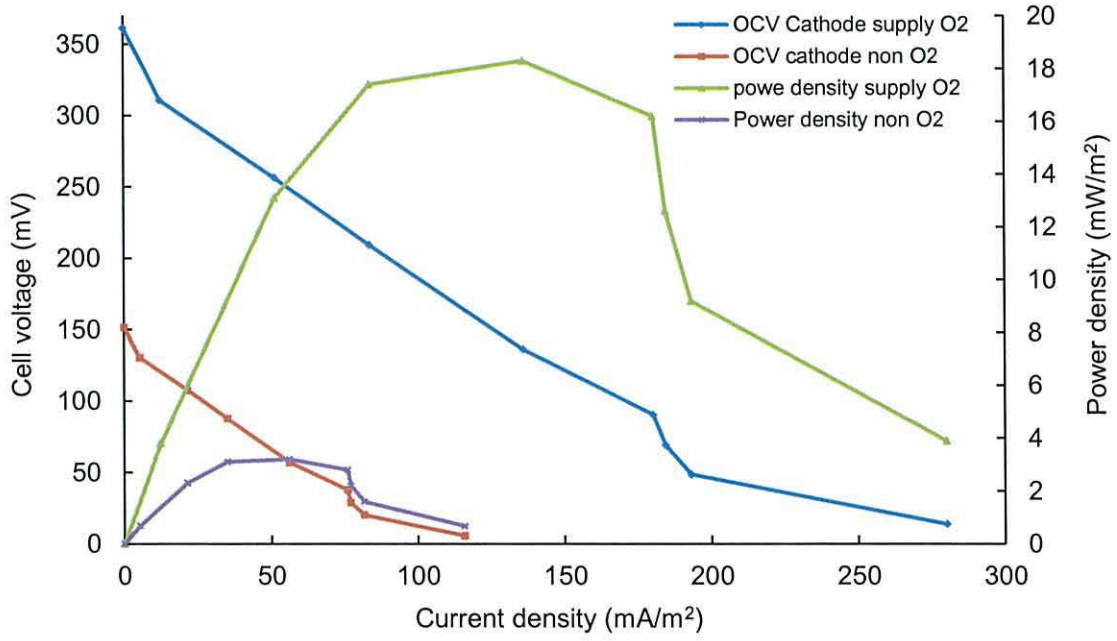

Figure 4. 15 - The effects of oxygen being added to the cathode chamber on the voltage generation, current density, and power density, experiments run in triplicate.

Table 4. 5 - Maximum voltage generation, current density, and power density of the MFC.

Electron acceptor	Open circuit voltage (mV)	Current density (mA/m^2)	Power density (mW/m^2)
None	152	116 (100Ω)	3.2 (2000 Ω)
Oxygen	364	280.3(100Ω)	18.3(2000 Ω)

4.4 Electrode potential

The OCP was measured of the electrodes (*anode and cathode*) of the MFC against a SCE as a function of current with different resistor circuits (Figure 4.16). The OCP of the anode was -156.7 mV, but the working potential decreased to -116.8 mV for current density up to 300 mA/m^2. The OCP of the cathode was 193.4 mV, but the working potential decreased to 39.7 mV for current density up to 300 m A/m^2 (Figure 4.16). It was observed that the OCV measurement result (364 mV) was different from the values achieved by taking the difference of the individual anode and the cathode potentials (350.1 mV). The possible explanation for this is that there is a potential difference between the interfacing liquids in the anode and cathode chambers.

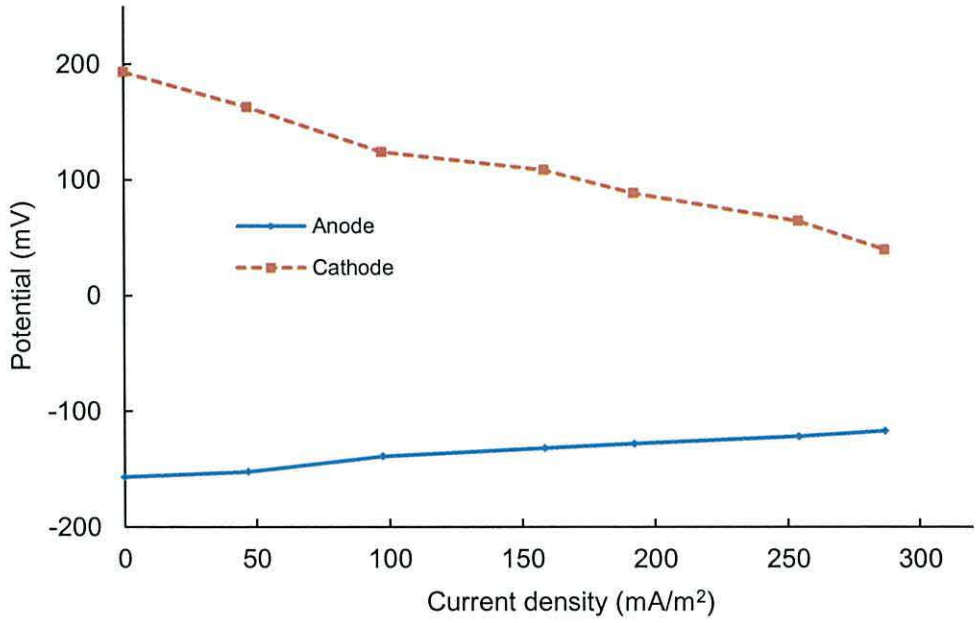

Figure 4. 16 - Anode (solid line) and cathode (dashed line) potential (vs. SCE reference electrode, 242mV against the NHE) as a function of current.

pH changes in a microbial fuel cell

A set of experiments were performed using cells of *Acidiphilium* sp. SJH bacteria (5.1 x 10^7 cells/ml), glucose 1800 mg/L, and a 10 mM ferric ion to measure pH changes, which was compared to that of the buffer solutions pH 2.5 experiment using potassium hydrogen phthalate 100 mM. In the buffer solutions the pH changed less than 0.3 units, both in the anode and cathode chambers after the substrate had been added, whilst the pH changes in the MFC without the buffer solution were

significantly higher than the buffer solution experiment. Protons are increased in the anode chamber during MFC operation, as a result pH decreased. This indicates that proton diffusion through the membrane is slower than its formation rate in the anode chamber. In the ORR protons are consumed with electrons in the cathode chamber (equation 4.4) and consequently, in the absence of pH control the pH will increase in the cathode chamber.[18] When the MFC utilising *Acidiphilium* sp. SJH bacteria was operated without a buffer solution, the maximum current density generated was much lower than with a buffer solution with pH changes to 4 in the cathode chamber and to 1 in the anode chamber (Figure 4.17).

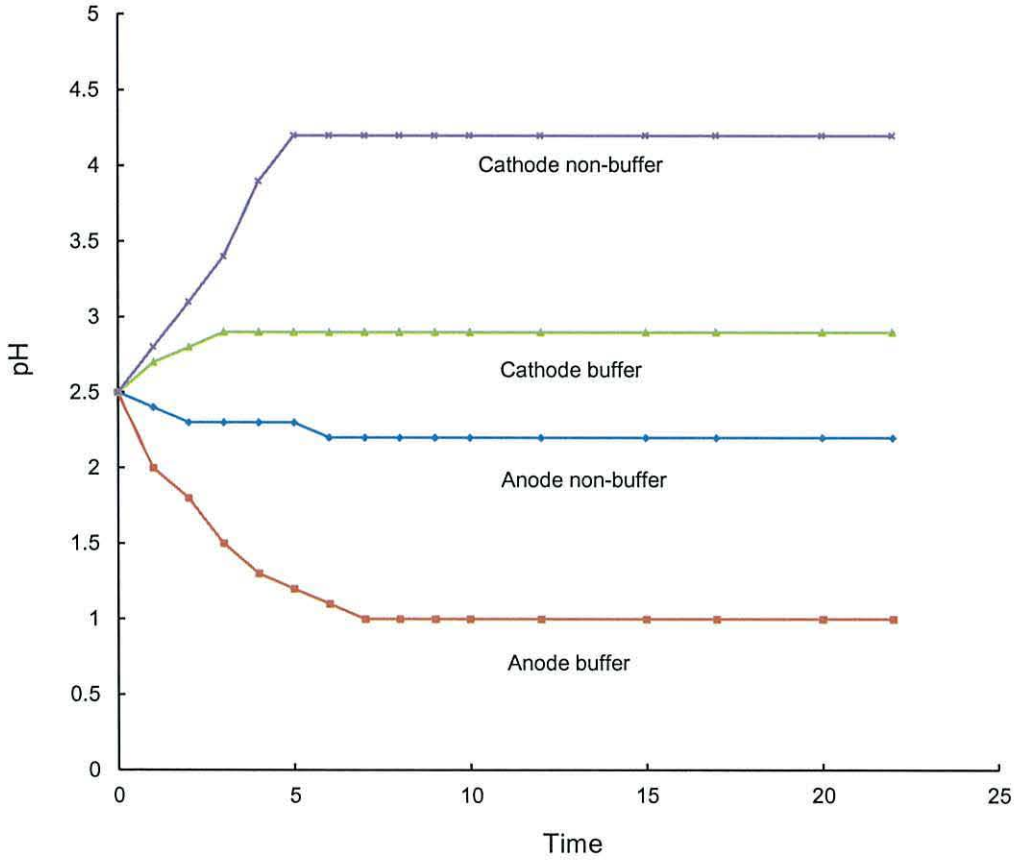

Figure 4. 17 - Trend of pH changes in MFC using non-buffered solution.

Voltage Generation and Effect of Nitrogen Sparging

As shown in (Figure 4.18), the sparging anode chamber containing cells of *Acidiphilium* sp. SJH bacteria (5.1 x 10^7 cells/ml), glucose 1800 mg/L, and with nitrogen gases, and the absence of sparging, the OCV at pH 2.5 (364, and 243 mV) respectively.

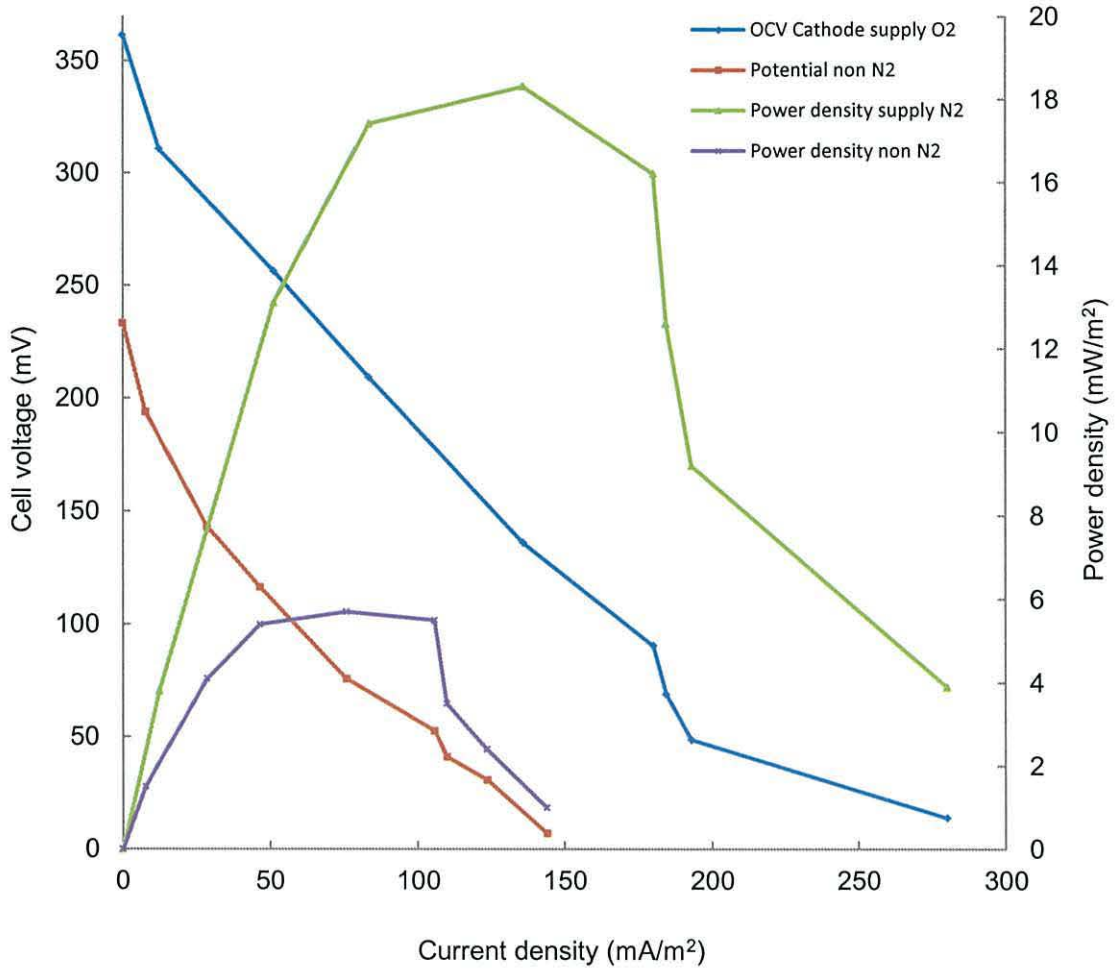

Figure 4. 18 - Effect of sparging and non- sparging of nitrogen on OCV, and power density in the H-type MFC reactor.

Figure 4.18 also illustrates the performance of the power densities and current density for MFC, without nitrogen gas sparging, the maximum power density and current density were 16.4 m W/m^2, and 120.3 m A/m^2 respectively. Power density and current density increased to 18.3 m W/m^2, and 136 m A/m^2 respectively with N_2 sparging. The oxidation processes of the degraded carbon source (*substrate*) by bacterial metabolic reactions result in the generation of high quantities of reducing power (*electron carrier*) in the form of NADH or NADPH. NADH/NAD fraction is commonly higher in the case of anaerobic microorganisms due to the absence of oxygen.[19,20] Oxygen ends the efficiency of the coupling mechanism, normally responsible for the stable cell voltage and anode potentials observed under anaerobic conditions, by direct oxidation of the electron shuttle and by facility of an alternative electron sink through a respiratory chain activity. This result suggests that oxygen is reduced in consuming the electron in the anodic chamber.[21]

Sandwich-type reactor

One of the easy reactors to construct and assemble is an H-type design. There are some difficulties in optimising its performance, due to large electrode separation, large dead volume in the head space, large reactor volume comparing to the small dimension of the electrode and small membrane areas, and the large amount of trapped bacterium in the narrow membrane joints. A new MFC reactor design using Sandwich-type chambers was designed and constructed in order to improve the performance of MFC and to increase the power density. Figure 4.19 shows the proposed design which will improve the performance of MFC and reduce the internal resistance by minimising electrode distances.[22]

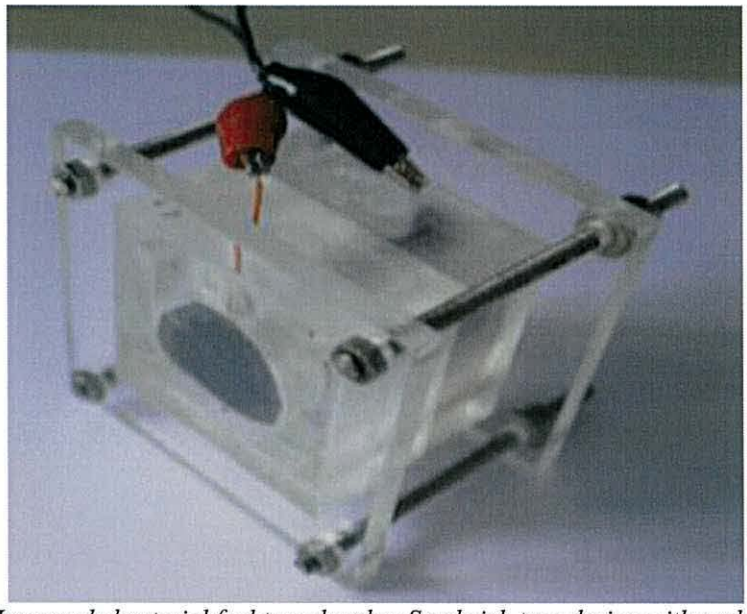

Figure 4. 19 - Homemade bacterial fuel two chamber Sandwich type design with carbon cloth (anode) and Platinum sheet (cathode) electrodes.

Open circuit voltage

The magnitude of the OCV over time for the MFC Sandwich-type reactor under optimum conditions (pH 2.5) is illustrated in (Figure 4.20). Figure 4.20 shows the OCV of the MFC with a Platinum sheet (1 cm^2) cathode supplied with oxygen as an electron acceptor in buffer solution pH 2.5, and an anodic chamber containing *Acidiphilium* sp. SJH (5.1 x 10^7 cells/ml), 10 mM ferric ion, and (900 mg/L) glucose against a fuel cell containing no bacteria.

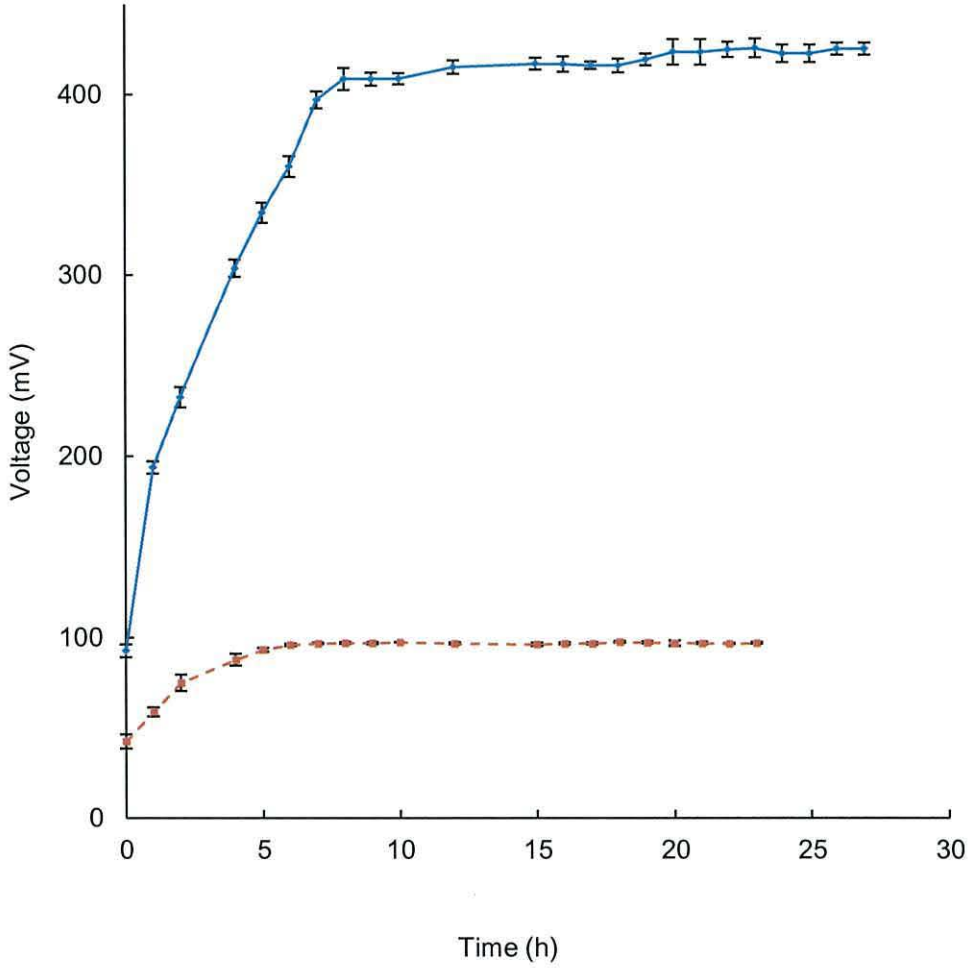

Figure 4. 20 - The resulting MFC voltage over time with (solid line) and without (dashed line) Acidiphilium sp. SJH, experiments run in triplicate (Error bars equal ±1 SD).

The initial voltage in both cases was less than 100 mV, which was due to a capacitive charge at the electrodes which can be seen, when no bacteria are present, increasing with time and reaching a steady state after approximately 10 hours. Figure 4.20 also illustrates that a maximum OCV of 424 mV was reached over 12 hours, at which point the voltage remained constant.

Polarisation curve

The polarisation curve represents the relationship between the power density and the OCV as a function of current density for the MFC utilising cells of *Acidiphilium* sp. SJH bacteria, ferric ion, and glucose were referenced to the anode, the cathode was made of a platinum sheet. The characteristics of MFC Sandwich type electricity generation were tested by a polarisation curve (Figure 4.21 on the following page). The data were collected to calculate the power generation and voltage across a range

of current densities attained by varying the resistance between the anode and cathode electrodes.

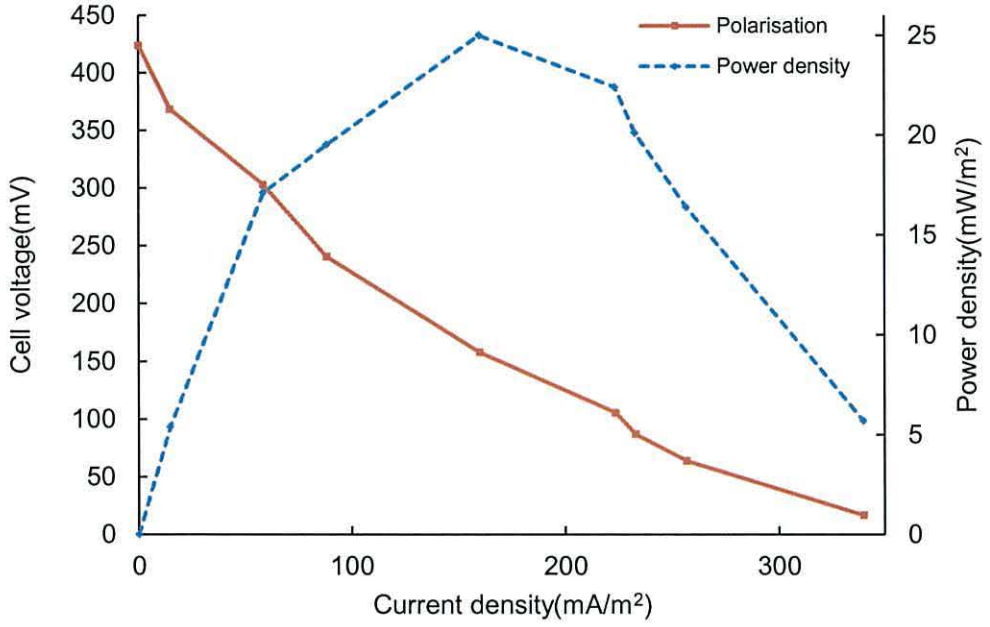

Figure 4. 21 - Power density (dashed line) and voltage (solid line) generated by the MFC as a function of current density, utilising an anodic carbon cloth and a cathodic Pt sheet. The maximum power density was 25 m W/m^2 at a current density of 160 m A/m^2.

The polarisation curve also showed that MFC keeps a voltage as a function of the current density production, that the OCV is 424 mV and that the voltage drops quickly to 303.4 mV at a current density of 58.5 m A/m^2, then linearly with current density after that point. The power density increased with current density to a maximum power point (25 mW/m^2) which occurred at 2000Ω. After this point, the power density dropped due to the increasing electrode overpotentials and ohmic losses.[23] The cell voltage and the current density were calculated from the polarisation curve; at the maximum power point value of power density, when the current density (I_{mp}) was 160 m A/m^2, with a corresponding cell voltage (V_{mp}) of 158 mV.

Electrode Potential

To further test the effect of the electrode spacing and reactor design on MFC performance, OCP was measured for the electrodes as a function of current with different resistor circuits (Figure 4.22). The OCP of the anode was -179.4 mV, but the working potential decreased to -34.4 mV for current density up to 350 m A/m^2.

The OCP of the cathode was 241.2 mV, but the working potential decreased to 48.2 mV for current density up to 350 m A/m^2 (Figure 4.22). There were significant differences in the OCP of the anode and cathode. This potential improvement on both anode and cathode could be a result of several factors. First, reducing the distance between the electrodes (8cm to 4cm), decreased the internal resistance in the system and reducing resistance for proton transfer from the anode to the cathode. Reducing the internal resistance could produce an observed increase in potential generation.[15] Second, it is also possible to find an increased size of PEM (0.78 cm^2 to 7 cm^2), and increasing anode surface area.[24]

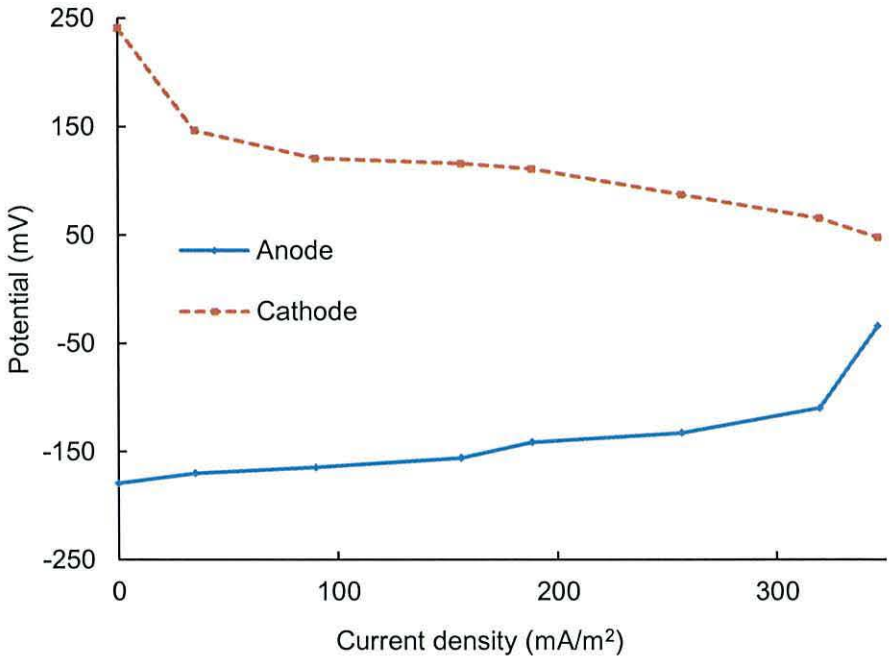

Figure 4. 22 - Anode (solid line) and cathode (dashed line) potential (vs. SCE reference electrode, 242mV against the NHE) as a function of current.

Current generation at variable fuel concentration

MFC were tested with ferric ion to measure high electrical current and stabilities that could be produced by *Acidiphilium* sp. SJH cells in the presence of various concentration of glucose. An MFC Sandwich-type reactor was used to investigate the effect of glucose on electricity generation. The decrease in concentration of glucose was observed with electricity production by analysing the samples taken from the anode chamber periodically.[25] *Acidiphilium* sp. SJH cells were run using different concentrations of glucose to determine the correlation between the glucose

concentration and the maximum current density. Figure 4.23 shows the current density of the MFC at various concentrations of glucose (180-1800 mg/L), and operated at a fixed external load (2000 Ω). The maximum current density increased with the glucose concentrations up to 540 ppm and attained a plateau. Table 4.6 shows the influence of glucose concentration on the maximum OCV, potential, current density, and stabilities across external load (2000 Ω). The voltage and current density increment produced by the MFC were proportional to glucose concentration range (180-1800 mg/L).Correlation was 0.9395 each mg/L of glucose equals 0.309 mA/m^2.

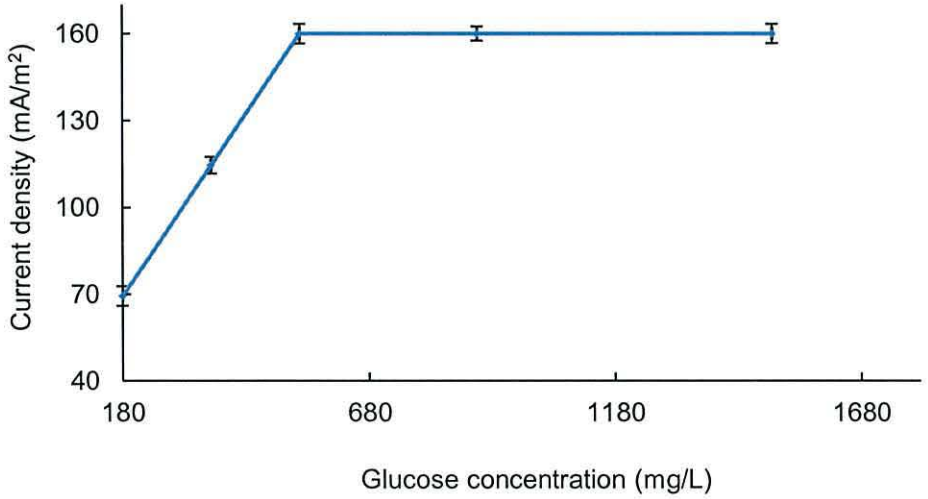

Figure 4. 23 - Current density generated using glucose at different concentrations, (2000Ω resistor) (Error bars ± SD), experiments run in triplicate.

Table 4. 6 - Effect of different concentration of glucose on electrical current and stability of MFC using by Acidiphilium sp. SJH cells.

Glucose concentration mg/L	Open circuit voltage		Potential mV (2000 Ω)	Current density mA/m^2 (2000 Ω)	Electrical stability (h)
	Potential mV	Current mA			
180	360	0	78.4	69.4	11
360	395	0	109.2	114.6	16
540	424	0	158.3	160	20

Effect of external resistance and current generation

When the OCV was stable, the MFC was operated with different resistance (100 Ω - 50 K Ω) across the anode and cathode. The potential was tested at each resistance. The current density and voltage data can be examined and recorded at each resistance. It was observed that the current from MFC was a function of external load. It was found that the lower the resistance the higher current density and vice versa (Figure 4.24).

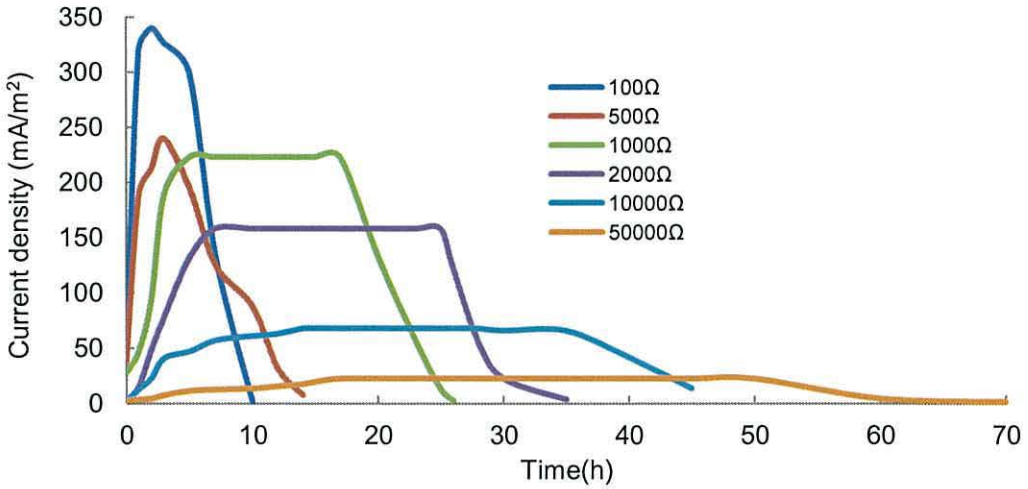

Figure 4. 24 - Differences in current density generation as a function of time from MFCs under different external resistances, concentration of glucose 540 mg/L.

Table 4.7 shows the time taken to reach the maximum current density decreased with decreasing external resistance. This observation may be due to the influence of different external resistances. At low resistance the electrons move more easily through the circuit than at high resistance, resulting in changed electron transfer rates and kinetic differences in fuel cell utilisation (*as previous work reported*).[26] Among the studied cases *Acidiphilium* sp. SJH, pH 2.5 operation in combination with buffer catholyte, and oxygen used as the electron acceptor, documented the highest current density 340 mA/m^2 (100 Ω), the maximum OCV 426 mV, and the maximum power density 25 mA/m^2 were obtained (2000 Ω).

Table 4.7 - Maximum current densities achieved for MFCs with different external loads and corresponding time.

External resistance	Peak current density (mA/m^2)	Time to achieve peak current density (h)
100 Ω	340 ± 20	2
500 Ω	320 ± 3.1	3
1000 Ω	223 ± 1.8	5
2000 Ω	158 ± 2.2	10
10000 Ω	68 ± 10	15
50000 Ω	23 ± 0.8	17

Power density as a function of external load

MFCs Sandwich type reactor was examined in the laboratory under external resistance. From these measurements, the optimal external resistance was found which showed the maximum power density. The power density generation of the MFC is shown in (Figure 4.25). Power density was a function of resistance circuit (50 KΩ - 100 Ω).Along with the external load increasing, the power density first increased then decreased. The maximum power density of 25 m W/m^2 was obtained

at 2000 Ω resistance in the ohmic region. The maximum power density of the MFC was obtained in the ohmic polarization region.[27]

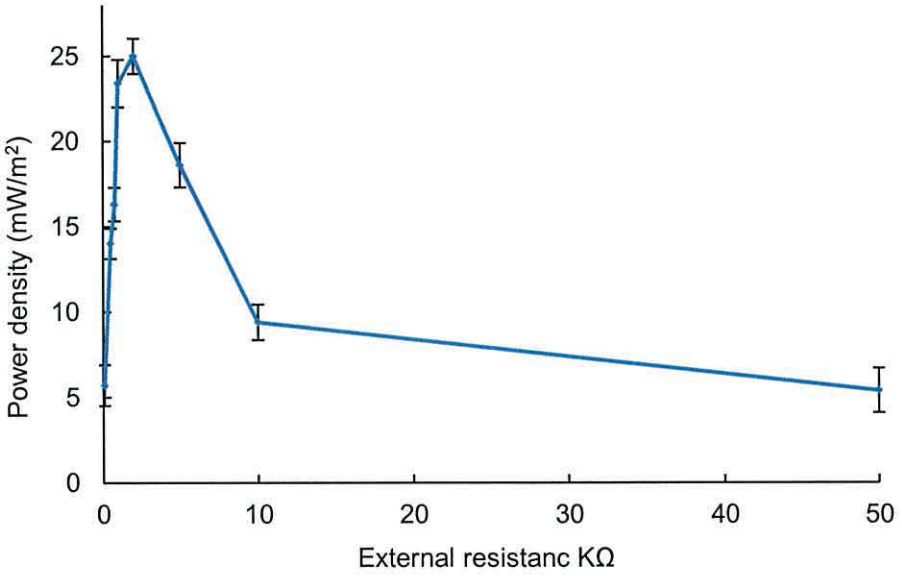

Figure 4. 25 - Power generated by the MFC as a function of external load, (Error bars ± SD), experiments run in triplicate.

Voltage generation

A repeatable cycle of electricity generation was obtained with *Acidiphilium* sp. SJH bacteria cells with an MFC Sandwich-type. At the beginning the MFC was operated in OCV for 10 hours. After a stable voltage was obtained for 15 hours this was connected with an external load 2000 Ω to test electricity generation. Successive additions of glucose (540 mg/L) produced a repeatable result. The voltage was tested; a consistent maximum voltage could be achieved for 2 h of 174 mV ± 6 mV (*Error bars ± SD*) declining to < 40 mV as the glucose was completely depleted, after 20 h (Figure 4.26). Figure 4.26 also illustrates when higher glucose concentration (1800 mg/L) in the anodic chamber resulted in a longer voltage production interval. This fact suggests that the MFC voltage is mainly established by the concentration ratio of Fe (III) and Fe (II). When most of the glucose had been consumed after 20-22 h, the reduction of Fe (III) was too slow to keep up with the electrode re-oxidation, which resulted in the increase in Fe (III) concentration.[4]

The total CE found here was 6.5 ± 1.2 % using (540 mg/L glucose) (n=3, using average shown in Figure 4.26) which can be measured according to Equation 4.5. Similar results were obtained in other experiments using the same system to a

different glucose concentration producing a maximum voltage of 158 ± 8 mV, with a slight change in CE of 7.1 ± 1.1 %.

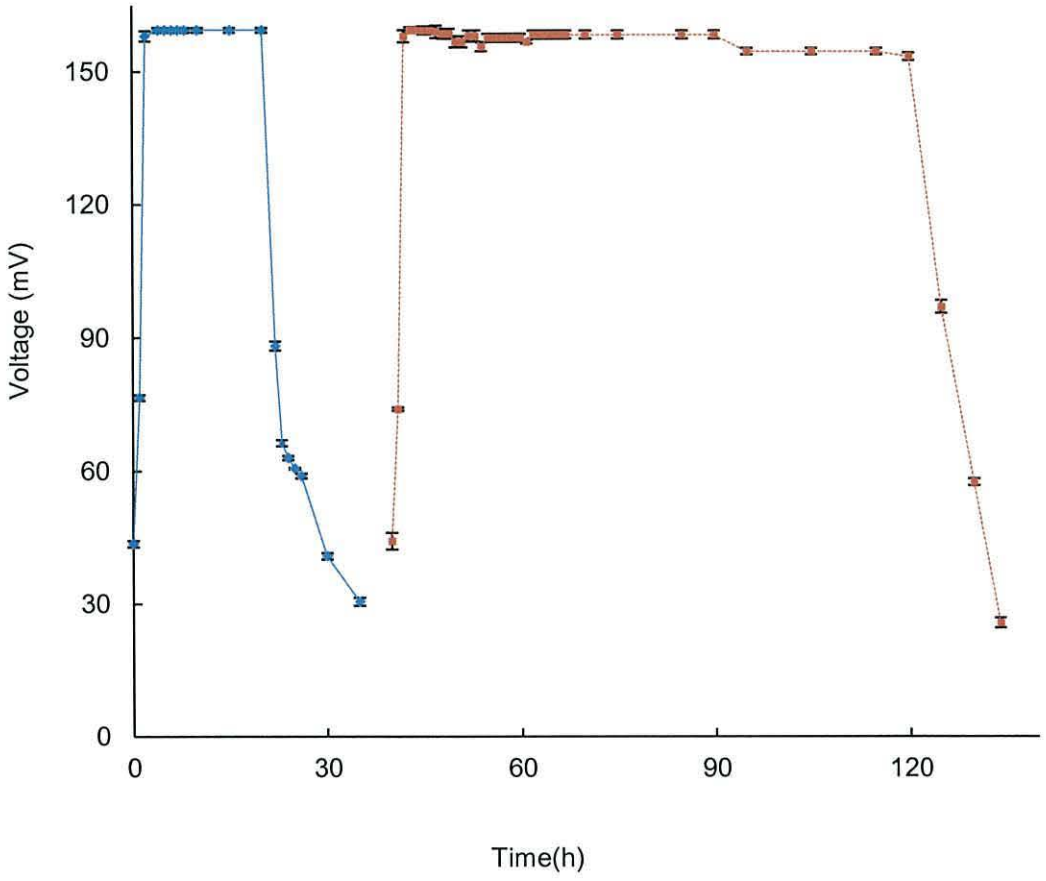

Figure 4. 26 - Voltage generation from glucose [540(solid line), 1800 mg/L(dashed line)] in the MFC (2000 Ω resistor), experiments run in triplicate (Error bars ± SD).

Power density as a function of time

According to the polarization curve of the MFC Sandwich-type, the external resistance was fixed at 1000 Ω (*optimal external resistance*). Figure 4.27 show the electricity was immediately generated from 900 mg/L glucose and was filled into the anode chamber. Power density reached the maximum of 25 m W/m^2 at 19 h, and then decreased slowly to 22.6 m W/m^2 at 80 h. After that it decreased sharply to the minimum at 85 h, the power densities started to decrease due to the substrate contained in the anode chamber being consumed. The power density was increasing for the first 19 h and then stabilised for 70 h with a maximum power density of 25mW/m^2 produced based on an anode surface area of 5 cm^2.

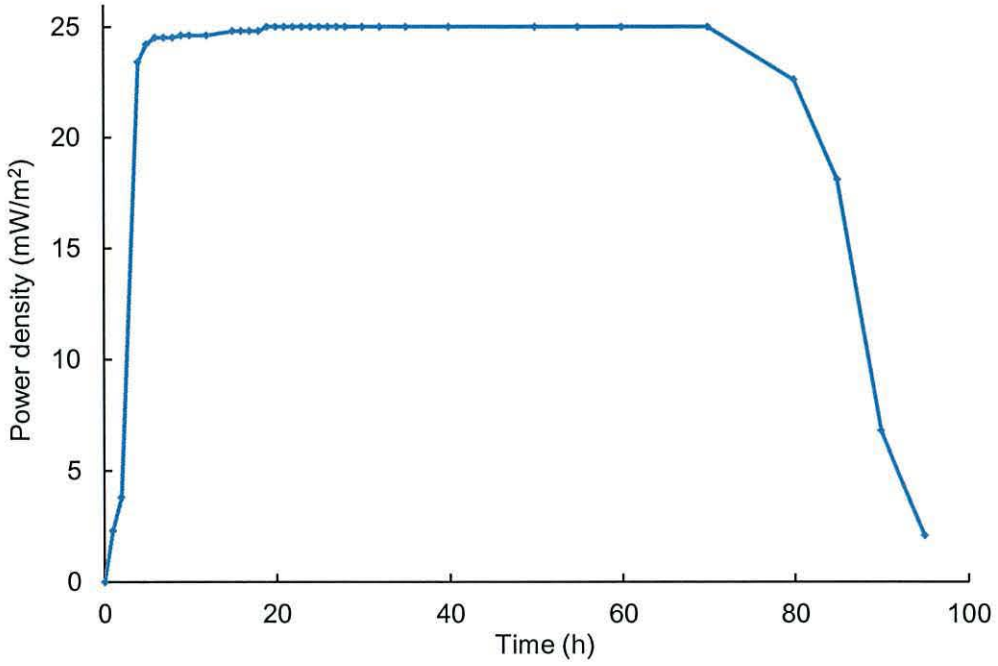

Figure 4. 27 - Power densities gained from Sandwich-type MFC under batch mode condition, (1800 mg/L glucose) (2000Ω).

4.5 Comparison Study

A comparison of production electrical current and voltage was obtained when *Acidiphilium* sp. SJH resting cells and growing cells were used in a glucose (1800 mg/L) fuel cell along with 10 mM Ferric iron as the electron shuttle under anaerobic conditions. Figures 4.28, and 4.29 on the following page show the current density and voltage obtained in *Acidiphilium* sp. SJH resting cells (5.1 x 10^7 cells/ml) (Figure 4.28) and growing cells (Figure 4.29) were used. The voltage rapidly increased to the maximum value (424 mV), and the amount of current density generated increased with resting the cells (Figure 4.28). The voltages produced by resting and growing cells were similar, whereas the quantity of current density produced by *Acidiphilium* sp. SJH resting cells was significantly greater (*about two fold greater*) than the amount of current density produced by growing cells. The maximum current density produced was determined at 89 h for growing cells (88 mA/m^2), and at 15 h for resting cells (164 mA/m^2) when the glucose levels were high. The decrease in concentration of glucose was observed with electricity production by analysing the samples taken from the anode chamber.

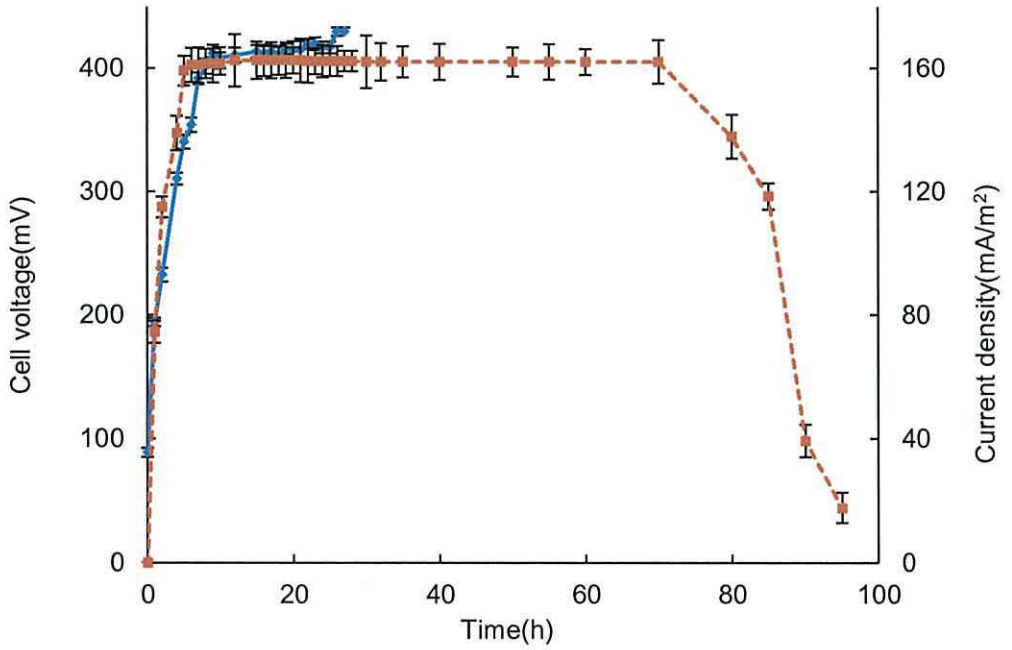

Figure 4. 28 - Current density(dashed line) (2000 Ω resistor), and voltage (solid line) obtained as a function of time when Acidiphilium sp. SJH resting cells were used in a glucose (1800 mg/L) MFC along with 10mM Ferric iron as the electron shuttle under anaerobic conditions, experiments run in triplicate. (Error bars ± SD).

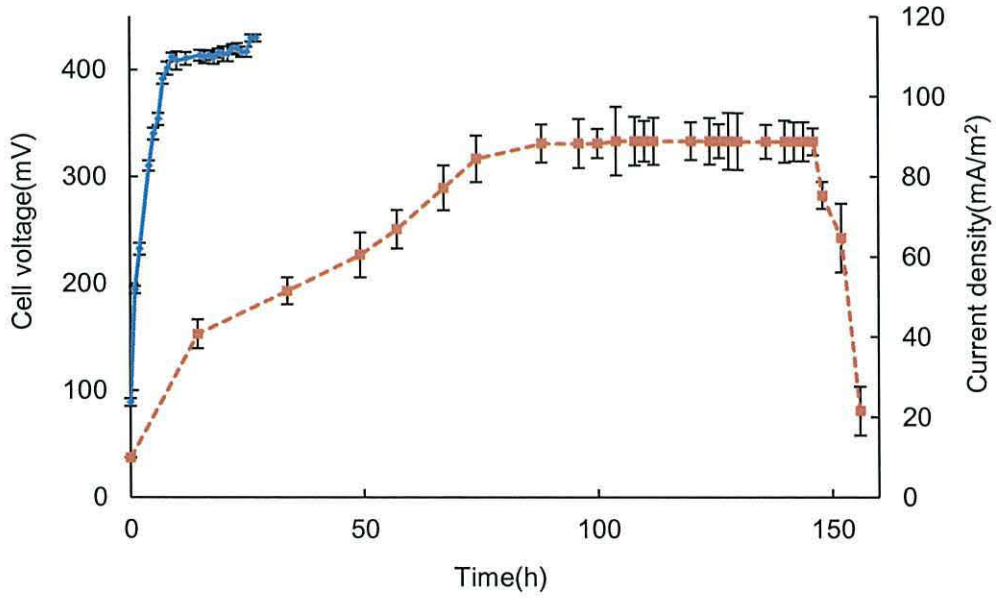

Figure 4. 29 - Current density(dashed line), and voltage (solid line) obtained as a function of time when Acidiphilium sp. SJH growing cells were used in a glucose (1800 mg/L) MFC along with 10 mM Ferric iron as the electron shuttle under anaerobic conditions, (Error bars ± SD).

Table 4.8 shows that the rate of glucose consumption and optical density were higher but the amount of electrical current produced was lower in growing cells than in resting cells. This indicates the influence of electrical generation in MFCs on physiological property. In resting cell tests the generation of electricity was expected as a consequence of ferric ion reduction by *Acidiphilium* sp. SJH and that this would result in lower levels of substrate oxidation and higher levels of enzyme system coupled to the bacterial cells (*reducing power*).

Table 4. 8 - glucose consumption and cell growth by growing and resting cells of Acidiphilium sp. SJH in MFC Ferric ion as electron shuttle.

Cells	Glucose (mg/L)	Current Density (mA/m^2)	Optical density (600 nm)
Growing	1800	118	1
Resting	540	223	0.2

4.6 Performance of different cathode materials on the OCP

The OCPs produced using different cathode material (*carbon cloth, carbon felt, and carbon Ketjen Black EC 600J*) with the same total cathode surface areas, (5 cm^2) were compared and examined in electrochemical tests (Figure 4.30 on the following page). OCPs of electrodes (Ketjen Black EC 600J, carbon cloth, and carbon felt) were 152.9, 140.4, and 124.8 mV respectively. The material used to construct the cathode electrode might play a role in the ORR activity.[28] It was observed that the carbon Ketjen Black EC 600J electrode could produce the higher potential than other electrodes for oxygen as an electron acceptor. The higher potential of carbon Ketjen Black EC 600J could be a result of higher surface area of Ketjen Black EC 600J at about 1413 m^2g^{-1}.[29]

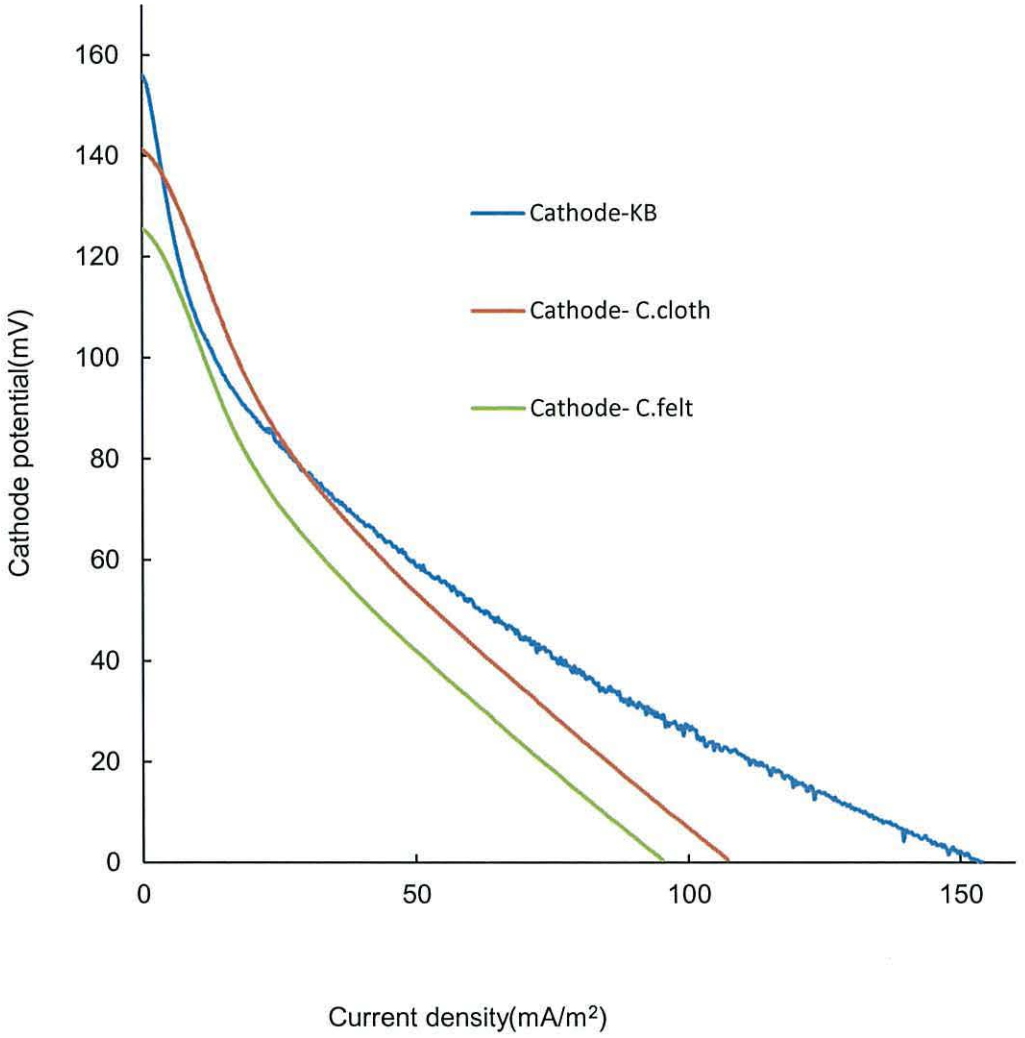

Figure 4. 30 - Cathode potentials (vs. SCE reference electrode, 242mV against the NHE) as a function of current density recorded in chemical cells for different cathode material (carbon cloth, carbon felt, and carbon Ketjen Black EC 600J).

4.7 Effect of the microbial fuel cell reactor design

A comparison was made of the MFCs performance between systems H-type and Sandwich-type design. The abilities of generating electricity of H-type and sandwich-type MFC design were compared using *Acidiphilium* sp. SJH bacteria cells, in a medium pH 2.5 with glucose as the carbon source and ferric ion as the electron shuttle, under optimal conditions. The MFC performance was estimated with a modified MFC system called a Two-chamber Sandwich design. This design leads to improvements in reactor performance and reduced internal resistance by minimizing electrode distances. These improvements lead to increased maximum

specific power output. 24 hours of operation demonstrated that the sandwich-type reached its highest voltage (424 mV) at 10 hours of operation. The H-type reactor generated about (361 mV) after 20 hours of operation (Figure 4.31). In these experiments, the sandwich-type reactor provided a maximum power density of 25 m W/m^2 per anode surface area compared to 18.3 m W/m^2 per anode surface area in the H-type reactor. This result indicated that the sandwich-type reactor was more efficient than the H- type reactor.

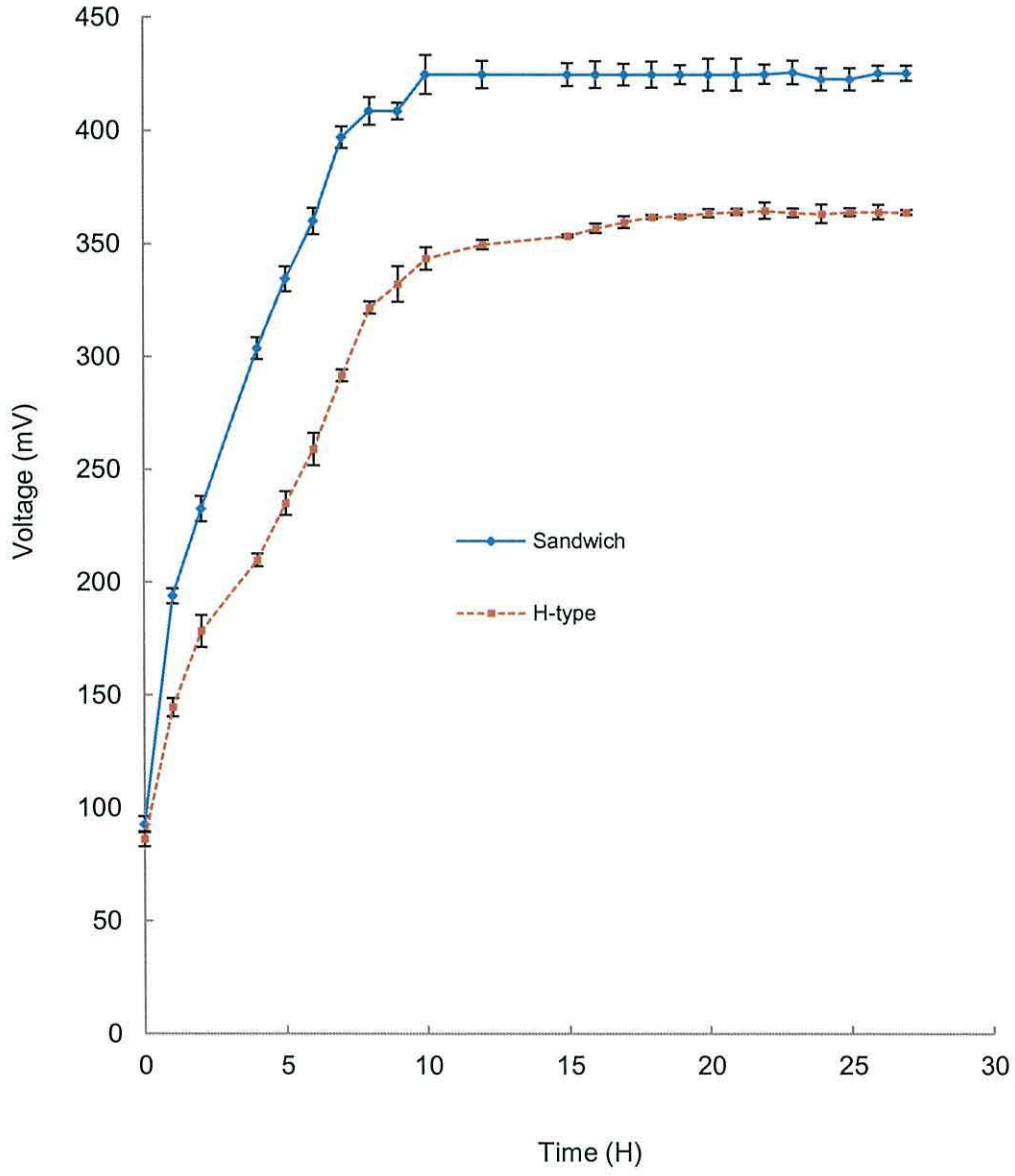

Figure 4. 31 - Comparison of operation efficiency on voltage generation between H-type (dashed line) and sandwich-type (solid line) reactors. (Error bars ± SD, experiments run in triplicate).

Table 4.9 shows the comparison between H-type and Sandwich type design. The power density and current density of MFCs Sandwich-type was increased with the reducing of anode and cathode distance, increasing anode surface area, and an increased size of PEM. This indicates that minimising the electrode spacing will help the protons transfer from anode to cathode; further improvement in reducing optimum resistance corresponded to a reduction of internal resistance.[30]

Table 4. 9 - The comparison between two design configurations.

MFCs	H-type	Sandwich
Anode	Carbon cloth	Carbon cloth
Cathode	Pt	Pt
Anode & cathode distance	8 cm	4 cm
Max. Power density	18.3 mW/m^2	25 mW/m^2
Max. Current density	140 mA/m^2	160 mA/m^2
Open circuit voltage	361 mV	425 mV
Surface area PEM	0.78cm^2	7 cm^2
Coulombic efficiency	6 %	7 %

4.8 Effect of Fe (III)-EDTA as an electron shuttle

The effect of Fe (III)-EDTA was studied as an electron shuttle to improve the efficiency of voltage output in MFC operating at low pH. Figure 4 32 shows the typical voltage generation *versus* time for MFCs containing *Acidiphilium* sp. SJH cells in the presence different concentrations of Fe (III) EDTA (1 mM, 5 mM,10 mM) as the electron shuttle and glucose (900mg/L) as the electron donor. Initially, during the period in which the MFC was left on OCV, the MFC voltage increased with time and reached a steady state after approximately 10 hours, Figure 4.32 also illustrates that a maximum OCV of 458 mV with (10mM) Fe (III)- EDTA was reached over12 hours, at which point the voltage remained constant. As (Figure 4.32) shows, high concentrations of Fe (III) - EDTA gives a good mediating result. The figure indicates that the chelating agent Fe (III) - EDTA is good electron shuttle in comparison with Ferric iron, particularly at the higher concentration (10 mM). Previous work by Tanaka *et al.*, using EDTA as a chelating agent's compound with iron as mediators with *E. coli* as microorganisms in MFC operating at neutral pH was similar to that shown in (Figure 4.32 on the following page).[31]

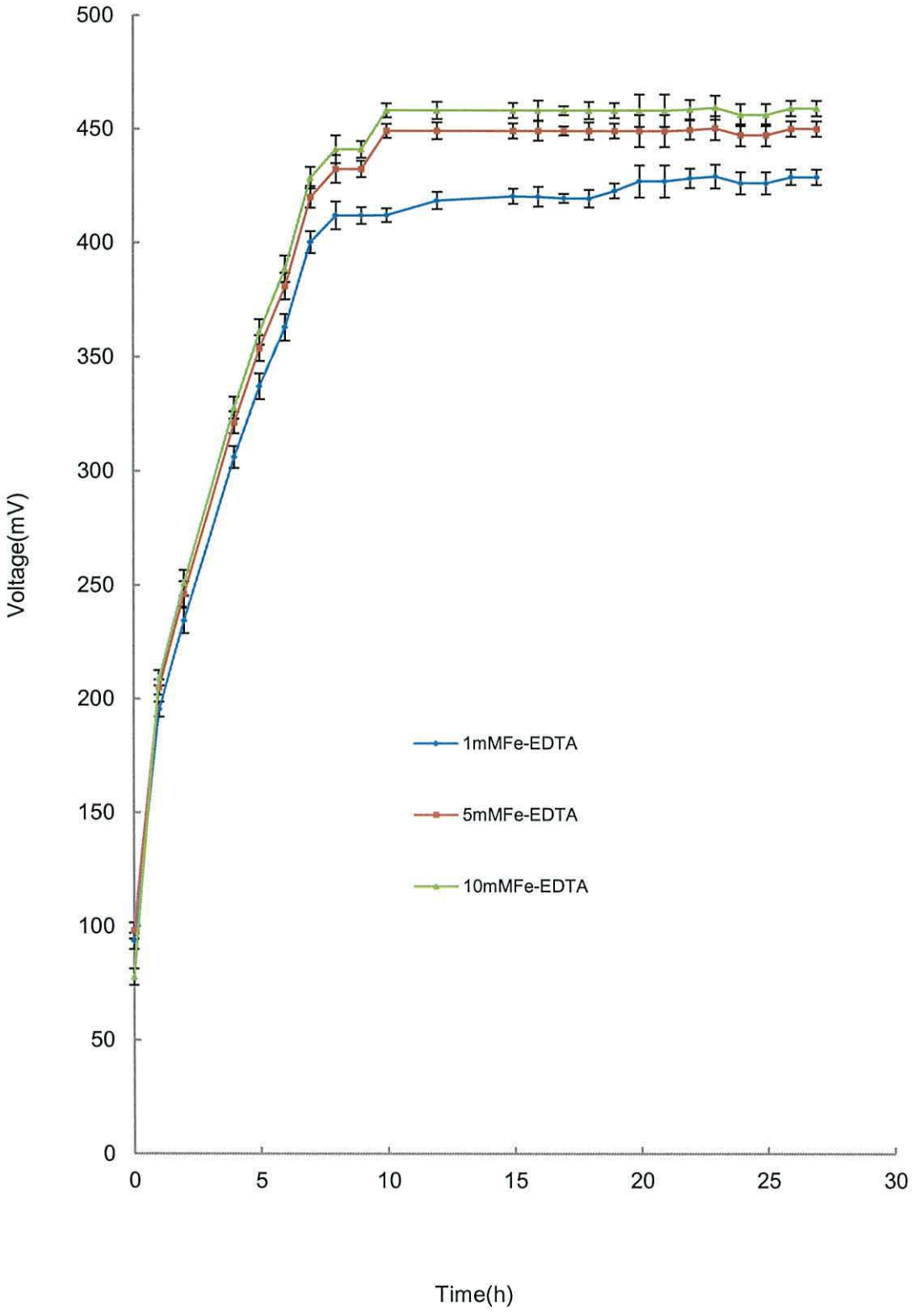

Figure 4. 32 - Voltage as a function of time of Acidiphilium sp. SJH cells in MFCs with different concentrations of Fe (III) EDTA, experiments run in triplicate.

Polarisation curve

The characteristics of MFC Sandwich type electricity generation were tested by a polarisation curve and the corresponding power density curve was generated (Figure 4.33). Polarisation curve, power density and open cell voltage as the function of current density produced in the MFC containing *Acidiphilium* sp. SJH cells (5.1 x 10^7 cells /ml) in the presence of Fe (III) - EDTA (10 mM) as the electron shuttle and glucose (900 mg/L) as the electron donor. The data were collected to calculate the power generation and voltage continued across a range of current densities attained by varying the resistance between the anode and cathode electrodes. From these measurements, the optimal external resistance was found (2000Ω) which showed the maximum power density. The maximum value of power density is 27.3 mW/m^2, which was occurred when the current density (I_{mp}) was 165m A/ m^2, with a corresponding cell voltage (V_{mp}) of 65 mV. The figure indicates that the chelating agent Fe (III)- EDTA is a good electron shuttle in comparison with Ferric iron, particularly at the concentration (10mM) showing increases in power density from 25 mW/m^2 to 27.3 mW/m^2 .

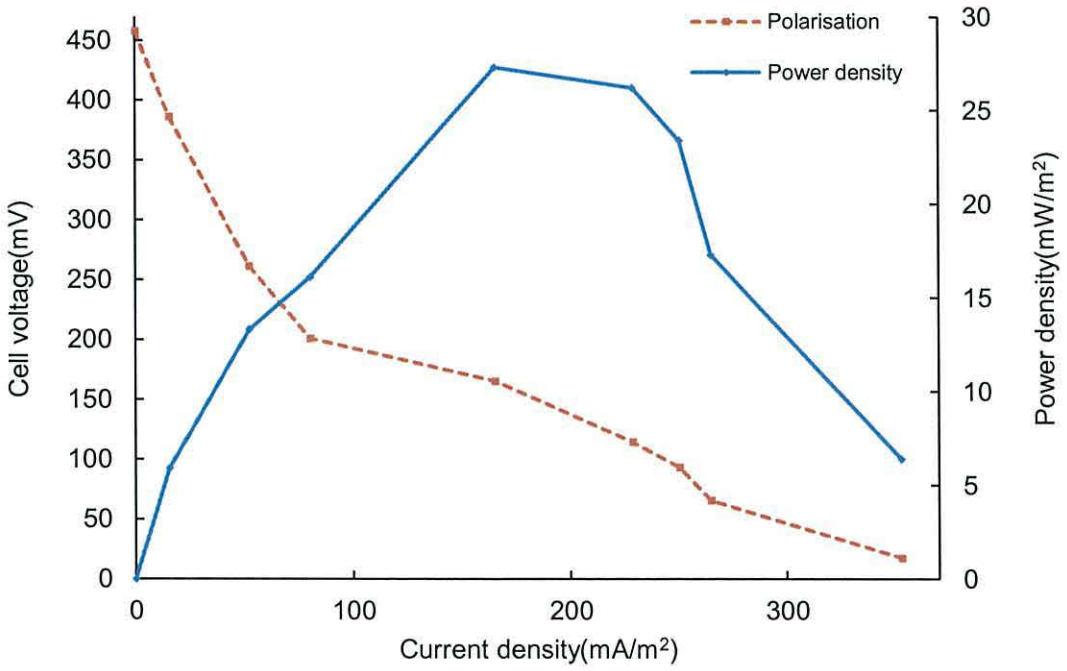

Figure 4. 33 - Power density (solid line) and voltage (dashed line) generated by the MFC as a function of current density, utilising Fe (III)- EDTA (10 mM) as electron shuttle and glucose (900mg/L) as electron donor. The maximum power density was 27.3mW/m^2 at a current density of 165 mA/m^2.

Electrode Potential

Additional tests were conducted the effect of the Fe-EDTA as an electron shuttle on power generation and compared with ferric ion. The OCP was measured of the electrodes of the MFC against a SCE as a function of current with different resistor circuits (Figure 4.34). The OCP and working potentials of the cathodes were not affected when using the Fe-EDTA as an electron shuttle. For example the OCP of the cathode with the Fe-EDTA and ferric ion were 239.2 mV, 241.1mV, respectively. Improvement on the anode potential was seen with Fe-EDTA -211 mV, and compared with ferric ion was -179.4 mV. Using Fe-EDTA as an electron shuttle made the anode potential more negative by 31.6 mV. This difference in anode potential increased the power density and Coulombic efficiency.

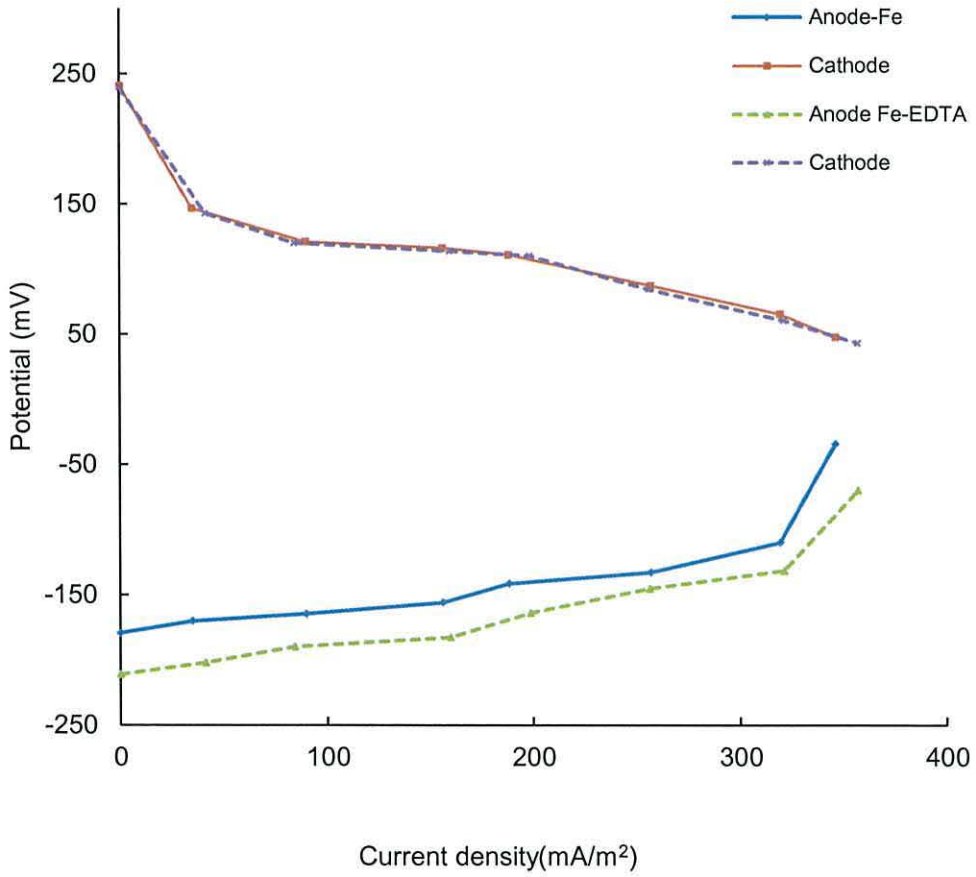

Figure 4. 34 - Anode with ferric ion and cathode (solid line) and anode with Fe-EDTA and cathode (dashed line) potential (vs. SCE reference electrode, 242mV against the NHE) as a function of current.

Current generation

In the MFCs (Figure 4.35), the efficiency of the Fe (III)- EDTA mediators was analysed by determining the electrical current of the *Acidiphilium* sp. SJH bacteria cells under a fixed resistance. When the MFC was connected across an external load (2000Ω), the electrical current output in the MFC directly reflected the change in concentration of Fe (III) - EDTA. This fact suggests that the electrical current output in the MFC is mainly established by the concentration ratio of Fe (III) -EDTA and Fe (II) - EDTA. During the period when *Acidiphilium* sp. SJH was metabolizing the glucose in the anode chamber, the reduction of Fe (III) -EDTA apparently outpaced the electrode re-oxidation reaction, as indicated by the low concentration of Fe (III)-EDTA accompanying the higher electrical current output. When most of the glucose had been consumed after 80 h, the reduction of Fe (III)-EDTA was too slow to keep up with the electrode re-oxidation, which resulted in the increase in Fe (III)-EDTA concentration.

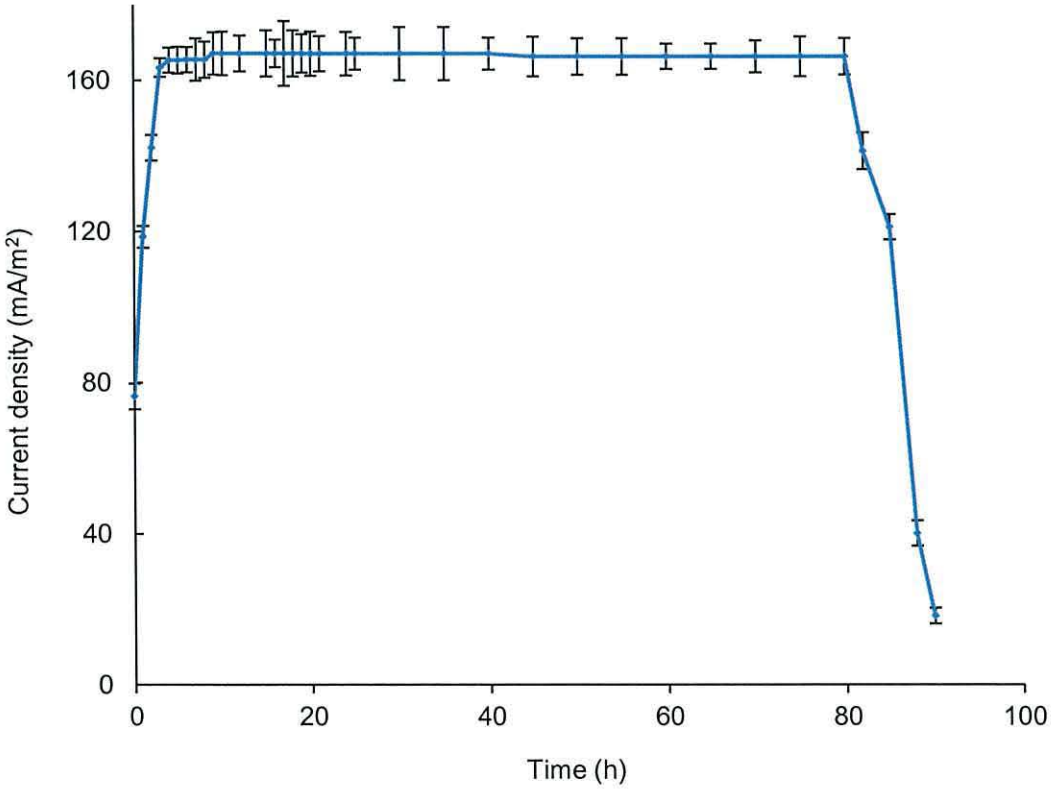

Figure 4. 35 - Current density (2000 Ω resistor), as a function of time when Acidiphilium sp. SJH resting cells were used in a glucose (1800 mg/L) MFC along with 10mM Fe(III)EDTA as the electron shuttle under anaerobic conditions. Three repetitive cycles (Error bars ± SD).

Coulombic efficiency

Coulombic efficiencies from the MFCs were obtained from electron recovery from glucose in the form of electricity. The amount of electrons recovered. *Acidiphilium* sp. SJH cells using sandwich design MFCs, containing ferric ion, and Fe (III) - EDTA as electron shuttles, for 20 h are listed in (Table 4.10). It can be seen to be effective more than 1 mM concentration as electron shuttle. It is clear that Fe (III) - EDTA was better than ferric ion because it increased both current and coulombic efficiency.

Table 4. 10 - Coulombic efficiencies of Acidiphilium sp SJH cells containing ferric ion, and Fe (III)-EDTA as electron shuttle, glucose (540mg/L).

	Coulombic efficiencies		
Electron shuttle	**1 mM**	**5 mM**	**10 mM**
Fe(III)	1.8± 0.6 %	6.6 ± 1.8 %	7.0 ± 1.2 %
Fe (III)- EDTA	1.4± 0.1 %	7.0 ± 2.4 %	7.5 ± 0.9 %

4.9 Conclusion

Two different designs of MFCs were presented operating at a low pH using iron-reducing heterotrophic bacteria (*Acidiphilium sp* SJH). Electricity generation in the presence of ferric ion, Fe (III) EDTA was demonstrated. The power outputs, coulombic efficiencies, and current densities were established for each MFC design (*H-type and sandwich type*) and a comparative study was carried out.

Results obtained from a comparison of the relationship between the power density and current density curves show that the H-type MFC has the maximum power density of 18.3 mW/m^2 and the sandwich type MFC has the maximum power density of 25 mW/m^2. These results show that the sandwich design will improve the performance of the MFC and reduce the internal resistance by minimising the electrode distances and membrane size. In contrast the change in power density was relatively small and this was postulated to be due to the high OCP of the anode electrode.

The results illustrate that the MFCs were operated with low external resistance (100 Ω) to produce high current density which dropped quickly with a shoulder. This behaviour was perhaps due to the limiting resistance within the system.

A comparison of the MFCs performance between the growing cells and resting cells of *Acidiphilium sp* SJH bacteria was also carried out. A higher current density (164 mA/m^2) was obtained at 15 h using resting cells compared to (88 mA/m^2) at 88 h for growing cells. These differences in the value of current density and time of reaction may be due to physiological property.

The reduction rate of Ferric ion by *Acidiphilium sp.* SJH at pH 2.5 was smaller than Fe (III) EDTA for the comparable coulombic efficiencies (7, 7.5 %) obtained from MFCs (sandwich design) using ferric ion or Fe (III) EDTA as the electron shuttle. This suggests a probability that ferric ion is more efficient when competing for the electron at the cell interaction step, but low effective in transferring the electron to the anode electrode.

4.10 References

1. James, J.; Benschoten, V.; Lewis, Y. J.; Heineman, W. R.; Roston, D. A.; and Kissinger, P. T. Cyclic Voltammetry Experiment. *J. Chem. Educ.* **1983**, *60*, 772 - 776.
2. Nicholson, R. S.; Theory and Application of Cyclic Voltammetry for Measurement of Electrode Reaction Kinetics. *Anal. Chem.* **1965**, *37*, 1351 - 1355.
3. Greef, R.; Peat, R.; Peter, L. M.; Pletcher, D. *Instrumental Methods in Electrochemistry*, 2nd ed. Ellis Horwood Limited, Market Cross House, Cooper Street, 1990.
4. Lovely, D. R.; and. Phillips, E. J. P. Rapid Assay for Microbially Reducible Ferric Iron in Aquatic Sediments. *Appl. Environ.Microbiol.* **1987**, *53*, 1536 - 1540.
5. Johnson, D. B.; Bridge, T. A. M. Reductive dissolution of ferric iron minerals by *Acidiphilium* SJH. *Geomicrobiol. J.* **2000**, *17*, 193 - 206.
6. Malki, M.; De Lacey, A. L.; Rodrıguez, N.; Amils, R.; and Fernandez, V. M. Preferential use of an anode as an electron acceptor by an acidophilic bacterium in the presence of oxygen. *Appl. Environ. Microbial.* **2008**, *74*, 4472 - 4476.
7. Johnson, D. B.; Bridge, T. A. M. Reduction of ferric iron by acidophilic hetrotrophic bacteria: evidence for constitutive and inducidle enzyme system in Acidiphilium spp. *J. Appl. Microbiol.* **2002**, *92*, 315 - 321.
8. Coupland, K.; and Johnson, D. B. Evidence that the potential for dissimilatory ferric iron reduction is widespread among acidophilic herotrophic bacteria. *FEMS Microbiol Lett.* **2008**, *279*, 30 - 35.
9. Bilgin, A. A.; Silverstein, J.; and Hemandez, M. Effects of Soluble Ferri-Hydroxide Complexes on Microbial Neutralization of Acid Mine Drainage. *Environ. Sci. Technol.* **2005**, *39*, 7826 - 7832.
10. Borole, A. P.; O'Neill, H.; Tsouris, C.; and Cesar, S. A microbial fuel cell operating at low pH using the acidophile *Acidiphilium cryptum Biotechnol.Lett.* 2008, *30*, 1367 - 1372
11. Logan, B. E. Exoelectrogenic bacteria that power microbial fuel cells. *Nat. Rev. Microbiol.* **2009**, *7*, 375 - 381.
12. Logan, B. E.; Regan, J. M. Microbial fuel cells - challenges and application *Environ. Sci. Technol.* **2006**, *40*, 5172 - 5180.
13. Wang, Y.; Niu, C. G.; Zeng, G. M.; Hu, W. J.; Huang, D. W.; Ruan, M. Microbial fuel cell using ferrous ion activated persulfate as a cathodic reactant *Int. J. Hydrogen Energy* **2011**, *36*, 15344 - 15351.
14. Fan, Y.; Hu, H.; and Liu, H. Sustainable Power in MFCs using Bicarbonate Buffer and Proton Transfer Mechanisms. *Environ. Sci. Technol.* **2007**, *41*, 8154 - 8158.
15. Cheng, S.; Liu, H.; and Logan, B. E. Increased power generation in a continuous flow MFC with advective flow through the porous anode and reduced electrode spacing. *Environ. Sci. Technol.* **2006**, ***40***, 2426 - 2432.
16. Zhao, F.; Harnisch, F.; Schröder, U.; Scholz, F.; Bogdanoff, P.; Herrmann, Challenges and Constraints of Using Oxygen Cathodes in Microbial Fuel Cells Ingledew. I *Environ. Sci. Technol.* **2006**, *40*, 5193 - 5199.

17. Ferguson, S. J.; and. Ingledew, W. J. Energetic problems faced by micro-organisms growing or surviving on parsimonious energy sources and at acidic pH: I. Acidithiobacillus ferrooxidans as a paradigm *Biochim. Biophys Acta* **2008**, *1777*, 1471 - 1479.
18. Jahav, G. S.; and Ghangrekar, M. M. Performance of microbial fuel cell subjected to variation in pH, temperature, external load and substrate concentration *Bioresour. Technol.* **2009**, *100*, 717 - 723.
19. Graef, M. D.; Alexeeva, S.; Snoep, J. L.; and Mattos, M. J. T. D. The Steady-State Internal Redox State (NADH/NAD) Reflects the External Redox State and Is Correlated with Catabolic Adaptation in *Escherichia coli J. Bacteriol.*, **1999**, *181*, 2351 - 2357.
20. Logan, B. E.; *Microbial Fuel Cells*, John Wiley and Sons, Inc. Hoboken, New Jersey, 2008.
21. Mohan, Y.; Kumar, S. M. M.; Das, D. Electricity generation using microbial fuel cells *Int. J. Hydrogen Energy* **2008**, *33*, 423 - 426.
22. Jang, J. K.; Pham, T. H.; Chang, I. S.; Kang, K. H.; Moon, H.; Cho, K. S.; Kim, B. H. Construction and operation of a novel mediator- and membrane-less microbial fuel cell. *Process Biochem.* **2004**, *39*, 1007 - 1012.
23. Logan, B. E.; Regan, J. M. Microbial Fuel Cells: Methodology and Technology. *Environ. Sci. Technol.* **2006**, *40*, 5181 - 5192.
24. Oh, S.; Logan, B. E. Proton exchange membrane and electrode surface areas as factors that affect power generation in microbial fuel cells. *Appl. Microbiol. Biotechnol.* **2006**, 70, 162 - 169.
25. Dubois, M.; Gilles, K. A. Hamilton, J. K.; Rebers, P. A.; and Smith, F. Colorimetric Method for Determination of Sugars and Related Substances. *Anal. Chem.*, **1956**, *28*, 350 - 356.
26. Picioreanu, C.; Katuri, K. P.; Head, I. M.; van Loosdrecht, M. C. M.; Scott, K. Mathematical model for microbial fuel cells with anodic biofilms and anaerobic digestion. *Water Sci. Technol.* **2008**, *57*, 965 - 971.
27. Benziger, J. B.; Satterfield, M. B.; Hogarth, W. H. J.; Nehlsen, J. P.; Kevrekidis, I. G. The power performance curve for engineering analysis of fuel cells. *J. Power Sources* **2006**, *155*, 272 - 285.
28. Ota, K.; Ishihara, A.; Mitsushima, S.; Lee. K.; Suzuki, Y.; Horifumi, H.; Nakagawa, T.; and Kamiya, N. Improvement of Cathode Materials for Polymer Eletrolyte Fuel Cell. *J.New Mater. Electrochem. Syst.* **2005**, *8*, 25 - 35.
29. Zhang, S. S.; Ren, X.; Read, J. Heat-treated metal phthalocyanine complex as an oxygen reduction catalyst for non-aqueous electrolyte Li/air batteries. *Electrochimica Acta* **2011**, *56*, 4544 - 4548.
30. Liu, H.; Cheng, S.; and Logan, B. E. Power Generation in Fed-Batch MFCs as a Function of Ionic Strength, Temperature, and Reactor Configuration. *Environ. Sci. Technol.* 2005, *39*, 5488 - 5493.
31. Tanaka, K.; Vega, C. A.; and Tamamushi, R. 612bis-Thionine and ferric chelate compounds as coupled mediators in MFCs. *Bioelectrochem. Bioenerg.* **1983**, *11*, 289 - 297.

Chapter 5

EVALUATION OF THE CATHODIC REACTION

5.1 Introduction

Within this chapter the reduction of oxygen at the cathode electrode was evaluated, and then a summary of the effect of differing cathode materials and their reactor configurations is reported. The final part of this study focused on the cathode utilising different electron acceptors.

5.2 Improvement of cathode materials

Effect of oxidative treatment of Ketjen Black

The generation of functional groups on the surface of Ketjen Black EC-600 carbon can be introduced by chemical oxidation treatments. After the oxidation treatment there is a significant change to the surface modification characterised by SEM, and IR spectra. SEM images were taken applying different magnifications between 100 and 5000. The SEM images of the functionalised and none functionalised Ketjen Black EC-600 is shown in (figures 5.1, A, and B), respectively. From the SEM images it can be seen that there is little change in morphological shape.

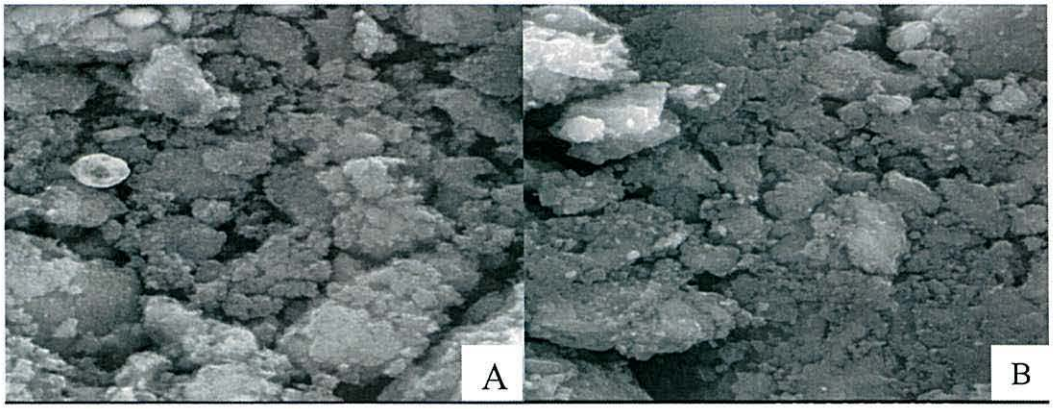

Figure 5. 1 - SEM image of the Ketjen Black EC-600 (A) functionalized, (B) none functionalized sample.

The IR peaks identified for Ketjen Black EC-600 carbon from the IR spectra are shown in Table 5.1. IR spectra for both functionalised and none functionalised samples for Ketjen Black EC-600 JD are shown in (figures 5.2, A, B). Chemical treatments such as wet oxidation in saturated ammonium peroxydisulphate can functionalise the surface of Ketjen Black EC-600 JD carbon with attached groups such as hydroxyl (-OH), carboxyl (-COOH), solfonated and carbonyl (-C=O) that are necessary to tether metal ions to the surface of the Ketjen Black EC-600 JD.[1,2] Commonly oxidation treatment process increases microporosity and surface area of

carbon black. The process involves the initial increase in the pore diameter giving rise subsequent increases in the internal as well as the total surface area. Further to the already started information, the oxidation treatment process is carried out in order to make carbon support wettable.[3] The peak at 1229 cm^{-1} corresponds to sulphonated groups. The peak at 1396 cm^{-1} which is due to the phenol/hydroxyl, there is also a band at 1718 cm^{-1} which can be assigned to the carbonyl (C=O) stretching frequencies for ketones, aldehyde, or carboxyl groups. The peak at 1600 cm^{-1} corresponds to the quinine is present in functionalised and none functionalised Ketjen Black EC-600. The band in the region of 1401.2 cm^{-1}could be –C–OH groups in phenol.[4] There is a large band at 3400 cm^{-1}, due to O-H of water. [5]

Table 5. 1- IR characterisation of the functionalised and none functionalised Ketjen Black EC-600.

None functionalised Ketjen Black carbon (cm^{-1})	Functionalised Ketjen Black carbon (cm^{-1})
1115 C-O (stretch of –COOH group)	1115 (sulphonated groups)
None	1396 (phenol/hydroxyl)
1618 (quinone)	1618 (quinone)
None	1718 (carbonyl (C=O) stretching)

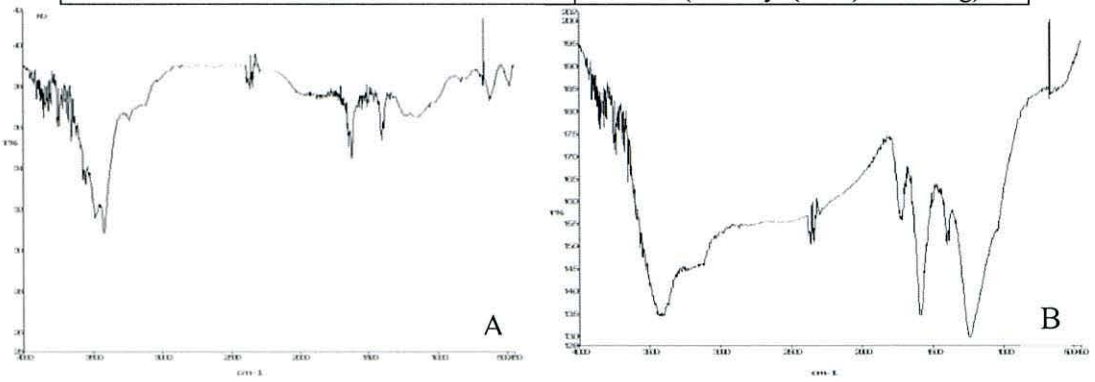

Figure 5. 2 - (A) FTIR spectra of none functionalized Ketjen Black carbon-600 JD, (B) functionalized Ketjen Black EC-600 JD.

Point of zero charge

Using the PZC method, where the final pH for Ketjen Black EC-600 was measured, a strong buffering effect was evident at pHs 4, 5, and 6, as shown by (Figure 5.3), for Ketjen Black EC-600 the PZC is 9 before oxidising treatments.

This study demonstrated that PZC plays an important role for the choice of platinum complex. For example if the surface of the carbon is positively charged at solution (pH< PZC) an anionic platinum complex is required i.e. $[PtCl6]^{2-}$, if the carbon surface is negatively charged at solution (pH> PZC) a cationic complex, that is $[Pt(NH3)4]^{2+}$, is required.[6]

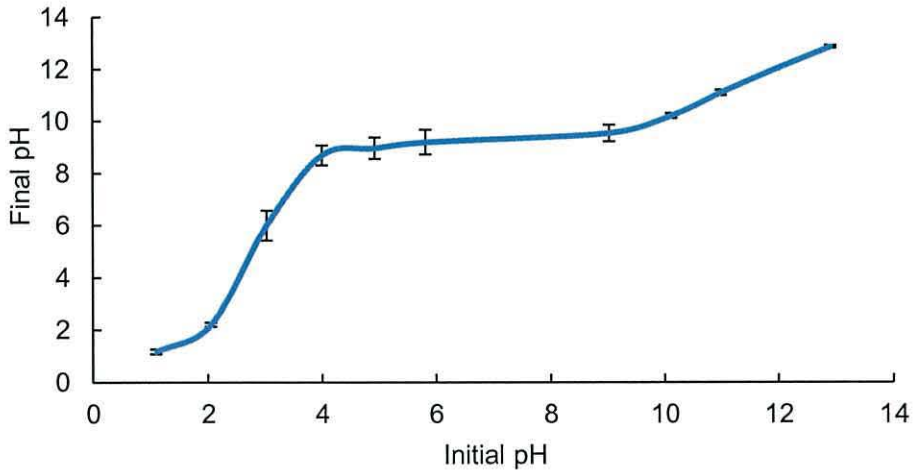

Figure 5. 3 - PZC measurement for Ketjen Black EC-600, experiments run in triplicate (Error bars equals ±1 SD).

A graph of initial pH *versus* final pH for sulphonated and unsulphonated Ketjen Black EC-600 shows in (Figure 5.4) it is clear that the pH of PZC of Ketjen Black EC-600 changes for both sulphonated samples compared with the unsulphonated sample, although it is indicated that sulphonic acid introduces the acidic group.[1] The PZC is attained from the horizontal axes of the graph. The PZC values for unsulphonated and sulphonated 24 and 48 hours Ketjen Black EC-600 are 9.1, 3.3, and 2.8, respectively.

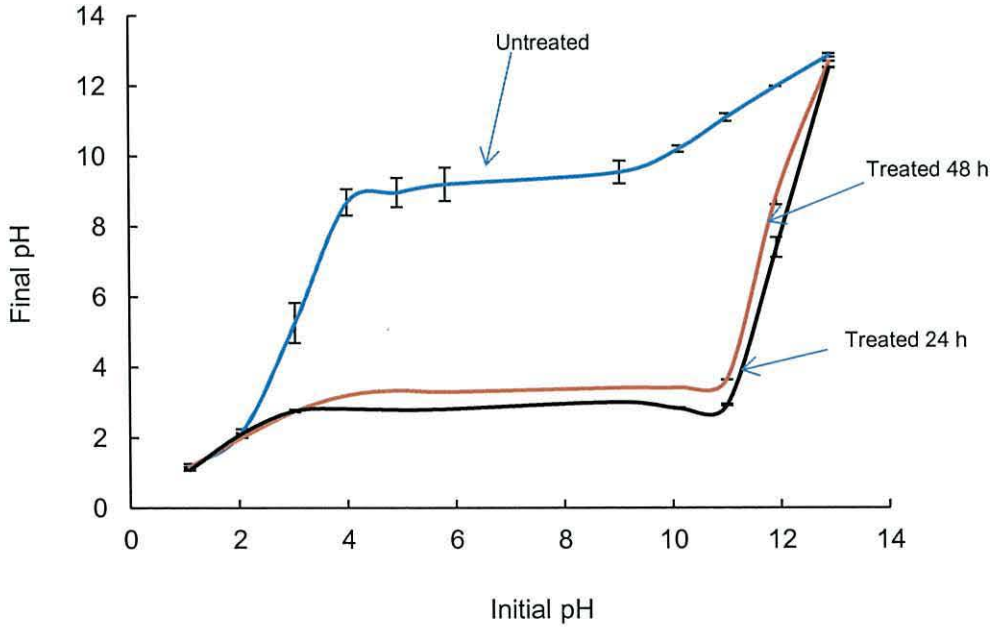

Figure 5. 4 - PZC for untreated, sulphonated Ketjen Black EC-600 JD, oxidation time 24,48h, experiments run in triplicate (Error bars equals ± 1 SD).

X-ray diffraction analysis

KB EC-600JD carbon black was used as the control and supporting carbon for platinum nano-sized particles. In order to know the platinum loading process, the formation of nano-sized platinum particles on the 22 wt % Pt/KB carbon support was established using X-ray diffraction (XRD). The face-centred cubic (FCC) nature of the reduced platinum ions was confirmed as shown in (Figure 5.5). The crystallinity, Pt (111), Pt (200) and Pt (220) of the platinum can clearly be seen; these are characteristic diffraction peaks for FCC and were found at diffraction angles of (2Theta) values of 40.2°, 46.7° and 68°, respectively. The resulting spectrum is in accordance with the standard powder diffraction expected for platinum nano sized particles.[7]

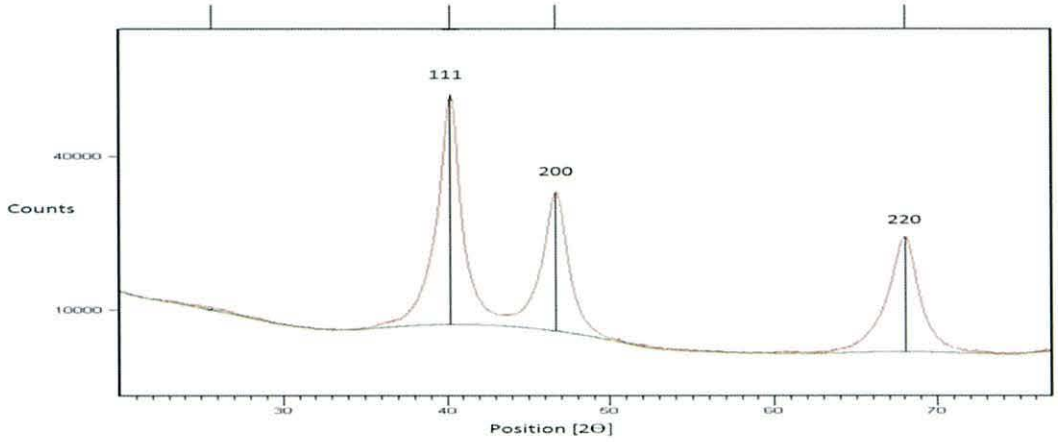

Figure 5. 5 - XRD analysis of 22 wt % Pt/K.B on carbon Ketjen Black support.

Transmission electron microscopy

In order to determine the size of the platinum particles and their dispersion on the surface of Ketjen Black carbon support the resulting Pt/KB electrodes were checked by Transmission Electron Microscopy (TEM). Figure 5.6 shows the TEM image of spherical platinum loaded on the surface of Ketjen Black EC-600 JD which is of a darker contrast; figure 5.6 also illustrates the homogenous nature of the Pt dispersion, well-separated nanoparticles, and in a narrow particle size range observed over the surface of Ketjen Black carbon. No significant accumulation was observed. The calculations yielded an averages diameter for the platinum particles of around 3 nm and the oxidised Ketjen Black EC-600 JD particles are visible in the TEM micrographs as large grey particles which range from 20 to 30 nm in diameter (Figure 5.6).

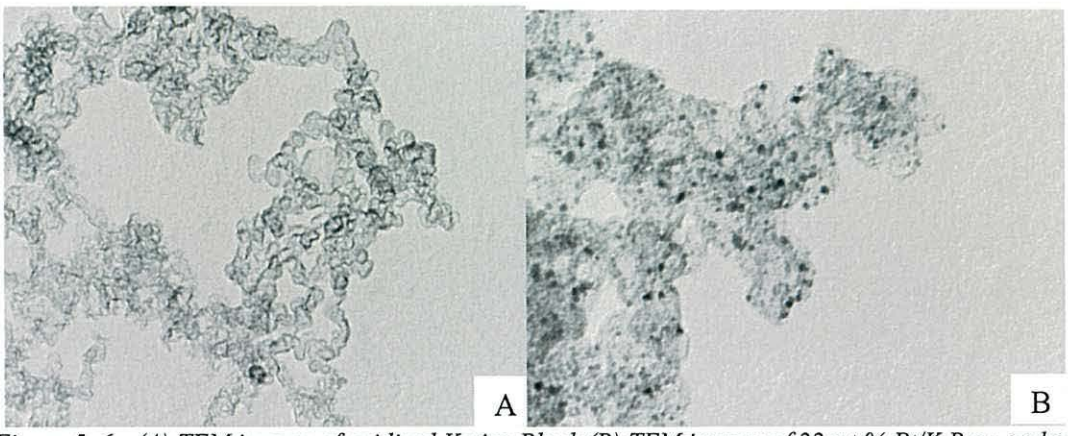

Figure 5. 6 - (A) TEM images of oxidised Ketjen Black,(B) TEM images of 22 wt % Pt/K.B on carbon Ketjen Black support (scale bar equals 100nm).

Previous work by Rimbu *et al.,* obtained an average diameter of 5.4 nm albeit with a different form of KB EC-300JD with a smaller surface area (800 m^2/g),[8] than the KB EC-600JD used (1400 m^2/g). As the particle size of the Pt is depends on the surface area of the carbon support, the average diameter of the particles fell within the expected size range.[9,10,11]

The size distribution of platinum nanoparticles is shown in the histogram in (Figure 5.7). It is clearly seen that the platinum nanoparticles, which correspond to the Pt loadings (22 wt % Pt/K.B) were relatively uniform. The distribution of particle sizes of (22 wt % Pt/K.B) was around 2 to 4 nm. This size distribution in the histogram was fairly narrow. The histogram describes the analysis of the size among 60 platinum particles per sample measured in the TEM image.

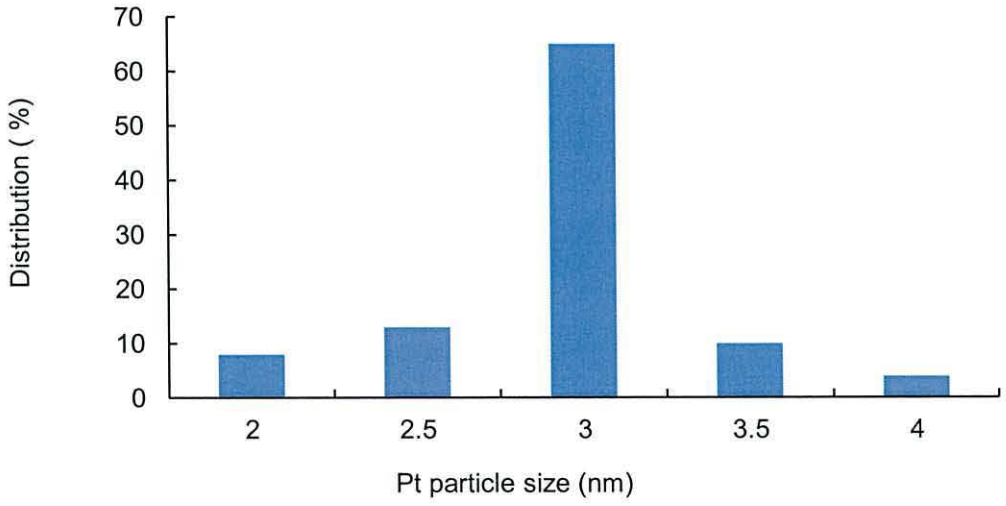

Figure 5. 7 - Particle size distribution of Pt particles for the22 wt % Pt/K.B on carbon Ketjen Black support.

Atomic absorption spectroscopy

The amount of platinum metal after the preparation of the Pt/KB was established *via* the use of Atomic absorption spectroscopy (AAS). The resulting data indicated that the KB contained 22 wt % Pt. This value is less than the expected value of 35 wt % indicating that losses occurred during the preparation or that not all platinum ions reduced to Pt metal.

5.3 Electrochemical characterisation

Study Oxygen reduction with different Pt loading using linear sweep voltammetry

In order to establish that the reduced platinum ions were able to act as a catalytic surface for the reduction of oxygen, linear sweep voltammetry (LSV) were obtained for the nano scale platinum loaded KB. The electrochemical measurements were carried out on a GC electrode that had been modified with 22 wt % Pt/KB *vs.* SCE at room temperature in O_2 saturated and 500 mM H_2SO_4 (Figure 5.8).

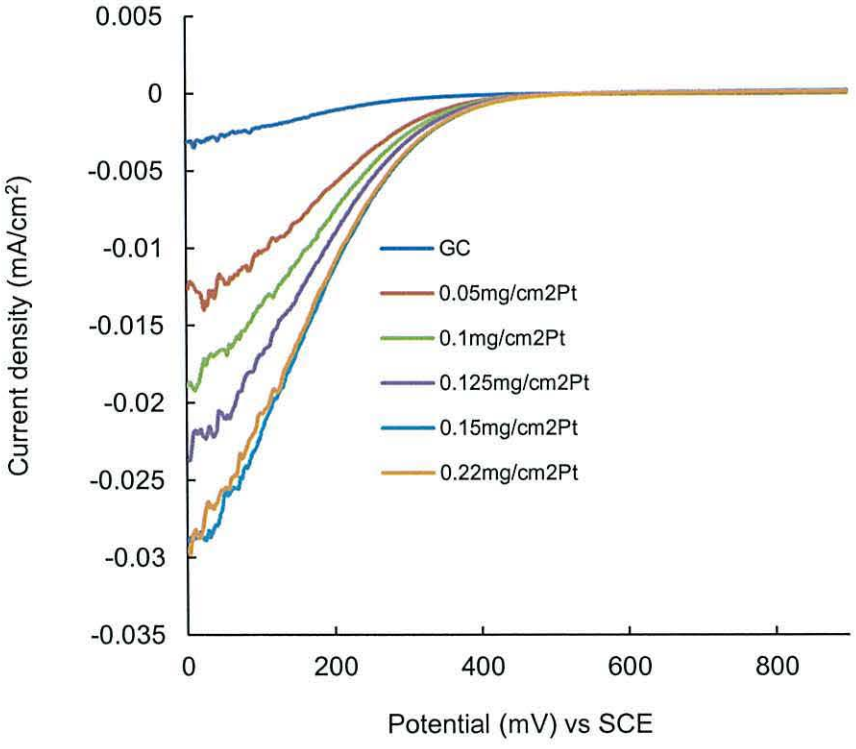

Figure 5. 8 - Oxygen reduction current densities: effect Pt loading (0.050 – 0.220 mg/cm^2) on KB modified GC electrode, in oxygen saturated 500 mM H_2SO_4 at a scan rate of 5 mV/s.

The oxygen reduction activity of Pt content (50 $\mu g/cm^2$- 220 $\mu g/cm^2$) are a distinguishing feature of the oxygen reduction increases (currents over the range 0 mV to 900 mV were produced), which is characteristic of nanoparticulate platinum on the surface of a carbon support (KB). The high cathodic current indicates that there is electrocatalytic activity of the functionalised Pt/KB electrode in the oxygen reduction region of the voltammogram.[12] The catalytic activity of the platinum on the Pt/KB coated on one side of the wet-proofed carbon cloth 5 cm^2 was also confirmed by voltammetry. Hence, in the comparatively complex mixture of platinum, KB and Nafion the surface of the platinum is exposed to the electrolyte solution and as such is suitable for the catalytic reduction of oxygen within the MFC.

Cathode performance versus platinum content

The performance of the cathode electrode with different platinum loading at a constant potential (20 mV) is shown in Figure 5. 9. It can be seen that the current density increased with platinum content up to 0.15 mg/cm^2 Pt. Figure 5.9 also illustrates that the current density slightly changed when the platinum loading increased to more than 0.15 mg/cm^2. It is interesting to observe that even with increasing amounts of platinum loading, the optimum performance of 0.22 mg/cm^2 shows only small increases in current density compared to the amount of platinum added. According to these results, an optimum platinum loading would be around 0.15 mg/cm^2 when 22 % Pt/K.B was used to make the cathode electrode.

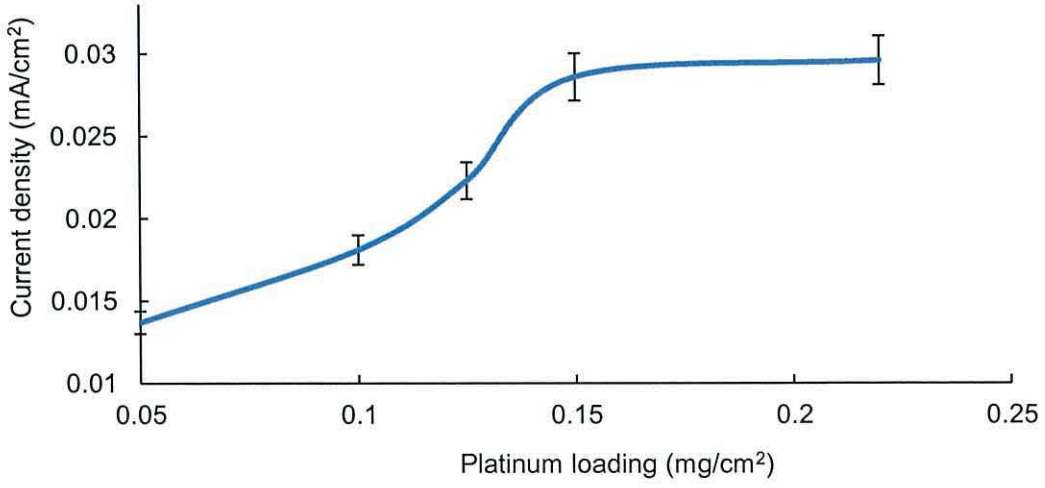

Figure 5. 9 - Current density vs. Pt loading for cathode electrode made using GC 22 % Pt/K.B experiments run in triplicate (Error bars equals ± 1 SD).

Efficiency study of Pt/KB catalyst

The efficiency of platinum nanoparticles loading on KB carbon [0.15 mg /cm^2 (22 wt % Pt/KB)] coated on side carbon cloth (5 cm^2) was carried out by measuring the current and power density during the MFC operation. Efficiency of the Pt/KB catalyst could be estimated from the corrosion of the KB carbon during the MFC operation. In Figure 5.10, it can be seen that the efficiency of the Pt/KB catalyst (0.15 mg/cm^2 (22 wt % Pt/KB)) decreases as the MFC hours of operation time increased, the efficiency decreases from 100 % to 89 % and 72 % after 10, 645, and 984 hours of operation time, respectively. This decline of efficiency is reflected by loss of platinum electrochemical surface area during the MFC operation. The platinum electrochemical surface area was lost at the cathode by the following mechanism: Firstly platinum as a nanoparticle were lost, this is due to carbon supported corrosion, secondly large platinum nanoparticles were forming a from a small dissolution platinum particles, thirdly aggregation of platinum nanoparticles by minimum surface energy.[13,14] Table 5.2 shows that both power density and current density decrease during an increase in the MFC hours of operation.

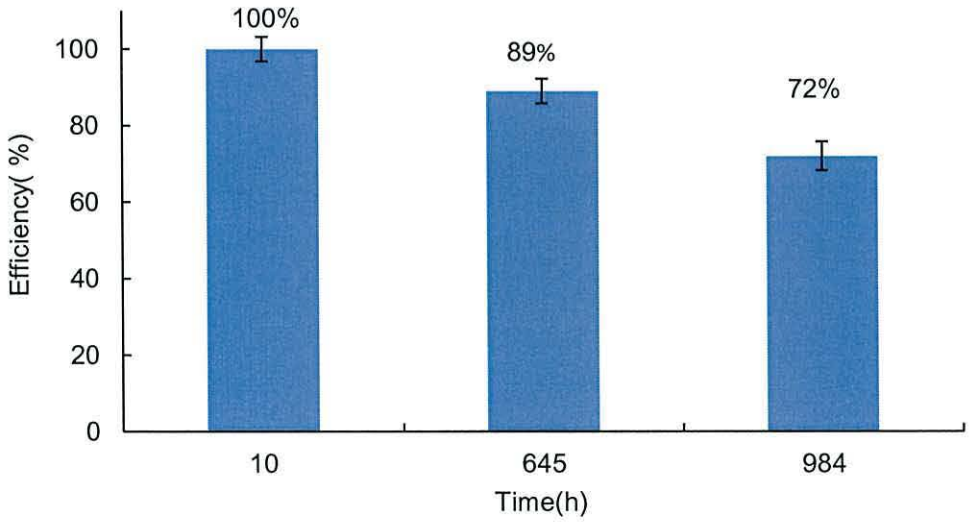

Figure 5. 10 - Efficiency of platinum nanoparticles loading on KB carbon [0.15 mg /cm^2 (22 wt % Pt/KB)] during MFC operation as a function of time. Three repetitive cycles (Error bars ± SD).

Table 5. 2- Effect of efficiency platinum nanoparticles loading on KB carbon [0.15 mg/cm^2 (22 wt % Pt/ KB] electrical current of MFC during operation in which the time increases.

Time (h)	Efficiency (%)	Current density (mA/m^2)(100Ω)	Power density (mW/m^2) (2000 Ω)
10	100	296 ± 2	20.7
645	89	284.6 ± 2	18.2
984	72	230.2 ± 2	15.4

5.4 Analysis of two-chamber microbial fuel cells

Microbial fuel cell performance using different Pt loadings

Platinum is a high cost and rare material, hence it is beneficial to reduce the amount used without affecting the performance. The experiments recognised activity and stability of the Pt/KB electrocatalyst with different Pt loading, in addition to solid Pt. The polarisation curve of the MFC experiment using *Acidiphilium* sp. SJH (5.1×10^7 cells/ml), ferric ion (10 mM), and glucose (900 mg/L) in buffer solution of pH 2.5 (potassium hydrogen phthalate, 100 mM) in the anode chamber is shown in figure 5.11 on the following page. The OCV of MFC using Pt electrode, and platinum nanoparticles loading on KB carbon [0.15 mg/cm^2 (22 wt % Pt/KB)] coated in one side of the wet-proofed carbon cloth (5 cm^2) in the cathode chamber supplied with air as an electron acceptor in buffer solution pH 2.5 were (424 mV, 381 mV) respectively.

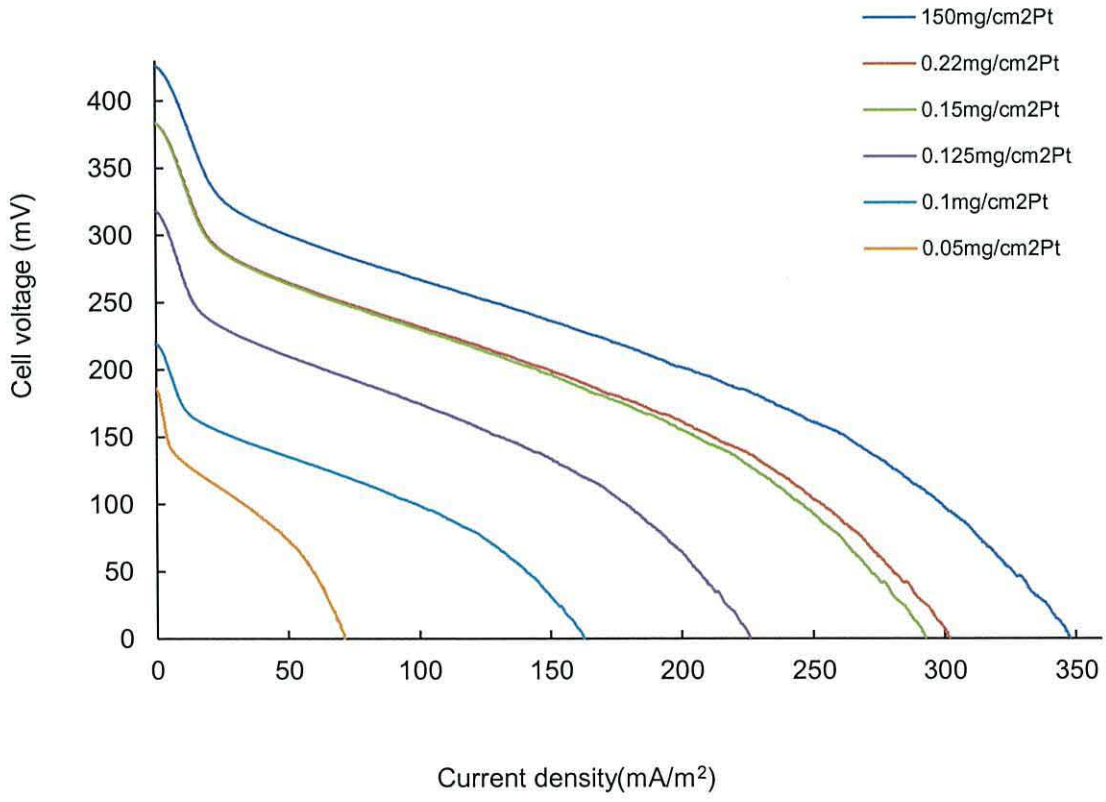

Figure 5. 11 - MFC polarisation curves with solid platinum electrode and various platinum nanoparticles loading on KB carbon (0.05-0.22mg/cm^2).

When platinum nanoparticles were loaded on KB carbon compared to a solid platinum electrode the modified cathode retained high efficiency. This indicates that the KB carbon can affect the catalyst activity as is also reflected in the OCV of the MFC. The use of nano particles which provide a large increase in surface area compared to a planer electrode. Figure 5.11 and Table 5.3 shows how the performance of the MFC correlates with Pt loading. OCV and current density increases were observed when the loading Pt increased from 0.05 to 0.22 mg/cm^2. However, the high quantity of OCV and current density were achieved when the loading reached 0.15 mg/cm^2. Figure 5.11 also illustrates that the current density slightly changed when the platinum loading increased to more than 0.15 mg/cm^2. Increasing the amount of platinum will offer only small increases in current density compared to the amount of platinum added.

Table 5. 3- OCV and current densities in MFCs for Pt electrode and various platinum nanoparticles loading on KB carbon.

Cathode electrode	OCV(mV)	Current(mA/m^2)(100 Ω)
Platinum electrode 0.15 g/ cm^2	424	340
0.05 mg/cm^2(22 wt % Pt/KB)	186	71
0.1 mg/cm^2(22 wt % Pt/KB)	220	160
0.125 mg/cm^2(22 wt % Pt/KB)	314	223
0.15 mg/cm^2(22 wt % Pt/KB)	381	293
0.22 mg/cm^2(22 wt % Pt/KB)	383	302

Electrode potential

The OCPs were measured for the electrodes (*anode and cathode*) of the MFC against a SCE as a function of current with different resistor circuits (100 to 50,000Ω) (Figure 5.12). The OCP of the anode was -176 mV, but the working potential decreased to -134.6 mV for current density up to 300 mA/m^2. The OCP of the cathode was 210.6 mV, but the working potential decreased to 21.4 mV for current density up to 300 mA/m^2 figure 5.12. It was observed that the OCP of the cathode using [0.15 mg/cm^2 Pt (22 wt % Pt/KB)] result in 225.6 mV (467.6mV NHE) this was lower than the theoretical cathode potential as energy losses occur at the cathode, indicating that further developments in the cathode construction are possible.

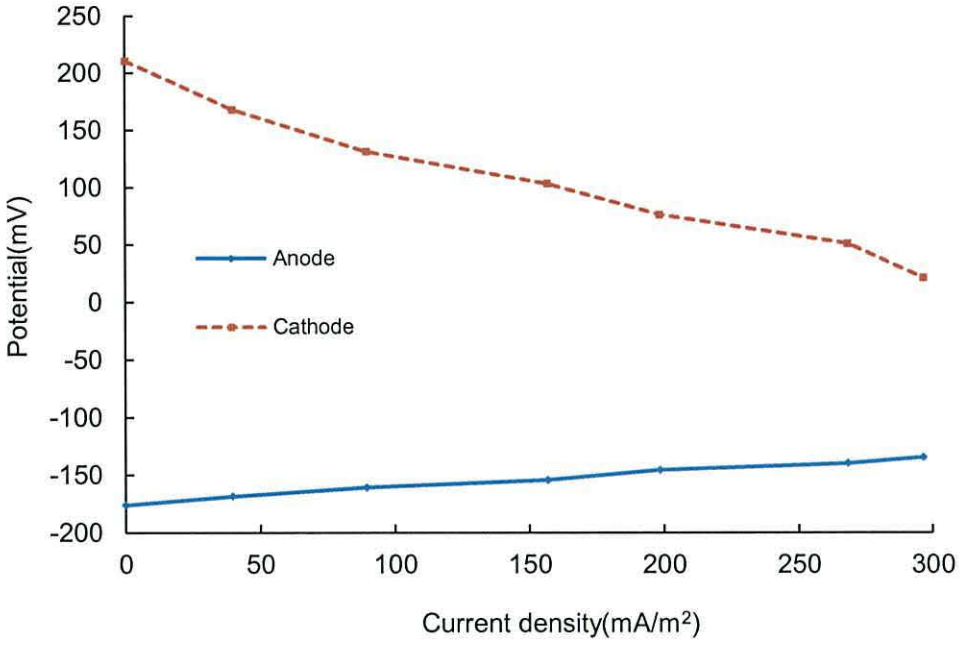

Figure 5. 12 - Anode (solid line) and cathode (dashed line) potential (vs. SCE reference electrode, 242mV against the NHE) as a function of current.

Polarisation curve

Polarisation and power density curves were obtained to calculate the maximum power density and current density against potential for the sandwich-type MFC utilising *Acidiphilium* sp. SJH bacteria (5.1 x 10^7 cells/ml), in the presence of glucose (900 mg/L) as electron donor and soluble ferric ion (10 mM) as the electron shuttle (Figure 5.13). When the OCV of the sandwich-type MFC reached the maximum it stabilised (388 mV). Sandwich-type MFC polarisations were operated with the distance between the anode and cathode of 4 cm at different resistance across the anode and cathode, under optimal conditions (pH 2.5, room temperature). The current density was determined using Ohms law based on the MFC voltage. From these measurements, the optimal external resistance was found which showed the maximum power density. The cell current and voltage data can be examined and recorded at the maximum power density. The polarisation curve also showed that MFC keeps a voltage as a function of the current density production, that the OCV is 388 mV and that the voltage drops quickly to 264 mV at a current density of 52.8 m A/m^2, known as activation losses region. There is then linear decrease in voltage with an increase in current density after that point, known as ohmic losses region. The last region known as mass transport losses occur at high current density and the quantity increases with increasing current density. The power density increased with current

density to a maximum power point (20.7 mW/m^2) which occurred at 2000 Ω. The cell voltage and the current density were calculated from the polarisation curve; at the maximum power point value of power density, when the current density (I_{mp}) was 150 m A/m^2, with a corresponding cell voltage (V_{mp}) of 150 mV.

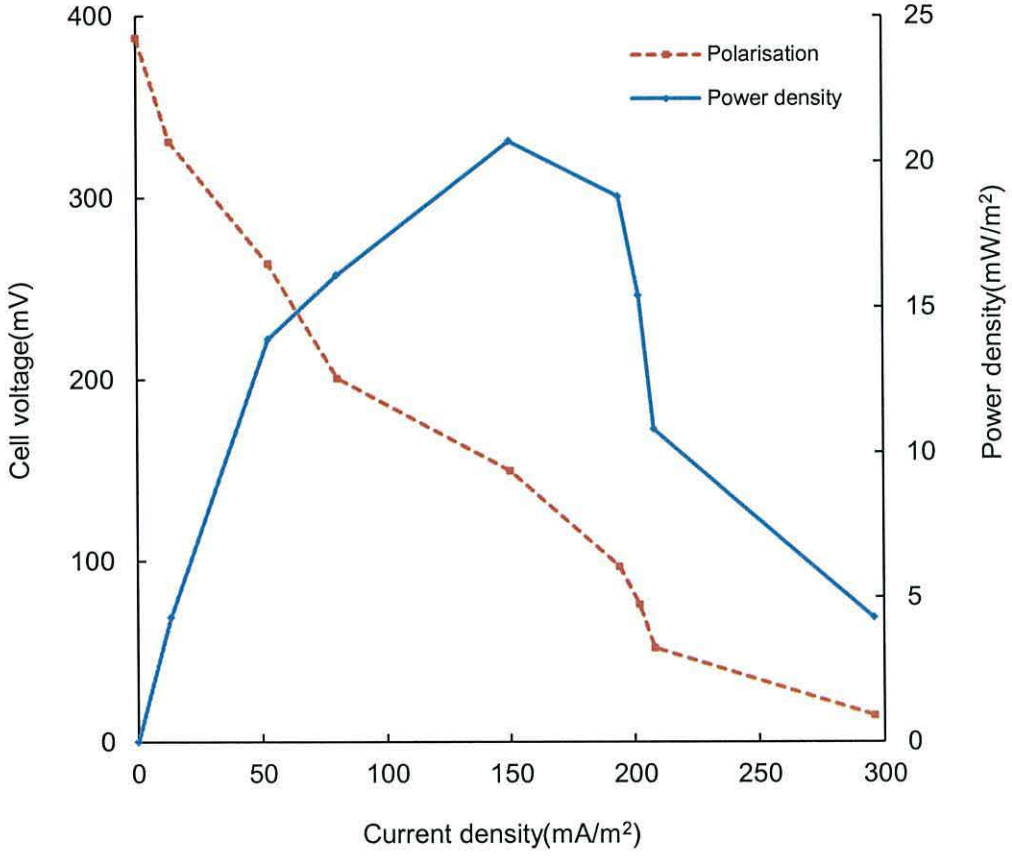

Figure 5. 13 - Sandwich-type MFC polarisation (dashed line) and power density (solid line) curve distance between the anode and cathode of 4 cm in buffer solution of pH 2.5.

The power generation using a two chamber MFC inoculated with *Acidiphilium* SJH was 20.7 mW/m^2 (figure 5.13) and compared to similar configurations reported in the literature. Borole and Neill obtained 12.7 mW/m^2 using *Acidiphilium cryptum* (pH≤ 4),[15] Bond *et al* obtained 14 mW/m^2 using a two-chambered microbial fuel cell,[16] while Bond and Lovley achieved 14.7 mW/m^2 (pH 7) using G. sulfurreducens and acetate-fed membrane (Nafion) fuel cells.[17] These power densities are higher than those reported for MFCs with *Shewanella putrefaciens* IR-1 and lactate (0.6 mW/m2; Kim *et al*,[18] or Rhodoferax ferrireducens and glucose (8 mW/m^2; Chaudhuri and Lovley.[19]

Effect of pure oxygen to gas cathode chamber

The most suitable electron accepter for an MFC is oxygen, which is commonly used because of its low cost, sustainability, and its high reduction potential.[20] A comparison of the MFCs performance between the cathodes supplied with pure oxygen as an external source of electron acceptors, and supplied with air is shown in (Figure 5.14). Sandwich-type MFC was operated when only pure oxygen was used to gas the cathode chamber; the maximum power density and CE were (18.2 mW/m^2, and 5.9 ± 1.3 %) respectively. Figure 5.14 also illustrates that the maximum power density was (20.7 mW/m^2, and 6.6 ± 0.9 %) respectively, when the cathode chamber was gassed with air. The resulting power densities showed a higher trend with the cell supplied with air obtaining a power density of 20.7mW/m^2 compared to18.2 mW/m^2 for the cell supplied with oxygen. The increase in the maximum power density using air versus pure oxygen was unexpected, because pure oxygen used to the cathode chamber was the most rate-limiting step.[21] These results suggest that more oxygen diffused to the anode chamber through the membrane to reduce the power density by taking electrons from the anode, when pure oxygen was used. The total CE found here was 6.6 ± 0.9 % using (1800 mg/L glucose).

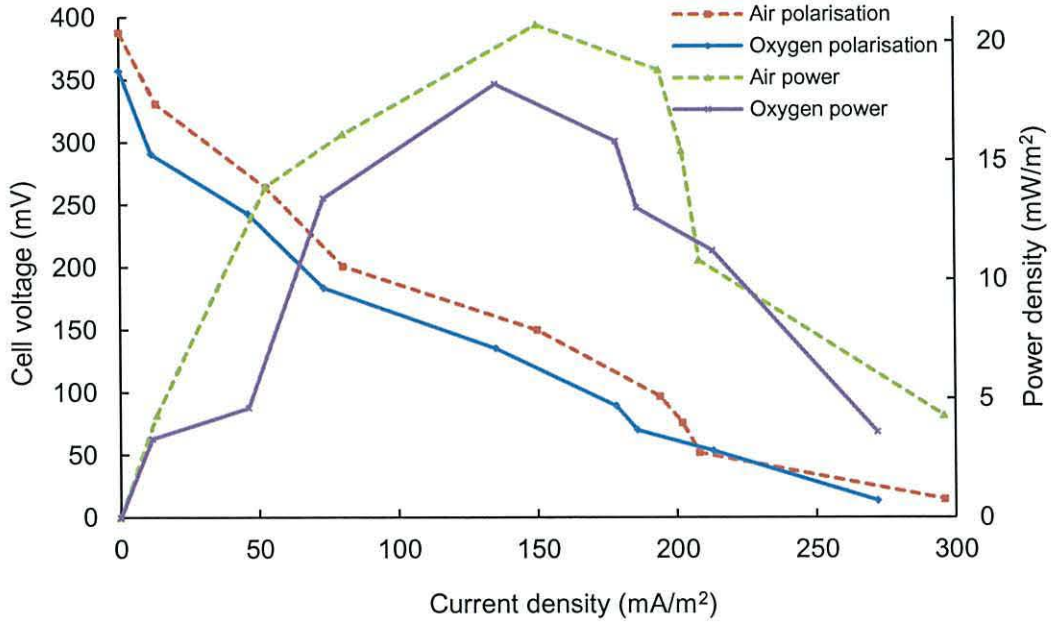

Figure 5. 14 - A comparison of the MFCs performance (polarisation and power density curve) between the cells supplied with pure oxygen(solid line) as an external source of electron acceptors, and supplied with air (dashed line) using [0.15 mg/cm² Pt (22 wt % Pt/KB)]cathode electrode.

5.5 Air-cathode two chamber microbial fuel cell

Air-cathode dual chamber MFC exposed directly to air can resolve the low solubility of oxygen in aqueous solution and eliminate biofilm formation on the surface cathode chamber, particularly due to the high sensitivity of precious metal catalysts. In addition, it eliminates the need for an aerated cathode.[22] Electricity generation using the characteristics of air-cathode two chamber MFC were tested by a polarisation curve utilizing *Acidiphilium* sp. SJH bacteria (5.1 x 10^7 cells/ml), in the presence of glucose (900 mg/L) as the electron donor and soluble ferric ion (10 mM) as the electron shuttle were referenced to the anode and the cathode was made of 150 $\mu g/cm^2$ (22 wt % Pt/KB) coated on wet-proofed carbon cloth, (*coated side*) placed facing the solution, with the uncoated side exposed to the air (Figure 5.15). The data were collected to calculate the power generation and voltage continued across a range of current densities attained by varying the resistance between the anode and cathode electrodes. The power density increased with current density to a maximum power point (17.4 m W/m^2) which occurred at 2000 Ω. The cell voltage and the current density were calculated from the polarisation curve; at the maximum power point value of power density, when the current density (132 I_{mp}) was mA/m^2, with a corresponding cell voltage (132 V_{mp}) of mV.

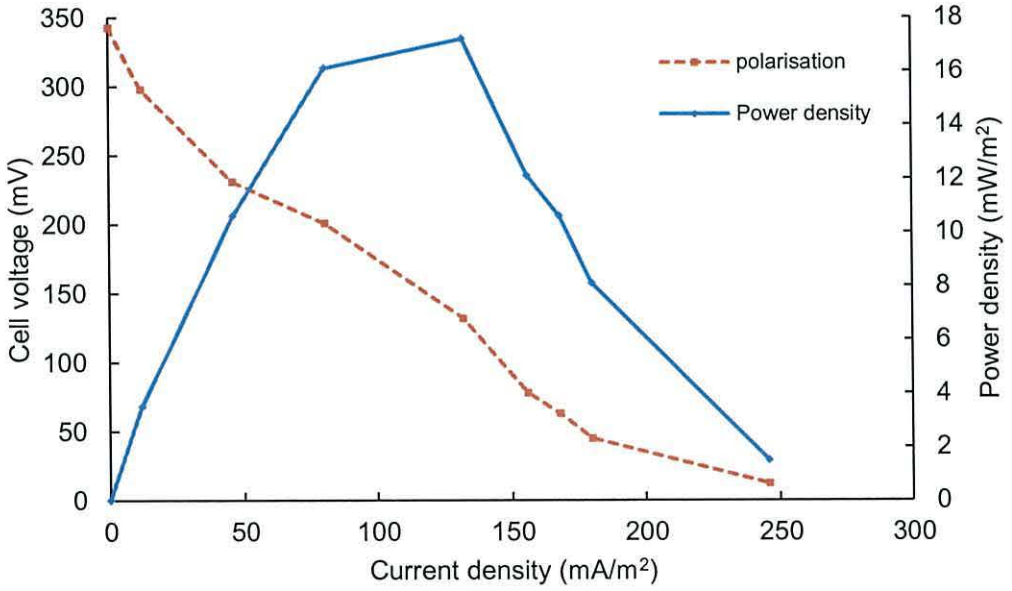

Figure 5. 15 - Air cathode MFC polarisation (dashed line) and power density (solid line) curve, using [0.15 mg/cm² (22 wt % Pt/KB)] coated on side carbon cloth (5 cm²) cathode electrode, and distance between the anode and cathode of 4 cm in buffer solution of pH 2.5.

A comparison of the MFCs performance between the cathodes of sandwich design supplied with pure oxygen as an external source of electron acceptors, and supplied with air and air-cathode design utilising the air diffusing electrode, (which obtained the oxygen from the atmosphere) is shown in (Table 5.4). The air-cathode dual chamber MFC exposed directly to air can resolve the low solubility of oxygen in aqueous solution. The OCV, current density, and power density of the air diffusing cathode was in the range of 343 mV, 132 mA/m^2, 17.2 mW/m^2 respectively. The voltage, current, and power remained stable, indicating the successful diffusion of oxygen through the air electrode.

Table 5. 4 - A comparison of the MFCs performance.

Reactor configuration	Electron acceptor	OCV mV	Current density mA/m^2	Power density mW/m^2
Sandwich	O_2 supply external source	357	135	18.3
Sandwich	Air supply external source	388	144	20.7
Air-cathode	O_2 supply from atmosphere	343	132	17.4

Spacing between electrodes in air cathode two chamber microbial fuel cells

A series of tests were conducted to study the effect of different electrode spacing (4, 3 and 2 cm) on power production in air cathode MFCs. When the distance between the anode and cathode were reduced from 4, to 3, and to 2 cm [anode was exposed to both sides of the fluid (3 cm) or fixed against a wall in a chamber with only one side exposed of the solution (4 and 2 cm)] and the cathode was made of 150 $\mu g/cm^2$ (22 wt % Pt/KB) coated on wet-proofed carbon cloth, (coated side) placed facing the solution, with the uncoated side exposed to the air; Figure 5.16 shows the power output observed at variable external loads and under different electrode spacing's between the anode and cathode electrodes. In this study reducing the electrode spacing, there may be little observable effects on the performance of MFCs. The performance was compared with that recorded from the normal run 4cm with the distance of 3and 2 cm. Under different external load, the power density increased with reductions in distance between the electrodes. The maximum power density increased from 17.4 to 18.6, and 19.8 mW/m^2 respectively, when the electrode spacing decreased from 4, t0 3 and to 2 cm. No further improvement in power density was observed with further reductions in electrode spacing between the anode and cathode. These results suggest that, under high internal resistance, there is a slight effect of electrode spacing on power output. A previous report by Jang *et al.,* obtained the maximum power density 1.3 mW/m^2 when the electrode spacing was

(10 cm) and 1.25 mW/m^2 when the electrode spacing was (30 cm).[23] However, previous studies have reported that, in a single-chamber fed-batch system, the power density increased with reductions in the distance between the electrodes (720 mW/m^2, 4 cm to 1210 mW/m^2, 2 cm).[24] Reducing electrode spacing between the anode and cathode can regularly decrease the area-specific electrolyte resistance and in turn the internal resistance, thus improving the performance of MFCs.[25] Thus, if the distance between the two electrodes are reduced, the protons have less distance to move, and the ohmic resistance is reduced. From the power density curves in (Figure 5.16) the internal resistance of the 4, 3, and 2 cm electrode spacing can be evaluated from maximum power density occurred at the point where the internal resistance was equal to the external resistance.[26] From the (figure 5.16), the maximum power density (17.4 mW/m^2 (4 cm), 18.6 m W / m^2 (3 cm), and 19.8 m W/m^2 (2 cm) can be converted to power production from the system:

$$P = P_{An}A_{An} = \left(19.8\frac{\text{mW}}{\text{m}^2}\right)(5\text{cm}^2)\frac{\text{Wm}^2}{10^3\text{mW}10^4\text{cm}^2} = \quad 0.99 \times 10^{-5}\text{W}$$

$$P = P_{An}A_{An} = \left(17.4\frac{\text{mW}}{\text{m}^2}\right)(5\text{cm}^2)\frac{\text{Wm}^2}{10^3\text{mW}10^4\text{cm}^2} = \quad 0.87 \times 10^{-5}\text{W}$$

Now the internal resistance can be estimated , as being equal to the external resistance, which were calculate from the currents of 141 mA/m^2 (2 cm), and 132 m A/m^2.

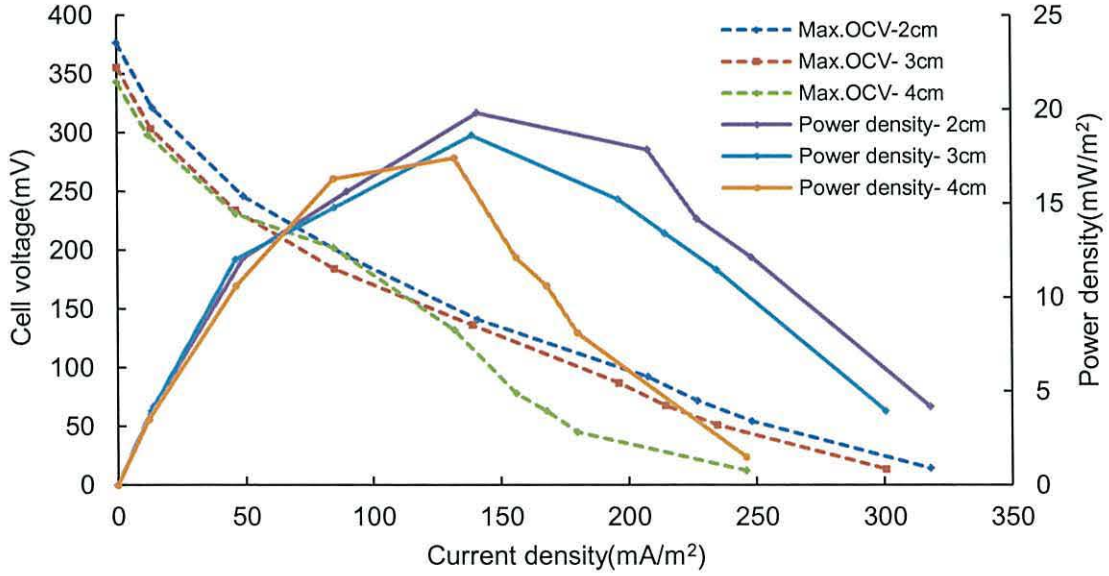

Figure 5. 16 - Polarisation and power density curve of the air cathode two chamber MFC operated with electrode spacing (4, 3, and 2cm).

The calculate internal resistance from power density curve = 1997 Ω 4 cm) electrode spacing and 1991 Ω for 2 cm electrode spacing. There was a small change in internal resistance. The reduction of electrode spacing (4 and 2 cm) had limited effect on power improvement due to the high internal resistance.

Platinum nanoparticles electrodeposited on carbon felt

The cyclic voltammograms of nanoparticles of platinum modified carbon felt is illustrated in (figure 5.17). Nanoparticles of platinum were electrodeposited on carbon felt by applying the potential between 100 and -500 mV from an aqueous electrolyte containing 1 mM Chloroplatinic acid hexahydrate and 1 mM of tri-sodium citrate. In this situation, the number of cycle was 30, and the scan rate was 50 mV/s. The current production increase with increasing number of cycles can be seen in Figure 5.17. This suggests that the formation of new nucleation sits was as a result of subsequent cycles. Recently, Zhao *et al* and Dulal *et al* have reported the formation of nanoparticles of platinum at the carbon fiber and multi-walled carbon nanotubes as carbon support.[27, 28]

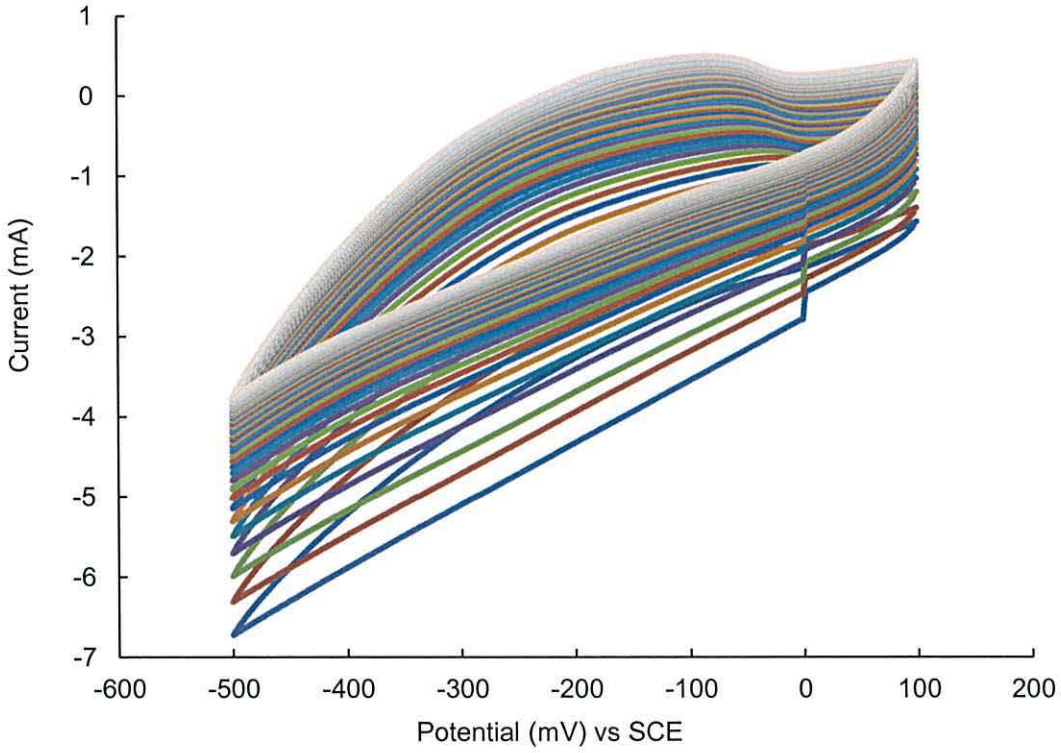

Figure 5. 17 - Cyclic voltammograms of nanoparticles of platinum modified carbon felt. The electrolyte contained 1mM Chloroplatinic acid hexahydrate and 1 mM of tri-sodium citrate. The scan rate was 50mV/s and the number of cycle was 30.

Scanning electron microscopy analyses of electrodeposited Pt particles

The surface morphologies of platinum particles electrodeposited on the surface carbon felt were observed by scanning electron microscopy (SEM) images. Figure 4.18 shows that platinum particles are, more or less, distributed and attached on the surface of the carbon felt. This experiment suggests that platinum (Pt^{4+}) complex covered on the surface of carbon felt can accept electrons to be reduced into platinum and the platinum can aggregate to form a nanoparticle directly by cycling potential scans between 100 and -500 mV. The observed platinum particles by SEM images are constituted by agglomerates of small particle size.

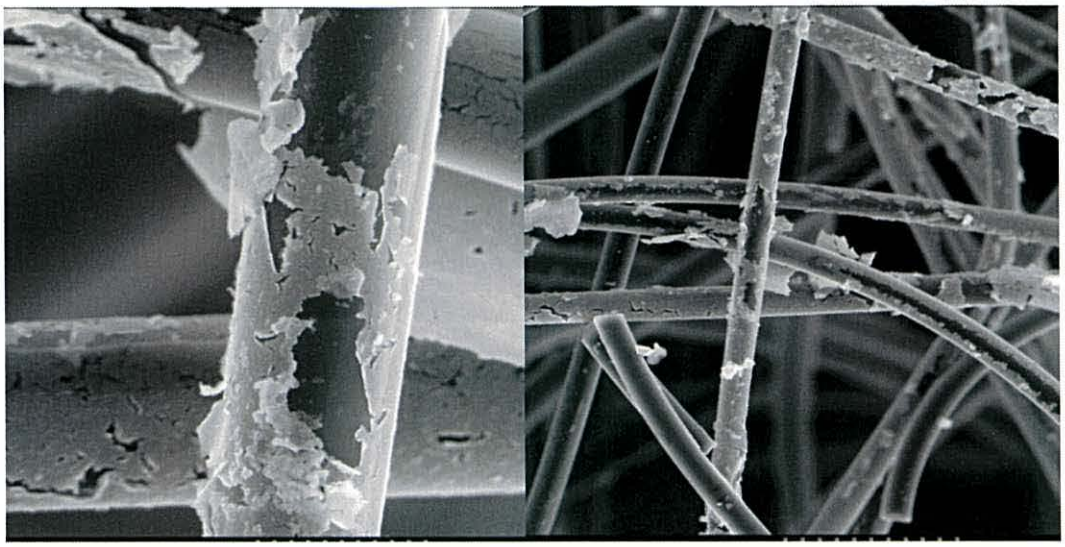

Figure 5. 18 - SEM images clearly showed the differences in size and morphology are observed when Pt is deposited on carbon felt, and the existence of agglomerates of several particles is observed.

Electrochemical characterisation of the platinum modified carbon felt electrode

Observation from the cyclic voltammetry suggest that platinum particles started appearing when this modified electrode was followed by cycling scans between 1500 and -400 mV in 0.5 M H_2SO_4 solution (pH 2.5), which are cyclic voltammetry profiles of platinum electrode in H_2SO_4 solution.[29] This test suggests that platinum particles are generated after reducing of Pt (IV) to Pt (0). As a comparison, cyclic voltammograms of nano-Pt/C. felt modified electrode and carbon felt electrode are shown together in Figure 5.19.

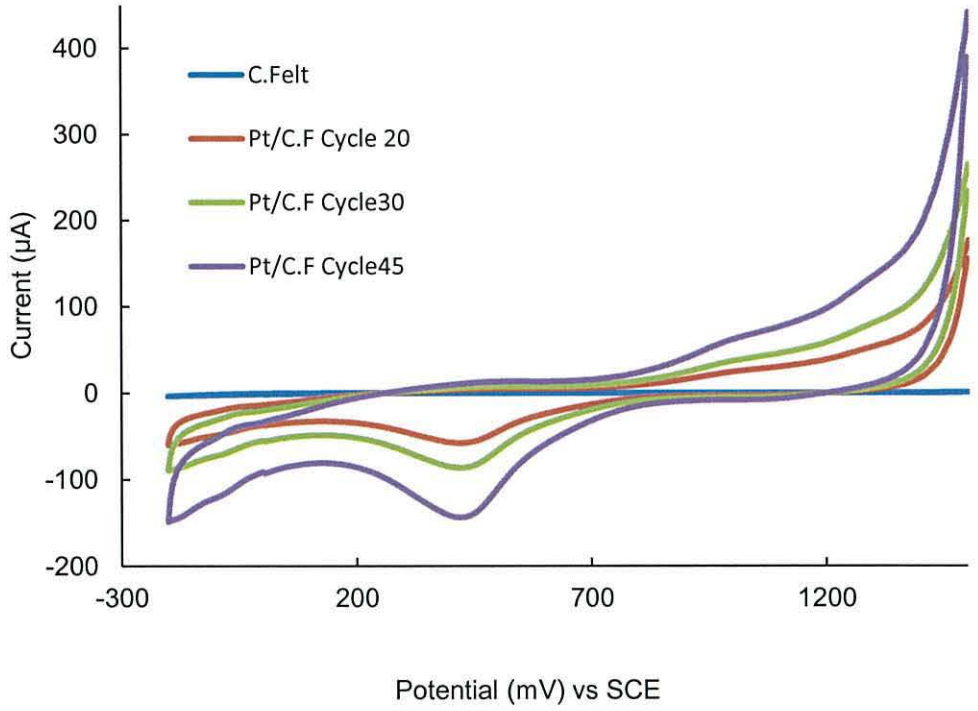

Figure 5. 19 - Cyclic voltammograms of Pt/C. Felt modified electrode obtained from cycling scans of carbon felt electrodes in 1 mM Chloroplatinic acid hexahydrate and 1 mM of tri-sodium citrate aqueous solution with cycling numbers with 20, 30, and 45 cycles, followed by cycling scans between1500 and -400 mV in 0.5M H_2SO_4 solution, scan rate: 50 mV/s.

As can been seen from figure 5.19 voltammogram for the carbon felt electrode had no observable redox peak. To study the effect of the platinum particles electrodeposited on the surface carbon felt the electrochemical activity of various Pt/C. felt modified electrodes were tested. These electrodes were obtained from different platinum particles electrodeposition by technique of cycling scanning carbon felt electrodes in 1 mM Chloroplatinic acid hexahydrate and 1 mM of tri-sodium citrate aqueous solution with cycling numbers from 20 to 45 cycles, followed by cycling scanning in 0.5 M H_2SO_4 solution between 1500 and -400 mV. Figure 4.19 also illustrates that an increase in the number of cycling scans from 20 to 45 cycles for Pt (IV) reduced to Pt (0) results in a significant improvement of the current and confirming that the deposited Pt/C. felt was rather stable.

Performance of electrodeposited Pt /C.felt cathode compared with Pt/KB cathode

Experiments were carried out under similar conditions and repeated three times to examine the performance of a sandwich-type dual chamber MFC with electrodeposited Pt (Pt /C. felt) and Pt/KB catalysts. The sandwich-type dual

chamber MFC with Pt /C. felt and Pt/KB in cathodes produced voltage after operation, and generated stable voltages at 2000 Ω. After the addition of glucose to the anode, it was observed that the cell voltage of the Pt/KB increased to a maximum value and could be achieved for 2 h of 144 mV (Figure 5.20), the maximum voltage was stable for 16 h and then gradually decreased to the minimum value of 40 mV as the glucose was completely depleted. Correspondingly, the Pt /C. felt in MFCs cathodes achieved a maximum cell voltage value of 128 mV and a minimum of 10 mV, as shown in (Figure 5.20).

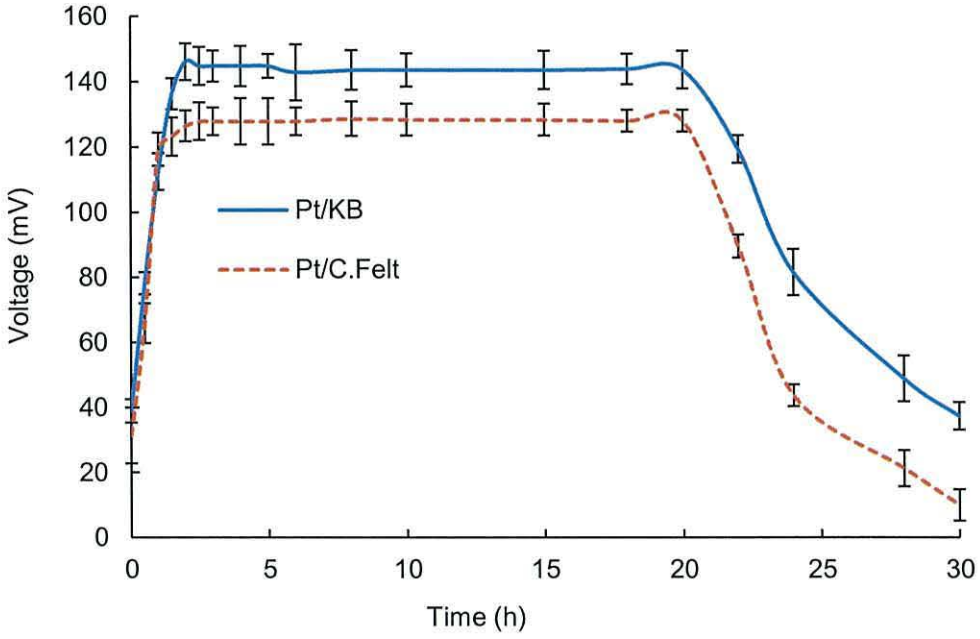

Figure 5. 20 - Voltage generated using catalyst of Pt/KB (solid line), and electrodeposited Pt (dashed line) from glucose [540mg/L] in the MFC (2000 Ω resistor), experiments run in triplicate (Error bars ± SD).

Clearly, the cathodes with Pt/KB generated higher voltages than the cathodes with Pt /C. felt. This indicates that the Pt/KB has better performance than Pt /C. felt in lowering the activation energy of the cathode and in improving the reduction reaction kinetics at the cathode.

Main differences in power production were observed in the study of polarisation and power density. As shown in (Figure 5.21), the OCV for Pt/KB was 388 ± 15 m V. This is significantly better than the Pt /C. felt (electro-deposited Pt) cathode (336 ± 19 mV). Moreover, the cathode with Pt/KB showed better cell voltage stability and a higher current density than the Pt /C. Felt cathode. The maximum power density generated using Pt/KB was 20.7 m W/m^2 at current density 144 m A/m^2. While, the

power density reached a maximum 16.3 mW/m^2, at a current density of 128 mA/m^2, using Pt /C. felt.

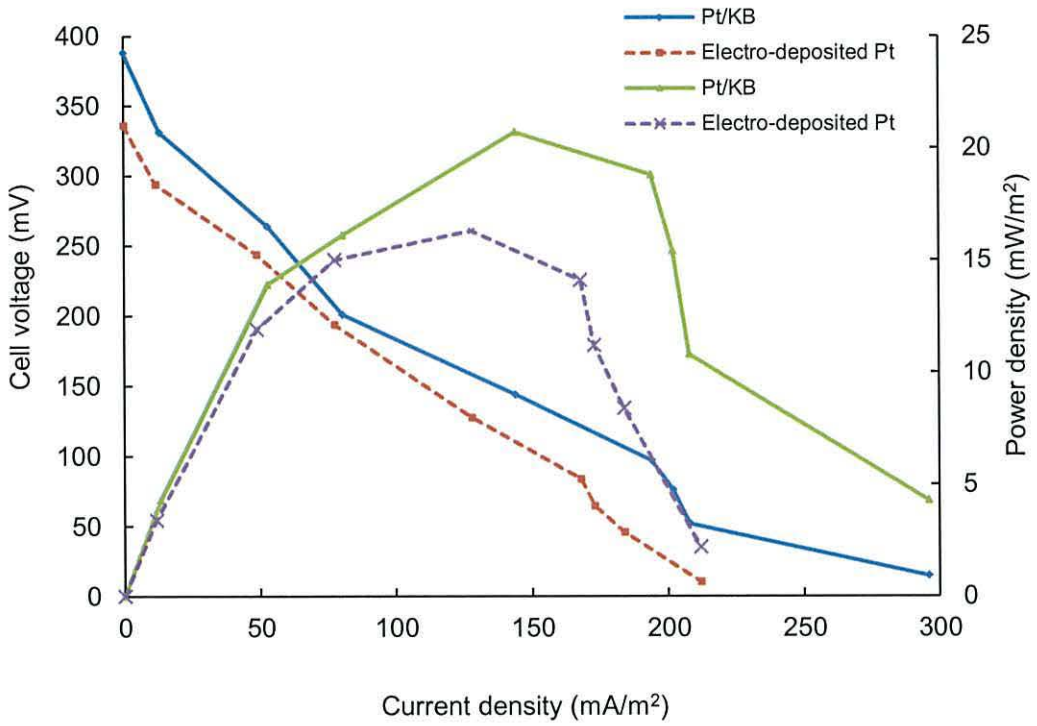

Figure 5. 21 - A comparison of the MFCs performance (polarisation and power density curve) between Pt/KB (solid line), and electrodeposited Pt (dashed line).

These results suggest that the cathode material made of Pt/KB /carbon felt had a lower ohmic resistance than the electrodeposited Pt (Pt /C. felt) cathode materials used in the experiment.

5.6 Electrochemical characterisation of electrodeposited Pt and Pt/KB

Linear sweep voltammetry (LSV) experiments were conducted to test the electrochemical performance of the (Pt/KB, electro-deposited Pt, and carbon felt) cathodes *vs.* SCE at room temperature in oxygen saturated and 500 mM H_2SO_4. Pt/KB as cathode catalyst had an important catalytic activity, while the cathode without catalyst (carbon felt) had a very low current response. Compared to the electro-deposited Pt cathode, the Pt/KB /carbon felt cathode showed better electrochemical performance with a higher current response (Figure 5.22). A higher reduction current was obtained with the Pt/KB electrode than with the electro-deposited Pt electrode. Lower catalytic activity of oxygen reduction currents were obtained for electro-deposited platinum on carbon felt, indicating that the carbon support affects catalytic activity. Obviously, the cathodic catalyst is vital for

improved overall performance of MFCs. These results clarified that Pt/KB /carbon felt cathode has a high catalytic activity for the ORR in the cathode chamber.

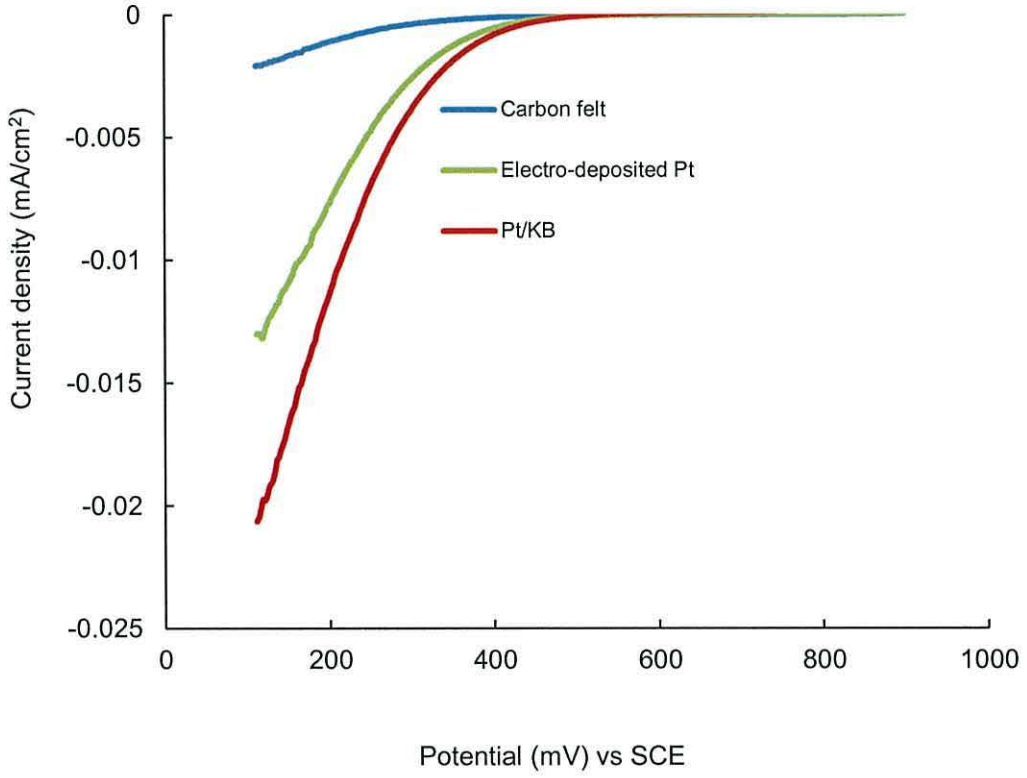

Figure 5. 22 - LSV of cathode with Pt/KB, electrodeposited Pt, and carbon felt. The scan rate was 5 m V/s, and the potential was scanned from 900 to 0 m V versus saturated calomel electrode.

5.7 Aqueous cathodes using different electron acceptor

Permanganate as the cathodic electron acceptor in microbial fuel cell

The performance of the electricity production in the dual compartment MFC was tested using permanganate as the cathodic electron acceptor in an acidic medium. An aqueous catholyte of potassium permanganate had a great influence on the potential difference across the cell terminals. The rate of reduction of the permanganate on the electrode surface is relatively faster than that of oxygen, thereby enhancing the kinetics of cathodic reactions. Figure 5.23 shows the OCV of the MFC with the aqueous catholyte of potassium permanganate used with a carbon cloth cathode and an anodic chamber containing *Acidiphilium* sp. SJH (5.1×10^7 cells/ml), ferric ion (10 mM), and glucose(10 mM) in buffer solution of pH 2.5 (potassium hydrogen phthalate, 100 mM). The potential raised from low voltage to maximum voltage (956 mV) over approximately 12 hours of operation reached a constant value. This

increase in OCV is most likely due to the high redox potential (1.70 V) of permanganate in acidic conditions as illustrated in Eq. (5-1),[30] and much of this potential is formed from the chemical energy of permanganate in acidic medium and not from the organic substrate.[26]

$$MnO_4^- + 4H^+ + 3e^- \rightarrow MnO_2 + 2H_2O \qquad E^\circ = 1.7V \qquad \text{Equation 5-1}$$

This reaction is based on the fact that the reduction of permanganate ions is not sustainable as they have to be replaced regularly.

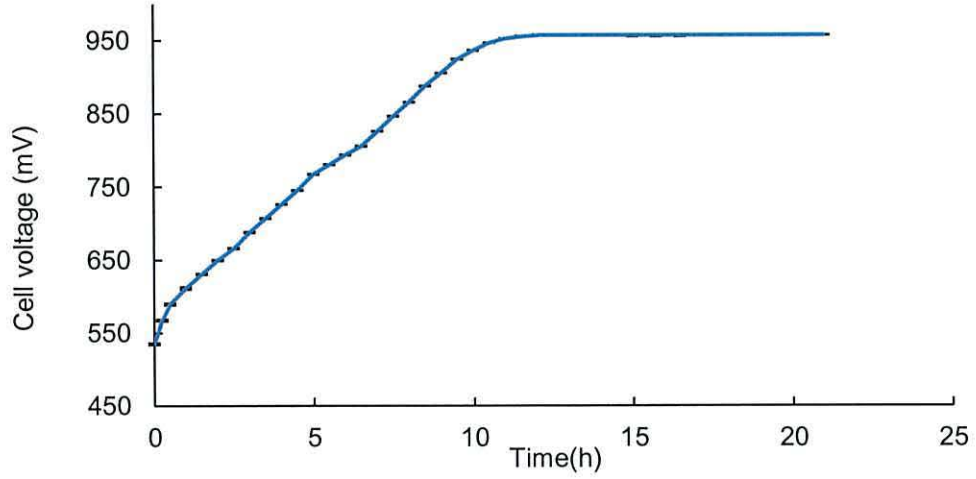

Figure 5. 23 - Voltage as a function of time of Acidiphilium sp. SJH cells in MFCs using aqueous catholyte of Potassium permanganate, experiments run in triplicate (Error bars equals ±1 SD).

Electrode potential

The individual OCP and working potentials of the electrodes (*anode and cathode*) of the MFC were measured based on the SCE as a function of current with different resistor circuits (100 to 50,000 Ω) (Figure 5.24 on the following page). The OCP of the anode was -162 mV, but the working potential decreased to -96 mV for current density up to 700 mA/m^2. The OCP of the cathode was 794 mV, but the working potential decreased to 212 mV for current density up to 700 m A/m^2 (figure 4.24). It was observed that the OCP of the cathode using the carbon cloth electrode and permanganate (10 mM, pH 3.5) was improved the cathode performance. Therefore, permanganate strong oxidising agent with high reduction potential is highly desirable to increase MFC efficiency.

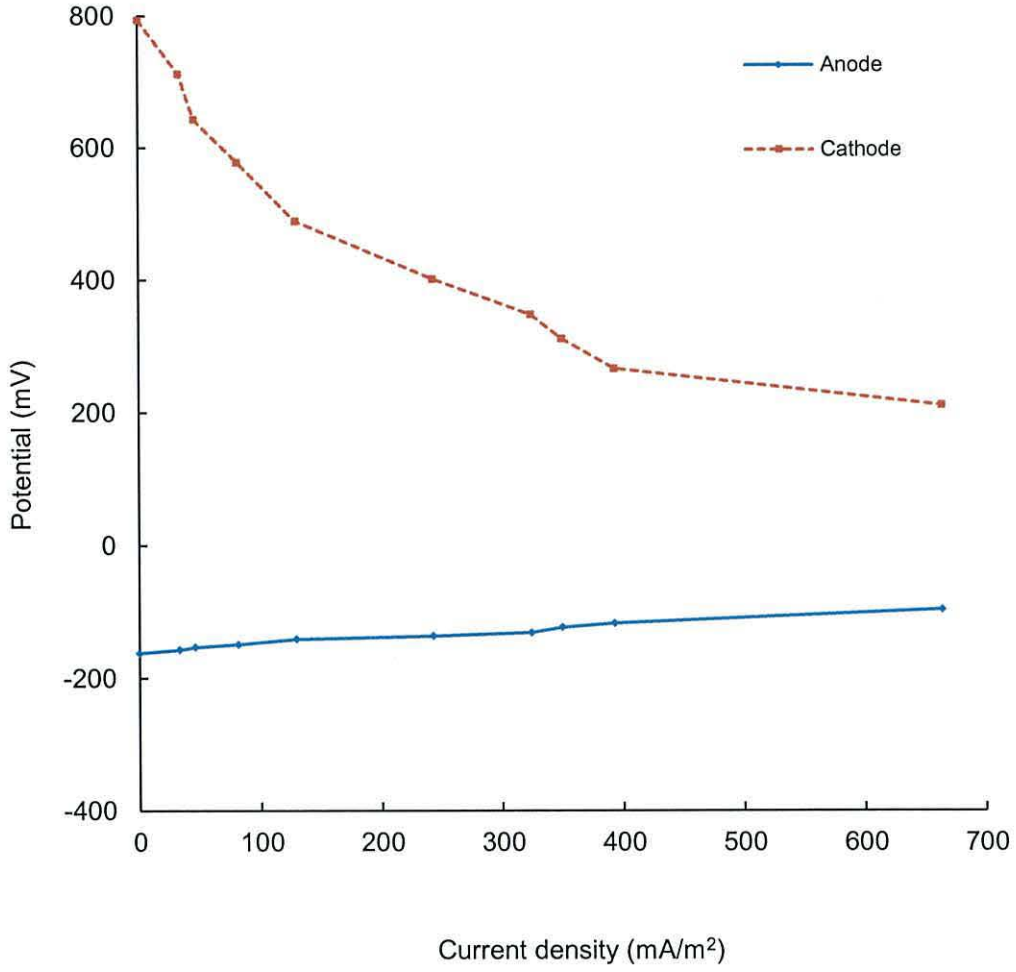

Figure 5. 24 - Anode (solid line) and cathode (dashed line) potential (vs. SCE reference electrode, 242mV against the NHE) as a function of current.

Effect of pH on OCV and cathode potential

When oxygen is not used at the cathode, no catalyst is needed and therefore wet proofed carbon cloth can be used. An aqueous catholyte of potassium permanganate was used as electron acceptor in cathode chamber of the MFC. To examine the effect of pH on the OCV and the cathode potential, the OCV and the cathode potential were calculated. Significant differences in OCV and cathode potential were observed. Figure 5.25 illustrates that the maximum OCV and cathode potential was achieved at pH 3.5, however the potential was decreased at pH 2.0 and 9.

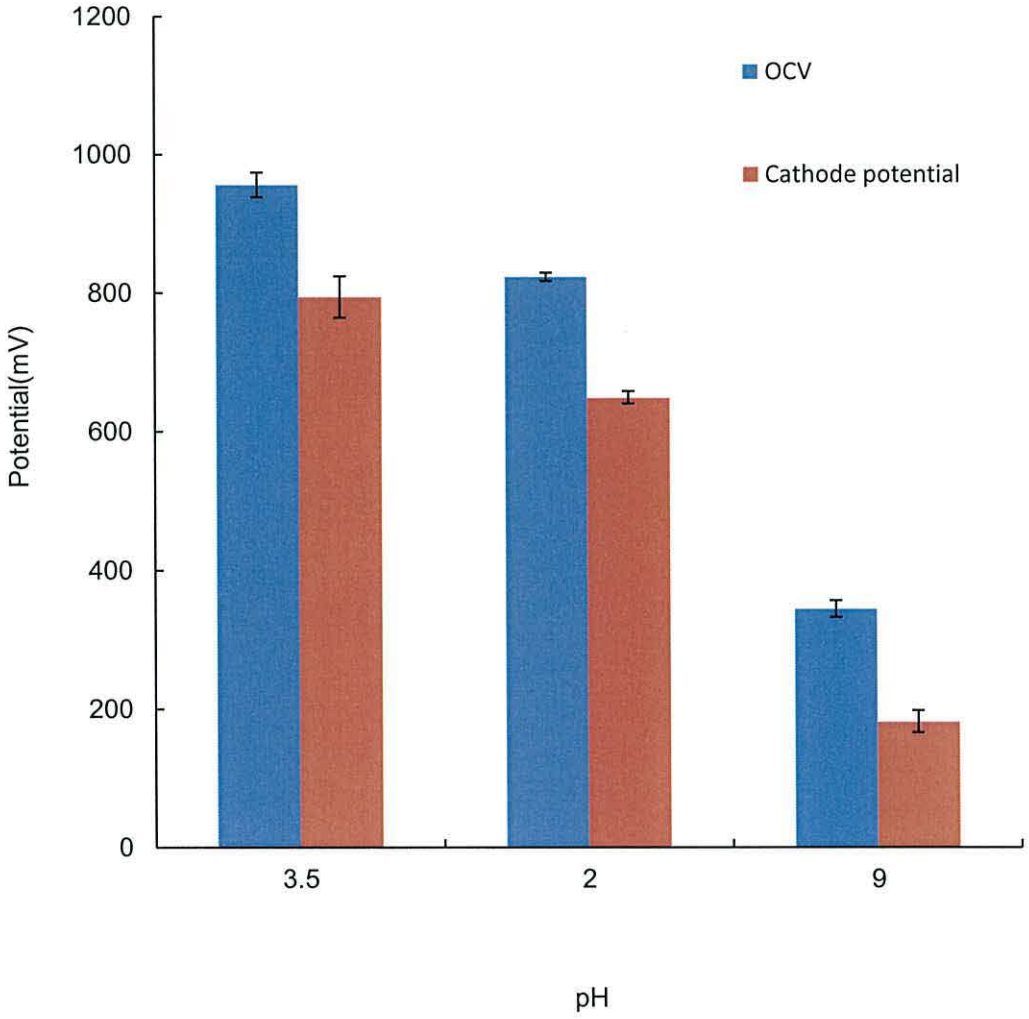

Figure 5. 25 - Effect of pH on OCV and cathode potential, 100 ppm permanganate concentration. Three repetitive cycles (Error bars ± SD).

The pH influence depends on the reduction potential (E°) of permanganate, and it was testified that the pH value determines whether reduction occurs via three, or five electrons exchange. These observations agree with the chemical equations shown below.[30,31] This indicated that proton availability is a limiting factor for the cathode reaction.[23]

$MnO_4^- + 4H^+ + 3e^- \rightarrow MnO_2 + 2H_2O$ $\quad E^{\circ} = 1.7V$ *Equation 5-2*

$MnO_4^- + 8H^+ + 5e^- \rightarrow Mn^{2+} + 4H_2O$ $\quad E^{\circ} = 1.51\,V$ *Equation 5-3*

$MnO_4^- + 2H_2O + 3e^- \rightarrow MnO_2 + 4OH^-$ $\quad E^{\circ} = 0.59\,V$ *Equation 5-4*

Table 5.5 shows the effect of pH on OCV and cathode potential on the basis of the reduction potentials. Potassium permanganate gives maximum OCV and cathode potential at pH 3.5. The pH influence on the OCV and cathode potential were investigated at pH 3.5. High pH produced a negative result on the OCV and cathode

potential when using permanganate as electron acceptor in the cathode chamber. Previous work by You *et al.,* obtained the maximum OCV and cathode potential at pH 3.5.[32]

Table 5. 5 - Reduction potential, OCV, and cathode potential at different pH.

pH	OCV V	Cathode potential V	Reduction potential(E°) V
3.5	0.956	0.764	1.71V
2	0.823	0.649	1.51V
9	0.345	0.182	0.59V

Effect of initial concentration permanganate on OCV and cathode potential

A series experiments were carried out to examine the role of initial concentration of permanganate (20, 100, 200 mg/L) on OCV and cathode potential in the MFC operating at pH 3.5. Figure 5.26 on the following page shows voltage generation versus initial concentration of permanganate. In this study the OCV and the cathode potential showed little observable change by increasing permanganate concentration. For example OCV and cathode potential would only increase 4 %, and 4.8 % respectively, when the permanganate concentration was increased 10 times (20 to 200 mg /L). No further improvement in OCV and the cathode potential was observed for further increases permanganate concentration. This means that the voltage generation value is insensitive to concentration of permanganate ion.

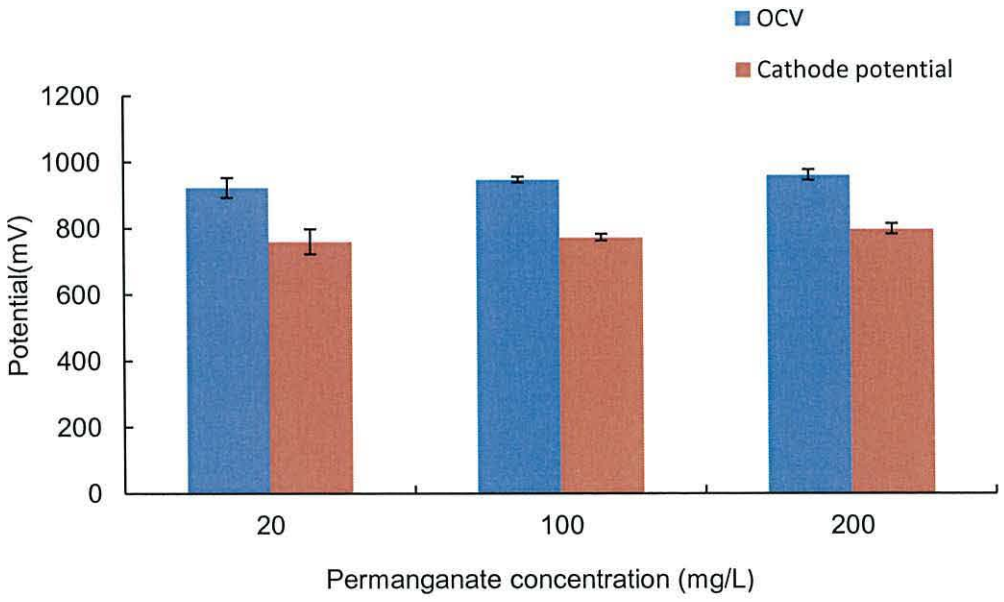

Figure 5. 26 - Effect of permanganate concentration on OCV and cathode potential, at pH 3.5. Three repetitive cycles (Error bars ± SD).

5.8 Power generation with different carbon electrode using permanganate

Different types of carbon electrode (carbon cloth, carbon felt, and Ketjen Black EC-600) were tested with dual chamber MFCs using an aqueous catholyte of potassium permanganate as the electron acceptor at pH 3.5. All tests of the dual chamber MFC could be described in the (Table 5.6). It was observed that Ketjen Black carbon could produce the highest voltage, current density, power density than carbon cloth and carbon felt electrode for permanganate as the electron acceptor at pH 3.5. It is suggested that types and construction of the carbon electrode might play a significant role in the activity of ORR that takes place at the cathode chamber for instance, treated Ketjen Black carbon has the advantage of high surface area and more attached functional groups on the surface. As the Ketjen Black carbon was examined as the cathode electrode, and potassium permanganate was used as the electron acceptor, the highest OCV (988 ± 13 mV), current density (702 m A/m^2),and the power density (702 mW/m^2) were obtained. In addition, it was established that the maximum power density clearly depended on electron acceptor.

Table 5. 6- Maximum (OCV), current density, and power density of H-type MFC at different carbon electrodes.

Electrode	Open circuit voltage mV	Max Current density mA/m^2	Max Power density mW/m^2
Ketjen Black carbon	988 ± 13	702	64.2
Carbon cloth	956 ± 90	664	58.9
Carbon felt	913 ± 17	633	54.1

Cathodic surface characterisation

The reduction of permanganate (100 mg/L) at different pH (2, 3.5) during the operation period (21hours) as electron acceptor in cathode chamber can be seen in (Figure 5.27). Scanning electron microscope (SEM) images (A) clearly exhibited deposits of MnO_2 formed on the surface of the carbon cloth (cathode) pH 3.5 in the dual chamber MFC, and (B) image of the carbon cloth in aqueous solution of Potassium permanganate at pH 2.0. Therefore, the more acidic aqueous solution of the permanganate ion (Mn^{7+}) is reduced to soluble Mn^{2+} as shown in equation 5.3.

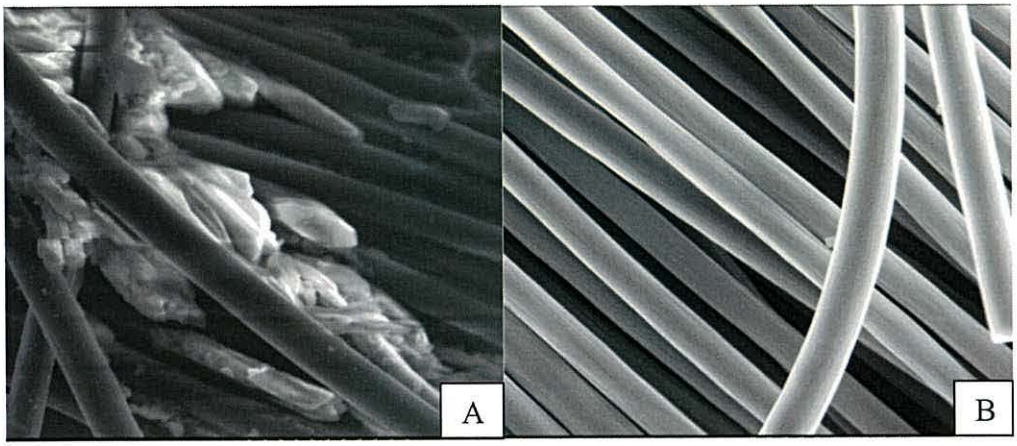

Figure 5. 27 - SEM image of (A) surface of the carbon cloth (cathode) pH 3.5, and (B) surface of the carbon cloth at pH 2.

Chromium [Cr (VI)] as the cathodic electron acceptor in microbial fuel cell

H-type MFCs were used to examine the chemical as a cathode electron acceptor in acidic medium experiments. An aqueous catholyte of hexavalent chromium had a great influence on the potential difference across the cell terminals. The rate of reduction of the chromium on the electrode surface is relatively faster than that of oxygen, thereby enhancing the kinetics of cathodic reactions. Figure 5.28 shows the OCV of the MFC when the aqueous catholyte of chromium[Cr(VI) was used with a carbon cloth cathode and an anodic chamber containing *Acidiphilium* sp. SJH (5.1 x 10^7 cells/ml), ferric ion(10 mM), and glucose(10 mM) in a buffer solution of pH 2.5 (potassium hydrogen phthalate, 100 mM). The potential rose from low voltage to maximum voltage (766 mV) in approximately 8 hours of operation when a constant value was reached. This increase in OCV is most likely due to the high redox potential (1.33 V) of chromium [Cr (VI)] in acidic conditions as illustrated in Eq.(5-5):

$$Cr_2O_7^{2-} + 14H^+ + 6e^- \rightarrow 2Cr^{3+} + 7H_2O \qquad E^e = 1.33\,V$$ Equation 5-5

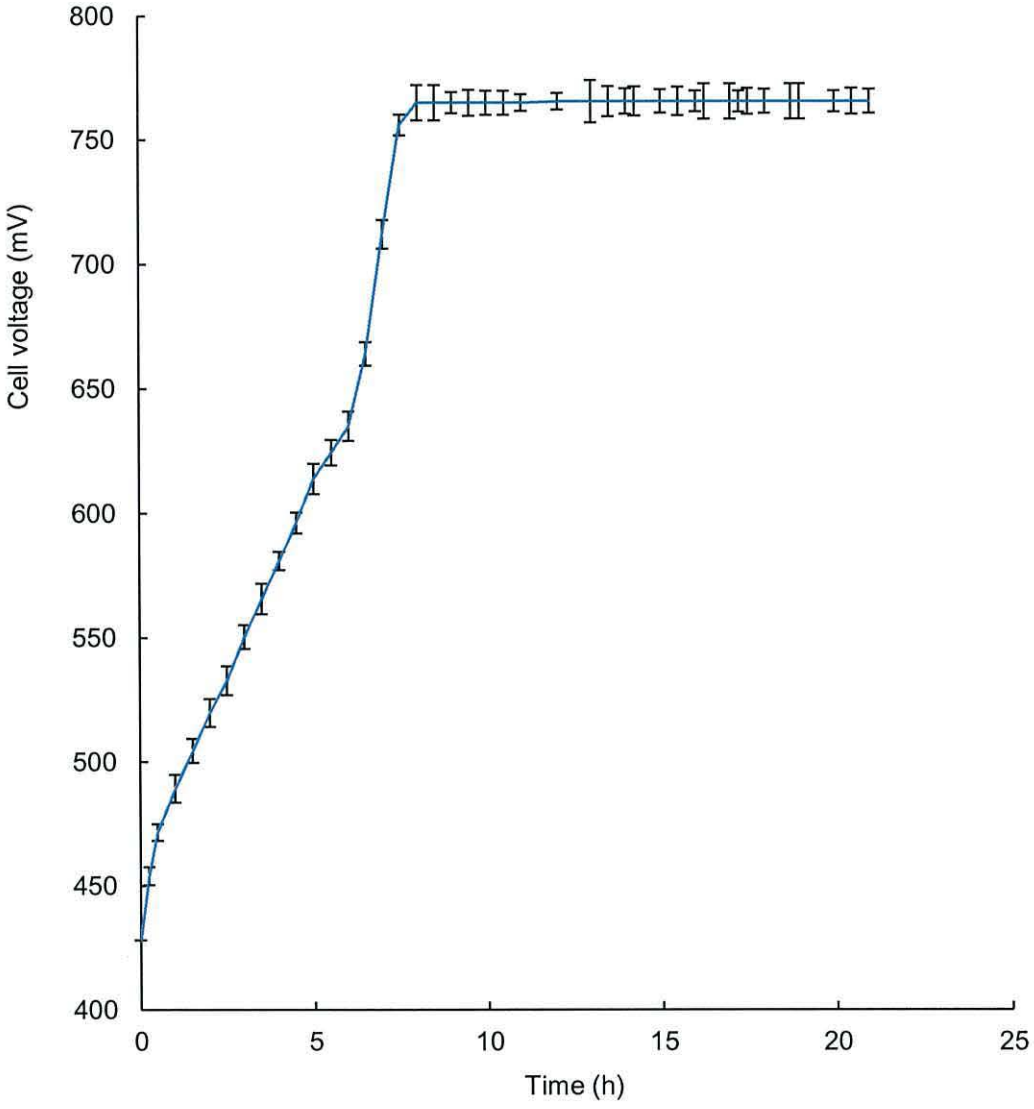

Figure 5. 28 - Voltage as a function of time of Acidiphilium sp. SJH cells in MFCs using aqueous catholyte of chromium [Cr (VI), experiments run in triplicate (Error bars SD).

Effect of pH on OCV and cathode potential

The OCV and cathode potential of the H-type two chamber MFC were determined to test the effects of pH. An aqueous catholyte of hexavalent chromium [Cr (VI)] (100 mg/L) was used as the electron acceptor in the cathode chamber of the MFC. To examine the effect of pH on the OCV and cathode potential, the OCV and cathode potential were calculated. Figure 5.29 illustrates that the maximum OCV and cathode potential was achieved at pH 2, however the potential was decreased at pH 3, 4, 5 and 6. A high pH produced a negative result on the OCV and cathode potential when using hexavalent chromium as the electron acceptor in the cathode chamber.

Previous work by Wang *et al.*, using anaerobic microorganisms as anodic biocatalyst at pH 7, and hexavalent chromium as the electron acceptor in the cathode chamber obtained the maximum OCV and cathode potential at pH 2.[33]

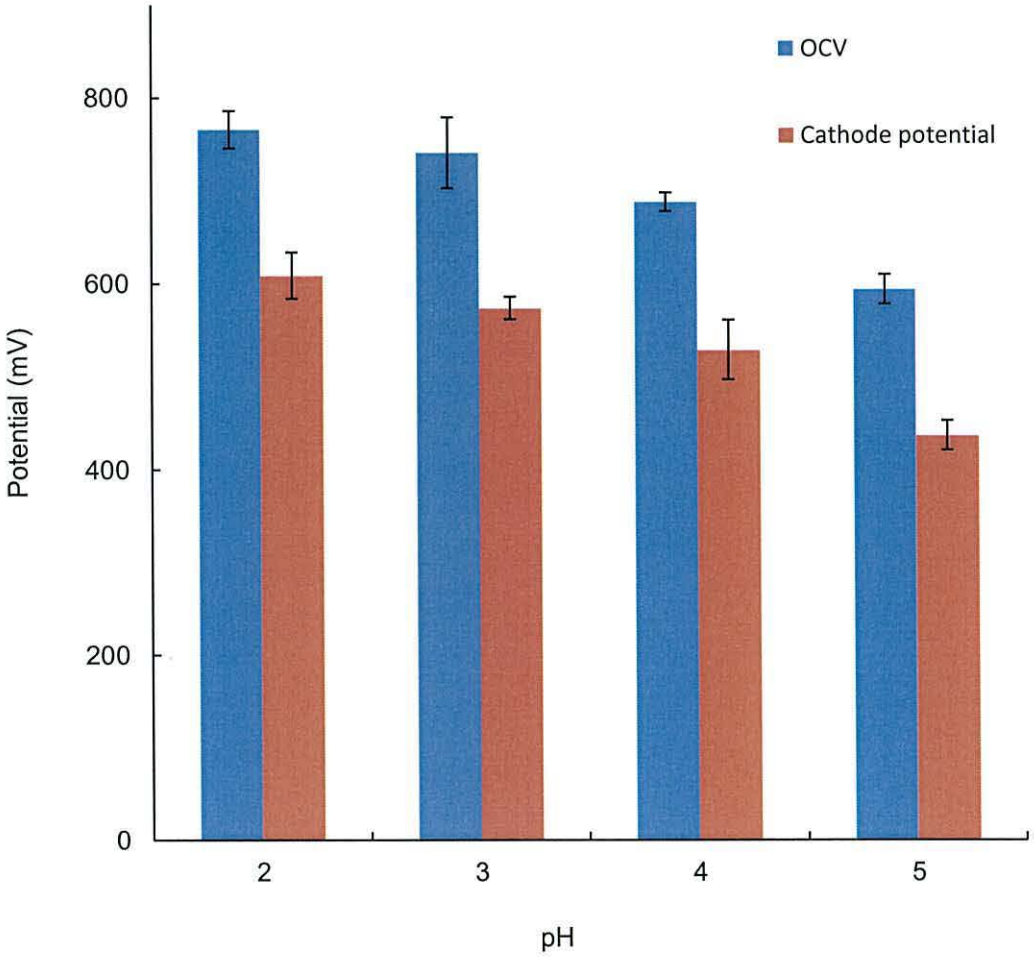

Figure 5. 29 - Effect of pH on OCV and cathode potential, 100 ppm hexavalent chromium concentration. Three repetitive cycles (Error bars ± SD).

Effect of initial concentration chromium on OCV and cathode potential

A two-chamber sandwich system was used to study the effect of different concentration of chromium [Cr (VI)] (20, 100, 200 mg/L) on OCV and cathode potential at pH 2. To examine the effect of concentrations of chromium on the OCV and cathode potential, the OCV and cathode potentials where calculated. Figure 5.30 shows voltage generation versus initial concentration of chromium [Cr (VI)]. In this study the OCV and cathode potential showed little observable change when increasing chromium concentration. For example OCV and cathode potential would only increase 9 % and 13 % respectively, when the chromium concentration increases 10 times (20 to 200 mg/L). No further improvement in OCV and cathode

potential was observed with further increases chromium concentration. This means the voltage generation value is insensitive to concentration of chromium ion.

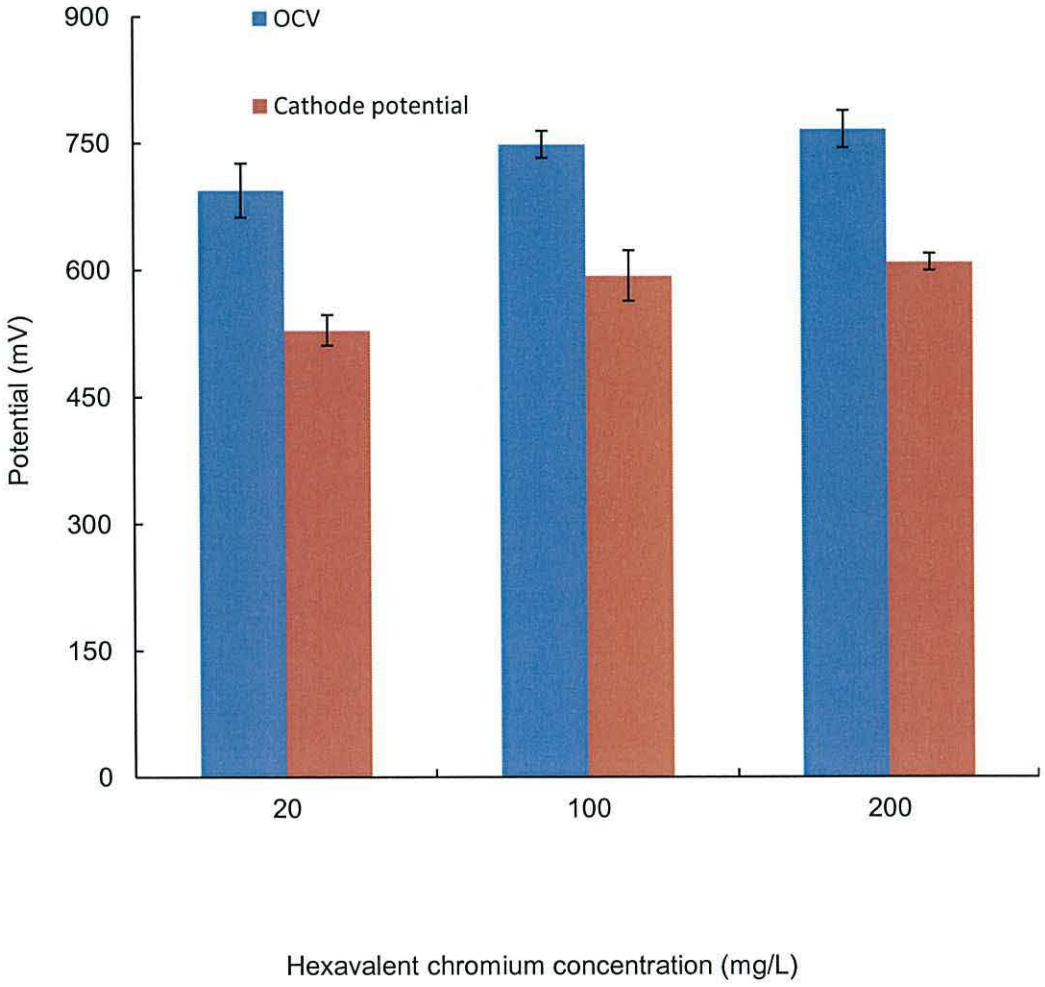

Figure 5. 30 - Effect of hexavalent chromium concentration on OCV and cathode potential, at pH 3.5. Three repetitive cycles (Error bars ± SD).

5.9 Power generation with permanganate, chromium and oxygen

As shown in (figure 5.31), power density was much greater using permanganate (10 mM, pH 3.5) and an uncoated carbon cloth electrode as the cathode compared to that obtained with chromium(pH 2) and an uncoated carbon cloth electrode, oxygen and 0.15mg/cm^2 Pt (22 wt % Pt/KB) coated on wet-proofed carbon cloth; and using a carbon cloth electrode (no platinum catalyst) as electron acceptors were performed in the two chamber MFCs. Power density was tested by a polarisation curve and the corresponding power density curve. The data were collected to calculate the power density and voltage continued across a range of current densities attained by varying the resistance (100 to 50,000 Ω) between the anode and cathode electrodes. From these measurements, the optimal external resistance was found (2000 Ω) which

showed the maximum power density. The maximum power density generated using permanganate was 58.9 m W/m^2 (carbon cloth electrode and permanganate) at current density 664 m A/m^2. While, the power density reached a maximum 45.5 mW/m^2, 20.7mW/m^2, 10.6 m W/m^2 at a current density of 520 mA/m^2, 296 mA/m^2,112 mA/m^2 using chromium ion, oxygen and 0.15mg/cm^2 Pt (22 wt % Pt/KB) coated on wet-proofed carbon cloth, and carbon cloth electrode(no platinum catalyst)with oxygen, respectively. The increase in power density when using permanganate as a function of this potential is formed from the chemical energy of permanganate in an acidic medium (pH 3.5). Here an OCV of 956 ± 9 mV, 766 ±17 mV, 388 ± 11 mV using chromium (pH 2), oxygen and 0.15 mg/cm^2 Pt, and 263 ± 17 mV using carbon cloth electrode and oxygen was obtained.

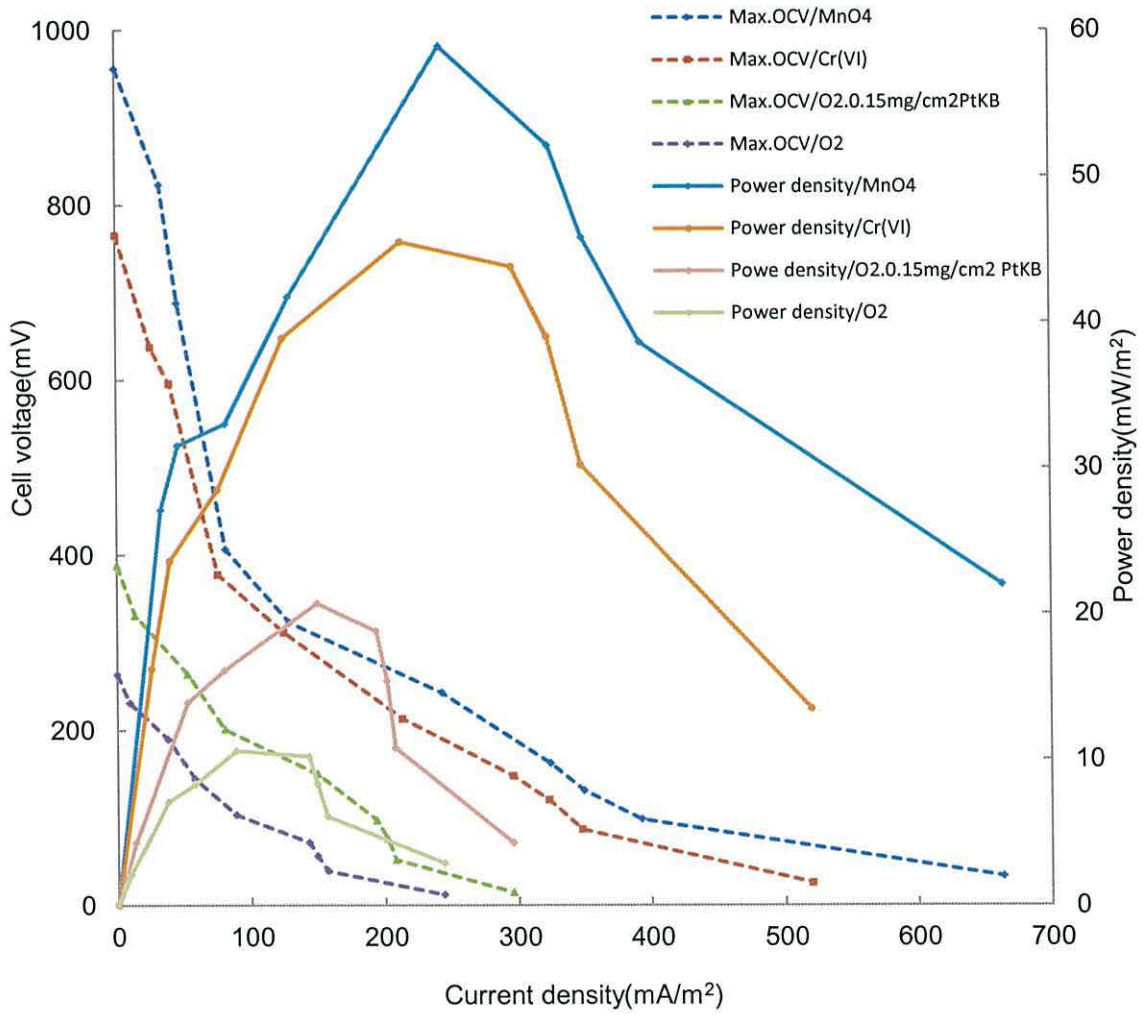

Figure 5. 31 - Power density and polarisation curve using permanganate (10mM), chromium [Cr (VI) (10mM), oxygen and 0.15mg/cm² Pt, and oxygen and carbon cloth.

The lower performance of the oxygen and carbon cloth cathode was mainly due to the high overpotentials of the cathode.[34] Table 5.7 shows the maximum power density achieved with the permanganate ion 10 is times greater than that found with oxygen and the carbon cloth cathode. This suggests that the ORR is related with large overpotential compared to permanganate. The OCV shows the potential difference between anode and cathode, in which the anode potential is measured on the basis of the substrate combustion rate, electron recovery from bacteria to anode, while cathode potential depends on the type of electron acceptor used, mass transfer and reduction potential of electron acceptor.

Table 5. 7- The comparison between permanganate ion, chromium [Cr (VI), and oxygen as electron acceptor in cathode chamber.

Cathode electrode	Electron acceptor	OCV mV	Current density $mA/m^2(100\Omega)$	Power density $mW/m^2(2k\Omega)$
Carbon cloth	Permanganate	956	664	58.9
Carbon cloth	Chromium	766	520	45.5
0.15 mg/cm^2 Pt (22 wt % Pt/KB)	Oxygen	388	296	20.7
Carbon cloth	Oxygen	263	244	10.6

The maximum power densities for MFCs reported in the previous studies cannot be explained only on the basis of aqueous catholyte solution. An important factor which has a direct influence on the maximum power density of an MFC is the difference in bacteria and MFC construction.[35] Recent studies have reported that using a graphite brush anode increases the surface area for bacteria while reducing the distance between the electrodes to decrease ohmic losses.[36]

Table 5.8 on the following page shows the comparison between two different electrodes (carbon cloth, and carbon felt) using three electron acceptors (permanganate ion, chromium [Cr (VI), and oxygen) were tested. It was found that carbon cloth electrode could produce the higher OCV, current density, and maximum power density than carbon felt for using permanganate ion, chromium [Cr (VI), and oxygen as electron acceptor in cathode chamber. The material used to construct the cathode electrode might play a role in the ORR activity,[37] plus the maximum power density clearly depend on the type of electron acceptor.

Table 5. 8- The comparison between carbon cloth, and carbon felt electrode using permanganate ion, chromium [Cr (VI), and oxygen as electron acceptor in cathode chamber.

Electron acceptor	Carbon cloth electrode			Carbon felt electrode		
	OCV mV	Current density 100 Ω	Max. Power density 2000 Ω	OCV mV	Current Density 100 Ω	Max. Power density 2000 Ω
Permanganate	956	664 mA/m^2	58.9 mW/m^2	922.4	588 mA/m^2	53.3 mW/m^2
Chromium	766	520 mA/m^2	45.5 mW/m^2	739.1	446 mA/m^2	39.1 mW/m^2
Oxygen	263	244 mA/m^2	10.6 mW/m^2	147	194 mA/m^2	9.6 mW/m^2

5.10 Conclusion

Platinum electrocatalysts supported on acid treatment KB carbon electrocatalysts were produced successfully. The dispersion at the nano-sized particles of catalytic materials, such as platinum into an electron conducting matrix, is a very convenient way to improve the electrocatalytic activity. The 22 wt % Pt/KB carbon support was prepared. TEM and XRD results reveal that well-separated platinum nanoparticles of around 3 nm in size were obtained on the KB carbon support and an optimum platinum loading established at 0.15 mg/cm^2.The platinum-modified cathode retained an equivalent of 80 ± 2 % efficiency compared to a solid platinum electrode, but contained only 0.1 % Pt.

Finding from results obtained showed that the reduction of electrode spacing had limited effect on power improvement due to the high internal resistance.

The results obtained were for the effect of three electron acceptors (permanganate, chromium [Cr (VI)] and oxygen) and two different carbon electrodes (carbon cloth and carbon felt) at the cathode chamber, using two chamber H-type reactor operating at low pH. Carbon cloth electrode provided a higher power density, current density, and OCV than carbon felt electrode for any electron acceptor.

5.11 References

1. Lakshmi, N.; Rajalakshmi, N.; and Dhathathreyan, K. S. Functionalization of various carbons for proton exchange membrane fuel cell electrodes: analysis and characterisation. *J. Phys. D: Appl. Phys.* **2006**, *39*, 2785 - 2790.
2. Parthasarathy, R.; Lin, X.; and Jaeger, H. M. Electronic Transport in Metal Nanocrystal Arrays: The Effect of Structural Disorder on Scaling Behavior. *Phys. Rev. Lett.* **2001**, *87*, 186807 - 186811.
3. Antonucci, P. L.; Alderucci, V.; Giordano, N.; Cocke D. L.; and Kim, H. On the role of surface functional groups in Pt carbon interaction. *J. Appl. Electrochem.* **1994**, *24*, 58 - 65.
4. Hollas, J. M. *Modern Spectroscopy*, John Wiley and Sons, Ltd. England, 2004.
5. Castilla, C. M.; Garcia, M.A. F.; Joly, J. P.; Toledo, I. B.; Marin, F. C.; and Utrilla, J.R. Activated carbon surface modifications by nitric acid, hydrogen peroxide, and ammonium peroxydisulphate treatments. *Langmuir*, **1995**, *11*, 4386 - 4392.
6. Spieker, W. A.; Regalbuto, J. R. A fundamental model of platinum impregnation onto alumina. *Chem. Eng. Sci.* **2001**, *56*, 3491 - 3504.
7. Swanson, H. E.; *and* Tatge, E. Standard X-ray diffraction powder patterns. *Natl. Bur. Stand. Circ.* **1953**, *539*, 69 - 70.
8. Rimbu, G. A.; Jackson, C. L.; and Scoti, K. Platinum/ carbon/ polyaniline based nanocompoosites as catalysts for fuel cell technology. *J. Optoelectron. Adv. Mater.* **2006**, *8*, 611 - 616.
9. Yu, E.; Cheng, S.; Scott, K.; and Logan, B. E. Microbial fuel cell performance with non-Pt cathode catalysts. *J. Power Sources* **2007**, *171*, 275 - 281.
10. Kim, M.; Park, J. N. Kim, H.; Song, S.; Lee. W. H. The preparation of Pt/C catalysts using various carbon materials for the cathode of PEMFC. *J. Power Sources* **2006**, *163*, 93 - 97.
11. Beattie, S. D.; Manolescu, D. M.; and Blair. S. L. High-Capacity Lithium–Air Cathodes. *J. Electrochem. Soc.* **2009**, *163*, A44 - A47.
12. Liu, Z.; Lin, X.; Lee, J. Y.; Zhang, W.; Han, M.; and Gan, L. M. Preparation and characterisation of platinum-based electrocatalysts on multiwalled carbon nanotubes for proton exchange membrane fuel cells. *Langmuir* **2002**, *18*, 4054 - 4060.
13. Li, L.; ZiDong, W.; Yi, Z.; XueQiang, Q.; MeiRong, X.; Jie, Z.; ZhiGang, S.; and CaiXin, S. DFT study of difference caused by catalyst supports in Pt and Pd catalysis of oxygen reduction reaction. *Sci. China Ser. B-Chem.* 2009, **52**, 571 - 578.
14. Wang, W.; Zheng, D.; Du, C.; Zou, Z.; Zhang, X; Xia, B.; Yang, H.; Akins, D. L. Carbon-supported Pd-Co bimetallic nanoparticles as electrocatalysts for the oxygen reduction reaction. *J Power Sources* **2007**, *167*, 243 - 249.
15. Borole, A. P.; O'Neill, H.; Tsouris, C.; and Cesar, S. A microbial fuel cell operating at low pH using the acidophile *Acidiphilium cryptum Biotechnol. Lett.* **2008**, *30*, 1367 - 1372.
16. Bond, D. R.; Holmes, D. E.; Tender, L. M.; Lovley, D. R. Electrode-Reducing Microorganisms That Harvest Energy from Marine Sediments *Sci.* **2002**, *295*,483 - 485.

17. Bond D. R.; and Lovley, D. R. Electricity Production by *Geobacter sulfurreducens* Attached to Electrodes. *Appl Environ Microbiol.* **2003**, *69*, 1548 - 1555.
18. Kim, H. J.; Park, H. S.; Hyun, M. S.; Chang, I. S.; Kim, M.; Kim, B. H. A mediator-less microbial fuel cell using a metal reducing bacterium, *Shewanella putrefaciens. Enzyme Microbiol. Technol.* **2002**, *30*, 145 - 152.
19. Chaudhuri, S. K.; Lovley, D. R. Electricity generation by direct oxidation of glucose in mediatorless microbial fuel cells *Nat. Biotechnol.* **2003**, *21*, 1229 - 1232.
20. Zhao, F.; Harnisch, F.; Schröder, U.; Scholz, F.; Bogdanoff, P. Herrmann, I. Challenges and Constraints of Using Oxygen Cathodes in Microbial Fuel Cells *Environ. Sci. Technol.* **2006**, *40*, 5193 - 5199.
21. Gil, G. C. Ghang, I. S.; Kim, B. H.; Kim, M.; Jang, J. K.; Park, H. S.; and Kim, H. J. Operational parameters affecting the performance of a mediator-less microbial fuel cell. *Biosen. Bioelectron.* **2003**, *18*, 327 - 334.
22. Erable, B.; Etcheverry, L.; and Bergel, A. Increased power from a two-chamber microbial fuel cell with a low-pH air-cathode compartment *Electrochem. Commun.* **2009**, *11*, 619 - 622.
23. Jang, J. K.; Pham, T. H.; Chang, I. S.; Kang, K. H.; Moon, H.; Cho, K. S.; Kim, B. H. Increased power from a two-chamber microbial fuel cell with a low-pH air-cathode compartment. *Process Biochem.* **2004**, *39*, 1007 - 1012.
24. Liu, H.; Cheng, S.; and Logan, B. E. Power Generation in Fed-Batch MFCs as a Function of Ionic Strength, Temperature, and Reactor Configuration. *Environ. Sci. Technol.* **2005**, *39*, 5488 - 5493.
25. Fan, Y.; Sharbrough, E; and Liu, H. Quantification of the Internal Resistance Distribution of Microbial Fuel Cells. *Environ. Sci. Technol.* **2008**, *42,* 8101 - 8107.
26. Logan, B. E. *Microbial Fuel Cells*, John Wiley and Sons, Inc. Hoboken, New Jersey, 2008.
27. Zhao, Y.; Fan, L.; Zhong, H.; and Li, Y. Electrodeposition and electrocatalytic properties of platinum nanoparticles on multi-walled carbon nanotubes: effect of the deposition conditions. *Microchim Acta* **2007**, *158*, 327 - 334.
28. Dulal, S. M. S. I.; Won, M.; Shim, Y. Carbon fiber supported platinum nanoparticles for electrooxidation of methanol and phenol *J. Alloys . Compounds* **2010**, *494*, 463 - 467.
29. Bard, A. J.; Faulkner, L. R. *Electrochemical Methods*, John Wiley & Sons, New York, 1980.
30. Walton, J.; Labine, P.; Reidies, A. *The chemistry of permanganate in degradative oxidations*, in: W. Eckenfelder, A. Bowers, J. Roth (Eds.), *Chemical Oxidation*, Technomic Publishing Co. Inc., Lancaster, Basel, **1991**.
31. Olya, M. E.; Aleboyeh, H.; Aleboyeh, A. Decomposition of a Diazo Dye in Aqueous Solutions by KMnO4 /UV/H_2O_2 Process. *Prog. Color Colorants Coat.* **2012**, *5*, 41 - 46.
32. .You, S; Zhao, Q; Zhang, J.; Jiang, J.; and Zhao, S. A microbial fuel cell using permanganate as the cathodic electron acceptor. *J. Power Sources* **2006**, *162*, 1409 - 1415.
33. Wang, G.; Huang, L.; Zhang, Y. Cathodic reduction of hexavalent chromium [Cr (VI)] coupled with electricity generation in microbial fuel cells. *Biotechnol Lett.* **2008**, *30*, 1959 - 1966.

34. Rismani-Yazdi, H.; Carver, S. M.; Christy, A. D.; Tuovinen, Cathodic limitations in microbial fuel cells: An overview *J. Power Sources* **2008**, *180*, 683 - 694.
35. Oh, S.; Min, B.; Logan, B. E. Cathode Performance as a Factor in Electricity Generation in Microbial Fuel Cells. *Environ Sci Technol.* **2004**, *38*, 4900 - 4904.
36. Logan, B. E.; Cheng, S.; Watson, V.; Estadt, G. Graphite fiber brush anodes for increased power production in air-cathode microbial fuel cells. *Environ Sci Technol.* **2007**, *41*, 3341 - 3346.
37. Ota, K.; Ishihara, A.; Mitsushima, S.; Lee. K.; Suzuki, Y.; Horifumi, H.; Nakagawa, T.; and Kamiya, N. Improvement of Cathode Materials for Polymer Eletrolyte Fuel Cell. *J. New Mater. Electrochem. Syst.* **2005**, *8*, 25 - 35.

Chapter 6

BIOFILM GROWTH

6.1 Introduction

In this chapter the development of the anode associated biofilm from *Acidiphilium SJH* bacteria at pH 2.5 is reported. No mediator was provided during the colonisation process. Both carbon felt and carbon cloth as working electrodes were individually addressed and placed in the same air-cathode single-chamber MFC to compare their electrochemical behaviour in the same biochemical conditions.

The anode surface modification was achieved by electro-deposition of polyaniline on the carbon felt. The performances of an unmodified carbon felt and modified with polyaniline based MFC are also compared.

6.2 Influence of anodic biofilm growth on bioelectricity production

Scanning electron microscopy characterisation on anodic biofilm growth

Bacteria colonisation on the electrode surface is more commonly referred to as biofilm.[1] The anode electrode can be modified to increase the cell output, in this regard experimental data showed that *Acidiphilium SJH* bacteria cells are able to colonise on the carbon felt surface of a MFC, and enhancing potential generation. The morphology of the biofilm on the carbon felt and carbon cloth electrodes were analysed by scanning electron microscopy (SEM). In order to show the SEM images of carbon felt and carbon cloth before biofilm formation Figure 6.1(A, B) and showing that the *Acidiphilium SJH* bacterial cells colonised on the surface of the carbon felt and carbon cloth (anode), the biofilm was developed for 30 days Figure 6.1(C, D), and individual cells can clearly be observed attached to the fibres of the carbon felt. The SEM images are illustrative of all electrode surfaces. The development of the anode associated biofilm can be observed in the entire electrode surface, presenting good homogeneity. Electronic communication has been made between the attached cells of the carbon felt and carbon cloth in which carbon felt, and carbon cloth are used as working electrodes in an electrochemical cell. Bacteria colonised on the anode biofilm may not always directly transfer electrons to the anode, however it may transfer indirectly through the interaction of other species in the cell.[2]

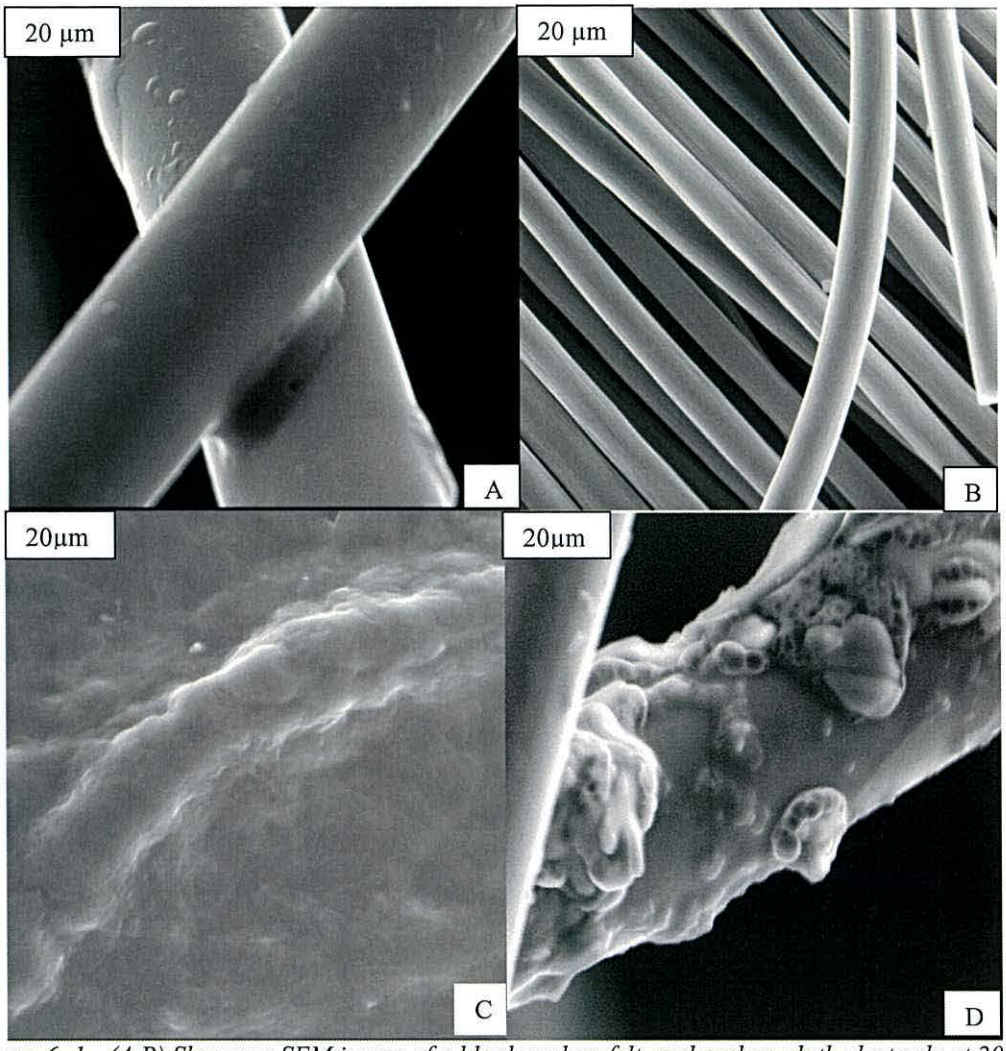

Figure 6. 1 - (A,B) Shows an SEM image of a blank carbon felt, and carbon cloth electrode at 2000X magnification with a scale of 20µm (C,D) shows an SEM image of carbon felt, and carbon cloth 30 days after inoculation with Acidiphilium SJH at 2000X magnification with a scale of 20 µm.

Cyclic voltammetry characteristics on anodic biofilm growth

It may be understood from CV that attached cells have the ability for electron transfer with the electrode. Voltammograms show the important variations in the redox peak shapes and positions at different key growth stages of biofilm formation with the electron transfer mechanism as a function of the biofilm growth. [3,4,5,6,7] Cyclic voltammetry characteristics on anodic biofilm growth are shown in (Figure 6.2). The voltammogram for the control (blank) anode had no observable redox peak. A little change was shown in the shape of the voltammogram for the anode OCV operation. A maximum current of 4 µA along, oxidation- reduction process cannot occur on the surface area of the biofilm. The voltammogram for the anodic biofilm growth (7days) operation recorded a maximum current of 13.3 µA along, no oxidation peak in the forward scan and a reduction peak at −120 mV (*vs.* SCE; 47 µA) in the reverse scan, while the voltammogram for the anodic biofilm growth

(21days) operation recorded no oxidation peak in the forward scan and a strong reduction peak at −112 mV (*vs.* SCE; 146 μA) in the reverse scan. In the case of the anodic biofilm growth (30 days) voltammogram, a maximum current of 40.5 μA was recorded, with a weak oxidation peak at 48 mV (*vs.* SCE; 14.69 μA) in the forward scan and a strong reduction peak at −105 mV (*vs.* SCE; 190 μA) in the reverse scan. As the density of the cells is high in the matrix, cell to cell contact is increased in the biofilm which stimulates the electron transfer mechanism.[8,9]

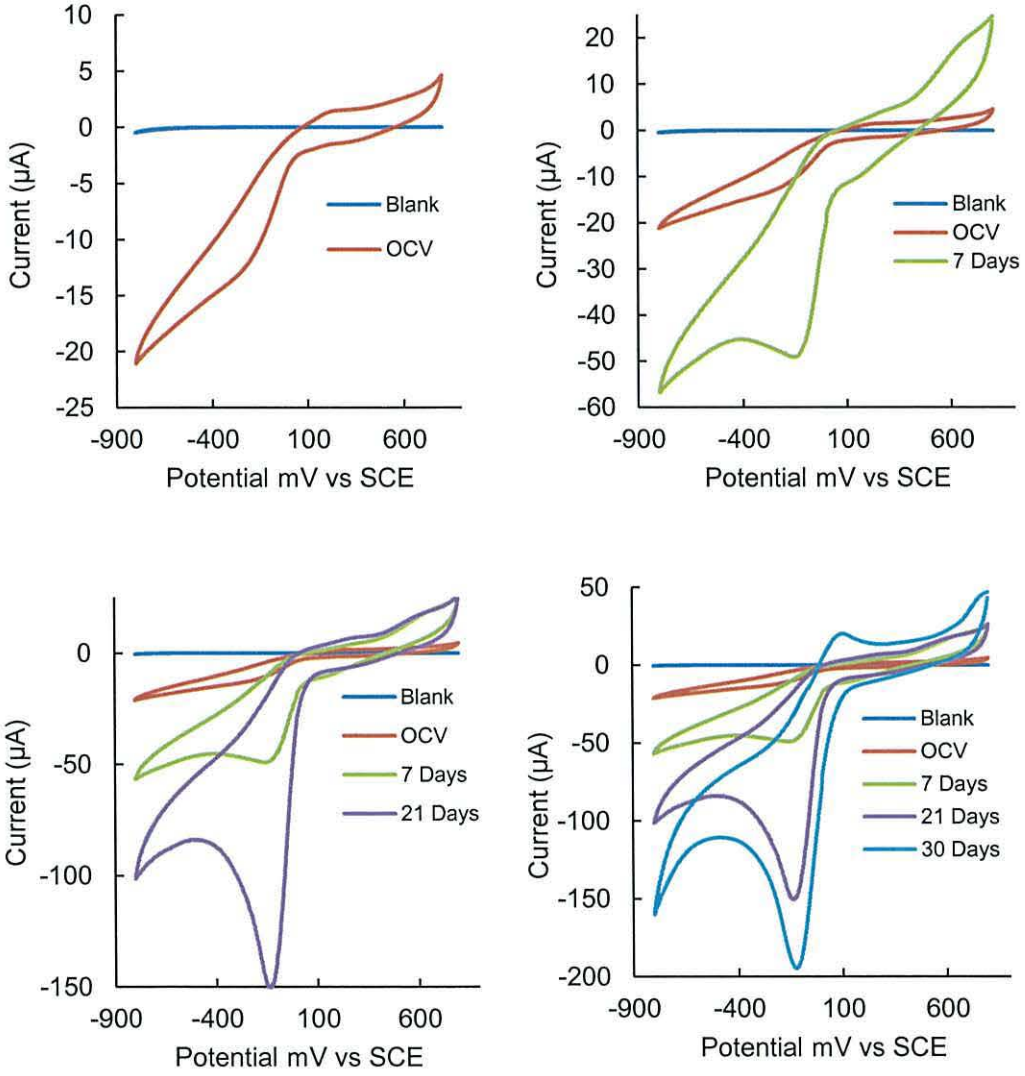

Figure 6. 2 - Cyclic voltammetry curves of anodic biofilm growth on carbon cloth at a different Period (7, 21, and 30days), 0.5 M H_2SO_4 pH 2.5, and scan rate of 5mV/s.

The colonise on the surface of a carbon cloth in MFC of *Acidiphilium SJH* bacteria have been explored using cyclic voltammetry. From the observations, when used as a working electrode the attached cells did not establish good electronic communication with the carbon cloth support in an electrochemical cell. Therefore a significant

amount of catalytic effect was not observed by cyclic voltammetry experiment. It may be suggested that the electrochemical characteristics of *Acidiphilium sp SJH* bacteria cells are versatile, depending on the composition of the culture medium; cyclic voltammetry was recorded with a biofilm-coated electrode.

A series of experiments was carried out to test the extent of anode associated biofilm formation on the surface of carbon felt electrodes. Figure 6.3 shows voltammogram profiles for the carbon felt anodes obtained for different durations (7, 21, and 30 days). The voltammogram for the fresh carbon felt anode had no observable redox peak. The anode associated biofilm growth (7 days) operation recorded a maximum current of 10.7μA along. No oxidation- reduction peak was found, while the shape of the voltammogram is different from that obtained for a fresh carbon felt electrode (blank). The voltammogram for the anodic biofilm growth (21days) operation recorded a maximum current of 54 μA along with weak oxidation peak at 41 mV (*vs.* SCE; 15.7 μA) in the forward scan, and no reduction peak was found in the reverse scan. In the case of the anodic biofilm growth (30 days) voltammogram, a strong oxidation peak in the forward scan of the voltammogram was observed at 1060 mV (*vs.* SCE, 78 μA). No reduction peak was found in the reverse scan. The possible explanation for the results is that the redox process cannot occur on the surface area of the 7days biofilm growth.

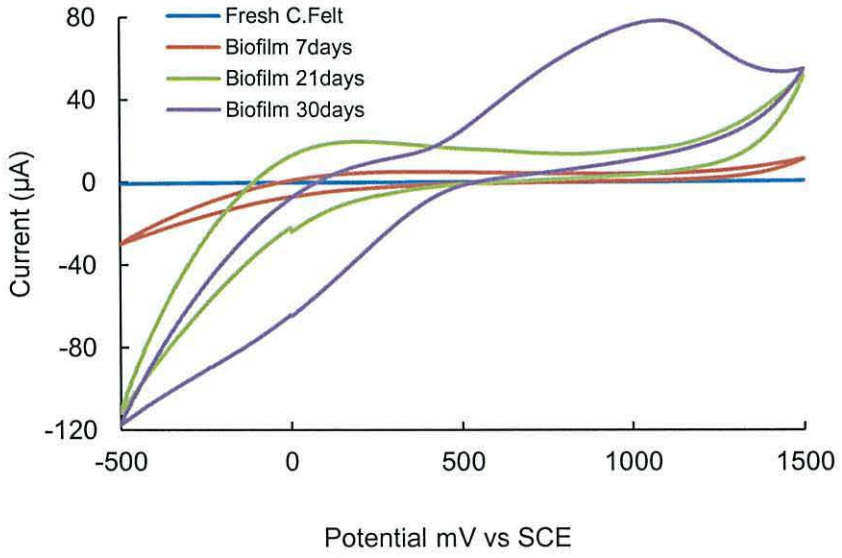

Figure 6. 3 - Cyclic voltammetry curves of anodic biofilm growth on carbon felt at a different Period (7, 21, and 30days), 0.5 M H_2SO_4 pH 2.5.Scan rate 5mV/s.

Observation from the cyclic voltammetry test suggests that a significant development in electrocatalytic activity was not observed with anodic biofilm growth on the surface of carbon felt. Previous work by Borole *et al.*, reported that electrocatalytic activity of biofilm can have a significant influence on the yield and efficiency of the conversion processes.[10]

Cyclic voltammograms of bacteria cell suspension

The electrochemical activities of washed cell suspensions of *Acidiphilium sp. SJH* bacteria were tested by cyclic voltammetry. Observation from the cyclic voltammetry showed a weak oxidation peak at 50mV (*vs.* SCE, 0.056 μA) in the forward scan and weak reduction peak at −150 mV (*vs.* SCE; 0.086 μA) in the reverse scan. (Figure 6.4). However, these features are not present in the blank growth liquid medium voltammetry. It was not clearly shown by cyclic voltammetry that *Acidiphilium sp. SJH* bacteria cells are electrochemically active. This experiment was repeated three times.

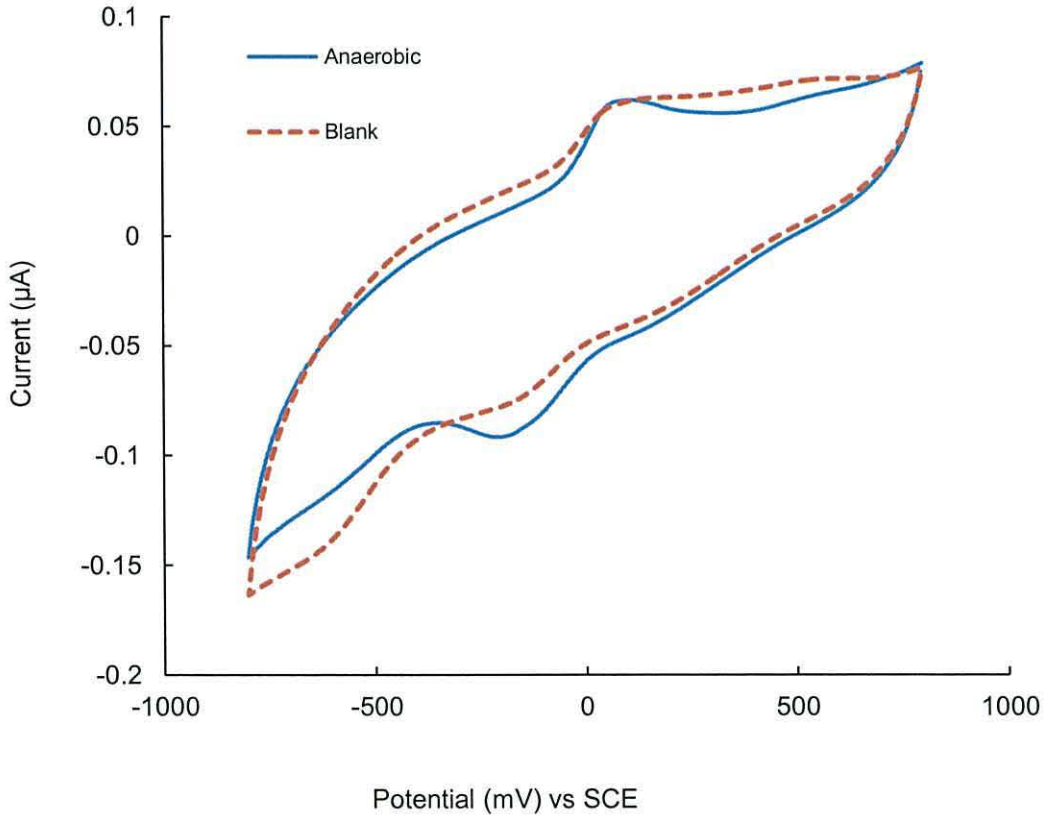

Figure 6. 4 - Cyclic voltammogram of Acidiphilium SJH bacteria grown anaerobically.

The ability of *Acidiphilium SJH* bacteria cells to reduce soluble ferric ion using glucose as an electron donor was tested under anaerobic condition. Ferric ion reduction was checked after 15 hours incubation, a control test was also carried out with *Acidiphilium SJH* bacteria, and ferric ion without glucose. After 15 hours incubation there was no change in the colour of the iron. Because an *Acidiphilium SJH* bacterium does not grow without glucose, there was no electron generation, and thus the ferric ion was not reduced. This simple method can be used for examination of the electrogenic activity of microorganisms.

These results suggest that the poor electrochemical activity of the *Acidiphilium* sp. *SJH* bacteria may be due to the fact that little consumed fuel (glucose) is used for electricity generation and most of it is consumed for bacteria metabolism,[11] and the electrochemical activity of the *Acidiphilium* sp. *SJH* bacteria might be associated with the ferric reductase not to outer membrane cytochromes.[12] The observed cyclic voltammetry was compared to previously reported electrochemical activity of bacteria and has been related to c-type cytochromes on the outer membrane of the bacteria cell wall.[13] It is not clear whether the observed poor electrochemical activity is as a result of c-type cytochrome or other redox proteins on the cell wall of the *Acidiphilium* sp. *SJH* bacteria. Mechanism of electron transfer used by biofilm cells directly influence the amount of energy that biofilms generate for growth and regulate components such as biofilm thickness, resistance and current density.[14]

An important feature in this process is the direct role of the anode associated biofilm in efficiently transferring electrons, in comparison with the functioning of non-biofilm. Bacteria cells in intimate contact with the electrode surface, for example, face different physical and chemical limitations during electron transfer than cells located in the upper biofilm layers, which are further away from the electrode surface and more exposed to nutrients. As a result, mechanism of direct electron transfer is often suggested to drive current production by bacteria cells closer to the electrode surface, whereas an indirect mechanism(s) is necessary to transfer electrons across the biofilm thickness.[10,15]

Direct electron transfer in MFCs though the anode associated biofilm was reported to be possible though microorganisms to the surface of the anode.[4] By physical phenomena (adherence) of the cell membrane or outer membrane cytochromes need

the interaction of the bacterial cell to the anode, contributing in the electron transfer from the bacterial cell to the electrode.[16] It has been recently suggested in other studies that some bacteria strains interconnect *via* conducting molecular nanowires to the electrode surface,[17,18] and self-mediated electron transfer excreted from the microorganisms.[19,3]

6.3 Poised potential electrode

In order to evaluate the performance of different anode potentials, the potentiostat-chronoamperometric experiments of MFCs with three different anode potentials were poised at 0 V, – 200 mV, and -400 mV *versus* SCE, utilising *Acidiphilium* sp. SJH bacteria cells, in 10 mM glucose solution. The current shape as a function of the poised potential applied to the GC electrode is shown in Figure 6.5. When the anode was poised at 0V, the current density increased at first, but reached a maximum within 3 hours, it then dropped quickly. The current density after 15 hours of operation was as low as 0.886 μ A/cm^2. While the anode electrode was poised at −200 m V, the current density was developed with a lower rate, however the increasing trend continued for 7–12 hours. The maximum current density reached about 7.2 μ A/cm^2 and then it decreased slightly; no sudden drop was shown within 15 hours. Increase in the current density was observed with a decrease in poised potential (-200mV, 7.2 μ A/cm^2) and decreased thereafter at poised potential (-400mV, 5.7 μ A/cm^2). Poised potential at (-200mV) produced a higher maximum current density 7.2 μ A/cm^2 compared to 0 mV and -400 mV (6.7 and 5.7 μ A/cm^2, respectively).

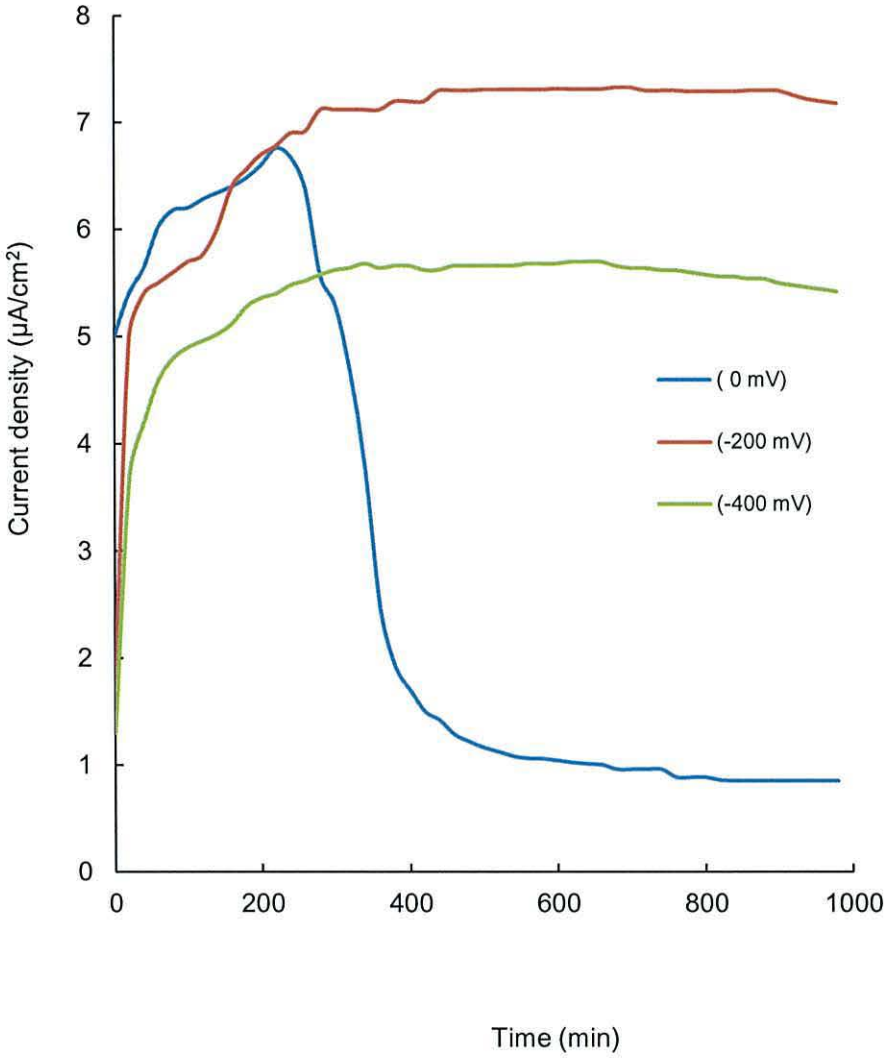

Figure 6. 5 - Chronoamperometric curves of the GC electrode poised at (0 mV, -200 mV, and -400 mV).

The results show an increment in current generation when the applied anode potential decreased from 0 mV to -200 mV followed by no increment when further decreased to -400 mV. Findings from recent research studies have suggested that in the functioning of MFC, the electron transfer mechanism is mediated by the influence of the anode potential on the bacterial activity.[20,21, 22,23]

Chronoamperometric assays were used to study comparison catalytic current production of *Acidiphilium sp. SJH* bacteria on GC electrode with and without a Ketjen Black EC-600 carbon modifier. Observation from the Chronoamperometric experiment showed that a GCE and a GCE coated with Ketjen Black EC-600 carbon polarised at the potential (-200 mV), produced oxidative currents (7.2 μ A/cm^2, 10.2

μ A/cm^2) respectively (Figure 6.6). These results illustrate that the surface modification of a GCE with Ketjen Black EC-600 carbon had a significant effect on the catalytic current density by 1.4 times. It has been recently suggested in other studies that there is a correlation between the anode associated biofilm on the solid surface and the electroactivity of the anode surface modification.[24,25]

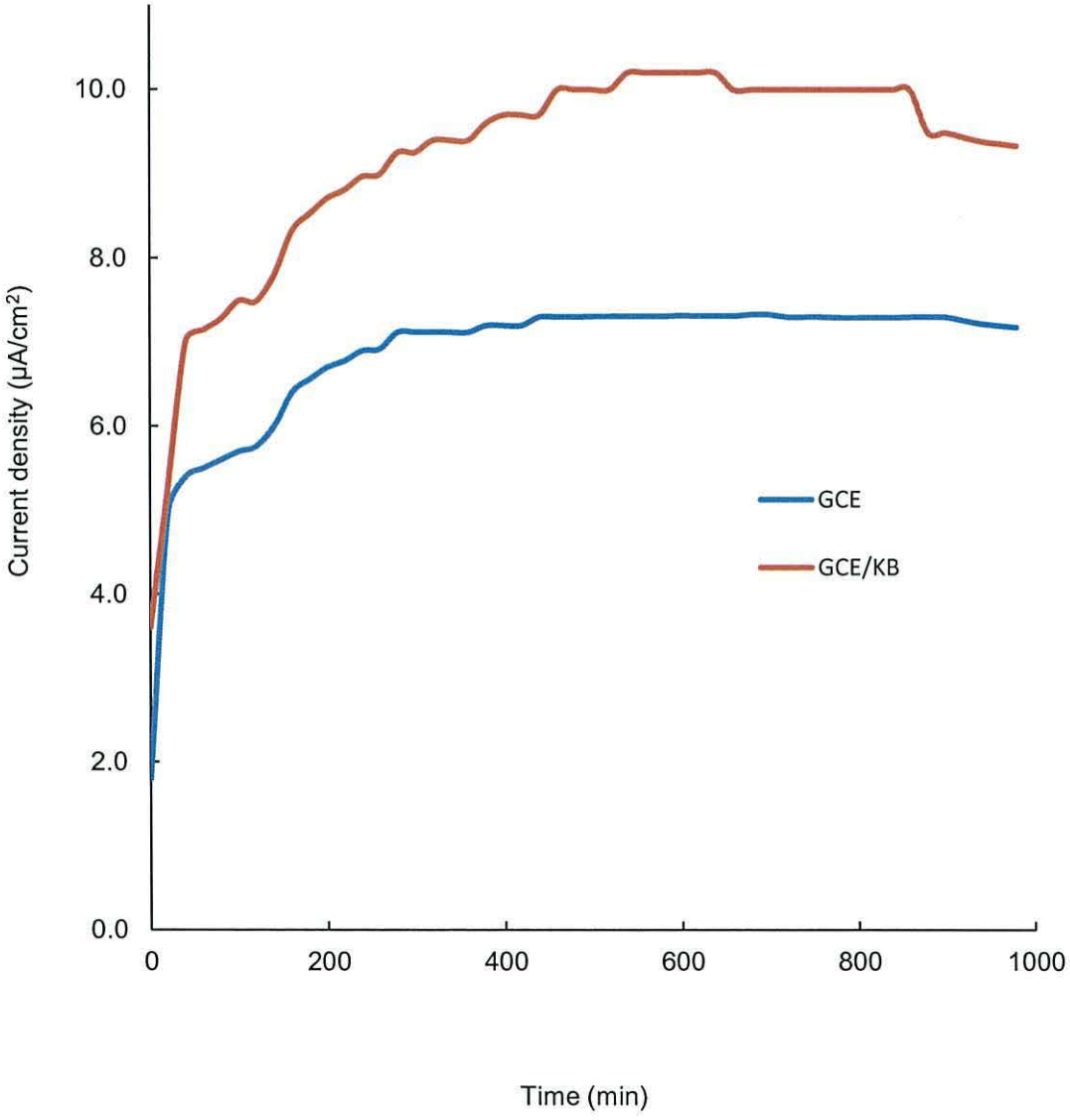

Figure 6. 6 - Comparison of catalytic current production of Acidiphilium sp. SJH bacteria on (GCE) and (GCE/KB) using Chronoamperometric technique.

6.4 Cell count

To determine whether *Acidiphilium sp. SJH* species might transfer to an electrode, the *Acidiphilium sp. SJH* cells were inoculated in an electrochemical cell, and the GC electrode was poised at a set of potentials ranging from -200 mV, -400 mV, and -600 mV against a SCE over the time. The number of *Acidiphilium* sp. SJH cells was assessed by measurement of the optical density at 600 nm (O.D = 0.2), and by direct cell counts (*Thoma chamber*) using a Leitz Wetzlar microscopic prior to and after oxidising potentials -200 mV, -400 mV, and -600 mV were applied. Figure 6.7 shows cell counts as a function of time. In the initial period (1h) before the potential cell numbers (5.9 x10^7 cell /ml) were applied, the cell numbers started to decrease from (1h to 3 h) after the operation. The final plateau in cell counts suggests the presence of a barrier to accumulation of the anode associated biofilm after this thickness. Figure 6.7 also illustrates that the applied potential had a positive effect on the bacteria electrode interface.

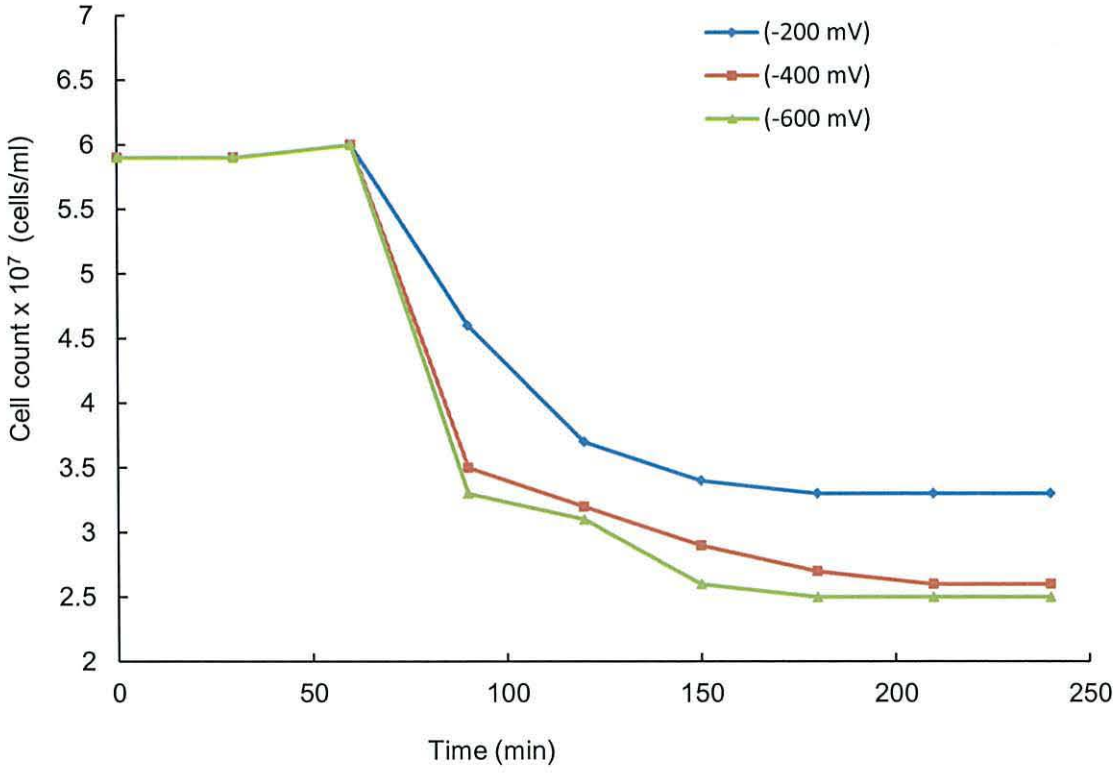

Figure 6. 7 - Effect of different poised potential on cell numbers of Acidiphilium sp. SJH bacteria as a function of time. Cell numbers were estimated by direct counts.

6.5 Cyclic voltammetry characteristics on short-term growth

Cyclic voltammetry analyses of *Acidiphilium* sp. SJH bacteria at different set potentials (-200 mV, -400 mV, and -600 mV) versus a SCE on the electro-catalytic activities of the anode an associated biofilm of short-term growth are shown in figure 6.8. Anodes at set potentials ranging from (-200 mV, -400 mV, and -600 mV) produced currents ranging from (0.11, 0.12, 0.12 μA) compared to (0.06 μA) of the GCE control. According to these voltammogram shapes, voltammograms derived from the anode electrode poised at (-400 mV, and -600 mV) shows similar anodic current production.

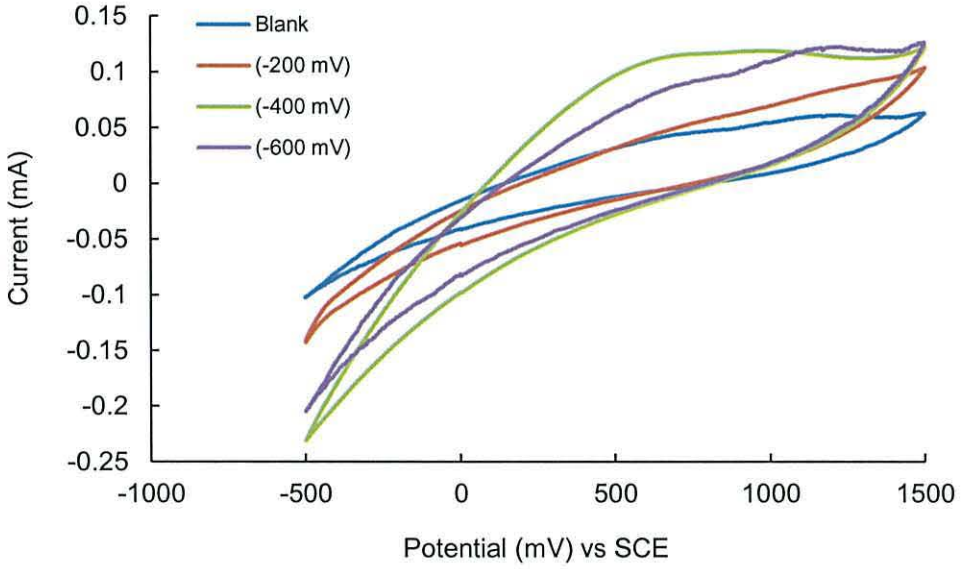

Figure 6. 8 - Cyclic voltammograms of anode electrode (GCE), blank, -200, -400, and -600 mV using SCE as the reference electrode, scan rate 5mV/s.

6.6 Influence of anodic biofilm growth on power output

Air-cathodes are supposed to be a more applied and simplifying system design for MFC cathodes; they are more interesting than other cathodes because they eliminate the need for an aerated catholyte as well as cost effectiveness and energy requirements.[26] Three air-cathode single-chamber MFCs were fabricated in house using a polyacrylic plastic cylindrical chamber 4cm long by 3cm in diameter (Figure 6.9). Polarisation and power density curves were obtained to calculate the maximum power densities and current densities for the air-cathode single-chamber MFC utilising *Acidiphilium* sp. SJH bacteria (5.1 x 10^7 cells/ml), in the presence of glucose (900 mg/L) as the electron donor, and soluble ferric ion (10 mM) as the electron

shuttle. When the OCV of the air-cathode single-chamber MFC reached the maximum it stabilised (400.4 mV) (Figure 6.10).

Figure 6. 9 - Homemade single chamber MFC with a carbon cloth (anode) and a carbon cloth modified with Pt/KB (air cathode).

Air-cathode single-chamber MFC polarisations were operated with the distance between the anode and cathode of 4 cm at different resistance across the anode and cathode, under optimal conditions (pH 2.5, room temperature). The potential was tested at each resistance and converted to power densities. The current density was determined using Ohms law based on the MFC voltage. From these measurements, the optimal external resistance was found (2000Ω) which showed the maximum power density. The cell current and voltage data can be examined and recorded at the maximum power density. The maximum value of power density was 21.3 mW/m^2, which occurred when the current density (I_{mp}) was 146 m A/ m^2, with a corresponding cell voltage (V_{mp}) of 146 mV. The air-cathode single-chamber MFC tested here provided an improvement in power density. This result suggests that reducing internal resistance in the MFC in order to improve power generation, as reported by others.[27,28]

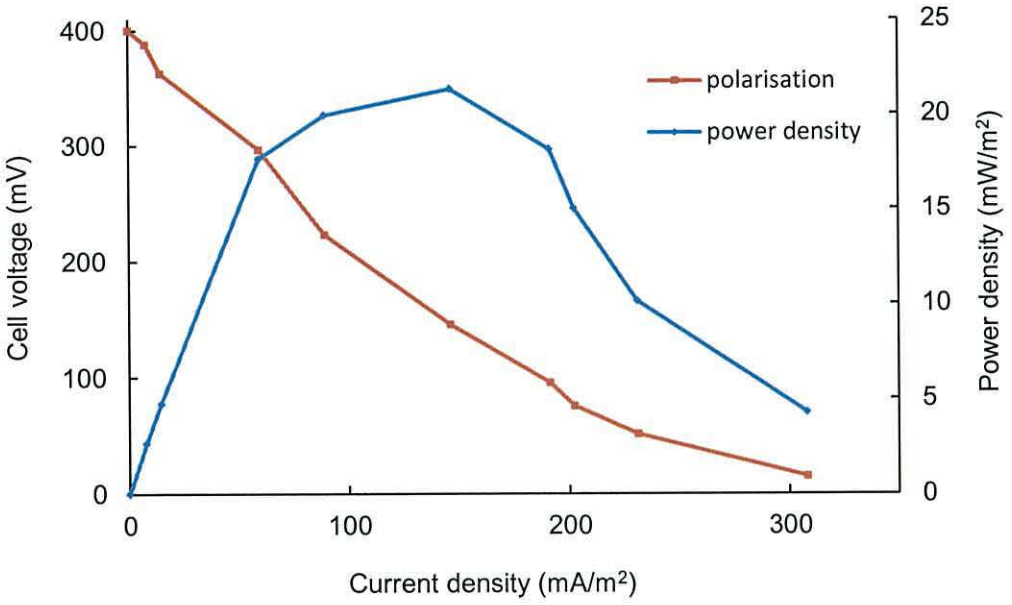

Figure 6. 10 - Polarisation curve measured at different resistances.

A comparison of maximum power densities as obtained when *Acidiphilium sp. SJH* cells were colonised on the carbon felt surface after 30 days of biofilm growth and *Acidiphilium sp. SJH* bacteria, as mentioned above. Later, two MFCs were obtained; the first cell contained a carbon felt electrode and *Acidiphilium sp. SJH* bacteria in the anode solution, and the second cell contained the carbon felt electrode-associated bacteria (30 days) and new medium solution. From these measurements (Figure 6.11), the optimal external resistance was found which showed the maximum power density, recorded with 30 days of anodic biofilm growth (25.9 m W/m^2) at 1 KΩ, and a lower power density was observed with OCV (21.3 m W/m^2) at 2 KΩ.

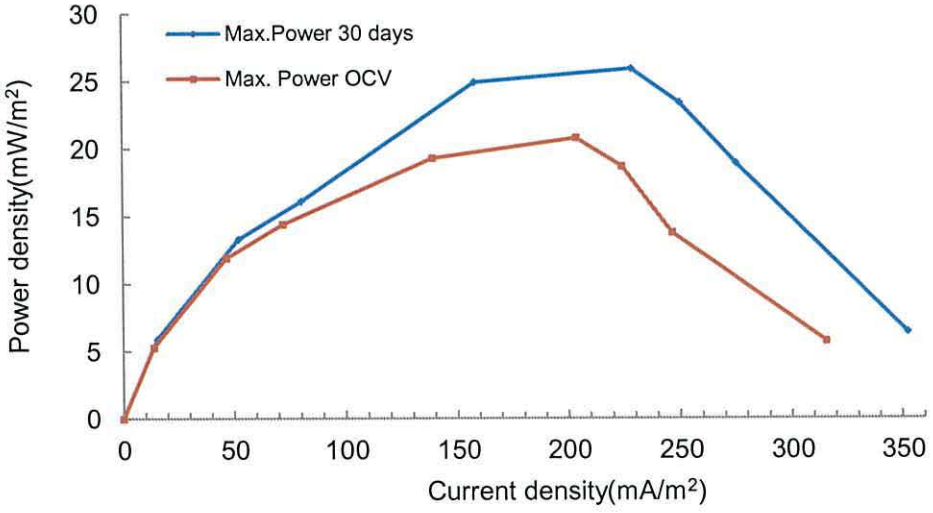

Figure 6. 11 - Power density generated by the MFC (Air cathode single chamber) using anodic biofilm growth (30 days), and OCV condition.

There were no important differences in power density between the air-cathode single-chamber MFC with anodic biofilm growth (30 days) of carbon felt surface and air-cathode single-chamber MFC with suspended *Acidiphilium* sp. SJH bacteria cells of fresh carbon felt. These results suggest that the power output increases due to the anode associated biofilm resulting in a reduction in the internal resistance.

Figure 6.12 shows the power density curves for the MFCs operated for different durations so as to yield anode associated biofilm. Power density curves were obtained to calculate the maximum power density of different anodic biofilm growth (7, 21, and 30 days). The maximum power density increased from 22.8 to 24.6, and 25.9 mW/m^2 respectively, when the anode associated biofilm increased from 7, 21, and 30 days. No further improvement was shown in power production in the period following the initial 30 days growth on the anode electrode. A direct influence of process performance was shown by the extent of biofilm growth on the surface of the anode of the MFC increasing the power density.[29]

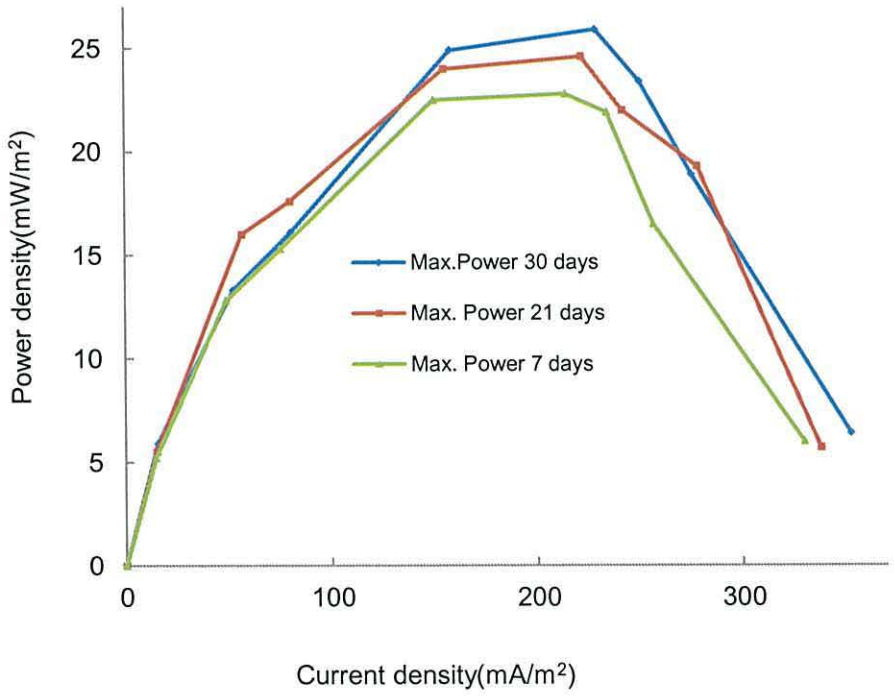

Figure 6. 12 - Power density generated by the MFC (Air cathode single chamber) using anodic biofilm growth on carbon cloth at a different period (7, 21, and 30 days).

Electrode Potential

The OCPs were measured for the electrodes (*anode and cathode*) of the air-cathode single chamber MFC against a SCE as a function of current with different resistor circuits (100 to 50,000 Ω) (Figure 6.13).

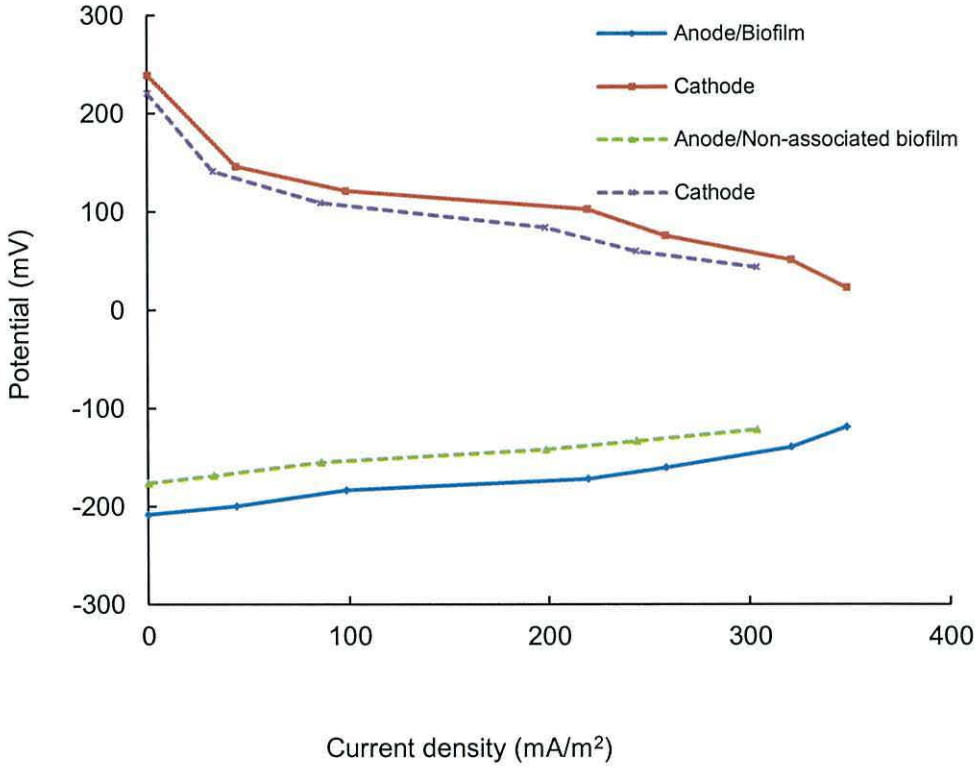

Figure 6. 13 - Anode associated biofilm and cathode (solid line) and anode non-associated biofilm and cathode (dashed line) potential (vs. SCE reference electrode, 242mV against the NHE) as a function of current.

The OCP of the anode associated biofilm was compared to the non-associated biofilm electrode. As shown in (figure 6.13) the anode associated biofilm had more negative potential than the non-associated biofilm electrode. The OCP of the anode associated biofilm was -208.2 mV(33.8mV NHE), but the working potential decreased to -118.7 mV for a current density up to 300 m A/m^2. In the non-associated biofilm electrode the OCP was -166.2 mV (76 mV NHE), but the working potential decreased to -121.3 mV for current density up to 300 m A/m^2. For both, anode associated biofilm and non-associated biofilm, the working potential increased slightly with current density. The OCP of the cathode with the non-associated biofilm electrode and anode associated biofilm were 235 mV (477 mV NHE), 239.4 mV (481.4mV NHE), respectively, but the working potential decreased to 43.7 mV, 23.4 mV for current density up to 300 m A/m^2, 350 m A/m^2, respectively. It was

observed that the OCP of the anode associated biofilm result -208.2 mV was increased when compared to non-associated biofilm electrode. The activity and performance of anode associated biofilm formed on the surface of the electrode indicated a further development in the MFC performance. Ren *et al*; reported that anodic biofilm growth can significantly reduce the overpotential and the charge transfer resistance of the electrode.[30]

Spacing between electrodes in air cathode single chamber microbial fuel cells

A series of tests were conducted to study the effect of different electrode spacing (4, and 2 cm) on power production in air cathode single chamber MFCs. Polarisation and power density curves were obtained to calculate the maximum power densities and current densities for the air-cathode single-chamber MFC utilising *Acidiphilium* sp. SJH bacteria (5.1 x 10^7 cells/ml), in the presence of glucose (900 mg/L) as the electron donor and soluble ferric ion (10 mM) as the electron shuttle. When the distance between the anode and cathode were reduced from 4, and to 2 cm [anode was fixed against a wall in a chamber with only one side exposed to the solution] and the cathode was made of 150 μg/cm^2 (22 wt % Pt/KB) coated on wet-proofed carbon cloth, (coated side) placed facing the solution, with the uncoated side exposed to the air; Figure 6. 14 shows the power output observed at variable external loads and under different electrode spacing between the anode and cathode electrodes. The maximum power density increased from 21.3 m W/m^2 to 30.2 m W/m^2, when the electrode spacing decreased from 4, to 2 cm.

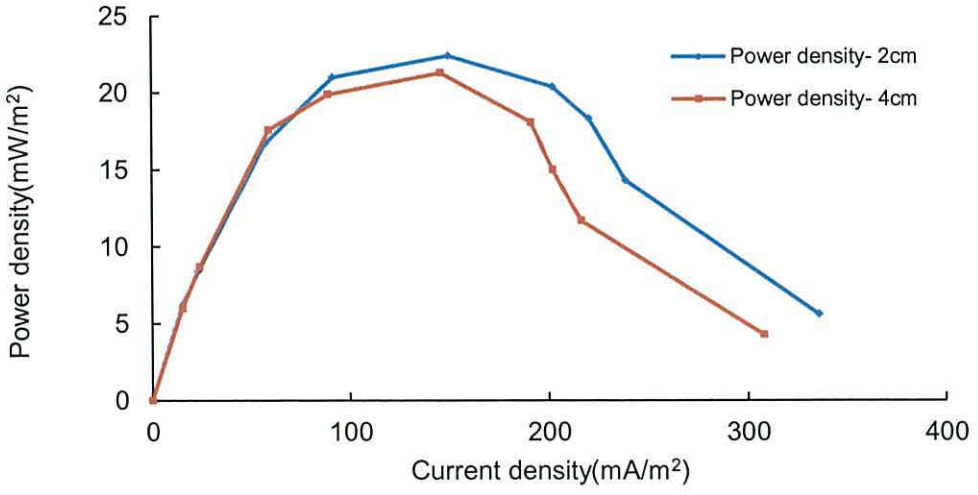

Figure 6. 14 - Power density generated as a function of current density of the air cathode single chamber MFC operated with different electrode spacing (4, and 2cm).

From the power density curves (Figure 6.14) the internal resistance can be evaluated of the 4, to 2 cm electrode spacing from maximum power density which occurred at the point where the internal resistance was equal to the external resistance.[31]

Now the internal resistance can be established as being equal to the external resistance, which can be calculated from the currents of 149.8 mA/m^2 (2 cm), and 146 m A/m^2. Thus, implies that the estimated internal resistances were 1996 Ω (2 cm), and 1998 Ω (4 cm). Internal resistances of the systems were found to be quite similar, despite the electrode spacing from 4 cm reduced to 2 cm (1998 Ω and 1996 Ω) respectively.

Figure 6. 14 also illustrates that there is a slight effect of electrode spacing on power output in the air cathode single chamber MFC. In this study reducing the electrode spacing and changes in reactor configuration show there may be little observable effects on the performance of MFC. The results suggest that when the internal resistance of the system is high the following factors have little influence on the power production of an MFC: anodic acidic medium which increases proton concentration, reducing the distance between anode and cathode, and the cathode being exposed directly to air. Logan *et al.*, reported that power production of an MFC is limited by the internal resistance.[32]In another study, maximum power density was obtained in a simple 2-bottle MFC built in H-type design was 2 mW/m^2 using a salt bridge as a membrane that had a high internal resistance (19,900 Ω).Using a proton exchange membrane instead of a salt bridge the internal resistance was reduced to 1290 Ω and power density increased to 40 mW/m^2.[27]

Performance of permanganate as the cathodic electron acceptor in microbial fuel cell

The dual compartment MFC was operated with anode associated biofilm (30days) referenced to anode compartment, and the permanganate catholyte was used as the cathodic electron acceptor in an acidic medium in order to evaluate the performance of permanganate. Figure 6.15 shows the OCV, maximum power density of the MFC with the aqueous catholyte of potassium permanganate used with a carbon cloth cathode and an anodic chamber containing anodic biofilm growth (30 days), and glucose (10 mM) in buffer solution of pH 2.5. The maximum power density generated using permanganate was 69.6 m W/m^2 at OCV 984.1 mV. While, the

power density reached a maximum 25.9 mW/m^2 at OCV 458 mV using oxygen and 0.15mg/cm^2 Pt (22 wt % Pt/KB). An aqueous catholyte of permanganate had a great influence on the potential difference across the cell terminals. The rate of reduction of the permanganate on the electrode surface is relatively faster than that of oxygen on (22 wt % Pt/KB), thereby enhancing the kinetics of cathodic reactions.

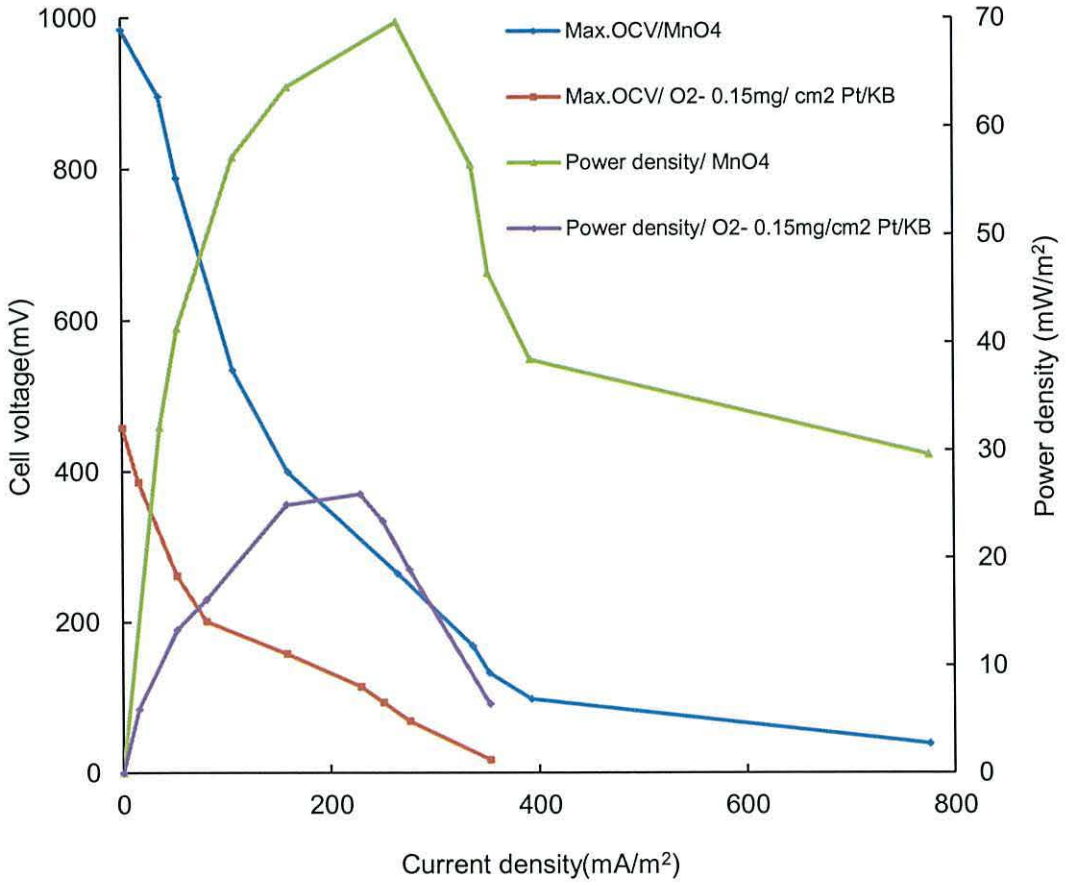

Figure 6. 15 - Power density and polarisation curve using anode associated biofilm (30days) with permanganate (10mM), and oxygen and 0.15mg/cm^2 Pt as electron acceptor in cathode chamber.

This increase in potential difference and power density due to the high redox potential (1.70 V) of permanganate is formed from the chemical energy of permanganate in acidic medium.[26]

6.7 Modification of the carbon felt by polyaniline film

Electrochemical polymerisation of aniline

The chemical modification process is supposed to be active by depositing or immobilising metals, metal oxides or other active compounds on the supports, such as carbon materials or conductive polymers, to improve the power generation of MFCs.[33] To examine the effect of covering of carbon felt with polyaniline on electrochemical performance of the anode, cyclic voltammetry technique was employed. For electrochemical polymerisation of polyaniline films modified with carbon felt, polyaniline films coated carbon felt was used as a working electrode, platinum wire as the counter electrode, and SCE as the reference electrode. Electropolymerisation of aniline proceeded coupling chemical reactions on the surface carbon felt was performed by cyclic voltammetry. Figure 6.16 shows the cyclic voltammograms during the electropolymerisation of aniline on carbon felt from a solution containing 200 mM aniline and 0.5M sulfuric acid for 15 cycles in the potential limits from −200 to 1500 mV at a sweep rate of 50 mV/s.

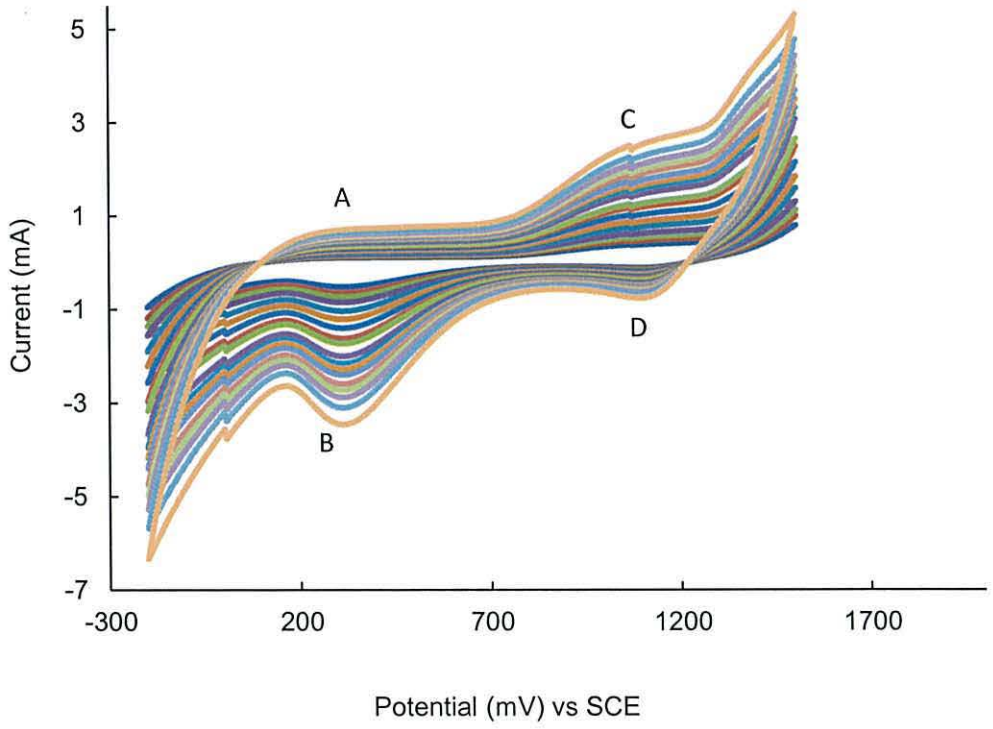

Figure 6. 16 - Cyclic voltammograms of polyaniline films modified with carbon felt. The electrolyte contained 200 mM aniline and 0.5M H_2SO_4 solution. The scan rate was 50mV/s and the number of cycles was 30.

The figure 6.16 shows the voltammogram profile of carbon felt changes in the first cycle and produces a polyaniline layer. Subsequently the polyaniline film was increased with an increasing number of cycles as proved by increasing in the peak current production. The two redox pairs with oxidation and reduction peaks were located at 240 mV, 1030 mV, 350 mV, and 1100 mV can be seen corresponding to the redox transition reactions of polyaniline. The peaks (A/B) indicated the pernigraniline forms of polyaniline, while the other peaks (C/D) rose from the development of the emeraldine form of polyaniline.[34] Previous work by Lai *et al* studied the effect of polyaniline modified carbon cloth anode improved electrochemical activity and lowered voltage drops.[35]

Surface morphology of modified carbon felt by polyaniline film

The surface morphologies of polyaniline modified and unmodified carbon felt anodes were tested by SEM. Figure 6.17 shows that polyaniline film had developed on the surface of the modified carbon felt anode compared to the unmodified carbon felt. The unmodified carbon felt consisted of a number of carbon fibres, each fibre with a smooth surface, Figure 6.17 left; while, in contrast, the polyaniline modification of carbon felt gave rise to a rough surface and a much more amorphous structure, Figure 6.17 right. Consequently, conductive polymers can change the morphology of the anode surface and increase the surface area of the anode, so it was expected that the increased anode surface could affect the power generation.

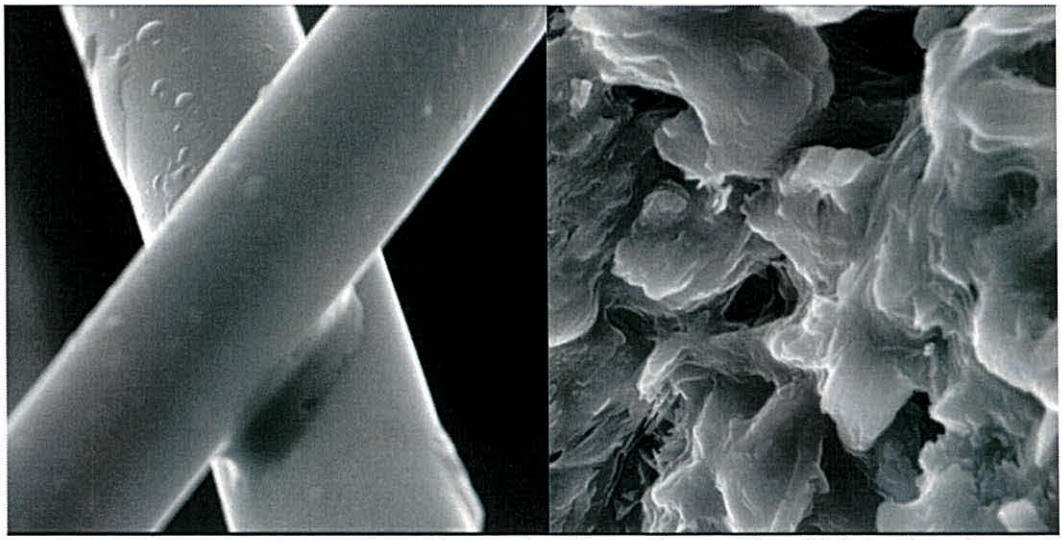

Figure 6. 17 - SEM image on an electrodeposited PANI sample on carbon felt by cyclic voltammetry X 3000.

Electrode Potential

To further test the effect of the carbon felt modified with polyaniline on the power output, OCPs and working potentials were measured for the electrodes (*anode and cathode*) of the air cathode two chamber MFC against a SCE as a function of current with different resistor circuits (100 to 50,000 Ω) (Figure 6.18). There were only small changes in the OCP and working potentials of the cathodes, despite the anode being modified or unmodified with polyaniline (223.8 ± 13 mV, 220.7 ±9 mV) respectively. There were important variations in the OCP and working potentials of the anode with the polyaniline modified and unmodified carbon felt anodes. Anode OCP when modified with polyaniline was mV (-191.5 ± 11mV); while for unmodified carbon felt the OCP was mV (-176.2 ± 9 mV). This difference in potential (- 15.3 mV) showed over a series of working potentials up to a current density of 321.3 mA/m^2. Improvement on the anode potential could result from different factors. First, the surface modification of the anode electrode may minimise the internal resistance in the MFC system. Low internal resistance could result in the observed improvement in the anode OCP. Second, it could be inferred that glucose degradation by bacteria produced electrons could be transferred to the anode modified with polyaniline more easily to reduce the over potential, which then enhanced electron transfer efficiency.

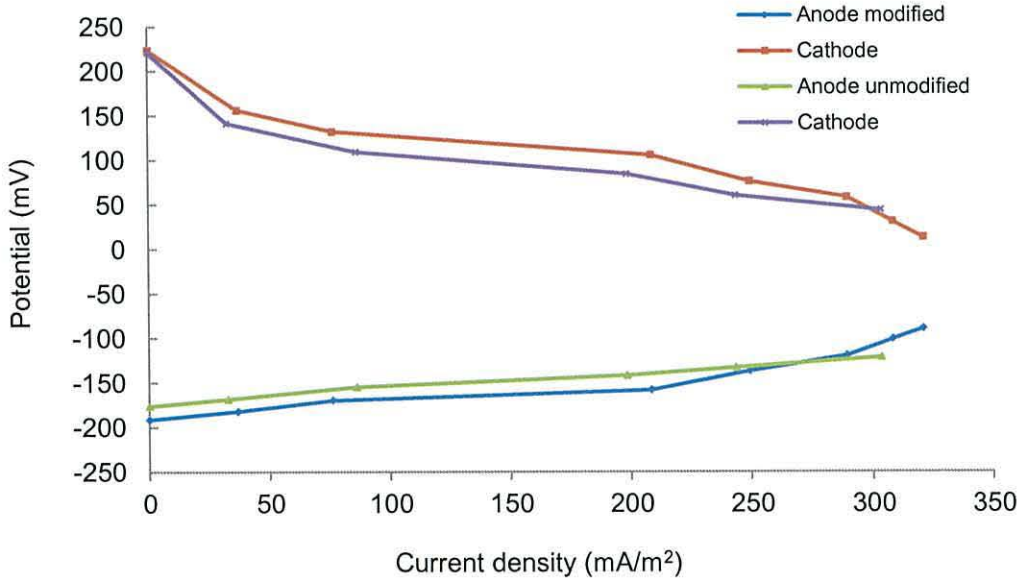

Figure 6. 18 - Anode modified with polyaniline and cathode (solid line) and unmodified anode and cathode (dashed line) potential (vs. SCE reference electrode, 242mV against the NHE) as a function of current.

Microbial fuel cell performance with modified carbon felt

The anode electrode significantly affects the electrical current of MFCs, for it is one of the parameters for electron transfer from bacteria to the anode electrode. Experimental tests were conducted with air cathode two chamber MFCs containing unmodified carbon felt and modified with polyaniline (PANI) as anodes, and the cathode was made of 150 $\mu g/cm^2$ (22 wt % Pt/KB) coated on wet-proofed carbon cloth, (coated side) placed facing the solution, with the uncoated side exposed to the air. Figure 6.19 shows OCV, polarisation and power density curves of MFCs with polyaniline modified and unmodified anodes. MFC with carbon felt modified with polyaniline showed an improvement in cell voltage generation, current density, and power density. The maximum power density generated using carbon felt modified with polyaniline was 23.7 m W/m^2, while the power density reached a maximum 21.3 mW/m^2 using unmodified carbon felt anode. In addition, the important factor which has a direct effect on MFCs applications is current density. It can be clearly seen that the carbon felt modified with polyaniline had a much higher current density than the unmodified carbon felt anode. Figure 6.19 also illustrates that the cell voltage of polyaniline modified MFC was stable, at about 419.8 mV, while that of the unmodified MFC was only about 400.3 mV.

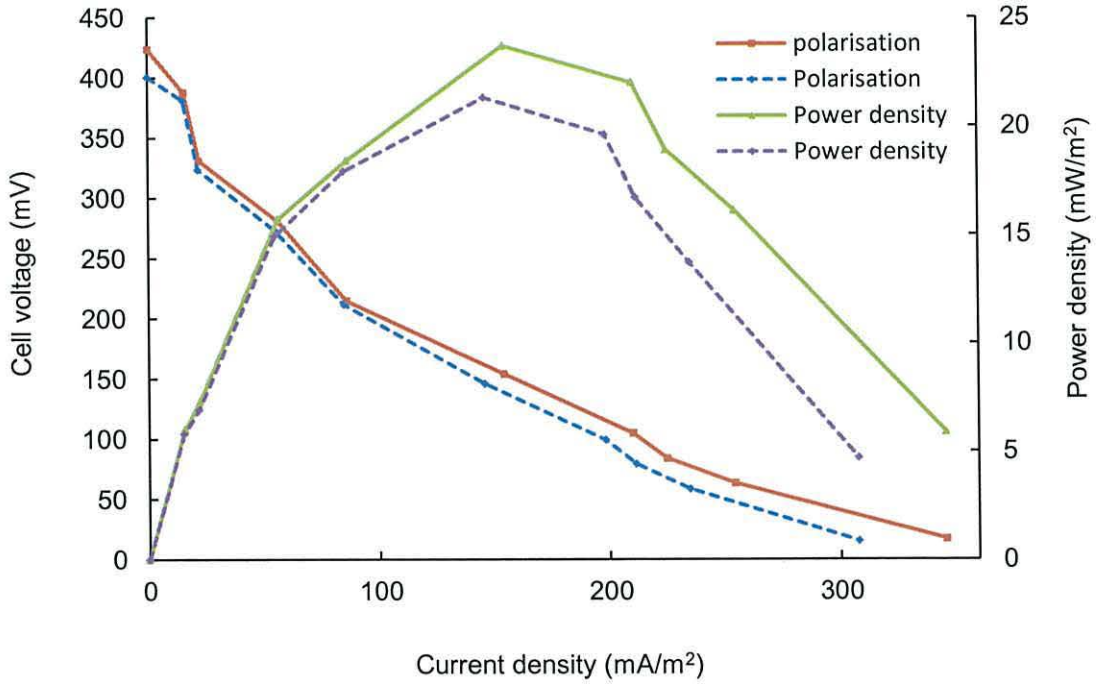

Figure 6. 19 - A comparison of the MFCs performance (polarisation and power density curve) between modified with polyaniline (solid line), and unmodified carbon felt (dashed line).

Polarisation and power density curves demonstrated that the carbon felt modified with polyaniline has a clear influence over the MFC system performance when compared with unmodified carbon felt anode (Figure 6.19).

The internal resistance of polyaniline modified carbon felt was approximately (1771 Ω) which was lower than that of unmodified carbon felt (1975 Ω).This comparison indicated that modified carbon felt with polyaniline may reduce the transfer resistance of MFCs and enhance electrons transferred from the bacteria to the anode surface.

6.8 Conclusion

In the present study it has been shown that the differences in the use of the different anode materials using the electron microscopy images of the anode associated biofilm. A thick and dense biofilm on carbon cloth can be observed. But the carbon felt electrode shows a different biofilm structure.

Experimental data showed that *Acidiphilium SJH* bacteria cells are able to colonise on the carbon felt surface of MFC enhancing potential generation. The extent of bacteria cell cover on the anodic surface showed a direct effect on MFC performance. The shape of voltammogram changes was specified with anode associated biofilm which shows a significant role of colonisation bacteria cells in directly exchanging electrons to the anode electrode. The power density curve showed the maximum power density at 1 kΩ as opposed to the maximum power density of OCV condition at 2 kΩ.

The modified carbon felt anode with polyaniline exhibited a direct influence on the MFC system performance and higher power density was achieved using air as the electron acceptor when the cathode was made of 0.15mg/cm^2 (22 wt % Pt/K.B) and the use of a single chamber.

6.9 References

1. Franks, A. E.; and Nevin, K. P. Microbial Fuel Cells, A Current Review. *Energies* **2010**, *3*, 899 - 919.
2. Pham, T. H.; Boon, N.; Aelterman, P.; Clauwaert, P.; De Schamphelaire, L.; Vanhaecke, L.; De Maeyer, K.; Hofte, M.; Verstraete, W.; Rabaey, K. Metabolites produced by *Pseudomonas sp.* enable a Gram-positive bacterium to achieve extracellular electron transfer. *Appl. Microbiol. Biotechnol.* **2008**, *77*, 1119 - 1129.
3. Rabaey, K.; Boon, N.; Siciliano, S. D.; Verhaege, M.; Verstraete, W. Biofuel Cells Select for Microbial Consortia That Self-Mediate Electron Transfer. *Appl. Environ. Microbiol.* **2004**, *70,* 5373 - 5382.
4. Dumas, C.; Basseguy, R.; Bergel, A. DSA to grow electrochemically active biofilms of *Geobacter sulfurreducens. Electrochim. Acta,* **2008**, *53*, 3200–3209.
5. Marsili, E.; Rollefson, J. B.; Baron, D. B.; Hozalski, R. M.; Bond, D. R. Microbial biofilm voltammetry: direct electrochemical characterisation of catalytic Electrode - attached biofilms. *Appl Environ Microbiol.* **2008**, *74*, 7329 - 7337.
6. Katuri, K. P.; Kavanagh, P.; Rengaraj, S.; Leech, D. Geobacter sulfurreducens biofilms developed under different growth conditions on glassy carbon electrodes: insights using cyclic voltammetry. *Chem. Commun.* **2010**, *46*, 4758 - 4760.
7. Martinez, A. A. C.; Harnisch, F.; Fitzgerald, L. A.; Biffinger, J. C.; Ringeisen, B. R.; Schroder, U. Cyclic voltammetric analysis of the electron transfer of Shewanella oneidensis MR-1 and nanofilament and cytochrome knock-out mutants. *Bioelectrochem.* **2011**, 81, 74 - 80.
8. Liu, Y.; Li, J. Role of *Pseudomonas aeruginosa* biofilm in the initial adhesion, growth and detachment of *Escherichia coli* in porous media. *Environ. Sci. Technol.* **2008**, *42*, 443 - 449.
9. Marsili, E.; Sun, J.; Bond, D. R. Voltammetry and Growth Physiology of Geobacter sulfurreducens Biofilms as a Function of Growth Stage and Imposed Electrode Potential. *Electroanal.* **2010**, *22*, 865 – 874.
10. Borole, A. P.; Reguera, G.; Ringeisen, B.; Wang, Z.; Feng, Y.; and Kim, B. H. Electroactive biofilms: Current status and future research needs. *Energy Environ. Sci.* **2011**, *4*, 4813 - 4834.
11. Logan, B. E. Exoelectrogenic bacteria that power microbial fuel cells. *Nat. Rev. Microbiol.* **2009**, *7*, 375 - 381.
12. Kim, H. J.; Park, H. S.; Hyun, M. S.; Chang, I. S.; Kim, M.; and Kim, B. H. A mediator less microbial fuel cell using a metal reducing bacterium, Shewanella putrefaciens. *Enzyme Microb. Technol.* **2002**, *30*, 145 - 152.
13. Myers, C. R.; and Myers, J. M. Localization of Cytochromes to the Outer Membrane of Anaerobically Grown Shewanella putrefaciens MR-1. *J. Bacteriol.* **1992**, *174*, 3429 - 3438.
14. Marcus, A. K.; Torres, C. I.; and Rittmann, B. E. Conduction-Based Modeling of the Biofilm Anode of a Microbial Fuel Cell. *Biotechnol. Bioeng.* **2007**, *98*, 1171 - 1182.

15. Huang, L.; Regan, J. M.; Quan, X. Electron transfer mechanisms, new applications, and performance of biocathode microbial fuel cells. *Bioresource Technol.* **2011**,*102*, 316 - 323.
16. Schroder, U. Anodic electron transfer mechanisms in microbial fuel cells and their energy efficiency. *Phys. Chem. Chem. Phys.* **2007**, *9*, 2619 - 2629.
17. Reguera, G.; Nevin, K. P.; Nicoll, J. S.; Covalla, S. F.; Woodard, T. L.; and Lovley, D. R. Biofilm and nanowire production leads to increased current in *Geobacter sulfurreducens* fuel cells. *Appl. Environ. Microbiol.* **2006**, *72*, 7345 - 7348.
18. Reguera, G.; Pollina, R. B.; Nicoll, J. S.; and Lovley, D. R. Possible Nonconductive Role of *Geobacter sulfurreducens* Pilus Nanowires in Biofilm. Formation. *J. Bacteriol.* **2007**, *189*, 2125 - 2127.
19. Rabaey, K.; Boon, N.; Hofte, M.; Verstraet, W. Microbial Phenazine production enhances electron transfer in biofuel cells. *Environ. Sci. Technol.* 2005, *39*, 3401 - 3408.
20. Busalmen, J. P.; Nunez, A. E.; Feliu, J. M. Whole Cell Electrochemistry of Electricity-Producing Microorganisms Evidence an Adaptation for Optimal Exocellular Electron Transport. *Environ. Sci. Technol.* **2008**, *42*, 2445 - 2450.
21. Srikanth, S.; Mohan, S. V.; Sarma, P. N. Positive anodic poised potential regulates microbial fuel cell performance with the function of open and closed circuitry. *Bioresour. Technol.* **2010**, *101*, 5337 - 5344.
22. Wagner, R. C.; Call, D.; and Logan, B. E. Optimal Set Anode Potentials Vary in Bioelectrochemical Systems. *Environ. Sci. Technol.* **2010**, *44,* 6036 - 6041.
23. Zhu, X.; Tokash, J. C.; Hong, Y.; Logan, B. E. Controlling the occurrence of power overshoot by adapting microbial fuel cells to high anode potentials. *Bioelectrochem.* **2013**, *90*, 30 - 35.
24. Dulon, S.; Parot, S.; Delia, M. L.; Bergel, A. Electroactive biofilms: new means for electrochemistry. *J. Appl. Electrochem.* **2007**, *37*, 173 - 179.
25. Rabaey, K.; Verstraete, W. Microbial fuel cells: novel biotechnology for energy generation. *Trends Biotechnol.* **2005**, *23*, 291 - 298.
26. Osman, M. H.; Shah, A. A.; Walsh, F. C. Review Recent progress and continuing challenges in bio-fuel cells. Part II: Microbial *Biosensor. Bioelectron.* **2010**, *26*, 953 - 963.
27. He, Z.; Minteer, S. D.; and Angenent, L. Electricity Generation from Artificial Wastewater Using an Upflow Microbial Fuel Cell. *Environ. Sci. Technol.* **2005**, 39, 5262 - 5267.
28. Min, B.; Cheng, S.; Logan, B. E. Electricity generation using membrane and salt bridge microbial fuel cells. *Water Res.* **2005**, *39*, 1675 - 1686.
29. Mohan, S. V.; Raghavulu, S. V.; and Sarma, P. N. Influence of anodic biofilm growth on bioelectricity production insingle chambered mediator-less microbial fue cell using mixed anaerobic consortia. *Biosen. Bioelectron.* **2008**, *24*, 41 - 47.
30. Ren, Z.; Ramasamy, R. P.; Owen, S. R. C.; Yan, H.; Mench, M. M.; and Regan, J. M. Time-course correlation of biofilm properties and electrochemical performance in single-chamber microbial fuel cells. *Bioresour. Technol.* **2011**, *102*, 416 - 421.
31. Logan, B. E. *Microbial Fuel Cells*, John Wiley and Sons, Inc. Hoboken, New Jersey, **2008**.
32. Logan, B. E.; Regan, J. M. Microbial fuel cells- challenges and application. *Environ. Sci. Technol.* **2006**, *40*, 5172 - 5180.

33. Zhou, M.; Chi, M.; Luo, J.; He, H.; Jin, T. An overview of electrode materials in microbial fuel cells. *J. Power Sources* **2011**, *196*, 4427 - 4435.
34. Gui, C. Q.; Ong, L. H.; Tan, T. C.; and Lee, J. Y. Extent of incorporation of hydrolysis products in polyaniline films deposited by cyclic potential sweep. *Electrochim. Acta* **1993**, *38*, 1395 - 1404.
35. Lai, B.; Tang, X.; Li, H.; Du, Z.; Liu, X.; Zhang, Q. Power production enhancement with a polyaniline modified anode in microbial fuel cells. *Biosens. Bioelectron.* **2011**, *28*, 373 - 377

Chapter 7

GENERAL CONCLUSION

7.1 Discussion and conclusions

Microbial fuel cells hold great promise for renewable and sustainable energy production and as a method for water treatment simultaneously. This work began with evaluating the electricity producing capacity of established *Acidiphilium SJH* bacteria operating at low pH in a MFC. Three MFC reactor designs were used through this study. H-type, sandwich-type dual chamber, and air cathode single chamber MFC. Based on the performances and experimental data for these three individual MFCs, H-type MFC, sandwich-type MFC, and air cathode single chamber MFC, the conclusion can be made that all of these three MFC reactor configurations are capable of generating electricity. Depending on the MFC structures, electrode materials and experiment conditions, their MFC performances were different.

The sandwich-type reactor provided a maximum power density of 25 m W/m^2, while the H-type MFC had the maximum power production of 18.3 m W/m^2. The coulombic efficiencies of these MFCs were not high, in the range from 6 % to 7 %, which showed that the efficiency of organic matter converting to electricity was very low based on these reactors and oxygen diffusion during long operation period. Improvement of cathode materials were explored in chapter 5, Platinum electrocatalysts supported on acid treatment KB carbon electrocatalysts were produced successfully. TEM and XRD results reveal that well-separated platinum nanoparticles. The formation of nano-scale (average diameter 3 nm) platinum particles highly dispersed within the Pt/KB cathode has been demonstrated, and an optimum platinum loading was established at 150 $\mu g/cm^2$. The platinum-modified cathode retained an equivalent of 80 ± 2 % efficiency compared to a solid platinum electrode, but contained only 0.1 % Pt. The sandwich-type MFC showed a maximum power density of 20.7 m W/m^2 with a Pt/KB modified carbon cloth cathode.

The modified Pt/KB cathode exhibited significant performance and higher power density was achieved when compared with the performance of platinum electrodeposition on the carbon felt electrode. Further, it was shown that carbon cloth, and carbon felt without a Pt catalyst can be used as cathode materials for MFC. The maximum power density generated using permanganate, chromium, and oxygen was 58.9 m W/m^2, 45.5 mW/m^2, and 10.6m W/m^2, respectively with a carbon cloth

electrode. The replacement or reduction of a Pt catalyst eliminates one of the main economic barriers for the extra industrial applications of MFCs technology.

Chapter 6 studied the formation of a biofilm of the *Acidiphilium sp. SJH* on the surface of the different anode materials (carbon felt, and carbon cloth) and the use of an air cathode single chamber MFC. Significant improvement in power generation occurred at 1 kΩ. The surface morphologies and electrochemical activity of the anode associated biofilm were observed by scanning electron microscopy, and cyclic voltammetry, respectively. In addition, the surface area value of the electrode might only provide limited information on the suitability of an electrode material for electrode associated biofilm formation. Electrode material construction characterisation may be a further significant factor for Electroactive biofilm formation.[1]

This work is needed to further elucidate the microecological importance of this finding. This chapter has also demonstrated surface modification of the carbon felt (anode) by polyaniline. In order to enhance the electron transfer from the microorganism to the anode, a chemically modified carbon felt surface quinoid (N=C=N) groups existing in polyaniline was developed. Surface modification of the anode electrode by polyaniline conductive film exhibited a better alternative for improving the performance of MFCs.

7.2 Further Work

Future studies will focus on the molecular analysis, such as total DNA extraction polymerase chain reaction (PCR), and denaturing gradient gel electrophoresis (DGGE) give additional information about *Acidiphilium sp. SJH* species composition.

Further, experiments will be on testing the electrogenic activity of *Acidiphilium sp. SJH*, and investigation into *Acidiphilium sp. SJH* is required to establish electricity from real wastewater in highly acidic environments (pH < 3).

This study is not planned as an exploration the bacteria–electrode material interaction in detail, which may be the topic of further study.

7.3 References

1. Liu, Y.; Harnisch, F.; Fricke, K.; Schröder, U.; Climent, V.; Feliu, J. M. The study of electrochemically active microbial biofilms on different carbon-based anode materials in microbial fuel cells. *Biosensor. Bioelectron.* **2010**, *25*, 2167 - 2171.